

THE PROPERTIES OF ION ORBITS IN  
THE CENTRAL REGION OF A CYCLOTRON

*by*

ROBERT JOHN LOUIS

B.Sc., University of Victoria, 1966  
M.Sc., University of Victoria, 1968

A thesis submitted in partial fulfilment of  
the requirements for the degree of

Doctor of Philosophy

in the Department  
of  
Physics

We accept this thesis as conforming to the  
required standard

THE UNIVERSITY OF BRITISH COLUMBIA  
January, 1971

In presenting this thesis in partial fulfilment of the requirements for an advanced degree at the University of British Columbia, I agree that the Library shall make it freely available for reference and study.

I further agree that permission for extensive copying of this thesis for scholarly purposes may be granted by the Head of my Department or by his representatives. It is understood that copying or publication of this thesis for financial gain shall not be allowed without my written permission.

Department of Physics

The University of British Columbia  
Vancouver 8, Canada

Date February 11, 1971

## ABSTRACT

The behaviour of ion orbits in the magnetic and electric fields at the centre of a cyclotron is studied in detail. The objective is to optimize the phase acceptance and beam quality for a 500 MeV  $H^-$  isochronous cyclotron.

Since accurate electric fields are necessary for orbit calculations, a numerical method for calculating these fields is examined in detail. The method is suitable for complicated electrode shapes and converges rapidly, yielding potentials in three dimensions with average errors of less than 0.01%. The magnetic fields used in the orbit calculations are measured on model magnets.

The axial motions are examined using a thick lens approximation for the accelerating gaps. A method is demonstrated for calculating the axial acceptance of the cyclotron as a function of RF phase. This method is used to evaluate the merits of various central geometries and injection energies. This method is also used to examine the effects of flat-topping the RF voltage by adding some third harmonic to the fundamental waveform. It is found that addition of the optimum amount of third harmonic increases the phase acceptance by about 20 deg. Finally, the effects of field bumps on the axial motions are investigated.

To allow accurate radial motion calculations to high energy, an approximate formula is developed which yields accurate (<1%) values for the changes in orbit properties of an ion crossing a dee gap. The geometry of the orbit on the first turn is discussed in detail. The radial centring is studied by tracking ions from injection to 20 MeV, and a method is described for choosing the starting conditions of the beam so as to minimize the radial betatron amplitude over a desired phase range.

The problems associated with using a three-fold symmetric magnetic field with a two-fold symmetric electric field are also discussed. Besides the well-known gap-crossing resonance, a previously ignored phase-oscillation effect is found to be important for cyclotrons operating on a high harmonic of the ion rotation frequency.

## TABLE OF CONTENTS

	Page
Chapter 1. INTRODUCTION	1
A. Problems in the Cyclotron Central Region	1
B. The TRIUMF Cyclotron	3
C. Equations of Motion	5
Chapter 2. ELECTRIC FIELD CALCULATIONS	8
A. Choice of Method	8
B. Finite Difference Approximation	9
C. Computational Details	13
D. Convergence Tests	17
E. The Practical Problem	21
Chapter 3. AXIAL MOTIONS	25
A. Introduction	25
B. Magnetic Field	26
C. Space Charge Forces	28
D. Electric Lens Effects	30
E. Calculation of Cyclotron Acceptance	34
F. Phase Space Acceptance for Various TRIUMF Central Geometries and Injection Energies	38
G. Effects of Third Harmonic in the RF on Axial Motions	41
H. Effects of Field Bumps	43
Chapter 4. RADIAL MOTIONS	47
A. Introduction	47
B. Basic Design	48
C. Problems with Three-Sector Magnetic Fields	55
D. Radial Centring	60
E. Effects of Finite Beam Emittance	68
Chapter 5. RADIAL LENS EFFECTS OF CYCLOTRON DEE GAPS	71
A. Introduction	71
B. Constant Gradient Approximation with No Magnetic Field	72
C. Sine Gradient Approximation	78
D. Constant Gradient Approximation with Third Harmonic in the Electric Field	80
E. Constant Gradient Approximation with Magnetic Field	81
F. Constant Gradient Approximation with Magnetic Field and Third Harmonic in the Electric Field	85
Chapter 6. SUMMARY AND CONCLUSIONS	88

CONTENTS (cont'd)

	Page
References	91
Figures	94
Appendix A. Theory of Successive Over-Relaxation	153
Appendix B. Boundary Conditions for Relaxation Calculations	160
Appendix C. New Relaxation Iteration Routines	176
Appendix D. Program AXCENT	192

## LIST OF TABLES

	Page
I. Largest eigenvalue ( $\lambda_m$ ) and best over-relaxation factor ( $\alpha_b$ ) for various size relaxation problems	14
II. Sequence of operations used to solve a 64x64x32 node relaxation problem	19
III. Average error after various numbers of iterations over the reduced problem	19
IV. Sequence of operations used to solve a 512x128x32 node relaxation problem	23
V. Gap factors given by numerical integration and by the constant gradient approximation (no magnetic field)	77
VI. Gap factors given by numerical integration and by the constant gradient approximation (isochronous magnetic field)	84

## LIST OF FIGURES

	Page
1.1 Central region of the TRIUMF cyclotron - median plane	94
1.2 Central region of the TRIUMF cyclotron - section through centreline of hill #3	95
2.1 Relaxation mesh organization; total number of nodes is $(p+1)(q+1)(r+1)$	96
2.2 Average error and average change per iteration vs number of sweeps over large volume	97
2.3 Average error vs number of sweeps over large volume for various values of $\alpha$	98
2.4 Number of nodes with a given error vs size of error for various number of sweeps over large volume	99
2.5 Number of nodes with a given error vs number of sweeps over large volume for various size errors	100
3.1 Magnetic axial focusing frequency ( $\nu_z$ ) vs energy for three- and six-sector magnetic geometries	101
3.2 Equivalent axial focusing frequency produced by space charge forces vs energy for various beam currents and axial beam heights	102
3.3 Cross-section of dees near accelerating region showing electric equipotentials and (schematically) an ion trajectory	103
3.4 Comparison between equivalent electric axial focusing frequencies predicted by the thin lens approximation and determined by numerical integration	104
3.5 Possible TRIUMF central geometry with three accelerating gaps in the first half-turn	105
3.6 Axial emittance ellipses required at injection for various RF phases	106
3.7 Axial acceptance vs RF phase for various injection energies (one accelerating gap in the first half-turn)	107
3.8 Axial acceptance vs RF phase for various injection energies (three accelerating gaps in the first half-turn)	108
3.9 Average axial acceptance (averaged from -30 deg to +60 deg) vs injection energy (one accelerating gap in the first half-turn)	109
3.10 Axial acceptance vs RF phase for various choices of the initial emittance ellipse	110

	Page
3.11 RF voltage waveforms with various amounts of third harmonic and phase shift between fundamental and third harmonic	111
3.12 Slope of RF voltage waveform with various amounts of third harmonic and phase shift between fundamental and third harmonic	112
3.13 Axial acceptance vs RF phase for various choices of the initial emittance ellipse, $\epsilon = 0.17$ , $\delta = 0$	113
3.14 Axial acceptance vs RF phase for various choices of the initial emittance ellipse, $\epsilon = 0.12$ , $\delta = 0$	114
3.15 Axial acceptance vs RF phase for various choices of the initial emittance ellipse, $\epsilon = 0.15$ , $\delta = -10$ deg	115
3.16 Total (magnetic and electric) equivalent axial focusing frequency vs energy for various RF phases	116
3.17 Transition phase (of total axial focusing from negative to positive) vs energy	117
3.18 Change in sine of RF phase required to keep ion at transition phase vs radius	118
3.19 Magnetic field bump required to keep ion at transition phase vs radius	119
4.1 Geometry of injection gap and first main gap for two RF phases	120
4.2 $y_c$ vs RF phase at injection gap for various injection gap positions	121
4.3 Energy gain in injection gap and first main gap vs RF phase at injection gap for various injection gap positions	121
4.4 RF phase at first main gap vs RF phase at injection gap for various injection gap positions	122
4.5 Phase oscillation amplitude vs centring error at various radii	123
4.6 RF phase vs half-turn number for various initial phases with no flutter in the magnetic field	124
4.7 Geometry of an orbit in a three-sector magnetic field	125
4.8 RF phase difference on succeeding half-turns as a function of orientation of the dee gap ( $\delta$ )	126
4.9 RF phase vs half-turn number for various initial phases with a three-sector magnetic field ( $\delta = 30$ deg)	127

	Page
4.10 Ratio of third harmonic amplitude in magnetic field to average field vs radius for (three-sector) field 1-14-5-70	128
4.11 Average orbit radius and maximum orbit scalloping vs radius for (six-sector) field 1-30-06-70	129
4.12 Geometry of an orbit in a six-sector magnetic field	130
4.13 Geometry of the difference between an equilibrium orbit and an accelerated orbit	131
4.14 Centre-point displacement along the dee gap vs energy showing values from numerical orbit tracks and from an analytic approximation	132
4.15 Accelerated phase plot inwards from 5 MeV, $\phi = -30$ deg	133
4.16 Accelerated phase plot inwards from 5 MeV, $\phi = 0$ deg	134
4.17 Accelerated phase plot inwards from 5 MeV, $\phi = +30$ deg	135
4.18 Accelerated phase plot outwards for various radii at first main dee gap, $\phi = 0$ deg	136
4.19 Accelerated phase plot outwards from inflector exit for various phases; ion with $\phi = 0$ is centred	137
4.20 Accelerated phase plot outwards from inflector exit for various phases; ion with $\phi = +17$ deg is centred	138
4.21 Betatron oscillation amplitude vs RF phase for various starting conditions	139
4.22 Phase histories of ions with various starting phases in a magnetic field with a field bump	140
4.23 Accelerated phase plot outwards from inflector exit for various phases using the magnetic field with the field bump; ion with $\phi = 17$ deg is centred	141
4.24 Accelerated phase plots with $\phi = 0$ deg for four points on the edge of the emittance ellipse a) matched to $v_r = 1$ , and b) chosen to reduce the radial oscillation amplitude over the phase range $-5$ deg to $+25$ deg	142
4.25 Accelerated phase plots with $\phi = +15$ deg for four points on the edge of the emittance ellipse a) matched to $v_r = 1$ , and b) chosen to reduce the radial oscillation amplitude over the phase range $-5$ deg to $+25$ deg	143
4.26 Accelerated phase plots with $\phi = +25$ deg for four points on the edge of the emittance ellipse a) matched to $v_r = 1$ , and b) chosen to reduce the radial oscillation amplitude over the phase range $-5$ deg to $+25$ deg	144

	Page
5.1 Cross-section of a dee gap showing electric equipotentials	145
5.2 Electric potential vs distance from dee gap centre showing actual values and constant gradient approximation	146
5.3 Geometry of an ion crossing a dee gap	147
5.4 Gap factors vs energy for $\phi_c = 0$ deg	148
5.5 Differences between gap factors obtained from numerical integration and those obtained from the constant gradient approximation as a function of energy, no magnetic field	149
5.6 Differences between gap factors obtained from numerical integration and those obtained from the constant gradient approximation as a function of energy, with an isochronous magnetic field	150
5.7 Differences between gap factors obtained from numerical integration and those obtained from the constant gradient approximation as a function of RF phase, with an isochronous magnetic field	151
5.8 Apparent displacement due to change in radius of curvature of the ion path while crossing the dee gap	152

## ACKNOWLEDGEMENTS

I would like to thank Dr. M.K. Craddock for supervising this work and for providing guidance and helpful suggestions throughout the course of my studies at U.B.C. I would also like to thank Dr. G.H. Mackenzie for several helpful discussions and Miss Ann Koritz, Mr. Neil Fraser and the staff of the Computing Centre at U.B.C. for their help in writing and debugging the computer programs. Finally I would like to thank Miss Ada Strathdee for her patience and perseverance while typing this thesis.

Financial support from the TRIUMF project throughout the course of this work is gratefully acknowledged.

## CHAPTER 1. INTRODUCTION

### A. Problems in the Cyclotron Central Region

The central region of a cyclotron requires special attention because the internal beam quality and phase acceptance are primarily determined during injection and the first few turns within the machine. During these initial turns, the beam has low energy and is therefore strongly influenced by the phase-dependent lens effects of the dee gaps. The objective of this work is to study the behaviour of ion orbits in the magnetic and electric fields at the cyclotron centre, and thereby to choose the beam injection conditions and magnet and electrode designs for optimum beam performance, i.e. a beam which is centred, has minimum spot size in both the radial and axial directions, and is in a phase interval which optimizes the acceleration process.

The usual studies of cyclotron central regions, for example Rose,<sup>1</sup> and others,<sup>2-4</sup> are concerned with machines with internal ion sources where the ion starts with zero energy and spends its first turn mainly within the electric field produced by the dee gap. With an external ion source, the problems are quite different; to solve them this study was undertaken.

Injection of ions into a cyclotron from an external source has been studied by Powell and Reece;<sup>5</sup> however, the injection energy in their case was 11 keV, compared to a maximum energy gain of 50 keV per turn, whereas in this case the injection energy is 300 keV, compared to 400 keV per turn. Also, the electrode geometry is very different.

This thesis considers ion injection for a  $H^-$  cyclotron where the ions are extracted by electron stripping and the duty cycle is determined by the phase band the central region will transmit and not by the extraction system, as in some cyclotrons with resonant extraction schemes. Thus there

is considerable emphasis on reducing phase-dependent effects in the central region.

The central region problems fall naturally into two groups, those concerning the axial motions and those concerning the radial motions.

The basic problem in the axial motion<sup>2</sup> is that the focusing provided by the magnetic field becomes very small near the centre of the machine, while the (phase-dependent) electric forces due to the dee gaps become very strong. It is well known<sup>1</sup> that the electric forces are defocusing for half of the RF cycle. Since these electric forces will be larger than the (focusing) magnetic forces at low energy, a detailed study of the axial motions is required if a large range of RF phases is to be accepted. The situation is further complicated by the fact that space charge effects will also tend to expand the beam. Space charge effects will be most important at low energy and high current.

The basic problem in the radial motion<sup>3</sup> is not lack of focusing but rather how to minimize the radial oscillation amplitudes of the ions. Since the ions are extracted when they reach a particular radius, a large spread in radial amplitudes means that ions from different turns may be present at the extraction radius, resulting in a large energy spread in the extracted beam. The initial motion of the ions in the cyclotron requires that the beam be injected off centre if it is to be centred at extraction; however, this effect is phase dependent, making it difficult to centre ions with a wide range of phases.

Since a knowledge of the electric fields involved is required for studies of both the axial and radial motions, Chapter 2 describes in detail a method for calculating these fields.

Chapter 3 considers the axial motions. A method is presented which

allows calculation of the axial acceptance of the accelerator as a function of RF phase. This method is used to study various injection energies and the effects of adding third harmonic to the RF. Finally, the effects of field bumps, used to induce phase slip, are considered.

Chapter 4 considers the radial motions. The geometry of the first turn and how this is influenced by the accelerating electrodes is studied in detail. The radial centring is studied by tracking ions from injection out to 20 MeV. Finally, the effects of a finite beam size are considered.

Chapter 5 describes an approximation which allows the changes in orbit properties of an ion crossing a dee gap to be evaluated to high accuracy without numerical integration through the electric field. The accuracy of the method is given as a function of RF phase and incident ion energy. This approximation is used in the tracking of the radial motions in Chapter 4 between 5 and 20 MeV where this approximation is very accurate.

## B. The TRIUMF Cyclotron

The studies described in this thesis were performed for the TRIUMF cyclotron,<sup>6</sup> which because of its unique design has several special problems.

The TRIUMF cyclotron is a six-sector, azimuthally varying field (AVF), isochronous machine, designed to accelerate 100  $\mu$ A of  $H^-$  ions to 500 MeV. The acceleration of  $H^-$  ions provides a convenient method of extraction by stripping two electrons from the  $H^-$  ions by passing the beam through a thin foil. This method gives an extraction efficiency of nearly 100% whereas conventional proton machines have not achieved efficiencies greater than 80% with a large duty cycle. Two other advantages of extraction by electron-stripping are variability of extraction energy by adjusting the foil position and simultaneous extraction of several beams at different energies.

The disadvantage of this technique is that the lifetime of the  $H^-$  ions requires that the maximum magnetic field that the ions pass through must be low (5.7 kG at 500 MeV)<sup>7</sup> to prevent dissociation of the  $H^-$  ions, and also there must be a vacuum  $< 7 \times 10^{-8}$  Torr to prevent  $H^-$  stripping by residual gas molecules. The low magnetic field means that the radius of the machine is very large (500 MeV orbit radius of 311 in.), and the central magnetic field (3.0 kG) is five or six times lower than in conventional cyclotrons.

The accelerating voltage is provided by four resonant cavities which provide 0.4 MeV energy gain per turn. The low magnetic field means that the ion rotation frequency is low (4.53 MHz). To allow the cavity resonators to fit inside the vacuum tank, the RF is operated at the fifth harmonic of the ion frequency. The fact that the accelerating structures are cavity resonators means that some third harmonic of the ion frequency can be introduced into the cavity, squaring the RF waveform and giving significant improvements in orbit properties.

The arrangement of the TRIUMF central region is shown in Figs. 1.1 and 1.2. The centre post is required to support part of the weight of the upper magnet cores, the magnetic force between the magnet pole pieces and the atmospheric load. The  $H^-$  beam is produced in an external (Ehlers) ion source and accelerated to 300 keV before being transported to the cyclotron and bent into the median plane by the spiral electrostatic inflector. The beam leaves the centre post at the "injection gap", which provides an auxiliary 100 keV (the dee-to-ground potential) acceleration on the first turn. The beam then spirals outward, gaining a maximum of 400 keV per turn.

Several types of operating conditions must be considered. One of the principal uses of the machine will be to produce mesons. In this case, the

current required is large, but the energy resolution is not important (since the mesons are produced in a secondary target). Therefore, the duty cycle may be maximized at the expense of energy resolution. It is also planned to produce a high resolution proton beam. In this case, high current is not required so a smaller duty cycle may be considered, giving smaller radial oscillation amplitude and thus improving energy resolution. It is also hoped that with the addition of third harmonic to the RF, separated turn acceleration will be possible, i.e. spatial turn separation will be maintained out to extraction so that the beam can be extracted from one turn, giving very high energy resolution (hopefully,  $\pm 50$  keV). Again, the phase band accelerated would be quite narrow.

### C. Equations of Motion

The force on a charged particle moving in electric and magnetic fields is given by the sum of the Lorentz and electric forces

$$\vec{F} = q(\vec{E} + \vec{v} \times \vec{B}) \quad (1.1)$$

$\vec{F}$  is the force on the particle which has charge  $q$ , mass  $m$  and velocity  $\vec{v}$ . The electric field is  $\vec{E}$  and the magnetic field is  $\vec{B}$ .

We define a Cartesian co-ordinate system with the  $z$  axis upwards in the axial direction (perpendicular to the plane of the orbits), the  $x$  direction is along the centreline of the dee gap, and  $y$  is perpendicular to the dee gap and the axial direction.

In a Cartesian system, eqn.(1.1) can be written

$$F_x = q \left[ E_x + (v_y B_z - v_z B_y) \right], \quad (1.2)$$

$$F_y = q \left[ E_y + (v_z B_x - v_x B_z) \right], \quad (1.3)$$

$$F_z = q \left( E_z + (v_x B_y - v_y B_x) \right). \quad (1.4)$$

The ion circulates in its orbit near the x-y plane; hence the components of the velocity in this plane ( $v_x$  and  $v_y$ ) are much larger than  $v_z$ . Due to the symmetry of the magnet, the magnetic field in the median plane is in the axial direction only, i.e.  $B_x = B_y = 0$ . Errors in the construction of the magnet may cause the magnetic median surface to be different from the geometric median plane, giving non-zero values of  $B_x$  and  $B_y$  in the geometric median plane; however, these will be small, and we may write eqns.(1.2) and (1.3) as

$$\frac{d}{dt}(mv_x) = q(E_x + v_y B_z), \quad (1.5)$$

$$\frac{d}{dt}(mv_y) = q(E_y - v_x B_z). \quad (1.6)$$

Eqns.(1.5) and (1.6) are relativistically correct, provided the changes in mass due to acceleration are not neglected. The relativistic mass is

$$m = \gamma m_0$$

where  $m_0$  is the rest mass and  $\gamma$  is the usual relativistic factor

$$\gamma = 1 + \frac{T}{m_0 c^2} = \left( 1 - \beta^2 \right)^{-\frac{1}{2}}$$

where  $T$  is the kinetic energy of the ion,  $c$  is the velocity of light and  $\beta = v/c$ .

The approximation used in deriving eqns.(1.5) and (1.6), i.e. that terms in  $v_z B_y$  and  $v_z B_x$  are negligible, has removed coupling between motion in the median plane and motion in the axial direction, greatly simplifying

the calculations. The solutions of eqns.(1.5) and (1.6) [obtained by numerical integration through realistic electric and magnetic fields] are discussed in Chapter 4.

The axial motion is described by eqn.(1.4). The terms in  $B_x$  and  $B_y$  cannot be neglected in this case since they are multiplied by the (large) velocities  $v_x$  and  $v_y$ . It is these terms which describe the axial magnetic focusing produced by flutter and spiral in the magnetic field when the ion is not in the median plane. The axial motion is discussed in Chapter 3.

## Chapter 2. ELECTRIC FIELD CALCULATIONS

### A. Choice of Method

Accurate orbit calculations in the centre region require a detailed knowledge of the electric and magnetic fields involved. The magnetic field can be obtained from measurements on model magnets. The electric field is produced by complicated electrode shapes (see Figs. 1.1 and 1.2) and hence cannot be calculated analytically. There are several methods which can be used to obtain the electric field in these circumstances:

- 1) Electroconductive analogies in which the potential is obtained by measuring the voltage in a conducting medium surrounding a model of the electrodes.<sup>8</sup> This method yields potentials (in two or three dimensions) with errors of about 0.3%.<sup>9</sup>
- 2) Numerical solution of Laplace's equation. This method yields potentials with average errors of 0.1% or less, depending on the time available for computation. This method is described in detail below.
- 3) The induced current method in which a vibrating charged probe induces a current in the electrodes proportional to the component of the required field at the probe in the direction of vibration of the probe.<sup>10</sup> This method gives field values with errors of 5.0% or less.
- 4) The magnetic analog in which the components of the magnetic field are a measure of the corresponding electric field components.<sup>11</sup>

Methods 3 and 4 yield field values which can be used directly in orbit calculations while methods 1 and 2 give potentials which must be numerically differentiated to obtain the field components.

From this point of view, method 3 or 4 is more attractive. However, methods 1, 3 and 4 require a model of the electrode structure to be built.

This means that changes in the electrodes require time-consuming and expensive changes in the model. In addition, these three methods involve mechanically-driven probes which are subject to alignment errors. Also, these methods use complicated electronic circuits which are subject to drift over long periods of time. For these reasons, the numerical solution of Laplace's equation which avoids these difficulties is the most attractive choice. Solving Laplace's equation for a complicated boundary shape is a difficult computational problem; however, the availability of large, fast computers enables large problems to be solved in a reasonable amount of time.

#### B. Finite Difference Approximation

We wish to find the electrostatic potential  $\phi$  which is the solution of Laplace's equation, i.e.

$$\nabla^2\phi = 0 \tag{2.1}$$

within the rectangular parallelepiped shown in Fig. 2.1. This volume is bounded by the planes  $x = 0$ ,  $x = ph$ ,  $y = 0$ ,  $y = qh$ ,  $z = 0$ ,  $z = rh$ . In the usual problem either the potential or its derivative is known on the surface of the volume (Dirichlet or Neumann boundary conditions, respectively) while the potential is unknown inside the volume. In the problems to be studied here every boundary plane has Dirichlet boundary conditions or is a plane of symmetry (described below). In addition, parts of the interior of the volume may have fixed potential values, i.e. the boundary conditions may extend inside the volume.

To solve eqn.(2.1) numerically we transform the differential equation to a difference equation and solve for the values of  $\phi$  at discrete nodes within the volume. Fig. 2.1 shows a rectangular grid with uniform spacing  $h$

in all three directions. The nodes occur at the intersections of the planes  $x = ih$ ,  $y = jh$  and  $z = kh$  where  $i = 0, 1, \dots, p$ ,  $j = 0, 1, \dots, q$  and  $k = 0, 1, \dots, r$ . The number of nodes in the grid ( $N$ ) is  $(p + 1)(q + 1)(r + 1)$ .

To derive the finite difference approximation, we consider the potential  $\phi_{ijk}$  at some node  $ijk$ . Expanding the potential in a Taylor series at the six nodes nearest to  $i, j, k$  we obtain

$$\phi_{i\pm 1, j, k} = \phi_{ijk} \pm h \left( \frac{\partial \phi}{\partial x} \right)_{ijk} + \frac{h^2}{2} \left( \frac{\partial^2 \phi}{\partial x^2} \right)_{ijk} \pm \frac{h^3}{6} \left( \frac{\partial^3 \phi}{\partial x^3} \right)_{ijk} + \frac{h^4}{24} \left( \frac{\partial^4 \phi}{\partial x^4} \right)_{ijk} + \dots$$

$$\phi_{i, j\pm 1, k} = \phi_{ijk} \pm h \left( \frac{\partial \phi}{\partial y} \right)_{ijk} + \frac{h^2}{2} \left( \frac{\partial^2 \phi}{\partial y^2} \right)_{ijk} \pm \frac{h^3}{6} \left( \frac{\partial^3 \phi}{\partial y^3} \right)_{ijk} + \frac{h^4}{24} \left( \frac{\partial^4 \phi}{\partial y^4} \right)_{ijk} + \dots$$

$$\phi_{i, j, k\pm 1} = \phi_{ijk} \pm h \left( \frac{\partial \phi}{\partial z} \right)_{ijk} + \frac{h^2}{2} \left( \frac{\partial^2 \phi}{\partial z^2} \right)_{ijk} \pm \frac{h^3}{6} \left( \frac{\partial^3 \phi}{\partial z^3} \right)_{ijk} + \frac{h^4}{24} \left( \frac{\partial^4 \phi}{\partial z^4} \right)_{ijk} + \dots$$

Adding these, we obtain

$$\phi_{i+1jk} + \phi_{i-1jk} + \phi_{ij+1k} + \phi_{ij-1k} + \phi_{ijk-1} + \phi_{ijk+1} = 6\phi_{ijk}$$

using (2.1) and neglecting terms in  $h^4$  and higher, we have,  $+ \frac{h^2}{2} \nabla^2 \phi + O(h^4)$ ;

$$\phi_{ijk} = \frac{1}{6} \left( \phi_{i+1} + \phi_{i-1} + \phi_{j+1} + \phi_{j-1} + \phi_{k+1} + \phi_{k-1} \right) \quad (2.2)$$

$$= b_{ijk} \cdot \begin{array}{l} \text{[interior points]} \\ \text{[boundary points]} \end{array}$$

In the right side of eqn.(2.2) we have abbreviated the notation by writing only those subscripts which are not equal to  $i, j$  or  $k$ .

Eqn.(2.2) describes a linear system of  $N$  equations which can be written

$$A d = b \quad (2.3)$$

where  $A$  is an  $N$  by  $N$  matrix containing the coefficients of the system,  $d$  is a column vector containing the unknown potential values

$$d = \begin{pmatrix} \phi_{111} \\ \vdots \\ \phi_{pqr} \end{pmatrix},$$

and  $b$  is a column vector containing the potential values for those nodes which fall in the boundaries.

Now the solution of eqn.(2.1) is reduced to the solution of the linear system eqn.(2.3). It should be noted that the order of the system 2.3 is equal to the number of nodes in the mesh, which will be of the order of many thousands or millions.

Direct methods for solving linear systems such as Gaussian elimination or use of determinants have two disadvantages in the present case. Firstly, they require that the matrix  $A$  be stored. This is clearly unnecessary since the elements of  $A$  can be generated using eqn.(2.2). Secondly, they require about  $N^3/3$  multiplications to solve a system of order  $N$ . To solve a system with  $N = 10^6$  would take  $10^{12}$  sec (many years) allowing 3  $\mu$ sec per multiplication. Such a system can be solved in about 2 hours using the iterative method described below.

Iterative methods offer two advantages over direct methods in this case. Firstly, they require only the current solution vector  $x$  to be stored and secondly, they are much more efficient for solving large systems when the coefficient matrix ( $A$ ) contains many zero elements.

Many iterative methods for solving systems such as 2.3 have been developed and studied theoretically. An excellent review of the methods available is given by Forsythe and Wasow.<sup>12</sup>

The method used here is based on a program developed by D. Nelson.<sup>13,14</sup> Basically this program uses successive over-relaxation by points to solve the linear system.\* This method is applied in a manner which allows extremely large problems to be solved using a modest amount of computer memory. The theory of successive over-relaxation by points is reviewed in Appendix A. The important results are as follows:

We start with an initial approximation (usually zero) to the potential at each node  $\phi_{ijk}^0$ ; then we obtain successive approximations using

$$\phi_{ijk}^{n+1} = \phi_{ijk}^n + \frac{\alpha}{6} \left( \phi_{i-1jk}^{n+1} + \phi_{i+1jk}^n + \phi_{ij-1k}^{n+1} + \phi_{ij+1k}^n + \phi_{ijk-1}^{n+1} + \phi_{ijk+1}^n - 6\phi_{ijk}^n \right) \quad (2.4)$$

where the best value of the "over-relaxation factor"  $\alpha$  for the ordinary successive over-relaxation method is given by

$$\alpha_b = \frac{2}{1 + \sin\theta} \approx 2 \left( 1 - \pi \sqrt{\frac{1}{3} \left( \frac{1}{p^2} + \frac{1}{q^2} + \frac{1}{r^2} \right)} \right) \quad (2.5)$$

where

$$\cos\theta = \frac{1}{3} \left( \cos\frac{\pi}{p} + \cos\frac{\pi}{q} + \cos\frac{\pi}{r} \right) \approx 1 - \frac{\pi^2}{6} \left( \frac{1}{p^2} + \frac{1}{q^2} + \frac{1}{r^2} \right). \quad (2.6)$$

So solving the system consists of iterating over the nodes of the mesh in some order, replacing the value of  $\phi$  of each node by the values given by eqn.(2.4). The order we shall choose is, giving the  $ijk$  values of the point to be iterated,

---

\* For this problem it appears that the Peaceman-Rachford method<sup>15</sup> gives faster convergence.<sup>16</sup> However, as has been pointed out by Young,<sup>16</sup> it is difficult to devise an efficient storage scheme which allows the matrix  $A$  to be accessed alternately by rows and columns. Any increase in convergence rate would probably be negated by increased time spent retrieving the data from the mass storage device.

$$\begin{array}{ccccccc}
 (0,0,0), & (1,0,0) & \dots & (p,0,0) & (0,1,0) & \dots & (p,1,0) & \dots & \dots & (p,q,0) \\
 (0,0,1) & \dots & \dots & & & & & & & \dots & (p,q,1) \\
 \vdots & & & & & & & & & & \vdots \\
 (0,0,r) & \dots & \dots & & & & & & & & (p,q,r)
 \end{array}$$

or the reverse order.

It is shown in Appendix A that the convergence of the method is determined by the largest eigenvalue of the matrix A. If the best value of  $\alpha$ , i.e.  $\alpha_b$ , is used, this eigenvalue is

$$\lambda_m = \frac{1-\sin\theta}{1+\sin\theta} \approx 1 - 2\pi \sqrt{\frac{1}{3} \left( \frac{1}{p^2} + \frac{1}{q^2} + \frac{1}{r^2} \right)} = \alpha_b - 1. \quad (2.7)$$

Values of  $\lambda_m$  and  $\alpha_b$  for the problems which are discussed in this chapter are given in Table I.

The number of iterations required to reduce the error by a factor f is approximately

$$n = \log f / \log \lambda_m. \quad (2.8)$$

### C. Computational Details

The program as described by Nelson<sup>14</sup> used an iteration subroutine coded in FORTRAN. This was rewritten in assembler language giving a factor of twelve increase in speed. In addition, the new iteration routine allows the iteration to be done in alternating directions. Details of these changes are given in Appendix C.

The advantage in iterating in alternating directions is that it ensures that the effect of the boundary conditions is quickly propagated through the volume. If, for example, uni-directional iteration was used going from small ijk to large ijk, and all boundaries were zero except the plane with the largest k value, many iterations would be required before

TABLE I

Largest eigenvalue ( $\lambda_m$ ) and best over-relaxation factor ( $\alpha_b$ ) for various size relaxation problems

Problem size	Total number of mesh points	$\lambda_m$	$\alpha_b$
32 x 32 x 16	16,384	0.7569	1.7569
64 x 64 x 32	131,072	0.8841	1.8841
128 x 32 x 8	32,768	0.6245	1.6245
256 x 64 x 16	262,144	0.7946	1.7946
512 x 128 x 32	2,097,152	0.8895	1.8895

the effect of the boundary at large  $k$  would be felt at small  $k$ . Alternating the direction of iteration avoids this difficulty.

The values of the  $\phi_{ijk}$ 's are stored on a mass storage device (tape, disc or drum). Subsets of this total "volume" are transferred to core storage, iterated over and returned to the mass storage device. To increase efficiency (by decreasing the number of data swaps) several iterations are done over each subset of the total volume while it is in core storage. This causes the convergence rate to be very slow; however, the program has a novel feature, described below, which allows good starting values to be found, hence reducing the number of iterations required. The iterations over the subsets of the total volume must be done carefully, to avoid discontinuities where the edges of these subsets occur. Consider the volume shown in Fig. 2.1 broken into blocks, each block containing  $16 \times 16 \times 8$  points; then there are  $b_1 = (p+1)/16$  blocks along the  $x$  co-ordinate,  $b_2 = (q+1)/16$  blocks along the  $y$  co-ordinate and  $b_3 = (r+1)/8$  blocks along the  $z$  co-ordinate. The data area in core storage in which the iterations are done (the physical work area) contains a  $2 \times 2 \times 2$  block subset of the total problem. The iteration is done as follows:

The physical work area is loaded starting at block co-ordinates  $(1,1,1)$  and then iterated. During this iteration all potentials on the boundaries of the physical work area are held fixed except boundaries which are symmetry planes of the total volume. The next load origin is  $(2,1,1)$ , and this iteration is repeated. Since two blocks along each co-ordinate are iterated each time while the increment between iterations is one block, discontinuities in the data should be reduced. The sequence of load points for the iteration is either

$$\begin{array}{l}
(1,1,1), (2,1,1) \dots (b_1,1,1),(1,2,1),(2,1,1) \dots (b_1,b_2,1) \\
(1,1,2), (2,1,2) \dots (b_1,1,2),(1,2,2),(2,1,2) \dots (b_1,b_2,2) \\
\vdots \\
(1,1,b_3) (2,1,b_3) \dots (b_1,1,b_3),(1,2,b_3),(2,1,b_3) \dots (b_1,b_2,b_3)
\end{array}$$

or the reverse one (alternating direction iteration over the blocks).

It should be noted that in one sweep over the data using this procedure  $8(b_1-1)(b_2-1)(b_3-1)$  blocks are iterated. On the average, this is

$$\frac{8(b_1-1)(b_2-1)(b_3-1)}{b_1 b_2 b_3} \quad (2.9)$$

iterations over each block.

The novel feature mentioned above which allows good starting values to be found operates as follows. After the boundary values have been assigned but before any iterations have been done, the mesh size is doubled reducing the problem to one with an eighth as many data points as the original problem. This process is repeated until the problem size is close to the size of the physical work area (32 x 32 x 16 points). This "reduced" problem is solved iteratively and expanded back to the original size problem. During the expansion process, the value assigned to each unknown point is the value for the nearest known node with smaller or equal  $i$ ,  $j$  and  $k$  values, i.e. if  $\phi_{ijk}$  is known, the program sets (omitting subscripts which are  $i$ ,  $j$  or  $k$ )

$$\phi_{i+1} = \phi_{j+1} = \phi_{i+1j+1} = \phi_{k+1} = \phi_{i+1k+1} = \phi_{j+1k+1} = \phi_{i+1j+1k+1} = \phi.$$

This procedure provides good starting values for the final iteration.

The boundary values are assigned either by calling a user-supplied subroutine which returns the value of the potential at each point, or by

the method given in Appendix B or by a combination of both.

In many situations, the boundary values at an edge of the problem are not known, but this edge is a plane of symmetry. In this case, the program calculates the potentials on the symmetry plane using the fact that the potentials outside it are the same as those inside. For example, if the  $i = 0$  plane were a plane of symmetry, then on this plane eqn.(2.4) would be

$$\phi_{0jk}^{n+1} = \phi_{0jk}^n + \frac{\alpha}{6} \left( \phi_{1jk}^{n+1} + \phi_{1jk}^n + \phi_{0j-1k}^{n+1} + \phi_{0j+1k}^n + \phi_{0jk-1}^{n+1} + \phi_{0jk+1}^n - 6\phi_{0jk}^n \right).$$

When estimating the convergence rate for a problem which contains planes of symmetry, it is important to remember that the errors are not zero at the plane of symmetry (as they would be if the plane were a boundary plane). Thus the errors and convergence rates will be those appropriate for the "effective size" of the problem, which is the size the problem would be if the symmetry properties were not utilized. Thus, if a problem contains one plane of symmetry, the effective size is twice the actual size, in general; if there are  $n$  symmetry planes, the effective size is  $2^n$  times the actual size.

#### D. Convergence Tests

To test the convergence and accuracy of the method, a problem for which the analytic solution was known was solved using the relaxation method. The problem is the one used by D. Nelson<sup>13</sup> as a test case; it consists of a  $64 \times 64 \times 32$  point "box" with boundary values of zero on all sides except the  $k = 32$  surface where the potential is

$$V = \sin\left(\frac{2\pi i}{64}\right) \sin\left(\frac{2\pi j}{64}\right).$$

The sequence of operations carried out in solving this problem is given in Table II.

The first question which must be answered is how many iterations are required on the reduced problem. To answer this, several runs were done. For each run  $n$  sweeps were done with  $\alpha = 1.5$ ,  $n$  with  $\alpha = 1.3$  and  $n$  with  $\alpha = 1.0$  (a total of  $3n$  sweeps). The value of  $\alpha$  used was reduced from 1.5 (close to the best value) to 1.0 to ensure that the difference equations are solved as exactly as possible when the iterations are finished. The problem was then expanded to full size, and two iterations were done on the full volume. All iterations were done with alternating directions. The results are summarized in Table III. In all cases the error is very small. Since iterating over the small volume is relatively fast, there is no large penalty paid for over-estimating the number of iterations required, and  $n = 100$  was chosen. For this case ( $n = 100$ ), the average change per iteration before expanding was  $< 10^{-6}$ , i.e. the reduced problem had been solved exactly to the precision of the arithmetic used. Thus the error of 0.25% after expanding is due to the expansion process.

Now the problem was expanded back to full size  $64 \times 64 \times 32$  points, and the convergence of this problem was investigated. Since we are doing the iterations over subsets of the problem each containing  $32 \times 32 \times 16$  points, the best value of  $\alpha$  is, from eqn.(2.5),  $\alpha_b = 1.75$ . Two other values of  $\alpha$  were used, 1.87 because this is  $\alpha_b$  for a problem containing  $64 \times 64 \times 32$  points and 1.50 for reasons discussed below. Fig. 2.2 shows the average error as a function of the number of iterations for these values of  $\alpha$ . The discrepancy in the error after two iterations over the

TABLE II

Sequence of operations used to solve a  $64 \times 64 \times 32$  node relaxation problem

Step	Operation	Problem size after this step	Number of iterations	Average change per iteration after this step
1	set boundary conditions	$64 \times 64 \times 32$	-	-
2	reduce to coarse grid	$32 \times 32 \times 16$	-	-
3	iterate ( $\alpha = 1.5$ )	$32 \times 32 \times 16$	100	$0.9 \times 10^{-3}$
4	iterate ( $\alpha = 1.3$ )	$32 \times 32 \times 16$	100	$0.6 \times 10^{-5}$
5	iterate ( $\alpha = 1.0$ )	$32 \times 32 \times 16$	100	$0.5 \times 10^{-6}$
6	expand to fine grid	$64 \times 64 \times 32$	-	?
7	iterate ( $\alpha = 1.5$ )	$64 \times 64 \times 32$	see Fig. 2.3	see Fig. 2.3

TABLE III

Average error after various numbers of iterations over the reduced problem

Case	n	Average error (%)
1	25	0.40
2	50	0.30
3	75	0.31
4	100	0.25
5	200	0.28

fine grid between Table II and Fig. 2.2 is due to different iteration directions where iterating over the fine grid. As expected,  $\alpha = 1.75$  produces the fastest convergence, but the convergence is satisfactory in all three cases. Eqn. (A.23) predicts that the number of iterations required to reduce the error by a factor  $f$  is  $n = \frac{\log f}{\log \lambda}$ . The value of  $\lambda_m$  appropriate to  $\alpha = 1.75$  is 0.75; hence the number of iterations required to reduce the error by a factor of 10 is  $\frac{-1}{\log_{10}(0.75)} = 8.0$ . As can be seen from Fig. 2.2, about 40 sweeps over the data are required to achieve the same reduction ( $\alpha = 1.75$ ). Since the problem contains  $4 \times 4 \times 4$  blocks of data, by eqn. (2.9), each sweep corresponds to

$$\frac{8(4-1)(4-1)(4-1)}{(4)(4)(4)} = 3.375.$$

iterations. Hence the 40 sweeps correspond to 135 iterations, indicating that the convergence is about sixteen times slower than the theoretically expected rate for ordinary successive over-relaxation. This slow convergence rate is probably due to the way in which the iterations are done, i.e. many iterations over a small subset of the total volume. However, with the good starting values provided by the reducing and expanding procedure, the convergence of the problem is acceptable.

For practical problems it has been found by the author and by D. Nelson<sup>13</sup> that  $\alpha = 1.5$  gives the best results. This is probably due to the fact that, in practical cases, fixed points occur within the volume. This means that the "wavelength" of the errors will be smaller than that assumed in eqn.(A.8), leading to smaller values of  $\alpha_b$ . Since  $\alpha = 1.5$  seemed to be best for "real" problems and since  $\alpha = 1.5$  still gives acceptable convergence for the test problem, only this value was studied further.

Fig. 2.3 shows the average error and the average change per iteration for the  $\alpha = 1.5$  case. The bars on the points giving the average error indicate the error at which the number of points vs error curve (Fig. 2.4) has fallen to half its peak value. As we would expect, since we are using  $\alpha > 1$ , the change per iteration is always larger than the error. Of course, there may be a few large local errors which do not produce a large average error.

Fig. 2.4 shows the distribution of errors for various numbers of iterations. The graph is actually a histogram; the vertical lines give the (approximately equal) intervals in which the numbers of points are counted. Several points are worth noting. Even after many iterations, about 0.04% of the points have errors larger than 5.0%, despite the average error being less than 0.04%. It appears that this situation will not change significantly even if many more iterations are done. It seems that the large errors must be removed before the smaller ones are affected. This is shown more clearly in Fig. 2.5 where the number of points with a given error is plotted as a function of the number of errors. It can be seen that the number of points with small errors remains relatively constant until the number of large errors has been reduced.

#### E. The Practical Problem

Problems which are useful in practice usually contain many more points than the case discussed in Section D. The same reducing and expanding procedure is followed, so that the starting values for the iterations on the large problem are quite good. However, since the number of points is larger, the convergence will be slower (as predicted by eqn.(A.22)) and each iteration will take longer.

The practical case discussed here is a 128 in. by 32 in. by 8 in. section from the centre of the TRIUMF cyclotron. The 8 in. dimension is in the axial direction and extends from the cyclotron median plane to the vacuum tank. The 128 in. dimension is along the dee gap, and the 32 in. dimension is perpendicular to the dee gap. The geometry in the median plane and the electric equipotentials calculated using this method are shown in Fig. 1.1. The geometry in the axial direction is shown in Fig. 1.2. It was felt that a 0.25 in. grid size adequately defined the boundaries; hence the problem contained  $512 \times 128 \times 32 = 2,097,152$  data points.

The sequence of operations used in solving this problem is given in Table IV. At the end of step 6, the change per iteration at each point is less than  $10^{-7}$ , so after expansion to  $256 \times 64 \times 16$  points, we would expect the average error to be about 0.40% as it was in the test case. The errors are of course unknown, but the average change per iteration at the beginning of step 8 was about 0.1%. The reason for this value being smaller than the value for the test case is probably that there are more fixed points in the real case. After 75 iterations over the  $256 \times 64 \times 16$  problem, the average change per iteration is less than  $10^{-6}$ . The iterations on the full-size problem (step 12) are very costly since we now have over two million data points; however, very few iterations are required. Step 12 consisted of four iterations over the full volume to smooth out any bumps left by the expanding process. The average change per iteration at the end of step 12 was less than 0.01%. Local errors will be larger than this, of course. In the test problem the largest errors were more than 100 times as large as the average error but only for 0.04% of the points; hence in this case we can expect local errors of the order of 1 or 2% at a very small number of points. However, the convergence of the

TABLE IV

Sequence of operations used to solve a  
512x128x32 node relaxation problem

Step	Operation	Problem size after this step	Number of iterations	Average change per iteration after this step
1	set boundary conditions	512 x 128 x 32	-	-
2	reduce to coarse grid	256 x 64 x 16	-	-
3	reduce to coarser grid	128 x 32 x 8	-	-
4	iterate ( $\alpha = 1.5$ )	128 x 32 x 8	100	$0.3 \times 10^{-3}$
5	iterate ( $\alpha = 1.3$ )	128 x 32 x 8	100	$<10^{-7}$
6	iterate ( $\alpha = 1.0$ )	128 x 32 x 8	100	$<10^{-7}$
7	expand	256 x 64 x 16	-	?
8	iterate ( $\alpha = 1.5$ )	256 x 64 x 16	25	$0.2 \times 10^{-4}$
9	iterate ( $\alpha = 1.3$ )	256 x 64 x 16	25	$0.2 \times 10^{-6}$
10	iterate ( $\alpha = 1.0$ )	256 x 64 x 16	25	$0.1 \times 10^{-6}$
11	expand to full size	512 x 128 x 32	-	?
12	iterate ( $\alpha = 1.5$ )	512 x 128 x 32	4	$<10^{-4}$

problem is very satisfactory. As can be seen in Fig. 1.1, the equipotentials have no unexpected kinks and fit the boundary conditions extremely well.

## Chapter 3. - AXIAL MOTIONS

### A. Introduction

The axial motions of ions within a cyclotron are influenced by three effects; magnetic forces due to slope, flutter and spiral of the magnetic field, electric forces due to the lens effect of the dee gap and space charge forces due to the electric field produced by the beam. The magnetic force is small and focusing at the centre of the machine. The electric force is very strong and phase dependent (focusing for some phases and defocusing for others). The space charge force is weak and always defocusing. It will be shown that the axial motions during the first few turns are controlled almost entirely by the electric forces.

Since one of the main design objectives of TRIUMF is to accelerate ions over a wide interval of the RF waveform (i.e. ions with large differences in their initial RF phase) careful design is required to prevent loss of those ions which start at unfavourable phases. The improvements which can be achieved by "squaring" the radio-frequency waveform (by adding a small fraction of 3rd harmonic to the fundamental) will be demonstrated.

Obviously, the axial displacement of the beam must not exceed the aperture of the dees but a more stringent limit on the amplitude of the axial oscillation is set by the fact that passage of the beam through regions where the forces are not linear causes distortion of the beam emittance. This causes a decrease in the "effective density" of the beam within the elliptical contour enclosing the beam's phase space. Recent work by Han<sup>17</sup> indicates that about 60% of the dee aperture is linear to within 5%.\* The axial motions must be adjusted so that as wide a range

---

\* C. Han integrated the equations of motion numerically through fields for three gap geometries. For a gap height of 1.6" and gap widths of 3.0", 6.5", and 7.4", the deviations from linearity were less than 5% over 60% of the gap height.

of phases as possible is transmitted. In addition, the beam must be matched to the magnetic field so that the amplitude of the axial oscillations is minimized.

### B. Magnetic Field

The axial restoring force ( $F_z$ ) exerted on an ion by the magnetic field can be expressed in terms of the axial oscillation frequency ( $\nu_z$ )<sub>m</sub> which an ion would have in the absence of other forces in the axial direction. The oscillation frequency is related to the force by

$$F_z = -m \omega_0^2 \left( \nu_z \right)_m^2 z,$$

where  $\omega_0$  is the ion rotation frequency. This is a linear approximation valid only for  $z \ll g$ , the magnet pole gap height. In a sector-focused cyclotron the oscillation frequency is given<sup>18</sup> approximately by

$$\left( \nu_z \right)_m^2 = -\mu' + F^2(1 + 2 \tan^2 \epsilon). \quad (3.1)$$

$-\mu' = \frac{r}{B} \frac{dB}{dr}$  describes the radial variation in the magnetic field. The azimuthal variation of the magnetic field is described by the flutter function  $F^2$  where

$$F^2 = \langle (B - \bar{B})^2 \rangle / \bar{B}^2.$$

$\bar{B}$  is the mean field at a given radius and the angular brackets denote a mean at one radius. Near the centre of the cyclotron the magnetic field is given to a good approximation by  $B = \bar{B} \left[ 1 + f \cos 6(\theta - \theta_m) \right]$  where  $f$  is the amplitude of the sixth harmonic component ( $= B_6 / \bar{B}$ ) and  $\theta_m$  is the azimuth angle of the peak field. If the azimuthal variation of the field is related to one harmonic only, the flutter function  $F^2$  is related to the amplitude of the harmonic  $f$  by  $F^2 = \frac{1}{2} f^2$ . The angle  $\epsilon$  is

the so-called "spiral angle" defined by  $\tan \epsilon = r d\theta_m / dr$ . For an isochronous field,  $\mu'$  is positive and, near the centre of the cyclotron, the spiral angle  $\epsilon$  is zero, hence the focusing provided by the magnetic field is due only to the "flutter" in the field. If the net effect of the magnetic field is to be focusing, the term due to the flutter must be larger than the defocusing term due to the field slope. Unfortunately, it is difficult to obtain large flutter in the central region of a cyclotron magnet because the vertical magnet gap is much larger than the horizontal distance between pole pieces. A typical plot of  $\left(\frac{v_z^2}{Z}\right)_m$  as a function of radius is shown in Fig. 3.1. We plot  $\left(\frac{v_z^2}{Z}\right)_m$  rather than  $\left(\frac{v_z}{Z}\right)_m$  since  $\left(\frac{v_z^2}{Z}\right)_m$  is proportional to the force exerted on the ion. Some cyclotrons use a magnetic "cone" in the central region to increase focusing. This consists of a central "bump" on the isochronous value of the field. This means that  $\mu'$  is negative, hence the magnetic focusing is increased. In addition, phase slip is introduced due to the fact that the field is not isochronous. The ions must be started at positive (late) phases so that they have slipped into phase by the time they have reached the isochronous field region. The positive phase histories are advantageous from the point of view of electric focusing.

In the absence of "squaring" of the RF, it will be shown that the phase acceptance has a sharp cutoff at -5 deg, i.e., only phases more positive than this can be accepted. A small field bump could be used to shift these positive phases into isochronism so that the range of phases which is accelerated is centred about 0 deg. It is shown in Section H of this chapter that this field bump does not contribute appreciably to the focusing.

A field bump will not be required when addition of third harmonic to the RF shifts the lower limit of the phase acceptance from -5 deg to -25 deg. Field bumps are undesirable for three reasons.

Firstly, the ions start off phase and since the error in centring depends on the cosine of the largest phase angle, the centring errors are increased.

Secondly, since the ions start off phase the energy gain is reduced. Because of the relatively high injection energy, this makes the clearance between the centre post and the beam small on the first turn.

Thirdly, the field bump will cause the beam to pass through the  $\nu_r = 1$  resonance (when  $\mu' \approx 0$ ) possibly leading to an increase in the radial oscillation amplitude.

Another way to increase the focusing is to increase the flutter. This may be achieved by cutting three of the pole pieces at a radius of 30 in., giving a three-sector geometry in the central region. This produced a  $\nu_z$  of about 0.2 from  $r = 10$  in. outwards; however, the large flutter with three-fold symmetry caused undesirable effects in the radial behaviour of the beam (see Chapter 4) and had to be abandoned.

Tests have also shown that a set of "floating" pole pieces 1.66 in. above and below the median plane between 12.5 in. and 30.0 in. radius, with six-fold symmetry, can also provide  $\left(\nu_z\right)_m \approx 0.2$  in the central region. However, it is virtually impossible to mount pole pieces in such a position without disturbing the alignment of the resonator hot arms.

At this time it seems that the best magnetic focusing that can be achieved is that shown by the solid curve in Fig. 3.1.

### C. Space Charge Forces

The ions in the beam produce an electric field which exerts a force on each ion in the beam. This is the space charge effect. This effect can be analyzed by considering the force on an ion on the surface of a bunch

due to the other ions in the bunch and the force due to the ions in other bunches. Reiser<sup>19</sup> has analyzed this problem; we find for the case of TRIUMF (400 kV voltage gain per turn and low magnetic field) that at low energy, more than 90% of the space charge force on an ion is due to the field produced by the other ions in the bunch. This force is directed radially outward from the centre of the bunch and can be written<sup>19</sup>

$$F = \frac{q I G}{4\epsilon_0 \Delta\phi v z_m}$$

where  $z_m$  and  $\Delta\phi$  are the maximum height and the length of the bunch in degrees of RF, respectively,  $v$  is the velocity of the ions,  $I$  is the average current,  $q$  is the charge on the ion,  $\epsilon_0$  is the permittivity of free space, and  $G$  is a factor which depends on the height-to-width ratio of the beam bunch.

The vertical oscillation frequency produced by this force is

$$\left(\frac{v^2}{z}\right)_{sc} = -\frac{q}{4\epsilon_0 m\omega^2} \frac{G}{z_m^2} \frac{I}{\Delta\phi} \frac{1}{v}. \quad (3.2)$$

In the case of TRIUMF, the source will produce about 2 mA, hence without bunching we can expect  $I/\Delta\phi = 5 \mu\text{A}/\text{deg}$ . Since the axial focusing is four or five times weaker than the radial focusing, we can expect beam width-to-height ratios of the order of 0.5. For this value, the geometrical factor  $G$  is 4.8. Fig. 3.2 shows how  $\left(\frac{v^2}{z}\right)_{sc}$  varies with energy for various values of  $I/\Delta\phi$  and  $z_m$ .

A graph showing the variation of  $G$  with the gap and height of the dee can be found in the paper by Reiser.<sup>19</sup>

This force is roughly the same order of magnitude as the magnetic force and can be accounted for by using an "effective" magnetic  $v_z^2$  which

is the difference between the actual magnetic  $v_z$  and the space charge  $v_z$  for the beam intensity under consideration.

#### D. Electric Lens Effects

The importance of electric focusing effects in cyclotrons was recognized soon after the invention of the cyclotron. Rose<sup>1</sup> developed approximate expressions for the lens effects of cyclotron dee gaps using the symmetry properties of the electric fields and a description of the field derived by Kottler.<sup>20</sup> These studies indicated that the lens properties arose from two effects. As can be seen in Fig. 3.3, the first part of the gap is focusing, while the second part is defocusing. These would cancel exactly, except that

- (i) the field is changing, and
- (ii) the ion is accelerated.

The deflection due to the field variation arises because the ion sees a different electric field in the second half of the gap than in the first. Since the first half of the gap is focusing and the second half is defocusing, there is a differential focusing effect. The change in  $z' = dz/dx$  due to this "field variation" effect is, to first order in  $qV_0/E_c$

$$(\Delta z')_{fV} = -\frac{qV_0}{E_c} \frac{1}{r} z \sin \phi_c \quad (3.3)$$

where  $V_0$  is the dee voltage and  $E_c$ ,  $r$  and  $\phi_c$  are the energy, radius and RF phase of the ion at the gap centre. This effect is linear in  $z$  and is focusing when the field is falling (positive phases) but defocusing when the field is rising (negative phases).

The second effect is due to the ion spending less time in the second half of the gap, hence the defocusing force in the second half of the gap

produces less deflection than an equal force would in the first half. This effect is always focusing and is given by

$$(\Delta z')_{ec} = -g \left( \frac{qV_0}{E_c} \right)^2 z \cos^2 \phi \quad (3.4)$$

where  $g$  is a numerical factor depending on the geometry.

There is also a collimation term due to the fact that the forward momentum  $p_x$  increases while the transverse momentum  $p_z$  remains constant; however, this term disappears when the change in  $p_z$  rather than  $z'$  is considered.

In addition, Rose predicts a change in axial position

$$\Delta z = \left( 1 - \frac{qV_0 \cos \phi}{E_c} \right) z_0. \quad (3.5)$$

Rose's analysis was extended by Cohen<sup>3</sup> who used an electric field developed by Murray and Ratner.<sup>21</sup> This more detailed analysis showed that the expressions developed by Rose are the first two terms in a series in  $\sqrt{1/E_c}$ . More recently, the analysis has been further extended by Reiser.<sup>22</sup> This most recent analysis includes the effect of the dee liner, i.e.,  $c$  is not  $\infty$  (see Fig. 3.3) as was assumed in the previous analyses. Reiser's expression for the deflection is

$$\Delta z' = -z_0 \left[ \frac{N(qV_0)}{r(E_c)} \sin \phi_c + \frac{2F(a,b,c)}{\pi b} \left( \frac{qV_0}{E_c} \right)^2 \cos^2 \phi_c \right] - \frac{qV_0}{E_c} \cos \phi_c z'_0 \quad (3.6)$$

where  $z_0$  is the axial displacement of the ion when it enters the lens,  $N$  is the harmonic ratio of the RF frequency to the ion frequency and  $F(a,b,c)$  is a dimensionless function which depends on the geometry ( $a$ ,  $b$  and  $c$  are described by Fig. 3.3).

The linearity in  $z$  of the above expressions for the deflection and displacement permits an enormous simplification in the axial motion calculations. However, this formula is based on the assumptions that the transit time of the particle across the gap is small and that the energy gain across the gap is much smaller than the incident ion energy. Since the electric forces become strong just where these approximations are likely to become invalid (i.e. at low energy), it is important to investigate the validity of this formula. For the case of TRIUMF, the RF operates at the fifth harmonic of the ion frequency ( $N=5$ ) and the transit times are of the order of 60 to 70 deg of RF on the first turn so the small transit time approximation is not valid; however, the relatively high injection energy (300 keV) means that the approximation that the energy gain is small compared to the incident energy is reasonably valid after a few accelerations. Recently, Han<sup>23</sup> has published a compilation of the focusing effects of cyclotron like gaps for geometries applicable to TRIUMF. These results were obtained by numerically integrating the equations of motion through electric fields calculated using the relaxation method described in Chapter 2. The data given in Han's Tables 6-1 to 6-7 provide a relevant source of numerical results to compare with the theory. To allow comparison of the electric forces to the magnetic and space charge forces, we can approximate the focusing effects at the dee gaps by an equivalent  $\left[ \frac{v_z^2}{z} \right]_e$  which would give the same deflection over a half-turn.

If  $\Delta z' \ll z_0/\pi r$

$$\frac{v_z^2}{z} = -\frac{F_z}{m\omega^2} = -\frac{d^2z}{\omega^2 dt^2} = -\frac{d^2z}{d\theta^2} = -\frac{1}{\pi} \Delta \left( \frac{dz}{d\theta} \right) = -\frac{r}{\pi} \Delta z'$$

For the numerical results given by Han<sup>23</sup>

$$\left(\frac{v_z}{c}\right)_e = \frac{r}{\pi} \left(\frac{1}{F_2}\right)$$

where  $F_2$  is the forward focal power of the lens.

Fig. 3.4 compares values of  $\left(\frac{v_z}{c}\right)_e$  obtained by exact numerical integration with those obtained from eqn.(3.6) for various phases and energies. The agreement is better for negative phases than for positive ones. In all cases the analytic description given by eqn.(3.6) overestimates the strength of the electric forces. It should be noted that for TRIUMF the injection energy is 300 keV, and the ion energy after the first main gap crossing is about 600 keV, so the approximation is valid to within 15% in the first turn. Hence we can use the expressions given in eqns.(3.5) and (3.6) and obtain a reasonable estimate of the axial motions.

It should be noted that the electric forces are much larger than the magnetic and space charge forces. In addition, the electric forces are defocusing for, roughly speaking, negative phases. This causes a sharp cutoff in the phase acceptance near 0 deg. This cutoff can be shifted to more negative phases by providing additional (for example, magnetic) focusing. To shift this cutoff to -30 deg at 500 keV, magnetic focusing equivalent to a  $\left(\frac{v_z}{c}\right)_m^2$  of (0.3) would be required to overcome the defocusing effects of the electric field.

This sharp cutoff for negative phases is due to the field variation effect. The deflection due to field variation is proportional to  $\sin\phi$ , hence rapidly becomes large for negative phases. The focusing due to the energy change is proportional to  $\cos^2\phi$  and is multiplied by a smaller coefficient than the field variation term. The relative magnitude of these two effects is shown in Fig. 3.4. The maximum contribution to

$(v_z)^2$  from the energy change term is given by the curve for  $\phi = 0$ . Hence the net effect of the electric field closely follows the field variation effect and is defocusing for negative phases.

### E. Calculation of Cyclotron Acceptance

Since the linear description of the electric lens effect is reasonably accurate, and the magnetic and space charge focusing can be described in a linear manner, we can track the axial motions of the ions using the matrix method for tracking beams as suggested by Penner.<sup>24</sup>

If the axial focusing frequency due to the combined effects of the magnetic field and space charge is  $\nu_z$ , then in a region where  $\nu_z$  is constant, the axial motion will be given by

$$z(s) = z_0 \cos \nu_z \theta + \frac{r z_0'}{\nu_z} \sin \nu_z \theta \quad (3.7)$$

$$z'(s) = -\frac{\nu_z z_0'}{r} \sin \nu_z \theta + z_0' \cos \nu_z \theta$$

where  $z_0$  and  $z_0'$  are the initial (axial) displacement and slope, respectively,  $\theta = s/r$  is the azimuthal angle subtended by the ion,  $s$  is the path length, and  $r$  is the radius of curvature of the ion.

We are dealing with low energies so we can use a non-relativistic energy-momentum relationship

$$z' = \frac{p_z}{k\sqrt{E}} \quad (3.8)$$

where  $p_z$  is the axial momentum,  $E$  is the kinetic energy and  $k = \sqrt{2m_0}$ .

It is convenient to measure momenta as  $\beta\gamma r_\infty$  where  $\beta$  and  $\gamma$  are the usual relativistic factors and  $r_\infty$  is the "cyclotron radius" ( $= m_0 c / qB_C$ ). This momentum is numerically equal to the radius of curvature the ion would have in the central magnetic field ( $B_C$ ). For the TRIUMF centre region

$$B_c = 3.0 \text{ kG}, \beta\gamma r_\infty (\text{in.}) = 18.94 \sqrt{E (\text{MeV})}.$$

Using eqn.(3.8), we can write the magnetic transfer matrix

$$\begin{pmatrix} z \\ \frac{pz}{k} \end{pmatrix} = \begin{pmatrix} \cos v_z \theta & \frac{r}{v_z \sqrt{E}} \sin v_z \theta \\ -\frac{v_z \sqrt{E}}{r} \sin v_z \theta & \cos v_z \theta \end{pmatrix} \begin{pmatrix} z_0 \\ \left(\frac{pz}{k}\right)_0 \end{pmatrix} \equiv T_m \begin{pmatrix} z_0 \\ \left(\frac{pz}{k}\right)_0 \end{pmatrix}. \quad (3.9)$$

The expressions given in eqns.(3.5) and (3.6) can also be written in this form. If we call the transfer matrix for the dee gap

$$T_e \equiv \begin{pmatrix} a & b \\ c & d \end{pmatrix}$$

then

$$a = 1 - \frac{qV_0}{E_c} \cos \phi \quad (3.10)$$

$$c = -\sqrt{E_f} \left[ \frac{N}{r} \left( \frac{qV_0}{E_c} \right) \sin \phi + \frac{2F(a,b,c)}{\pi b} \left( \frac{qV_0}{E_c} \right)^2 \cos^2 \phi \right] \quad (3.11)$$

where  $E_c$  and  $E_f$  are the ion energies at the centre and end of the dee gap, respectively.

The expressions derived by Rose and Cohen do not include any dependence of the final position on the initial divergence, i.e.  $b$  is assumed to be zero. The numerical results given by Han indicate  $d \approx 1$ , and since Liouville's Theorem required  $ad - cb = 1$ , we choose

$$d = 1 \quad (3.12)$$

$$b = \frac{1}{c}(ad - 1). \quad (3.13)$$

The fact that  $b$  is non-zero means that there is a displacement term which depends on the initial slope ( $z_1'$ ). The existence of this term is confirmed in the numerical results given by Han; however, it is a small effect.

Now that the transfer matrices for the various parts of the trajectory are known, the complete trajectory can be calculated by the usual matrix multiplication method

$$\begin{pmatrix} z_2 \\ \frac{p_{z_2}}{k} \end{pmatrix} = T_1 \begin{pmatrix} z_1 \\ \frac{p_{z_1}}{k} \end{pmatrix}$$

$$\begin{pmatrix} z_3 \\ \frac{p_{z_3}}{k} \end{pmatrix} = T_2 \begin{pmatrix} z_2 \\ \frac{p_{z_2}}{k} \end{pmatrix}$$

$$\begin{pmatrix} z_3 \\ \frac{p_{z_3}}{k} \end{pmatrix} = T_2 T_1 \begin{pmatrix} z_1 \\ \frac{p_{z_1}}{k} \end{pmatrix} .$$

A method for analyzing optic systems, much more powerful than trajectory tracking, has been developed by Steffen.<sup>25</sup> This method allows the tracking of elliptical beam phase space areas through the system. It is usual to consider elliptical emittances, since ellipses can be specified by only three parameters, and make a good approximation to the actual phase space shape, which would presumably be polygonal.<sup>26</sup> We will use Steffen's notation to describe the phase space ellipses. If the ellipse is described by the equation

$$\gamma z^2 + 2 \alpha z \frac{p_z}{k} + \beta \left( \frac{p_z}{k} \right)^2 = \epsilon$$

then, as derived by Steffen, the maximum displacement and momentum are

$$z_{\max} = \sqrt{\epsilon \beta}$$

$$\frac{p_z \max}{k} = \sqrt{\epsilon \gamma} .$$

If we define the transfer matrix which transforms the vector

$$\begin{pmatrix} z \\ \frac{p_z}{k} \end{pmatrix}$$

by

$$\begin{pmatrix} z_2 \\ \frac{p_{z_2}}{k} \end{pmatrix} \equiv \begin{pmatrix} c & s \\ c' & s' \end{pmatrix} \begin{pmatrix} z_1 \\ \frac{p_{z_1}}{k} \end{pmatrix}$$

then Steffen shows that the ellipse parameters are transformed according to

$$\begin{pmatrix} \beta_2 \\ \alpha_2 \\ \gamma_2 \end{pmatrix} = \begin{pmatrix} c^2 & -2cs & s^2 \\ -cc' & cs' + sc' & -ss' \\ c'^2 & -2c's' & s'^2 \end{pmatrix} \begin{pmatrix} \beta_1 \\ \alpha_1 \\ \gamma_1 \end{pmatrix}.$$

This allows tracking of the beam ellipse through the system by multiplication of 3x3 matrices.

Since the electric and space charge forces decrease with increasing energy, the only important focusing force outside the central region is the magnetic field. At this point (where electric forces have become negligible) the beam must be matched to the magnetic field; that is, the amplitude of the axial oscillations must be minimized and a beam of uniform envelope obtained. For a constant  $v_z$  the phase space ellipse which minimizes  $z_{\max}$  is given by

$$\begin{aligned} \alpha_m &= 0 \\ \gamma_m &= \frac{v_z \sqrt{E}}{r} = \text{constant} \cdot v_z \\ \beta_m &= \frac{1}{\gamma_m}. \end{aligned}$$

Once the central region geometry has been decided, the transfer matrix from injection to the radius where electric forces are negligible can be calculated (T). Now if this matrix is inverted ( $T^I$ ), the phase space ellipse required at injection to provide a beam matched to the magnetic field is

$$\begin{pmatrix} \beta_i \\ \alpha_i \\ \gamma_i \end{pmatrix} = T^I \begin{pmatrix} \beta_m \\ \alpha_m \\ \gamma_m \end{pmatrix}.$$

Unfortunately, due to the fact that the electric forces are phase dependent,  $T^I$  will be different for every initial RF phase. This means that the required initial phase space shape will be phase dependent; however, the initial phase space shape cannot easily be varied with phase. The best that can be done is to choose the initial ellipse shape for one RF phase and accept the fact that for other phases only those ions whose points in phase space fall within the chosen ellipse shape will be accelerated with  $z < z_{\text{ideal envelope}}$ . This provides a method for calculating the phase acceptance of an accelerator. The ellipse shape required for one phase is chosen as the one to be provided; then the overlap of the ellipses for other phases with the chosen ellipse gives the acceptance of the accelerator for each phase.

#### F. Phase Space Acceptance for Various TRIUMF Central Geometries and Injection Energies

Early in the design of TRIUMF it was necessary to fix the injection energy and injection geometry. The original suggestion was that the injection energy should be 150 keV; however, it was soon realized that the strong and phase-dependent electric forces would allow only a poor duty factor for

this injection energy. Raising the injection energy would alleviate this problem and also reduce the spread in orbit centre points due to different energy gains for different RF phases, thus improving the radial beam quality. However, a higher injection energy makes bunching, chopping and the design of the spiral electrostatic inflector more difficult. Thus we must investigate the axial motions to determine how the phase acceptance varies with injection energy and make a compromise between increased phase acceptance and the difficulties mentioned above.

Various initial orbit geometries had been suggested, ranging from the one injection gap case shown in Fig. 1.1 to the multi-gap case shown in Fig. 3.5.

At the time of these studies it was hoped that a three-sector magnetic field could be used in the central region. Model tests showed that this three-sector geometry produced a magnetic  $v_z$  of about 0.2, and so the axial motion studies were done with this value. The three-sector magnetic geometry was later replaced by a six-sector geometry for reasons which are explained in Chapter 4. The six-sector geometry produces much smaller values of  $v_z$  at small radius (see Fig. 3.1); however, tests with smaller  $v_z$  values show that the conclusions reached here are still valid even with much reduced values of  $v_z$ .

Most of the geometries studied had posts defining the first two gaps. It was estimated that these posts would reduce the electric forces by a factor of 4, and this is included in the calculations.\*

For each geometry the transfer matrices and the ellipse shapes required at injection were calculated. Fig. 3.6 shows the ellipses

---

\* The study by Han<sup>23</sup> indicates that the presence of posts in the dee gap actually reduces the focusing forces by a factor of six or seven.

required for one geometry. The cyclotron acceptance was calculated as discussed above. For comparison purposes, the overlap of the ellipses with the ellipse for 20 deg is used, since this is approximately in the middle of the acceptance interval and gives as good matching with other phases as is possible.

Fig. 3.7 shows the overlap with the ellipse for a phase of +20 deg for injection energies of 150, 306 and 472 keV with one 100 keV gap in the first turn. The sharp cutoff at about -15 deg is due to the defocusing action of the electric field. Fig. 3.8 shows the overlap with the ellipse for a phase of +20 deg for injection energies of 120, 286 and 454 keV with three 100 keV gaps in the first turn. This geometry gives no significant improvement in the phase acceptance, and the multi-gap geometry worsens the radial centre point spread and complicates the resonator design; hence multi-gap geometries were abandoned.

The data for the one gap geometries is summarized in Fig. 3.9. The average acceptance (averaged from -30 deg to +60 deg) seemed to flatten out above 300 keV, and this seemed to be the highest reasonable energy from the point of view of bunching and inflection, so it was decided to raise the injection energy from 150 to 300 keV.

Now after it was decided that a three-sector magnetic geometry could not be used, the code was rewritten to accept a magnetic  $v_z$  varying with radius, and the calculations for 300 keV injection energy were repeated using the much smaller  $v_z$  measured on the six-sector magnet model (Fig. 3.1). Fig. 3.10 shows the acceptance as a function of phase for this case for various choices for the initial ellipse. If the 20 deg ellipse is chosen as the axial phase space shape of the beam at injection, over 90% of the beam would be accepted at phases greater than 10 deg while the fraction of

the beam accepted would be 64% at 0 deg, 30% at -10 deg and zero for phases less than -10 deg. For this choice of initial ellipse shape the amplitude of the beam envelope does not exceed 0.55 in. for phases between -10 deg and 60 deg.

#### G. Effects of Third Harmonic in the RF on Axial Motions

The unique features of the TRIUMF resonators allow the addition of higher odd harmonics to the fundamental mode.<sup>27</sup> If the third harmonic of the fundamental is added, the resonators operate as a  $3\lambda/4$  cavity as well as a  $\lambda/4$  cavity. We now have an RF voltage given by

$$V = V_0 \left[ \cos \phi - \epsilon \cos (3\phi + \delta) \right] \quad (3.14)$$

where  $\epsilon = (\text{amplitude of third harmonic})/(\text{amplitude of fundamental})$  and  $\delta$  is the phase of the third harmonic with respect to the fundamental. Small positive values of  $\epsilon$  are required to square or "flat-top" the fundamental. A fraction  $\epsilon = 1/9$  produces perfect flat-topping at 0 deg, while more third harmonic than this produces a slight dip in the total voltage at 0 deg (see Fig. 3.11).

Now we must modify the formulae describing the lens effects of the gaps (eqns. 3.10 to 3.13) to reflect the fact that the accelerating voltage is given by eqn.(3.14) instead of a pure cosine waveform. The field variation term given in eqn.(3.3) is essentially proportional to  $dV/d\phi$ , i.e. to the rate at which the field is changing, and the energy change term given in eqn.(3.4) depends on the square of the energy gain. Hence with the RF voltage given by eqn.(3.14) we have

$$c = \sqrt{E_f} \left[ \frac{N}{r} \left( \frac{qV_o}{E_c} \right) \left( \sin \phi - 3\epsilon \sin(3\phi + \delta) \right) + \frac{2F(a,b,c)}{\pi b} \left( \frac{qV_o}{E_c} \right)^2 \left( \cos \phi - \epsilon \cos(3\phi + \delta) \right)^2 \right] \quad (3.15)$$

and

$$a = 1 - \frac{qV_o}{E_c} \left( \cos \phi - \epsilon \cos(3\phi + \delta) \right). \quad (3.16)$$

[cf. eqns. (3.10) and (3.11) for no third harmonic.]

As before,

$$\begin{aligned} d &= 1 \\ b &= \frac{1}{c}(ad - 1). \end{aligned}$$

The negative limit on the axial phase acceptance is determined by the most positive phase for which the total force acting on the ion is defocusing (see Section H of this chapter). The electric force is defocusing due to the field variation effect when the field is increasing, since the (always focusing) energy gain effect is much smaller than the field variation effect. Hence we want to choose  $\epsilon$  and  $\delta$  so that the negative of the slope of the voltage ( $\propto v^2$  due to the field variation effect)

$$- \frac{d}{d\phi} \left( \frac{V}{V_o} \right) = +\sin \phi - 3\epsilon \sin(3\phi + \delta) \quad (3.17)$$

remains positive over as wide a range as possible. Fig. 3.12 shows  $-\frac{d}{d\phi} \left( \frac{V}{V_o} \right)$  for various values of  $\epsilon$  and  $\delta$ . The widest interval where  $-\frac{d}{d\phi} \left( \frac{V}{V_o} \right)$  remains positive is produced by  $\delta = -10 \pm 2$  deg and  $\epsilon = 0.15 \pm .01$ ; however, when  $\delta \neq 0$ , the presence of the beam causes coupling between the first and third harmonics in the resonators, so that the third harmonic becomes detuned increasing, by a large amount, the power required to maintain the third

harmonic voltage. These coupling effects are not yet fully understood, so we will consider two cases,  $\delta = 0$  and  $\delta \neq 0$ . When  $\delta = 0$  the limit on  $\epsilon$  is set by the value which causes  $-\frac{d}{d\phi}\left(\frac{V}{V_0}\right)$  to become negative;  $\epsilon = 0.17$ , for example, produces a "hole" in the phase acceptance for  $5 \text{ deg} < \phi < 25 \text{ deg}$  (see Fig. 3.13) due to the fact that  $-\frac{d}{d\phi}\left(\frac{V}{V_0}\right)$  is negative there. With  $\delta \neq 0$ , the maximum value of  $\epsilon$  which can be tolerated is  $\epsilon = 0.12 \pm .01$ . The phase acceptance produced by this value is shown in Fig. 3.14. If we allow non-zero values of  $\delta$ , the best choice is  $\delta = -10 \text{ deg}$ ,  $\epsilon = 0.15$ . The phase acceptance for this case is shown in Fig. 3.15.

The optimum values of  $\epsilon$  and  $\delta$  will depend to some extent on the final details of the magnetic field, the current being accelerated and on the RF system, since the amount of power required to keep the peak voltage at 100 keV increases as  $\epsilon$  increases; however, the use of third harmonic in the RF appears to shift the cutoff in acceptance due to electric defocusing from  $-5 \text{ deg}$  to  $-25 \text{ deg}$ .

These conclusions are based purely on approximate analytic formulae and should be confirmed by numerical orbit tracking, i.e. by integrating the equations of motion numerically through three dimensional electric and magnetic fields.

#### H. Effects of Field Bumps

By a field bump we mean here an increase in the magnetic field above the isochronous value. The usual procedure in cyclotrons is to make the bump largest at the centre of the cyclotron and decrease with radius. This produces additional axial magnetic focusing due to the negative field gradient [see eqn.(3.1)]. In addition, the bump causes the phase of the ions to change, since the magnetic field is no longer isochronous. The change in

the sine of the phase angle is given by Smith and Garren<sup>28</sup>

$$\Delta(\sin \phi) = -\frac{2\pi Nq^2 B_c}{m_0 \Delta E} \int \delta B r dr = \frac{1}{6858 \text{ G}\cdot\text{in}^2} \int \delta B r dr. \quad (3.18)$$

$\delta B$  is the field bump,  $B_c$  is the central magnetic field,  $\Delta E$  is the energy gain per turn,  $N$  is the harmonic number, and  $q$  and  $m_0$  are the ion charge and mass, respectively, and the constant is appropriate to the TRIUMF cyclotron. If  $\delta B > 0$ , the ions "catch up", i.e. positive phase (late) ions (favourable for electric focusing) are brought into phase as the energy increases and the electric focusing becomes less important than the magnetic flutter focusing. In a conventional cyclotron with the RF not operating at a high harmonic of the ion frequency, a carefully chosen field bump can be of great help in overcoming the electric forces, since the two effects mentioned above both help to increase the useful phase acceptance.

For the case of TRIUMF, the operation of the RF at the fifth harmonic of the ion frequency means that the electric focusing is very strong, and the two advantages mentioned above are reduced. For example, a bump of 25 G at 10 in. diminishing to zero at 25 in. gives the required phase shift of about 30 deg and an equivalent  $\sqrt{2}$  due to the field gradient of 0.01. As can be seen from Fig. 3.4, however, this is much smaller than the force produced by the electric fields, and hence would have only a small effect on the phase acceptance. Larger field bumps cannot be used because (i) they produce more phase shift, causing ions to be shifted to a phase where the electric forces are defocusing, and (ii) ions starting at large positive phases will not gain enough energy to clear the centre post on the first turn. A field bump can, however, be used to shift the range of phases which is accepted (-5 deg to +25 deg) to a range which is centred about

0 deg. This must be done carefully so that none of the useful phase range is shifted to a phase where the electric field is defocusing before the magnetic focusing is strong enough to make the total focusing positive. Fig. 3.16 shows the total effective  $v_z^2$  produced by the magnetic and electric fields. It can be seen that the sharp cutoff in phase acceptance at -5 deg demonstrated in Fig. 3.10 is caused by the fact that ions with phases more negative than -5 deg experience a force which is defocusing at about 1.5 MeV. Since Fig. 3.16 shows at what energy the total focusing becomes positive as a function of phase, we can calculate how the phase of the ions should be "programmed" so that the ion is brought into isochronism as soon as possible but not subjected to defocusing forces. Fig. 3.17 shows the phase at which the focusing becomes positive as a function of energy. An ideal magnetic field would produce no phase gain out to 1.5 MeV; then it would cause the phase of the ion whose phase was -5 deg at 1.5 MeV to become more negative, as shown in Fig. 3.17. The amount of phase gain desired is determined by the phase range to be accepted. If we aim to accept all ions with phases between -5 deg and +45 deg, the amount of phase gain is given by  $\Delta \sin \phi$  where, after the phase gain has taken place,

$$[\sin(-5^\circ) + \Delta \sin \phi] = -[\sin(45^\circ) + \Delta \sin \phi].$$

This gives  $\Delta \sin \phi = -0.31$ , and the final range of phases is  $\pm 23.4$  deg. The phase history shown in Fig. 3.17 is produced by the  $\Delta \sin \phi$  shown in Fig. 3.18. The field bump required to produce this variation in  $\Delta \sin \phi$  is shown in Fig. 3.19. A bump with such a sharp cutoff cannot be produced in practice; however, a bump with the same  $\int \delta B r dr$  as the one shown in Fig. 3.19, and which shifts the phases no faster than the bump shown in Fig. 3.19, could be used. It should be noted that the positive slope of

this bump will decrease  $\left(v_z\right)_m^2$  by about 0.005. Another disadvantage is that the ions will spend 5 or 6 turns far from the optimum phase. This may cause a large spread in centre points to develop unless the radial starting conditions are carefully chosen. This problem is considered in Chapter 4.

Of course, with third harmonic in the RF, the negative phase limit due to electric focusing is -25 deg and a field bump is not required.

## Chapter 4. RADIAL MOTIONS

### A. Introduction

The central region of the cyclotron must be designed with two general objectives in mind. Firstly, the geometry of the electrodes must be arranged so that ions with the desired range of phases can be accelerated without hitting the electrodes. Secondly, the central region must produce a beam which is centred to within the desired tolerances.

We have shown in Chapter 1 that the motion in the median plane and the axial motion are independent to a good approximation. This chapter will discuss motion in the median plane only.

Fig. 1.1 is a section through the median plane of TRIUMF. The beam is injected down the axis of the cyclotron, then bent into the median plane by the spiral electrostatic inflector. The problem of the inflector is discussed elsewhere.<sup>29</sup> We will assume that at the exit of the inflector we have a mono-energetic beam whose shape in phase space is a free parameter. The fact that the RF operates at the fifth harmonic of the ion frequency allows the "injection gap" to provide an extra 100 keV acceleration on the first turn. This eases the geometrical problems somewhat but causes the co-ordinate of the orbit centre point, perpendicular to the gap, to vary with phase. After reaching the first main gap, the ions are accelerated and spiral outward as in an ordinary two-dee cyclotron. The main geometrical constraint is clearance of the centre post on the first turn. Ions more than 45 deg from peak phase will hit the dee and be lost; however, centring requirements limit the acceptable phases to a range smaller than this.

The use of fifth harmonic acceleration means that transit time effects are large. This reduces the energy gain at low energy. To alleviate this situation, the dee gap is tapered in both the horizontal and axial

directions (see Figs. 1.1 and 1.2) so that the electric fields are compressed and the energy gains are increased. In addition, the injection gap and first main gap are defined by posts which compress the electric field further and decrease axial focusing effects, as described in Chapter 3. These refinements make the geometry quite complicated and necessitate numerical tracking of the orbits at least out to the radius where the taper ends (30 in. or about 3 MeV). The orbit tracking was done using a slightly modified version of the computer program PINWHEEL.<sup>30</sup> The magnetic fields were obtained from measurements on a 1:20 model magnet, and the electric fields were calculated using the methods described in Chapter 2.

#### B. Basic Design

The first ion orbit in the cyclotron is shown schematically in Fig. 4.1. After leaving the inflector the ions travel, under the influence of the magnetic field only and with centre of curvature  $S$ , until they reach the injection gap. At the injection gap the ions are accelerated, and hence the centre of curvature changes. In addition, if the centre line of the injection gap is at an angle to the beam, the ions are deflected. Since the energy gains and deflections are phase dependent, the centre points and radii of curvature will be different for different phases. The ions now travel, again under the influence of the magnetic field only, to the first main gap where they are again accelerated. Due to the phase-dependent effects at the injection gap, the radius and RF phase at which the first main gap is crossed will depend on the initial RF phase and so will the centre points. In designing the central geometry it is desirable to choose the position and orientation of the injection gap so that as wide a phase

interval as possible clears the centre post on the first turn and is close enough to being centred to be useful.

As far as the placement of the injection gap is concerned, the quantities of interest are the radius, RF phase, energy and angle at which ions with various initial phases cross the first main gap.

To get a first order description of the effects we can use the approximation that the energy gains are instantaneous and give the ions  $93.0 \cos\phi$  keV at the injection gap and  $174.5 \cos\phi$  keV at the first main gap. These values are based on the results of numerically integrating ion trajectories through the gaps. We will also use a non-relativistic expression for the radius of curvature of the ion which, for a 3 kG magnetic field, is

$$r(\text{in.}) = 0.60 \sqrt{E(\text{keV})} = 18.94 \sqrt{E(\text{MeV})}. \quad (4.1)$$

Since in most cases we will be interested in differences between ions with different phases, we will label the ion whose centre of curvature is  $(x_c, 0)$  [i.e. its centre of curvature is on the centreline of the dee gap] by the subscript 1. We label an ion at some other phase by the subscript 2. Quantities referring to the injection gap are further labelled with the superscript  $ig$ , while those referring to the first main gap have superscript  $mg$ .

The geometry of the orbit near the injection gap and first main gap is shown in Fig. 4.1. If the ion reaches the injection gap making an angle  $\beta$  to the gap axis, then for a peak dee voltage  $V_0$  an ion with charge  $q$  experiences a force  $-q\nabla V \cos\phi^{ig} \cos\beta$  along the orbit and a force  $-q\nabla V \cos\phi^{ig} \sin\beta$  perpendicular to the orbit. The injection gap causes a

straightening or "collimating" deflection, given by

$$A = \tan^{-1} \left( \frac{\Delta p \sin \beta}{p + \Delta p \cos \beta} \right) \approx \frac{\Delta E}{2E} \cos \phi^{ig} \sin \beta \quad (4.2)$$

where  $p$  and  $\Delta p$  are the initial momentum and momentum gain, respectively.

The approximation is valid if  $\Delta p \ll p$ . Because of radial centring considerations, two quantities of interest are the radius and angle at which the ions cross the first main gap, or the differences in these quantities for different phases. The length  $a$  is given by

$$a^2 = r_1^2 + r_2^2 - 2r_1r_2 \cos (A_2 - A_1) \quad (4.3)$$

and the angle  $E$  by

$$E = \sin^{-1} \left( \frac{r_2}{a} (A_2 - A_1) \right). \quad (4.4)$$

The radius difference at the first main gap ( $\delta r$ ) is given by

$$\delta r = a \cos(E-\psi) - r_1 + \sqrt{r_2^2 + a^2 \sin^2(E-\psi)}. \quad (4.5)$$

The angle at which the ions cross the centreline of the gap is given by

$$C = \sin^{-1} \left( \frac{a}{r_2} \sin(E-\psi) \right). \quad (4.6)$$

The RF phase at which the ion reaches the main gap is given by

$$\phi^{mg} = \phi^{ig} + 5(\psi + A_2 - A_1 - C). \quad (4.7)$$

The co-ordinate of the centre point perpendicular to the dee gap is given by

$$y_c = -a \sin(E-\psi). \quad (4.8)$$

It appears from eqns.(4.2) and (4.5) that if  $\beta \neq 0$ , the radius and angle at which the ion crosses the main gap can be varied with phase. This would be useful because it provides a method of improving the "match" between the orbit starting conditions provided by the injection gap and those required for centred orbits. However, because of the posts, the injection gap acts as a lens (similar in properties to the lenses studied in Chapter 3). Han<sup>23</sup> has studied the properties of a lens similar to the injection gap and found that it is convergent for positive phases and divergent for negative phases. The deflections due to the lens effects are larger than those produced by placing the injection gap at an angle to the beam. This effect has been confirmed by numerical orbit tracks through electric fields with the injection gap at various angles. Since radial centring considerations require  $r^{mg}$  for both positive and negative phases to be less than  $r^{mg}$  for zero phase, slanting the injection gap to the ion path does not improve the centring and will not be considered further.

Now with  $\beta = 0$ , eqns.(4.2) to (4.8) are much simplified and will be stated again:

$$A_1 = A_2 = 0$$

$$a = r_1 - r_2 \approx \frac{r_0}{2} \frac{\Delta E^{ig}}{\sqrt{E_0}} (\cos\phi_1 - \cos\phi_2) \quad (4.9)$$

$$E = 0$$

$$\delta r = a \cos\psi - r_1 + \sqrt{r_2^2 + a^2 \sin^2\psi} \quad (4.10)$$

$$\sin C = \frac{r_2 - r_1}{r_2} \sin \psi = \frac{a}{r_2} \sin \psi \quad (4.11)$$

$$y_c = (r_1 - r_2) \sin \psi = -r_2 \sin C \quad (4.12)$$

$$\approx \frac{r_o}{2} \frac{\Delta E^{ig}}{E_o} \sin \psi (\cos \phi_1 - \cos \phi_2)$$

$$\phi^{mg} = \phi^{ig} + 5\psi - 5C. \quad (4.13)$$

The subscript o refers to quantities before the injection gap is reached.

In the central region of TRIUMF the radius of curvature is given by eqn.(4.1). The quantities  $\Delta E^{ig}$  and  $E_o$  are 93 and 300 keV, respectively; hence the constant appearing in eqn.(4.12) is  $\frac{r_o}{2} \frac{\Delta E^{ig}}{E_o} = 1.61$  in.

The first order choice for the available parameters is  $\psi = 36$  deg and  $\phi_1^{ig} = 0$  deg, i.e. the ion with zero phase at the injection gap has  $y_c = 0$  after the injection gap. If we use this geometry, then the centre points predicted by eqn.(4.12) are as shown by the solid curve in Fig. 4.2. The energy gain calculated as  $93 \cos \phi^{ig} + 174.5 \cos \phi^{mg}$ , with  $\phi^{mg}$  given by eqn.(4.13), is shown by the solid curve in Fig. 4.3. As expected, the centre points for all ions which gain less energy than the ion with zero phase lie above the centreline of the dee (positive values of  $y_c$ ). The asymmetry in the energy gain is due to the fact that negative phases are favoured by this arrangement, which delays all non-zero phases. Consider two ions which reach the injection gap with phases  $\phi^{ig} = \pm 30$  deg; the energy gains will be identical here but the ions will arrive at the main gap at  $\pm 30$  deg -  $5C$ , as predicted by eqn.(4.13). Since  $C$  is about -0.55 deg for this case, the ion with phase -30 deg at the injection gap will reach the main gap at -27.25 deg, and the ion with phase +30 deg at

the injection gap will reach the main gap at +32.25 deg. The phase at the main gap as a function of phase at the injection gap for this case is shown by the solid line in Fig. 4.4.

The different values of  $y_c$  for various phases are inherent in the use of the injection gap at an angle to the main gap. This centring is undesirable because it leads to a phase oscillation. An orbit with radius of curvature  $r$  and off centre by an amount  $y_c$  must turn through an angle of  $\pi + 2y_c/r$  between dee gap crossings. This means that the ion will arrive at one gap early by  $10y_c/r$  deg of RF phase and late at the next gap by the same amount. Fig. 4.5 shows the magnitude of this phase oscillation as a function of  $y_c$  for various values of  $r$ . Fig. 4.2 indicates that we can expect values of  $y_c$  of about 0.10 in. for an ion with phase of +30 deg. This leads to a phase oscillation amplitude of 4 deg at a radius of 14 in. (the radius of the first turn). The existence and order of magnitude of these phase oscillations are confirmed by the phase histories shown in Fig. 4.6. These phase histories are from a numerically integrated orbit. The +30 deg ion has an oscillation amplitude of about 4.5 deg, in good agreement with the expected value. The asymmetry between positive and negative phases in Fig. 4.6 is probably due to the zero phase ion not being exactly centred. The phase oscillation damps out as the energy (and hence  $r$ ) increases. The magnitude of the centring errors (and hence the phase oscillations) can be reduced by centring the spread of  $y_c$ 's about the centreline of the dee instead of having all the  $y_c$  of one sign, as was assumed for the solid curve in Fig. 4.2. This is achieved by moving the injection gap closer to the main gap without changing its orientation. To centre the spread of  $y_c$ 's for a phase interval of  $\pm\Delta\phi$ , the phase of the ion whose  $y_c$  value is zero is  $\phi_1^{ig} = \cos^{-1} \left[ (1 + \cos\Delta\phi)/2 \right]$ ; hence

$$\sin \frac{\phi_1^{ig}}{2} = \frac{1}{\sqrt{2}} \sin \frac{\Delta\phi}{2} \quad (4.14)$$

So, if we wanted to centre the  $\gamma_c$ 's for a phase range of  $\pm 45$  deg, we would choose  $\phi_1^{ig} = 31.4$  deg. This produces the  $\gamma_c$  and  $\Delta E$  values shown by the dashed lines in Figs. 4.2 and 4.3. In order to make  $\gamma_c$  zero for a phase of 31.4 deg, the injection gap must be shifted 0.12 in. (see Fig. 4.2) closer to the main gap. The maximum phase oscillation is now reduced to about  $\pm 5$  deg rather than  $\pm 10$  deg. The phase change between injection gap and main gap [given by eqn.(4.13)] is now less than 180 deg; hence we are shifting the ions towards negative phases for ions with  $|\phi^{ig}| < 31.4$  deg where they tend to be defocused in the axial direction on subsequent turns. In fact it is useful to reduce the angle  $\psi$  (i.e. rotate the injection gap towards the main gap about the centre point for  $\phi_1$ ). This reduces the energy spread for positive phases; for example  $\psi = 32$  deg produces the energy gain curve given by the dotted line in Fig. 4.3. The maximum is shifted towards positive phases because reducing  $\psi$  reduces  $\psi^{mg}$  [see eqn.(4.13)]; hence positive phases gain more energy. The reduced energy spread alleviates the problems of centring and clearing the centre post on the first turn. However, as can be seen from eqn.(4.13) and the dotted curve on Fig. 4.4, reducing  $\psi$  to 32 deg causes a large phase shift (about 23 deg) towards negative phases. The small shift towards negative phases required to centre the spread of  $\gamma_c$ 's is tolerable, since it produces a large improvement in the centring; however, reducing  $\psi$  to, say, 32 deg produces an unacceptably large shift towards negative phases. Hence  $\psi$  must be chosen so that the ion with phase  $\phi_1^{ig}$  [see eqn.(4.14)] has  $\gamma_c = 0$  after passing through the injection gap. The radius of the injection gap

is fixed because the injection energy is fixed; hence the injection gap position is determined.

### C. Problems with Three-Sector Magnetic Fields

As demonstrated in Chapter 3, the lower limit on the phase acceptance is set by axial focusing requirements. The acceptable range of phases can be increased if a phase-independent focusing force can be found to counteract the defocusing effects of the electric field. The only phase-independent source of axial focusing is the magnetic field; hence efforts were made to increase  $(v_z)_m$  near the centre of the machine. Increasing  $(v_z)_m$  requires that the "flutter" of the magnetic field be increased. Unfortunately, the central geometry of TRIUMF makes this very difficult because the magnet gap is large and there are six sectors, making the spacing between the magnet sectors small at small radius. One way of increasing the flutter is to transform the field from a six-sector geometry to a three-sector geometry in the central region. This is done by cutting off alternate magnet pole pieces at  $r = 40$  in. and adding to the remaining pole pieces steel wedges (see Fig. 1.2) extending to the centre of the cyclotron. This produces a field which is dominated by the third harmonic rather than the sixth. This "three-sector geometry" produced a considerable improvement in  $(v_z)_m$ , as is shown by the dashed line in Fig. 3.1. With the three-sector geometry,  $(v_z)_m$  is greater than 0.1 for  $r > 10$  in. However, the large third harmonic caused undesirable effects in the radial orbit behaviour.

There are two effects caused by the three-sector geometry, an increase in phase oscillation amplitude and the gap crossing resonance. Which of these effects is most important depends on the orientation of the electric

field to the magnetic field. We define this orientation by the angle  $\delta$  shown in Fig. 4.7.

The phase oscillation effect results because, if  $\delta \neq 0$ , the orbit covers 2 valleys and 1 hill on one half-turn and 1 valley and 2 hills on the next half-turn. Hence, the lengths of the orbit on successive half-turns are different, as can be seen in Fig. 4.7. If the  $n^{\text{th}}$  harmonic dominates the variation in the magnetic field, the orbit equation may be written in the approximate form (e.g. Walkinshaw and King<sup>31</sup>)

$$r = r_0 \left( 1 + \frac{1}{n^2-1} \frac{B_n}{\bar{B}} \cos n\theta \right) \quad (4.15)$$

where  $r_0$  is the radius of the (circular) orbit if the field had no azimuthal variation,  $B_n$  is the amplitude of the  $n^{\text{th}}$  harmonic in the field and  $\bar{B}$  is the average field. For the present case with  $n=3$ ,

$$r = r_0 (1 + a \cos 3\theta) \quad (4.16)$$

$$\text{where } a = \frac{1}{8} \frac{B_3}{\bar{B}}$$

Now we wish to calculate the path length ( $s$ ) between dee gaps. Using eqn.(4.16), we have

$$\begin{aligned} \frac{ds}{d\theta} &= \left[ \left( \frac{dr}{d\theta} \right)^2 + r^2 \right]^{\frac{1}{2}} \\ &\approx r_0 \left( 1 + a \cos 3\theta \right). \end{aligned}$$

The approximation which has been made is that  $B_3 \ll 8 \bar{B}$ . Hence, over one half-turn we have

$$\frac{s_1}{r_0} = \int_{\theta=\delta}^{\theta=\delta+\pi} (1 + a \cos 3\theta) d\theta = \pi + \frac{1}{12} \frac{B_3}{B} \sin 3\delta \quad (4.17)$$

and over the following half-turn

$$\frac{s_1}{r_0} = \int_{\theta=\delta+\pi}^{\theta=\delta+2\pi} (1 + a \cos 3\theta) d\theta = \pi - \frac{1}{12} \frac{B_3}{B} \sin 3\delta \quad (4.18)$$

So, between successive gap crossings the phase oscillates by  $5 \times \frac{1}{12} \frac{B_3}{B} \sin 3\delta$  (since the RF operates on the fifth harmonic of the ion frequency).

The variation of this phase change as a function of  $\delta$  is shown in Fig. 4.8 for a third harmonic amplitude ( $B_3$ ) which will produce  $v_z = 0.2$ . Phase histories for a numerical orbit track corresponding to the worst case ( $\delta = 30$  deg) are shown in Fig. 4.9. The amplitude of the phase oscillation is about 8.5 deg for the zero phase ion (for which the phase oscillation would be zero without the three-sector magnetic field). This is in reasonable agreement with the theory. Since any phase oscillation such as this will decrease the duty factor,<sup>32</sup>  $\delta$  must be small, i.e. the centreline of the dee gap should be close to the line running from a hill top at  $\delta = 0$  to the opposite valley bottom at  $\delta = 180$  deg. To keep the amplitude of the phase oscillation less than 5 deg, we must have  $\delta < 16$  deg. The effect of this phase oscillation is important here because the RF operates at the fifth harmonic of the ion frequency. It has been dismissed as unimportant for three-sector cyclotrons operating with  $N = 1$ .<sup>33</sup>

This phase oscillation effect can be eliminated by placing the dee gap along a hill-valley centreline ( $\delta = 0$  in Fig. 4.7). Unfortunately, this orientation maximizes another undesirable effect, the gap crossing

resonance. This is essentially a shift in the orbit centre points along the dee gap caused by a larger magnetic field at one dee gap than the other. This effect has been discussed in detail by Gordon,<sup>33</sup> but we can make an estimate of the effects as follows. Referring again to Fig. 4.7, we can refer to the dee gap on the right side by the subscript 1 and on the left side by the subscript 2; then the magnetic fields at the gap are

$$B_1 = \bar{B} + B_3 \cos \delta, \quad (4.19)$$

$$B_2 = \bar{B} - B_3 \cos \delta.$$

Since these effects are important at low energy, the radius of curvature can be approximated by

$$\rho(\text{in.}) = \frac{56.92}{B(\text{kG})} \sqrt{E(\text{MeV})}.$$

If the increase in energy at the dee gap is  $\Delta E$  MeV, the change in radius of curvature at the gap, assuming the ions always cross normally, is

$$\Delta\rho(E) = \frac{56.92}{B} \left( \sqrt{E + \Delta E} - \sqrt{E} \right). \quad (4.20)$$

The radial position of the ion does not change appreciably as the gap is crossed, so the change in radius of curvature is reflected in a change in the position of the centre of curvature. As the ion alternately crosses gaps 1 and 2, the centre of curvature oscillates back and forth approximately along the centreline of the dee. If the magnetic fields are different at the two gaps, there is a net drift of the centre of curvature towards the higher field, given by

$$\delta\rho = 56.92 \left[ \sum_{\substack{i=1 \\ \text{odd } i}}^k \frac{1}{B_1} \left( \sqrt{E_{i+1}} - \sqrt{E_i} \right) - \sum_{\substack{i=2 \\ \text{even } i}}^{k+1} \frac{1}{B_2} \left( \sqrt{E_{i+1}} - \sqrt{E_i} \right) \right] \quad (4.21)$$

where  $E_{i+1} = E_i + \Delta E_i$ ;  $i$  is the half-turn number and  $\Delta E_i$  is the energy gained at the  $i^{\text{th}}$  dee gap.

Using eqn. (4.19) and the fact that  $B_3/\bar{B} \ll 1$ , this can be expressed as

$$\delta\rho \approx \frac{56.92}{B} \sum_{i=1}^k \left[ \frac{\Delta E_i}{2\sqrt{E_i}} \left[ (-1)^{i+1} - \frac{B_3}{B} \cos 3\delta \right] \right]. \quad (4.22)$$

The first term in the square bracket is the displacement of the orbit centre from the cyclotron centre. This term oscillates, hence its sum depends on the differences of the  $\Delta E$ 's. The second term in the square bracket is the centre point drift due to the third harmonic component in the magnetic field. This term always has the same sign, hence will accumulate rapidly if  $B_3$  is large.  $B_3$  varies widely with radius (see Fig. 4.10); hence the sum depends on the magnetic field used. Numerically summing the series for the values of  $B_3$  shown in Fig. 4.10, and using  $\Delta E_i = 0.2$  MeV at all gaps, produced a centring error of 0.3 in. Numerical tracking of ions through the measured magnetic field using the computer code GOBLIN gave a centring error of about 0.5 in. for this field. Eqn. (4.22) shows that the centre point drift due to  $B_3$  is proportional to  $\cos 3\delta$  and hence could be eliminated to this approximation by choosing  $\delta = 30$  deg. This means that the dee gap runs along a hill-valley interface, but this is unfortunately the situation which produces the large phase oscillations discussed above.

The drift in centre point could be reduced by putting a first harmonic in the magnetic field. The first harmonic causes the centre point to drift and could be arranged to cancel out the drift due to the gap crossing resonance, as has been described by Gordon<sup>33</sup> and van Kranenburg *et al.*<sup>34</sup> However, producing a first harmonic varying accurately enough with radius would be extremely difficult and necessitate special coils or shimming of

the magnet. In addition, the compensation is exact for only one RF phase.

In summary, aligning the dee gap along the centreline of a hill (or valley) produces a phase oscillation of about 10 deg. Aligning the dee gap along a hill-valley interface excites the gap-crossing resonance causing a centring error of about 0.5 in., which can be only partially cancelled by a first harmonic in the magnetic field. Orientations between the two described above do not bring the phase oscillation and the centre point drift within acceptable limits, and hence the three-sector magnetic field has not been adopted.

#### D. Radial Centring

The central region of a cyclotron must produce a beam which is centred at extraction. By centred we mean that the oscillations of the orbit centre point approach the geometric centre of the machine as the energy increases. In TRIUMF the large energy gain per turn and low magnetic field produce large oscillations of the centre point at low energy. The centre point at injection must be off centre by about half the radius gain per half-turn (see, e.g., Gordon<sup>33</sup>) if the orbit centre point is to approach the centre of the machine as the energy becomes large. This centre point displacement required because of the acceleration can be derived in a manner similar to the derivation of eqn.(4.22). If we assume circular orbits, then the change in centre of curvature at one gap is

$$x_{c_i} - x_{c_{i+1}} = \rho_i - \rho_{i+1}$$

and at the next gap

$$x_{c_{i+2}} - x_{c_{i+1}} = \rho_{i+1} - \rho_{i+2}$$

Hence over one turn the change in centre point is

$$x_{c_{i+2}} - x_{c_i} = -\rho_{i+2} + 2\rho_{i+1} - \rho_i. \quad (4.23)$$

If the energy gain per gap crossing ( $\Delta E$ ) is  $\ll$  the energy  $E$  and the change in radius per gap crossing ( $\Delta r$ ) is  $\ll$  the radius  $r$ , we can approximate eqn.(4.23) by a differential equation

$$\frac{dx_c}{dE} = -\frac{\Delta E}{2} \frac{d^2\rho}{dE^2}. \quad (4.24)$$

Now if the centre point ( $x_c$ ) at infinite energy is zero, i.e. the beam is centred, integrating eqn.(4.24) once yields

$$x_c(E) = \frac{\Delta E}{2} \frac{d\rho}{dE} = \frac{r_\infty}{2} \frac{\Delta E}{m_0 c^2} \frac{1}{\beta\gamma^3}. \quad (4.25)$$

where  $\rho$  and  $\delta$  are the usual relativistic factors and  $r_\infty$  is the cyclotron radius  $= \frac{m_0 c}{qB_c}$  ( $\approx 410$  in. for TRIUMF). The right-hand side of eqn.(4.25) is just one-half the radius gain per half-turn at energy  $E$ . The above estimate provides a good starting point for finding central orbits, especially at high energy. However, at low energy where the geometry is complicated by the presence of the injection gap, we must resort to numerical orbit tracks to optimize the centring.

The determination of what constitutes a centred orbit is complicated by several factors. The azimuthal variation of the magnetic field causes scalloping of the orbit; hence the instantaneous centre point depends on the azimuthal angle. The average orbit radius and maximum scalloping are shown in Fig. 4.11 as a function of energy.

The quantities we will mainly be concerned with in this section are  $r$ ,

the radius of the ion from the geometric centre of the cyclotron, and  $p_r$ , the radial momentum. The momentum will be written in the form

$$p = \beta \gamma r_{\infty} . \quad (4.26)$$

In these units, the momentum of the ion is represented by its radius of curvature in the central magnetic field ( $B_c$ ). The radial momentum is that component of the momentum which is directed in the radial direction, i.e.

$$p_r = p \frac{dr}{ds} = p \frac{\dot{r}}{v} = p \sin \chi$$

where  $\tan \chi = \frac{dr}{rd\theta}$ . In the central region, the flutter in the magnetic field is small, hence the orbit scalloping is small, and we can roughly approximate  $B$  by  $B_c$  and  $p_{\theta}$  by  $p$ ; then the component of the centre point perpendicular to the dee gap ( $y_c$ ) equals  $p_r$  at  $\theta = \delta$ , i.e. the dee gap.

The essential features of the central orbits of TRIUMF are shown in Fig. 4.12. The magnetic field has six-fold symmetry. The centreline of the dee gap is 5.5 deg from the centreline of a valley. The azimuthal angle  $\theta$  is measured from the centreline of the dee gap as shown.

One way to remove the complicating effects of orbit scalloping, and to determine how close the orbit is to an ideal centred orbit, is to calculate, at some azimuthal angle, the difference between the radius and radial momentum of the actual accelerated orbit (a.o.) and an equilibrium orbit (e.o.) at the same energy. An e.o. is a fixed energy orbit which closes upon itself, has average centre of curvature at the centre of the machine, and is stable for small displacements in radius and momentum. The e.o.'s are calculated by the program CYCLOPS.\* Now for any energy at one azimuth,

---

\* CYCLOPS was kindly made available to TRIUMF by Dr. M. Gordon of Michigan State University.

we know the radius and radial momentum ( $r_{e0}$  and  $p_{re0}$ ) of the equilibrium orbit. Hence, when tracking an a.o., we can calculate the differences in radius and momentum between the e.o. and the a.o. at this azimuth. If an orbit is to be centred at the final energy, the differences between the e.o. and the a.o. during acceleration (i.e.  $\Delta r = r_{ao} - r_{e0}$  and  $\Delta p_r = p_{rao} - p_{re0}$ ) are due to centre point displacements along the dee gap only (changes in  $x_c$ ) due to acceleration. Hence, as the energy increases and the changes in  $x_c$  decrease, the values of  $\Delta r$  and  $\Delta p_r$  (due only to a non-zero value of  $x_c$ ) will decrease, and the a.o. will approach the e.o. The locus of the point  $(\Delta r, \Delta p_r)$  in phase space on successive turns (at one azimuth angle) as the acceleration proceeds forms an "accelerated phase plot". The gross features of the accelerated phase plot depend on the amount the instantaneous centre point of the a.o. differs from the instantaneous centre point of the e.o. ( $\Delta x_c$  and  $\Delta y_c$  in the x- and y-directions, respectively) and on the azimuthal angle at which the accelerated phase plot is calculated.

Suppose at some angle  $\theta_0$  the a.o. has energy  $E$ , radius  $r_{ao}$  and radial momentum  $p_{rao}$ . We interpolate in a table of equilibrium orbit radii and radial momenta values for azimuth  $\theta_0$  to obtain  $r_{e0}$  and  $p_{re0}$ , which are the radius and radial momentum of the equilibrium orbit at energy  $E$ . Now if we neglect the variation in the magnetic field along  $\theta_0$  between  $r_{e0}$  and  $r_{ao}$ , then the radii of curvature are the same, i.e.  $\rho_{e0} = \rho_{ao} \equiv \rho$ , and we have the situation shown in Fig. 4.13. The angle  $\chi$  will be small since  $p_r$  is much less than  $p$  and  $\Delta p_r$  will also be much less than  $p$  hence we can approximate the arc  $\rho \frac{\Delta p}{p}$  by a straight line and the centre point components are related to the differences in radius and radial momenta by

$$\begin{pmatrix} \Delta y_c \\ \Delta x_c \end{pmatrix} = \begin{pmatrix} \cos(\theta_0 - \chi) & \sin(\theta_0 - \chi) \\ -\sin(\theta_0 - \chi) & \cos(\theta_0 - \chi) \end{pmatrix} \begin{pmatrix} \frac{\rho \Delta p_r}{p} \\ \Delta r \end{pmatrix}. \quad (4.27)$$

Thus the accelerated phase plot removes the "motions" in the orbit centre point due to scalloping of the orbit and allows the actual errors in centring to be determined. Fig. 4.14 shows  $\Delta x_c$  calculated using eqn.(4.27) [using  $\Delta r$  and  $\Delta p_r$  values from a numerical track of a centred orbit] compared to the values of  $\Delta x_c$  predicted by eqn.(4.25).  $|x_c|$  is plotted rather than  $x_c$  to allow comparison of the curves for  $\theta_0 = 54.5^\circ$  and  $\theta_0 = 234.5^\circ$ . The values of  $x_c$  are all negative for  $\theta_0 = 54.5^\circ$  and all positive for  $\theta_0 = 234.5^\circ$ . The agreement is fairly good; however, the only way to do the final optimization of the centring seems to be to work backwards from the centred orbit. That is, we start an ion on a centred orbit at high energy and numerically track it backwards into the centre of the machine. If we do this for several RF phases, we will know what the starting conditions should be if ions with various phases are to be centred. Using a typical magnetic field (01-03-06-70), ions with various starting phases were tracked backwards into the centre of the machine.

The procedure which is used for tracking orbits is as follows. For energies less than 5 MeV the program PINWHEEL is used. This solves the relativistic equations of motion using measured magnetic fields and electric fields calculated by the method described in Chapter 2. For energies greater than 5 MeV the program GOBLIN is used. This program solves the relativistic equations of motion using measured magnetic fields but approximating the effects of the electric fields by the "impulse" approximation

described in Chapter 5. The transition is made at 5 MeV because above this energy there is no significant radial variation in the field across the dee gap, while for energies below 5 MeV there is such a variation because of the tapering of the electrodes.

The ions were started at 20 MeV at the centreline of a valley ( $\theta = -5.5$  deg), with  $\Delta p_r = 0$  and with  $\Delta r$  equal to one-half the turn separation per half-turn, as indicated by eqn.(4.25). The accelerated phase plots at  $\theta_0 = 54.5$  deg and  $\theta_0 = -125.5$  deg (see Fig. 4.12), i.e. at the centreline of a valley, are shown in Figs. 4.15, 4.16 and 4.17 for ions with starting phases of  $-30$  deg,  $0$  and  $+30$  deg, respectively. For the ideal case where  $y_c$  is always zero and  $x_c$  becomes zero at high energy, then eqn.(4.27) shows that the  $\Delta p_r$  and  $\Delta r$  values will always lie on the straight line passing through  $\Delta r = 0$  and  $\Delta p_r = 0$  and at an angle of  $\pi - \theta_0$  to the  $\Delta r = 0$  axis. This is the straight line shown in Figs. 4.15, 4.16 and 4.17. Using eqn.(4.27) and the data shown in Fig. 4.16, the values of  $x_c$  shown in Fig. 4.14 were calculated. Extrapolation of this curve down to 0.4 MeV (the energy of the beam between the injection gap and the first main gap) indicates that the beam should be off centre by about  $1.32 \pm .05$  in. at this energy. Since the radius of curvature of the beam is 11.88 in., this means that the radius at which the first main gap should be crossed is  $13.20 \pm .05$  in. Accelerated phase plots for three different choices of radius at the first main gap crossing are shown in Fig. 4.18. The arrow on Fig. 4.18 gives twice the radial oscillation amplitude. The curve for  $r = 13.20$  in. clearly leads to the smallest amplitude radial oscillation. To determine what happens to other phases an ion was tracked backwards from  $r = 13.20$  in. at the first main gap through the injection gap, into the centre post, providing initial conditions for outward tracks. Using these

initial conditions, trajectories were followed outwards for various phases, producing the phase plot shown in Fig. 4.19. The -25 deg ion gives a radial oscillation amplitude of about 0.5 in., while the +25 deg ion gives an amplitude of about 0.8 in. These oscillations are much too large, as they would lead to a very large energy spread at extraction. In order to achieve more than a very narrow phase band, the starting conditions must be adjusted to favour ions which start with phases other than zero. Since the difference in the accelerating conditions which causes the large oscillation amplitudes to develop is essentially the energy gain, which varies roughly as  $\cos \phi$ , it is reasonable to centre an ion whose phase corresponds to the average cosine in the phase band to be accelerated.

Since in the absence of third harmonic in the RF we are restricted essentially to positive phases, we will choose starting conditions so that various positive phases are centred and observe how this affects the magnitude of the radial oscillations. Fig. 4.20 shows accelerated phase plots for ions with the same phase range as in Fig. 4.19 but with starting conditions chosen to give centred orbits for starting a phase of +17 deg. Phase plots such as shown in Fig. 4.20 were calculated using starting conditions to give centred orbits for initial phases of +15 deg, +17 deg, +19 deg and +21 deg. The results are summarized in Fig. 4.21. For a phase range of -5 deg to +25 deg, the amplitudes of the radial oscillations are minimized if an ion with initial phase of 15 deg to 17 deg is centred. If a small amplitude of oscillation were desired (and a small phase width could be tolerated), one would choose the case where the 0 deg ion was centred.

To first order the energy resolution obtainable in the extracted beam is related to the radial oscillation amplitude by the energy gain per turn.

For the case of TRIUMF, the maximum energy gain per turn (400 keV) produces a 0.064 in. increase in radius at 500 MeV. When operating with a wide phase spread, the beam will be spread out fairly uniformly with radius, so that a  $\pm 0.064$  in. oscillation will worsen the energy resolution by  $\pm 400$  keV (or alternatively  $\pm 0.1$  in. will produce  $\pm 600$  keV).

Eqn. (4.25) shows that the  $x_c$  required to allow for centre point motions due to acceleration is proportional to  $\Delta E$  and hence is also proportional to  $\cos\phi$  since  $\Delta E \approx qV_0 \cos\phi$ . Therefore, if the zero phase ion is centred at high energy and has centre point  $x_c^{E_1}$  at injection and  $x_c^{E_2}$  at some other energy, an ion with some other phase ( $\phi$ ) will have a centring error  $(1 - \cos\phi)x_c^{E_1}$  at injection. If this centring error did not alter the behaviour of the centre point motions with energy, we would expect this initial centring error to produce a centring error  $(1 - \cos\phi)(x_c^{E_1} - x_c^{E_2})$  at energy  $E_2$ . The dashed line in Fig. 4.21 shows this centring error as a function of phase at injection. Fig. 4.21 shows that the oscillation amplitude is much larger than this, so some mechanism is causing this centring error to produce a large amplitude radial oscillation. One such mechanism is described in Section E of this chapter.

Of course, the ion beam will contain particles with various displacements and divergences from the central ray, and we must investigate how the beam as a whole is centred. This is discussed in the next section.

In Section H of Chapter 3 it was shown that a field bump could be used to shift the acceptable range of phases so that the accepted phase interval is centred about zero degrees. Fig. 4.22 shows the phase histories for four ions in a field which has the bump described in Fig. 3.19 added to it. As expected, the initial phase interval of 0 deg to +50 deg is shifted to about -21 to +25 deg. The dashed line shows the theoretically expected

phase shift for the ideal bump. Note that the phase change is never faster than ideal, so no ions which are initially focused are shifted to defocusing phases. Accelerated phase plots for ions with various starting phases in the magnetic field with the bump added are shown in Fig. 4.23. The starting conditions are adjusted to favour the +17 deg ion (as in Fig. 4.20 without the field bump). The oscillation amplitudes for phases of 0 deg, +15 deg and +30 deg are 0.13, 0.12 and 0.42 in., respectively, while without the bump they are 0.20, 0.14 and 0.46 in. Thus the effect of the bump is to slightly decrease the oscillation amplitudes in this case. We would expect (from Fig. 4.21) that large positive phases would have very large oscillation amplitudes, and this is confirmed in Fig. 4.23, which shows that the ion that starts at +45 deg is unacceptable. This undesirable behaviour for large positive phases is not significantly improved if we arrange the starting conditions to favour the +21 deg ion. Note that the radial centring requirement effectively sets a positive phase limit of about +25 deg, so that the field bump used (designed for a phase interval of -5 deg to +45 deg, see Section H of Chapter 3) is too large. However, the effects of the bump on the radial motion are small.

#### E. Effects of Finite Beam Emittance

Now we will consider how the centring varies over a beam with a realistic size. The expected emittance of the TRIUMF ion source is  $0.50 \pi$  in. mrad (at 300 keV). We will assume that this is not significantly increased by the transport system up to the point of injection into the cyclotron dees. To minimize the amplitude of the radial oscillations we want to choose the initial ellipse shape to match the radial focusing, as described in Chapter 3 for axial focusing. Since the lens effects of the

dee gaps are small, we first try matching to the magnetic focusing, for which  $v_r \approx 1.0$  in the central region. To see how the emittance is transformed as the beam is accelerated, four particles were tracked, starting on the edge of the emittance ellipse. Figs. 4.24(a), 4.25(a) and 4.26(a) show accelerated phase plots for these four points for initial phases of 0 deg, +15 deg and +25 deg, respectively. As can be seen from these figures, the ellipse is "stretched" as the acceleration proceeds, producing a large amplitude radial oscillation. This is due to an effect explained by Mackenzie.<sup>35</sup> Briefly, the effect is important in this case because of the low field and large energy gain per turn causing the initial orbits to be far from the equilibrium orbits. Consider the trajectories in phase space of two ions with initial phases of  $+\phi$  and  $-\phi$ . An initial displacement from the origin ( $\Delta r \neq 0$  or  $\Delta p_r \neq 0$ ) will cause precession through an angle of approximately (if  $v_r$  is close to 1)  $\pi(v_r - 1)$  during a half-turn in the magnetic field. Since  $\Delta r \neq 0$  or  $\Delta p_r \neq 0$  means that the beam is not centred, the ions arrive at the next dee gap later or earlier than they left the previous gap (as described in Section B). Hence the energy gain is not the same for the  $+\phi$  ion as for the  $-\phi$  one. This means that on the next half-turn one ion will be closer to its e.o. than the other to its e.o., and while they both precess through the same angle, the  $-\phi$  ion will precess so as to reduce its displacement from the origin in phase space, while the displacement of the  $+\phi$  ion increases if  $v_r > 1$ . The effect is reversed if  $v_r < 1$ . These displacements in phase space cause "stretching" of the emittance ellipse, producing a large amplitude radial oscillation. This effect is important when the ion energy is small and when  $v_r$  is different from one, so that the precession is large. Numerical orbit tracks have shown that the effect is unimportant above 10 MeV.

The amplitude of these oscillations can be reduced by choosing a different initial ellipse shape. If, for example, we choose an ellipse which is reduced by a factor of two in the  $\Delta r$  direction but increased by a factor of two in the  $\Delta p_r$  direction from the ellipse that is matched to  $v_r = 1$ , we obtain the phase plots shown in Figs. 4.24(b), 4.25(b) and 4.26(b) for the same three initial phases as used previously. These phase plots show that the oscillation amplitude is reduced to 0.25 in. over the phase range 0 deg to +25 deg. This represents an effective increase by a factor of almost four in the oscillation amplitude due to the phase-dependent acceleration.

## CHAPTER 5. RADIAL LENS EFFECTS OF CYCLOTRON DEE GAPS

### A. Introduction

The calculation of radial motions in a cyclotron at low energies requires a detailed knowledge of the electric field produced by the dees. The calculation or measurement of this field is a difficult problem (see Chapter 2), and the numerical integration of the equations of motion through the field is a slow procedure. To integrate the equations of motion from injection to extraction would require a prohibitively large amount of computer time. It is therefore useful to have an approximate method of calculating the radial motions. One way of doing this is to represent the radial motion as half-turns in a purely magnetic field separated by accelerating impulses induced by the electric fields at the dee gap. The magnetic field is approximated by an isochronous field with  $\nu_r$  (the radial oscillation frequency) constant over each half-turn and determined by interpolation in the values computed by the equilibrium orbit code for the real field. The effects of the dee gaps are approximated by instantaneous changes in the energy ( $\delta E$ ), RF phase ( $\delta t$ ), radial position ( $\delta x$ ) and angle to the gap ( $\delta \xi$ ) when the ion reaches the azimuthal angle of the centre line of the dee gap. Thus in a two-dee cyclotron such as TRIUMF the ion will pass through a 180 deg long magnetic field region (with  $\nu_r$  constant), then have its energy, radial position, RF phase and angle to the dee gap instantaneously changed as it crosses the gap, then pass through another magnetic field region and dee gap, etc. This chapter investigates various approximations which give the quantities describing the dee gap ( $\delta E$ ,  $\delta t$ ,  $\delta x$  and  $\delta \xi$ ). The results from the approximations are compared to numerical orbit tracks through a real electric field.

Since we have  $v_r$  constant over each half-turn, we can approximate the radial motion in the magnetic field by a sinusoidal oscillation about the equilibrium orbit. There will also be a significant oscillation at the principal flutter frequency, but this will produce no change over 180 deg in a six-sector machine.

We will call the amplitude of this oscillation  $\Delta r$  and the slope  $\frac{\Delta p_r}{p}$  where  $p$  and  $p_r$  are the total and radial momenta, respectively. The transformation of these quantities are given by an equation equivalent to eqn.(3.9), i.e.

$$\begin{pmatrix} \Delta r \\ \frac{\Delta p_r}{p} \end{pmatrix} = \begin{pmatrix} \cos v_r \theta & \frac{r}{v_r} \sin v_r \theta \\ -\frac{v_r}{r} \sin v_r \theta & \cos v_r \theta \end{pmatrix} \begin{pmatrix} \Delta r_0 \\ \left( \frac{\Delta p_r}{p} \right)_0 \end{pmatrix} \quad (5.1)$$

where  $r$  is the radius of curvature and  $\theta$  is the azimuthal angle in the magnetic field.

Now we need a description of the changes in momentum and position produced by the dee gaps. Fig. 5.1 shows a typical dee gap. The radial motion of the ion is confined close to the median plane  $z = 0$ . Fig. 5.2 shows a plot of the instantaneous electric potential in the median plane. This figure suggests that a first approximation to the effects of the dee gap can be obtained by assuming that the gradient of the electric field is constant over some region and zero elsewhere.

#### B. Constant Gradient Approximation with No Magnetic Field

We assume the gap is as shown in Fig. 5.3, uniform in the x-direction, with a gap width of  $\ell$  and a total voltage across the gap of  $V_0$ . At time  $t = 0$ , the ion is at  $x = x_0$ ,  $y = \ell/2$  with velocity  $\dot{x} = \dot{x}_0$ ,  $\dot{y} = \dot{y}_0$ ,  $\left( \dot{x} \equiv \frac{dx}{dt}, \dot{y} \equiv \frac{dy}{dt} \right)$ . The phase of the accelerating voltage at  $t = 0$  is  $\phi_0$  and

its frequency is  $\omega$ . The equations of motion are

$$\ddot{x} = 0 \quad (5.2)$$

$$\ddot{y} = \frac{qE}{m} = k \cos(\omega t + \phi_0) \quad (5.3)$$

where  $k = \frac{qV_0}{m\ell}$ ,  $q$  and  $m$  being the charge and mass of the ion, respectively.

Integrating eqn.(5.2) gives

$$\dot{x} = \dot{x}_0 \quad (5.4)$$

$$x = x_0 + \dot{x}_0 t \quad (5.5)$$

Integrating eqn.(5.3) gives

$$\dot{y} = \dot{y}_0 + \frac{k}{\omega} \left[ \sin(\omega t + \phi_0) - \sin(\phi_0) \right] \quad (5.6)$$

$$y = y_0 + \dot{y}_0 t + \frac{k}{\omega} \left[ \frac{1}{\omega} \left[ \cos(\phi_0) - \cos(\omega t + \phi_0) \right] - t \sin(\phi_0) \right] \quad (5.7)$$

In practical cases, the electrodes which produce the field are located above and below the median plane, and so the width of the field there is larger than the physical gap between the electrodes (as demonstrated in Fig. 5.1). We therefore treat  $\ell$  as a free parameter to obtain the best agreement with numerically integrated orbits. The time required for the ion to cross the gap  $\tau$  (the transit time) is also as yet unknown. Within the validity of the approximation, the width of the electric field will depend only on the geometry, while the transit time will depend on the electric field and the velocity of the ion; hence we choose  $\ell$  so that the constant gradient approximation gives the same energy gain as the numerical results for one case, i.e. one incident energy and RF phase. Now, using this value of  $\ell$ , we calculate the transit time  $\tau$  which is the value of  $\tau$

that solves eqn.(5.7) when  $\dot{y} - y_0 = -\ell$ , i.e.

$$\ell + \dot{y}_0 \tau + \frac{k}{\omega} \left[ \frac{1}{\omega} \left( \cos \phi_0 - \cos(\omega \tau + \phi_0) \right) - \tau \sin \phi_0 \right] = 0. \quad (5.8)$$

This can be solved by any standard numerical technique, for example the Newton-Raphson method.<sup>36</sup> Once  $\tau$  is known, the changes in  $x$ ,  $y$ ,  $\dot{x}$  and  $\dot{y}$  across the gap can be calculated. We will call the above approximation the iterative approximation, since it requires an iterative solution of eqn.(5.8) to find the transit time.

Now, within the validity of the approximation, the value of  $\ell$  found to be best in one case should also give the best results for other incident energies and phases. To select an appropriate value of  $\ell$ , the best method seems to be to compare the results of numerical integrations to the results predicted by the constant gradient approximation at high energy, where we expect the approximation to be most valid.

Since the iterative solution of eqn.(5.8) may be time consuming, one is tempted to look for simpler approximations. If the transit time is small enough so that we can approximate  $\sin \omega t$  by  $\omega t$  and  $\cos \omega t$  by 1, then we obtain the "linear" approximation

$$\dot{y} = \dot{y}_0 + kt \cos \phi_0 \quad (5.9)$$

$$y = y_0 + \dot{y}_0 t \quad (5.10)$$

and the transit time is

$$\tau = \frac{\ell}{\dot{y}_0}. \quad (5.11)$$

In this case the assumption of small transit time is equivalent to assuming that the velocity of the ion is constant across the gap.

A more exact approximation is obtained if we keep terms up to  $(\omega t)^2$  in

the expansions of  $\sin\omega t$  and  $\cos\omega t$ ; then we obtain the "quadratic" approximation which is

$$\dot{y} = \dot{y}_0 + k \left( t \cos\phi_0 - \frac{\omega}{2} t^2 \sin\phi_0 \right) \quad (5.12)$$

and

$$y = y_0 + \dot{y}_0 t + \frac{k}{2} t^2 \cos\phi_0. \quad (5.13)$$

The transit time is obtained from eqn.(5.13) when  $y = -\frac{l}{2}$  and is

$$\tau = \frac{-\dot{y}_0 + \sqrt{\dot{y}_0^2 + 2k l \cos\phi_0}}{k \cos\phi_0}. \quad (5.14)$$

This approximation is equivalent to assuming that the ion velocity across the gap is the average of the initial and final velocities.

A still better approximation can be obtained by retaining one more term in the expansion of  $\sin\omega t$ ; then we obtain the "cubic" approximation

$$\dot{y} = \dot{y}_0 + k \left( t \cos\phi_0 - \frac{\omega}{2} t^2 \sin\phi_0 - \frac{\omega^2 t^3}{6} \cos\phi_0 \right). \quad (5.15)$$

The last term in eqn.(5.15), which was neglected in eqn.(5.12), is usually as large as the second last term in eqn.(5.15). In the cubic approximation we still calculate the transit time using eqn.(5.14).

The validity of these approximations was tested by comparing the changes in  $x$ ,  $\dot{x}$ ,  $y$  and  $\dot{y}$  to those given by numerical integration through a real electric field. The numerical calculations solve the exact relativistic equations of motion. The various constant gradient approximations assume that the mass is constant across the gap; however, the mass used is the relativistic mass appropriate to the initial ion energy. The electric field used was that for the gap shown in Fig. 5.1, i.e. a total gap height of 4.0 in. and a total gap width of 6.0 in. In the TRIUMF

cyclotron the field produced by a gap of these dimensions is reached at a radius of 40 in. (about 5 MeV). The value of  $\lambda$  was selected so that the iterative approximation gave the same energy gain as the numerical integration for  $\phi_0 = 0$  deg and  $E_0 = 100$  MeV. The value selected was 8.97 in., considerably larger than the physical gap width of 6.0 in. The gradient used for the approximation is shown by the dashed line in Fig. 5.2.

In this case, there is no force in the x direction; hence  $p_x$  remains constant and displacements in the x-direction are just  $\dot{x}t$ . The change in  $p_y$  causes the energy of the ion to increase. We will express the energy gain by the so-called gap factor G,

$$G = \frac{\Delta E}{qV_0 \cos\phi_c} \times 100\%, \quad (5.16)$$

where  $\Delta E$  is the actual energy gained by the ion and  $\phi_c$  is the RF phase at which the ion crosses the centre of the gap.

Fig. 5.4 compares the energy gain obtained by numerical orbit tracking in the real field for  $\phi_c = 0$  deg with the energy gains predicted by the various constant gradient approximations. The small transit time approximations give very much less accurate results than the approximation based on exact computation of the transit time, and hence they will not be considered further.

Values of G for various phases and energies from the iterative constant-gradient approximation and from numerical integration are given in Table V. Figure 5.5 shows the differences between the values calculated by numerical integration and those from the iterative constant gradient approximation. In all cases, over a phase range of -45 deg to +45 deg and an energy range of 1 to 100 MeV, the differences are less than 0.5%.

The errors displayed in Fig. 5.5 are inherent in the constant gradient

TABLE V

Gap factors given by numerical integration and by the  
constant gradient approximation (no magnetic field)

Energy (MeV)	-45		-30		-15		0		+15		+30		+45	
	N	IA												
1	78.599	78.319	78.921	78.840	79.242	79.302	79.512	79.683	79.697	79.963	79.780	80.131	79.730	80.177
2	88.718	88.726	88.775	88.888	88.847	89.034	88.905	89.157	88.935	89.249	88.925	89.306	88.852	89.323
5	95.351	95.349	95.318	95.381	95.304	95.412	95.291	95.440	95.272	95.462	95.241	95.478	95.183	95.467
10	97.663	97.633	97.627	97.642	97.601	97.651	97.580	97.660	97.559	97.668	97.351	97.674	97.487	97.680
20	98.833	98.790	98.802	98.791	98.780	98.794	98.762	98.796	98.743	98.800	98.720	98.803	98.687	98.806
50	99.529	99.488	99.508	99.487	99.493	99.487	99.479	99.487	99.466	99.488	99.449	99.490	99.426	99.492
100	99.759	99.722	99.742	99.720	99.730	99.720	99.719	99.719	99.709	99.720	99.697	99.721	99.681	99.723

N = numerical results

IA = results from iterative approximation

approximation and not a result of an inappropriate choice of  $\ell$ , since changing  $\ell$  merely displaces the family of error curves.

The other quantity of interest is the transit time. In all cases, the transit time was within 0.1% of the expected time of  $\ell/v_a$  where  $v_a$  is the average of the initial and final velocities.

Thus in this case the effect of the gap can be approximated by instantaneous changes at the centre line of the gap as follows:  $\delta E$  is the energy change appropriate to the velocity change given by eqn.(5.6),  $\delta t$  and  $\delta x$  are zero and  $\delta \xi$  is the change in angle due to the energy gain. This change in angle results because  $p_y$  changes while  $p_x$  remains constant and is

$$\delta \xi = \tan^{-1} \frac{p_x}{p_y + \Delta p} - \tan^{-1} \frac{p_x}{p_y} \quad (5.17)$$

where  $\Delta p$  is the increase in momentum given by eqn.(5.6), and  $p_x$  and  $p_y$  are the initial momentum components.

### C. Sine Gradient Approximation

To improve the results given by the constant gradient approximation, we should use an electric field which more closely approximates the real field. Fig. 5.2 suggests that a better approximation than a linearly varying potential (constant gradient) might be a potential of the form

$$\frac{V}{V_0} = \cos(\omega t + \phi_0) \cos\left(\frac{\pi}{L}\left(y - \frac{L}{2}\right)\right) \quad (5.18)$$

where  $L$  is a wavelength which describes the electric field. If we define the average velocity  $v_a = \ell/\tau$  (gap width  $\ell \neq L$ , see below), the equation of motion is, in so far as the actual velocity can be approximated by the

average velocity,

$$\ddot{y} = k\pi \cos(\omega t + \phi_0) \sin \frac{\pi v_a t}{L}. \quad (5.19)$$

Integrating eqn.(5.19) [assuming  $v_a$  is constant] gives

$$\dot{y} - \dot{y}_0 = \frac{k\pi}{2} \left[ \frac{\cos\phi_0 - \cos\left(t(\omega + \pi v_a/L) + \phi_0\right)}{\omega + \pi v_a/L} \right. \quad (5.20)$$

$$\left. + \frac{\cos\left(t(\omega - \pi v_a/L) + \phi_0\right) - \cos\phi_0}{\omega - \pi v_a/L} \right]$$

and

$$y - y_0 = \dot{y}_0 t + \frac{k\pi}{2} \left[ \frac{\sin\phi_0 - \sin\left(t(\omega + \pi v_a/L) + \phi_0\right)}{(\omega + \pi v_a/L)^2} + \frac{t \cos\phi_0}{\omega + \pi v_a/L} \right. \quad (5.21)$$

$$\left. + \frac{\sin\left(t(\omega - \pi v_a/L) + \phi_0\right) - \sin\phi_0}{(\omega - \pi v_a/L)^2} - \frac{t \cos\phi_0}{\omega - \pi v_a/L} \right].$$

It was found that the results were improved if we allowed the gap width ( $\ell$ ) to be less than the wavelength which describes the electric field ( $L$ ). Thus we use only part of one cycle of the sine function to describe the electric field gradient. Of course, if  $\ell < L$ ,  $V_0$  must be increased to

$$\frac{V_0}{\cos\left(\frac{\pi}{L}\left(\frac{\ell}{2} - \frac{L}{2}\right)\right)}$$

to maintain the same total voltage across the gap.

Since  $v_a$  and the time required to cross the gap are both unknown, we must solve eqn.(5.21) for the transit time  $\tau$  when  $\dot{y} - \dot{y}_0 = -\ell$ . We define  $v_a \equiv \ell/\tau$  so the transit time is given by

$$\begin{aligned}
 \ell + y_0 \tau + \frac{k\pi}{2} \left[ \frac{\sin\phi_0 - \sin(\omega\tau + \pi\ell/L + \phi_0)}{(\omega + \pi\ell/L\tau)^2} + \frac{\tau \cos\phi_0}{\omega + \pi\ell/L\tau} \right. \\
 \left. + \frac{\sin(\omega\tau - \pi\ell/L + \phi_0) - \sin\phi_0}{(\omega - \pi\ell/L\tau)^2} - \frac{\tau \cos\phi_0}{\omega - \pi\ell/L\tau} \right] = 0.
 \end{aligned} \quad (5.22)$$

This approximation was compared to the results of numerical integration through the real field as described above for the constant gradient approximation. Over a phase interval of -45 deg to +45 deg and an energy interval of 1 to 100 MeV, the errors for the sine gradient approximation were several times larger than for the constant gradient approximation; hence the sine gradient approach was not pursued further.

#### D. Constant Gradient Approximation with Third Harmonic in the Electric Field

Since it is planned to "flat-top" the RF voltage by adding a small fraction of third harmonic to the fundamental, it is useful to derive the constant gradient approximation for the case where the RF voltage is given by

$$\frac{V}{V_0} = \cos(\omega t + \phi_0) - \epsilon \cos(3\omega t + \phi_0 + \delta). \quad (5.23)$$

$\epsilon$  is the fraction of third harmonic and  $\delta$  is the phase of the third harmonic with respect to the fundamental. The equation of motion in the y-direction is now

$$\ddot{y} = k \left[ \cos(\omega t + \phi_0) - \epsilon \cos(3\omega t + \phi_0 + \delta) \right] \quad (5.24)$$

which when integrated gives

$$\dot{y} - \dot{y}_0 = \frac{k}{\omega} \left[ \sin(\omega t + \phi_0) - \sin\phi_0 - \frac{\epsilon}{3} \left( \sin(3\omega t + \phi_0 + \delta) - \sin(\phi_0 + \delta) \right) \right] \quad (5.25)$$

and

$$y - y_0 = \dot{y}_0 t + \frac{k}{\omega} \left[ -\frac{1}{\omega} \left( \cos(\omega t + \phi_0) - \cos \phi_0 \right) - t \sin \phi_0 \right. \\ \left. + \frac{\epsilon}{3} \left[ \frac{1}{3\omega} \left( \cos(3\omega t + \phi_0 + \delta) - \cos(\phi_0 + \delta) \right) - t \sin(\phi_0 + \delta) \right] \right]. \quad (5.26)$$

The validity of eqns.(5.25) and (5.26) have not been checked by comparison with numerical integration. However, it is reasonable to expect them to be at least as accurate as (5.6) and (5.7) when the RF voltage is not changing more rapidly than it does for the fundamental only. Fortunately, the phase region of interest is precisely where the waveform given by (5.23) is flat, so that eqns.(5.25) and (5.26) should be of as much utility as (5.6) and (5.7).

#### E. Constant Gradient Approximation with Magnetic Field

We now consider the case where the ion being accelerated sees a magnetic field B perpendicular to its plane of motion and an electric field with constant gradient. The equations of motion are

$$\ddot{x} = \frac{q}{m} B \dot{y} \quad (5.27)$$

and

$$\ddot{y} = k \cos(\omega t + \phi_0) - \frac{q}{m} B \dot{x} \quad (5.28)$$

where as before  $k = qV_0/m\lambda$ .

If we assume that the magnetic field is isochronous, then the ion rotation frequency is constant and equal to  $qB/m$ . Integrating eqn.(5.27) once and using  $\omega = NqB/m$  (the RF frequency), we obtain

$$\dot{x} - \dot{x}_0 = \frac{\omega}{N}(y - y_0) \quad (5.29)$$

and

$$\ddot{y} = k \cos(\omega t + \phi_0) - \frac{\omega}{N} \left[ \dot{x}_0 + \frac{\omega}{N}(y - y_0) \right]. \quad (5.30)$$

The solutions to eqns.(5.29) and (5.30) are, for  $N \neq 1$ ,

$$\begin{aligned} x = x_0 - \frac{N}{\omega} \left( \dot{y}_0 + \frac{k}{\omega} \frac{N^2}{1-N^2} \sin\phi_0 \right) \left( \cos\frac{\omega t}{N} - 1 \right) & \quad (5.31) \\ + \frac{N}{\omega} \left( \dot{x}_0 - \frac{k}{\omega} \frac{N}{1-N^2} \cos\phi_0 \right) \sin\frac{\omega t}{N} \\ + \frac{k}{\omega^2} \frac{N}{1-N^2} \left( \sin(\omega t + \phi_0) - \sin\phi_0 \right), \end{aligned}$$

$$\begin{aligned} \dot{x} = \left( \dot{y}_0 + \frac{k}{\omega} \frac{N^2}{1-N^2} \sin\phi_0 \right) \sin\frac{\omega t}{N} & \quad (5.32) \\ + \left( \dot{x}_0 - \frac{k}{\omega} \frac{N}{1-N^2} \cos\phi_0 \right) \cos\frac{\omega t}{N} + \frac{k}{\omega} \frac{N}{1-N^2} \cos(\omega t + \phi_0), \end{aligned}$$

$$\begin{aligned} y = y_0 - \frac{N\dot{x}_0}{\omega} + \frac{N}{\omega} \left( \dot{y}_0 + \frac{k}{\omega} \frac{N^2}{1-N^2} \sin\phi_0 \right) \sin\frac{\omega t}{N} & \quad (5.33) \\ + \frac{N}{\omega} \left( \dot{x}_0 - \frac{k}{\omega} \frac{N}{1-N^2} \cos\phi_0 \right) \cos\frac{\omega t}{N} + \frac{k}{\omega^2} \frac{N^2}{1-N^2} \cos(\omega t + \phi_0), \end{aligned}$$

and

$$\begin{aligned} \dot{y} = \left( \dot{y}_0 + \frac{k}{\omega} \frac{N^2}{1-N^2} \sin\phi_0 \right) \cos\frac{\omega t}{N} & \quad (5.34) \\ - \left( \dot{x}_0 - \frac{k}{\omega} \frac{N}{1-N^2} \cos\phi_0 \right) \sin\frac{\omega t}{N} - \frac{k}{\omega} \frac{N^2}{1-N^2} \sin(\omega t + \phi_0). \end{aligned}$$

The transit time  $\tau$  is given by

$$\begin{aligned} l = \frac{N}{\omega} \left[ -\dot{x}_0 + \left( \dot{y}_0 + \frac{k}{\omega} \frac{N^2}{1-N^2} \sin\phi_0 \right) \sin\frac{\omega\tau}{N} \right. & \quad (5.35) \\ \left. + \left( \dot{x}_0 - \frac{k}{\omega} \frac{N}{1-N^2} \cos\phi_0 \right) \cos\frac{\omega\tau}{N} \right] + \frac{k}{\omega^2} \frac{N^2}{1-N^2} \cos(\omega\tau + \phi_0). \end{aligned}$$

Note that eqn.(5.35) takes into account the increase in path length due to the magnetic field.

Cohen,<sup>3</sup> Comiti<sup>37</sup> and Reiser<sup>38</sup> have derived equations similar to eqns.(5.33) and (5.34), but they give no method for calculating the transit time nor any indication of the accuracy of their approximations.

For the case without a magnetic field, displacements in the x-direction depend on  $p_x$  only, since the electric field produces no component of force in the x-direction. Similarly, when a magnetic field is present the change in  $p_x$  should be that due to the magnetic field only, as if the electric field were not present. That this is true is verified by the work of Comiti<sup>37</sup> and by the results of numerical integration in the present case.

The energy gains predicted by eqn.(5.34) and those obtained from numerical integration are given in Table VI. The value of  $\ell$  (the gap width) used was the one chosen for the zero magnetic field case, i.e. 8.97 in. The differences in the gap factor  $G$  are shown in Fig. 5.6. The errors in this case are about ten times larger than for the case where no magnetic field was present. This is possibly due to the fact that the curvature of the ion path causes the ion to spend more time near the edges of the field where the constant gradient approximation is least accurate. However, over the region of interest ( $-30 \text{ deg} < \phi < +30 \text{ deg}$  and  $E > 5 \text{ MeV}$ ), the errors are still less than 1%. Fig. 5.7 shows the phase variation of the error in  $G$ . A more accurate description of the energy gain could be obtained by fitting some function to the curves shown in Fig. 5.7 and using this as a correction to the energy gain predicted by eqn.(5.34).

The errors in timing caused by assuming that the change in energy occurs discontinuously at the centre of the gap are about 1.5 deg (RF) at -45 deg and 1 MeV, 0.2 deg at 0 deg and 1 MeV, decreasing rapidly with energy (<0.01 deg at 100 MeV).

TABLE VI

Gap factors given by numerical integration and by the constant gradient approximation (isochronous magnetic field)

Energy (MeV)	-45		-30		-15		0		+15		+30		+45	
	N	IA	N	IA										
1	75.487	78.126	77.009	78.654	78.199	79.124	79.207	79.510	80.118	79.795	81.026	79.965	82.086	80.013
2	86.375	88.681	87.395	88.844	88.166	88.991	88.824	89.115	89.454	89.208	90.131	89.265	90.990	89.284
5	93.836	95.345	94.459	95.378	94.919	95.409	95.318	95.437	95.709	95.459	96.151	95.475	96.745	95.484
10	96.590	97.634	97.028	97.643	97.352	97.652	97.631	97.661	97.908	97.669	98.225	97.676	98.652	97.681
20	98.080	98.791	98.390	98.793	98.618	98.795	98.816	98.798	99.013	98.801	99.240	98.804	99.547	98.807
50	99.064	99.489	99.264	99.488	99.411	99.488	99.539	99.489	99.667	99.489	99.814	99.491	100.014	99.493
100	99.429	99.722	99.577	99.721	99.685	99.720	99.778	99.720	99.872	99.721	99.979	99.722	100.126	99.724

N = numerically integrated results

IA = results from iterative approximation

In the present case (with a magnetic field), there is an apparent displacement of the ion due to the change of radius of curvature. The numerical integration of the ion orbit is done over a distance  $d$  in the  $y$ -direction. If the radius of curvature before the gap is  $\rho_1$ , and after the gap is  $\rho_2$ , the displacement we would expect from  $y = \frac{d}{2}$  to  $y = -\frac{d}{2}$ , if the change in radius of curvature occurs discontinuously at the centre of the gap with no displacement along the gap, is

$$\begin{aligned} \Delta x &= \rho_2 \cos \left( \sin^{-1}(d/2\rho_2) \right) - (\rho_2 - \rho_1) - \rho_1 \cos \left( \sin^{-1}(d/2\rho_1) \right) \\ &\approx \frac{d^2}{8} \left( \frac{1}{\rho_1} - \frac{1}{\rho_2} \right). \end{aligned} \quad (5.36)$$

In Fig. 5.8 the values of  $\Delta x$  found from eqn.(5.36) are compared with the numerically tracked orbits. The agreement is excellent. This means that  $\delta x$ , the displacement of the orbit at the dee gap, is effectively zero, and the energy gain results in a displacement of the centre of curvature.

Thus, in this case as in the case where no magnetic field was present, we approximate the effect of the gap by instantaneous changes at the centre line of the gap as follows:  $\delta E$  is the energy change corresponding to the velocity change given by eqn.(5.34),  $\delta t$  and  $\delta x$  are given zero values, and  $\delta \xi$  is the "collimation" given by eqn.(5.17).

#### F. Constant Gradient Approximation with Magnetic Field and Third Harmonic in the Electric Field

Using the RF voltage given by eqn.(5.23) and including the effects of an isochronous magnetic field, the equations of motion are

$$\dot{x} - \dot{x}_0 = \frac{\omega}{N} (y - y_0) \quad (5.37)$$

and

$$\ddot{y} + \frac{\omega^2}{N^2} y + \frac{\omega}{N} \left( \dot{x}_0 - \frac{\omega}{N} y_0 \right) = k \left( \cos(\omega t + \phi_0) - \varepsilon \cos(3\omega t + \phi_0 + \delta) \right). \quad (5.38)$$

For  $N \neq 1$ , the solutions to eqns. (5.37) and (5.38) are

$$\begin{aligned} \dot{x} = & \left[ \dot{y}_0 + \frac{k}{\omega} N^2 \left( \frac{\sin \phi_0}{1-N^2} - \frac{3\varepsilon}{1-9N^2} \sin(\phi_0 + \delta) \right) \right] \sin\left(\frac{\omega t}{N}\right) \\ & + \left[ \dot{x}_0 - \frac{k}{\omega} N \left( \frac{\cos \phi_0}{1-N^2} - \frac{\varepsilon}{1-9N^2} \cos(\phi_0 + \delta) \right) \right] \cos\left(\frac{\omega t}{N}\right) \\ & + \frac{k}{\omega} \frac{N}{1-N^2} \cos(\omega t + \phi_0) - \frac{\varepsilon k}{\omega} \frac{N}{1-9N^2} \cos(3\omega t + \phi_0 + \delta), \end{aligned} \quad (5.39)$$

$$\begin{aligned} x - x_0 = & -\frac{N}{\omega} \left[ \dot{y}_0 + \frac{k}{\omega} N^2 \left( \frac{\sin \phi_0}{1-N^2} - \frac{3\varepsilon}{1-9N^2} \sin(\phi_0 + \delta) \right) \right] \left[ \cos\left(\frac{\omega t}{N}\right) - 1 \right] \\ & + \frac{N}{\omega} \left[ \dot{x}_0 - \frac{k}{\omega} N \left( \frac{\cos \phi_0}{1-N^2} - \frac{\varepsilon}{1-9N^2} \cos(\phi_0 + \delta) \right) \right] \sin\left(\frac{\omega t}{N}\right) \\ & - \frac{1}{\omega^2} \frac{kN}{1-N^2} \left( \sin(\omega t + \phi_0) - \sin \phi_0 \right) \\ & - \frac{1}{3\omega^2} \frac{\varepsilon k N}{1-9N^2} \left( \sin(3\omega t + \phi_0 + \delta) - \sin(\phi_0 + \delta) \right), \end{aligned} \quad (5.40)$$

$$\begin{aligned} \dot{y} = & \left[ \dot{y}_0 + \frac{k}{\omega} N^2 \left( \frac{\sin \phi_0}{1-N^2} - \frac{3\varepsilon}{1-9N^2} \sin(\phi_0 + \delta) \right) \right] \cos\left(\frac{\omega t}{N}\right) \\ & - \left[ \dot{x}_0 - \frac{k}{\omega} N \left( \frac{\cos \phi_0}{1-N^2} - \frac{\varepsilon}{1-9N^2} \cos(\phi_0 + \delta) \right) \right] \sin\left(\frac{\omega t}{N}\right) \\ & - \frac{k}{\omega} \frac{N^2}{1-N^2} \sin(\omega t + \phi_0) + \frac{3\varepsilon k}{\omega} \frac{N^2}{1-9N^2} \sin(3\omega t + \phi_0 + \delta), \end{aligned} \quad (5.41)$$

$$y - y_0 = -\frac{N\dot{x}_0}{\omega} + \frac{N}{\omega} \left[ \dot{y}_0 + \frac{k}{\omega} N^2 \left( \frac{\sin \phi_0}{1-N^2} - \frac{3\varepsilon}{1-9N^2} \sin(\phi_0 + \delta) \right) \right] \sin\left(\frac{\omega t}{N}\right) \quad (5.42)$$

.....

$$\begin{aligned}
& + \frac{N}{\omega} \left[ \dot{x}_0 - \frac{k}{\omega} N \left( \frac{\cos \phi_0}{1-N^2} - \frac{\epsilon}{1-9N^2} \cos(\phi_0 + \delta) \right) \right] \cos\left(\frac{\omega t}{N}\right) \\
& + \frac{k}{\omega^2} \frac{N^2}{1-N^2} \cos(\omega t + \phi_0) - \frac{\epsilon k}{\omega^2} \frac{N^2}{1-9N^2} \cos(3\omega t + \phi_0 + \delta).
\end{aligned}$$

These equations have not been compared to the results of numerical integrations, but the differences should be comparable to those quoted in the previous section over the region of interest.

## CHAPTER 6. SUMMARY AND CONCLUSIONS

The motion of the ions at the centre of a cyclotron has been studied with particular reference to the TRIUMF cyclotron.<sup>6</sup> The object was to investigate the factors determining the phase acceptance and beam quality of the cyclotron, and to consider how the design might be adjusted to optimize these quantities.

The calculation of both axial and radial motion requires knowledge of the electric and magnetic fields. The magnetic fields used were measured on model magnets. The electric fields were calculated by numerically solving Laplace's equation using the relaxation method. The convergence and accuracy of this method was investigated in detail. Numerically solving a problem for which the solution could be found analytically showed that the numerical solution contained average errors less than 0.01%. The method uses a novel feature to obtain accurate starting values for the iteration, and the solution time for a very large problem ( $2 \times 10^6$  data points) is about 3 hours on an IBM 360/67.

The axial motions were studied using the thick lens description of the dee gaps developed by Rose,<sup>1</sup> Cohen<sup>3</sup> and Reiser.<sup>22</sup> A method was developed for calculating the axial acceptance of the accelerator as a function of RF phase. It was found that the axial acceptance exhibits a sharp cut-off at about -5 deg, i.e. ions with phases more negative than -5 deg cannot be accelerated. This effect results because, for negative phases, the field is rising, and the field variation effect causes the dee gaps to defocus the ions. This effect is more important for TRIUMF than for other cyclotrons because the RF operates at the fifth harmonic of the ion frequency, causing the electric forces to be much stronger. The negative phase limit can be shifted to more negative values by flat-topping

the RF waveform. This flat-topping can be produced by adding some third harmonic of the RF frequency to the fundamental waveform. It is shown that addition of 12% of third harmonic in phase with the fundamental shifts the cut-off due to the field variation effect to about -15 deg. This situation can be further improved by adding 15% of third harmonic shifted 10 deg from the fundamental. For this case the negative phase limit is shifted to about -25 deg.

The effect of field bumps is investigated. For the case of TRIUMF a radially decreasing field bump at the cyclotron centre cannot produce enough axial focusing to overcome the strong electric forces. However, a carefully designed field bump can be used to shift the phases of the ions. It is shown how to design a field bump to shift those phases initially favoured by electric focusing (positive phases) into phase with the peak of the RF voltage when electric focusing is less important. This is done without shifting the ions to phases where they are defocused by the electric field.

The radial motions of the ions in the first turn were studied to find the best position of the injection gap. A position close to 36 deg back along the orbit from the main gap was found to provide the best centring and phase histories.

To allow economical orbit tracking out to high energies, an analytic description of the changes in radial orbit properties on crossing a dee gap was developed. The results of this approximation differ from the exact changes (found by numerical integration) by less than 1% for energies above 5 MeV.

The beam centring was studied by tracking ions through realistic electric and magnetic fields (to 5 MeV), then to 20 MeV by integrating

through the magnetic field and using the approximation mentioned above. The results of these orbit tracks showed that the transformation of the radial beam ellipse is quite phase dependent. This may be reduced by reducing phase-dependent effects at the dee gaps. The energy resolution of the beam is investigated by tracking ions to 20 MeV. The radial oscillations present at 20 MeV are reduced by a factor of about 1.5 during acceleration to 500 MeV due to adiabatic compression. The finite emittance of the beam also worsens the energy resolution by  $\pm 300$  keV.

If the ion with initial RF phase of 0 deg is centred large radial oscillations develop for ions with other initial RF phases. For example, if we require an energy resolution of  $\pm 600$  keV, then half of this can be allowed to the coherent radial oscillations, meaning that the oscillation amplitude allowed is 0.05 in. at 500 MeV or 0.07 in. at 20 MeV. This allows a phase acceptance of 16 deg. For an energy resolution of  $\pm 1200$  keV the phase acceptance is 26 deg. For the case where large duty cycle is required, the largest phase acceptance is obtained if an ion in the centre of the phase interval is centred (rather than the ion with 0 deg initial phase). For  $\pm 1200$  keV energy resolution, for example, the phase acceptance can be increased to -17 deg to +26 deg by centring the ion with initial phase of 17 deg.

In summary, the axial motions place a positive limit  $>60$  deg on the phase acceptance. The negative limit is -5 deg without third harmonic, -15 deg with 12% of third harmonic in phase with the fundamental, and -25 deg with 15% of third harmonic shifted by 10 deg from the fundamental. The radial motions allow a phase acceptance of -8 deg to +6 deg for an energy resolution of  $\pm 600$  keV or -17 deg to +26 deg for an energy resolution of  $\pm 1200$  keV, in both cases with RF fundamental only.

## REFERENCES

1. M.E. Rose, "Focusing and Maximum Energy of Ions in the Cyclotron", Phys. Rev. (Ser. II) 53, 392 (1938)
2. D. Böhm and L.L. Foldy, "Theory of the Synchro-Cyclotron", Phys. Rev. (Ser. II) 72, 649 (1947)
3. B.L. Cohen, "The Theory of the Fixed Frequency Cyclotron", Rev. Sci. Instr. 24, 589 (1953)
4. M. Reiser, "Initial Acceleration and Radial Focusing in the Non-uniform Electric Field at the Ion Source of the Cyclotron", Michigan State University Cyclotron Project, Report MSUCP-16 (1963)
5. W.B. Powell and B.L. Reece, "Injection of Ions into a Cyclotron from an External Source", Nucl. Instr. Meth. 32, 325 (1965)
6. E.W. Vogt and J.J. Burgerjon, editors, "TRIUMF Proposal and Cost Estimate" (1966)
7. G.M. Stinson *et al.*, "Electric Dissociation of H<sup>-</sup> Ions by Magnetic Fields", TRI-69-1 (1969)
8. T.E. Zinneman, "Three-dimensional Electrolytic Tank Measurements and Vertical Motion Studies in the Central Region of a Cyclotron", University of Maryland, Department of Physics and Astronomy, Technical Report No. 986 (1969)
9. D. Vitkovitch, *Field Analysis* (D. van Nostrand, London, 1966), 205
10. V.P. Pronin and A.N. Safonov, "Measurement of the Electrical Field in the Central Region of the Dubna Synchrocyclotron by the Induced Current Method", Communications of the Joint Institute for Nuclear Research, Dubna, No. JINR-P9-4851 (1969)
11. J.M. van Nieuwland, H.L. Hagedoorn, N. Hazewindus and P. Kramer, "Magnetic Analogue of Electric Field Configurations Applied to the Central Region of an AVF Cyclotron", Rev. Sci. Instr. 39, 1054-5 (1968)
12. G.E. Forsythé and W.R. Wasow, *Finite-Difference Methods for Partial Differential Equations* (J. Wiley, New York, 1960)
13. D. Nelson, H. Kim and M. Reiser, "Computer Solutions for Three-Dimensional Electromagnetic Field Geometries", IEEE Trans. Nucl. Sci. NS-16, 766 (1969)
14. D. Nelson, "The Relaxation Code - Solutions of Laplace's Equation for Non-Analytical Three-Dimensional Geometries", University of Maryland, Department of Physics and Astronomy, Technical Report No. 960 (1969)
15. D.W. Peaceman and H.H. Rachford, Jr., "The Numerical Solution of Parabolic and Elliptic Differential Equations", J. Soc. Ind. Appl. Math. 3, 28 (1955)

16. D. Young, "The Numerical Solution of Elliptic and Parabolic Partial Differential Equations" in *Modern Mathematics for the Engineer: Second Series*, ed. E. Bedanbach (McGraw-Hill, New York, 1961), 373-419
17. C. Han, private communication, July 25, 1969
18. J.R. Richardson, "Sector-Focusing Cyclotrons" in *Progress in Nuclear Techniques & Instrumentation*, Vol.1, ed. F.M. Farley (North-Holland, Amsterdam, 1965), 3-101
19. M. Reiser, "Space charge effects and current limitations in cyclotrons", IEEE Trans. Nucl. Sci. NS-13, 171 (1966)
20. F. Kottler, "Elektrostatik der Leiter" in *Handbuch der Physik*, Vol. 12, ed. W. Westphal (J. Springer, Berlin, 1927), 466-85
21. R.L. Murray and L.R. Ratner, "Electric Fields within Cyclotron Dees", J. Appl. Phys. 24, 67 (1953)
22. M. Reiser, "First-Order Theory of Electrical Focusing in Cyclotron-Type Two-Dimensional Lenses with Static and Time-Varying Potential", University of Maryland, Department of Physics and Astronomy, Technical Report No. 70-125 (1970)
23. C. Han, "Computer Results for the Focal Properties of Two- and Three-Dimensional Electric Lenses with Time-Varying Fields", University of Maryland, Department of Physics and Astronomy, Technical Report No. 70-126 (1970)
24. S. Penner, "Calculations of Properties of Magnetic Deflection Systems", Rev. Sci. Instr. 32, 150 (1961)
25. K.G. Steffen, *High Energy Beam Optics* (Interscience, New York, 1965)
26. A.P. Banford, *The Transport of Charged Particle Beams* (E. Spon, London, 1965)
27. K.L. Erdman *et al.*, "A 'Square-Wave' RF System Design for the TRIUMF Cyclotron" in Proceedings, International Cyclotron Conference, 5th, Oxford, 1969 (Butterworths, London, to be published)
28. L. Smith and A.A. Garren, "Diagnosis and Correction of Beam Behaviour in an Isochronous Cyclotron", Proc. International Conference on Sector-focused Cyclotrons & Meson Factories, Geneva, 1963 (CERN, Geneva 1963)
29. L. Root and E.W. Blackmore, private communication (1970)
30. M. Reiser and J. Kopf, "Electrolytic Tank Facility and Computer Program for Central Region Studies for the MSU Cyclotron", Michigan State University Cyclotron Project, Report No. MSUCP-19 (1964)
31. W. Walkinshaw and N.M. King, "Linear Dynamics in Spiral Ridge Cyclotron Design", Atomic Energy Research Establishment, Harwell, England, Report No. AERE-GP/R-2050 (1956)

32. M.K. Craddock and J.R. Richardson, "Magnetic Field Tolerances for a Six-Sector 500 MeV  $H^-$  Cyclotron"; TRIUMF Report TRI-67-2 (1968)
33. M.M. Gordon, "The Electric Gap-crossing Resonance in a Three-sector Cyclotron" in Proceedings, International Conference on Sector-focused Cyclotrons, Los Angeles, 1962, (North-Holland, Amsterdam, 1962), 268-80
34. A.A. van Kranenburg, H.L. Hagedoorn, P. Kramer and D. Wierds, "Beam Properties of Philips' AVF Cyclotrons", IEEE Trans. Nucl. Sci., NS-13, 41-7 (1966)
35. G.H. Mackenzie, "Orbit Dynamic Calculations for TRIUMF", to be published (IEEE Trans. Nucl. Sci., NS-18, 1971)
36. C.E. Froberg, *Introduction to Numerical Analysis* (Addison-Wesley, Reading, Mass., 1965)
37. S. Comiti and R. Giannini, "Etude de la géométrie centrale du synchrocyclotron avec source 'calutron' à extraction haute fréquence", CERN Report No. 70-9 (1970)
38. M. Reiser, "Central Orbit Program for a Variable Energy Multi-Particle Cyclotron", Nucl. Instr. & Meth. 18,19, 370 (1962)
39. S.P. Frankel, "Convergence Rates of Iterative Treatments of Partial Differential Equations", Math. Comput. 4, 65 (1950)
40. D. Young, "Iterative Methods for Solving Partial Difference Equations of Elliptic Type", Trans. Amer. Math. Soc. 76, 92 (1954)
41. R. Courant, "Partielle Differenzengleichungen und Differentialgleichungen", in Atti, International Congress of Mathematicians (New Series), 3rd, Bologna, 1928 (Bologna, N. Zanichelli, 1929)

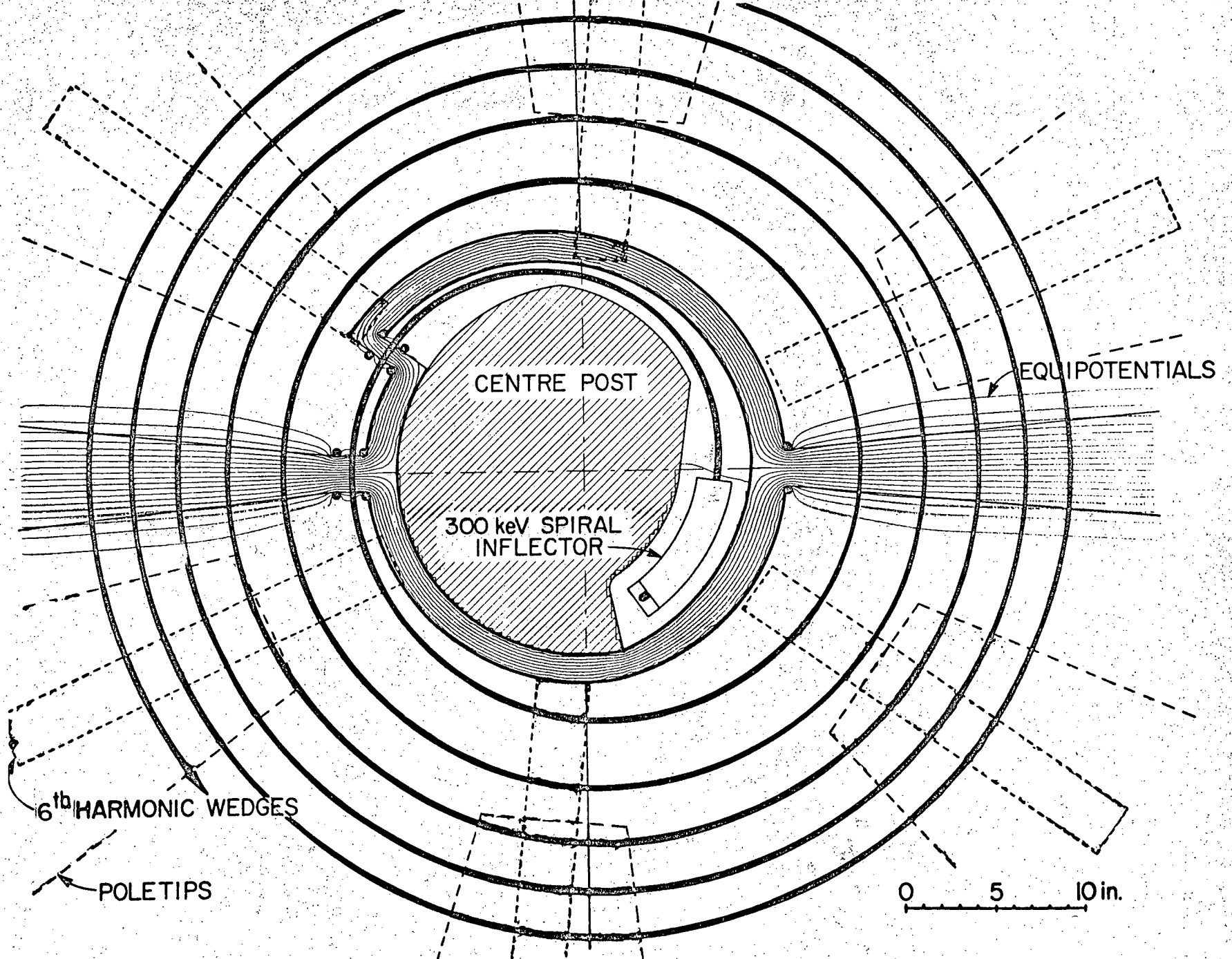


Fig. 1.1 Central region of the TRIUMF cyclotron - median plane

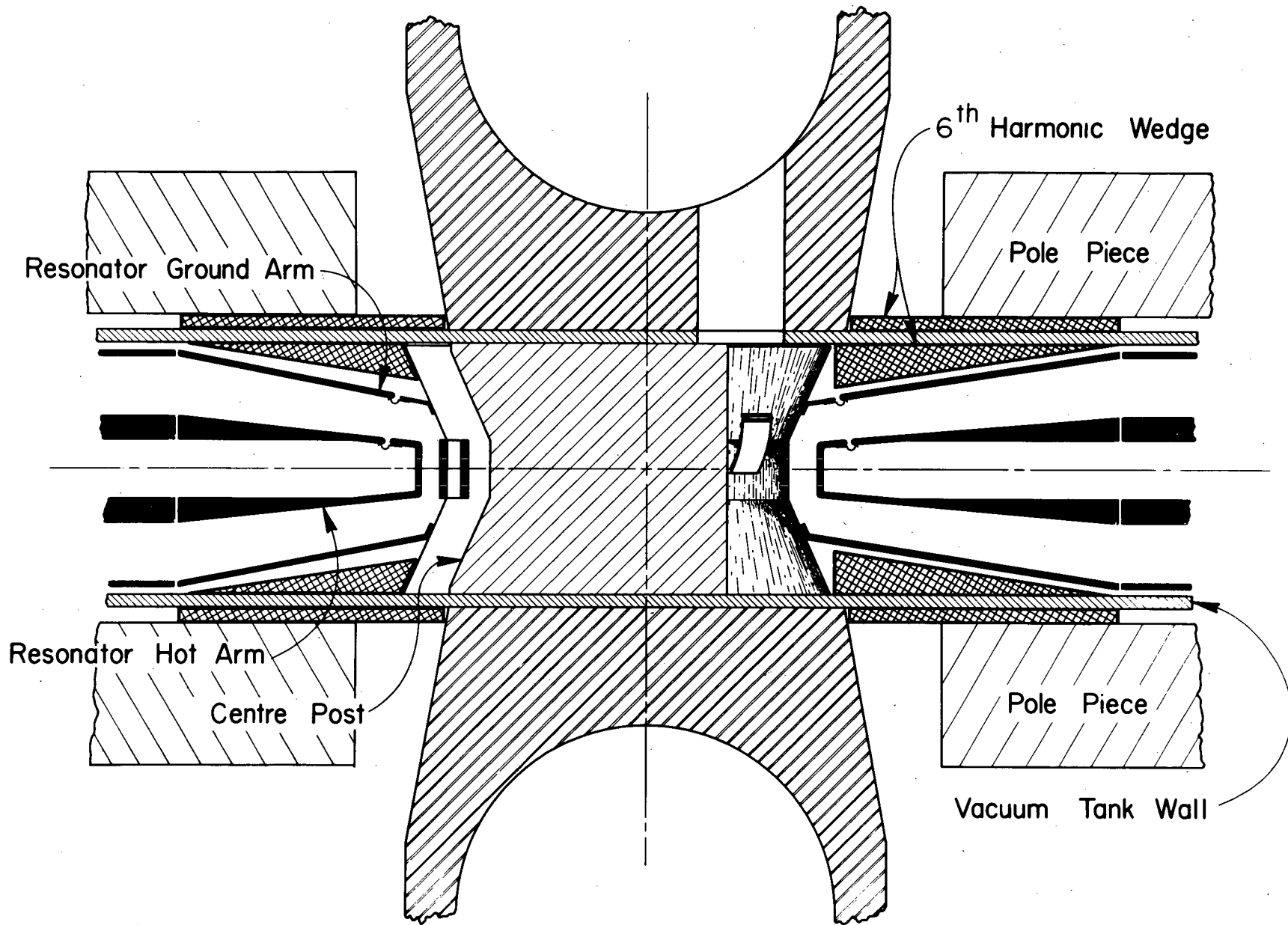


Fig. 1.2 Central region of the TRIUMF cyclotron - section through centreline of hill #3

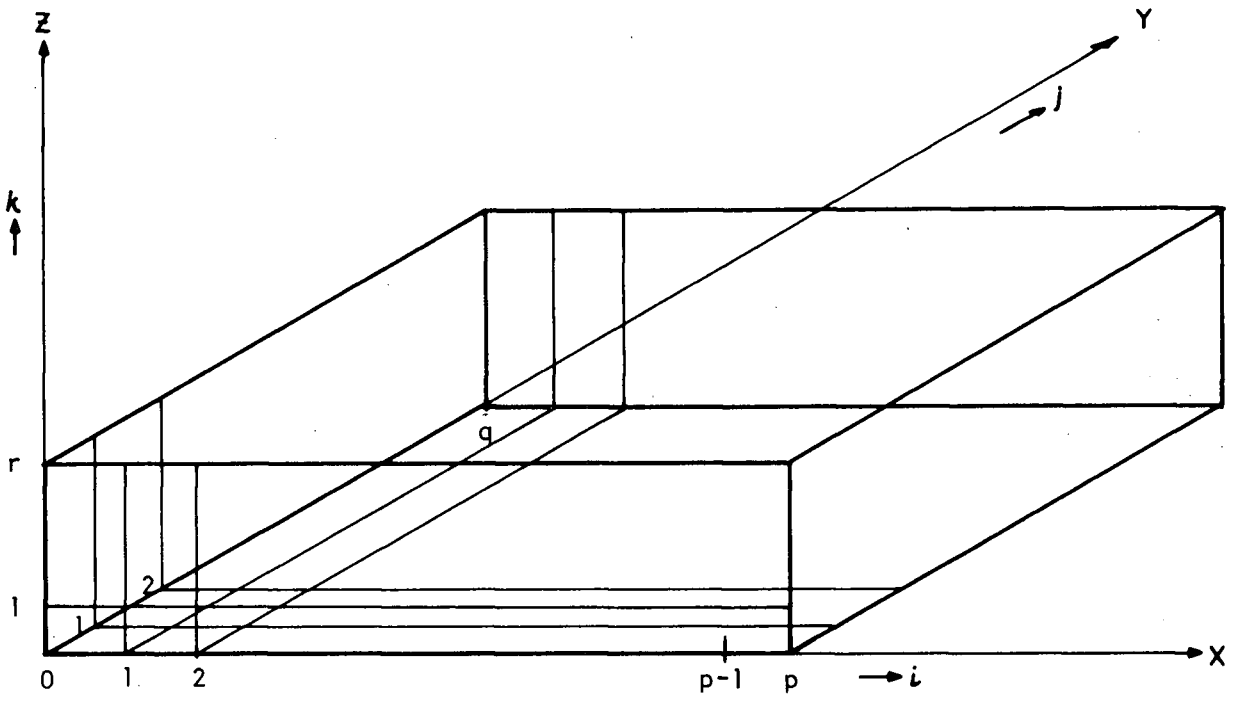


Fig. 2.1 Relaxation Mesh Organization. Total number of nodes is  $(p+1)(q+1)(r+1)$ .

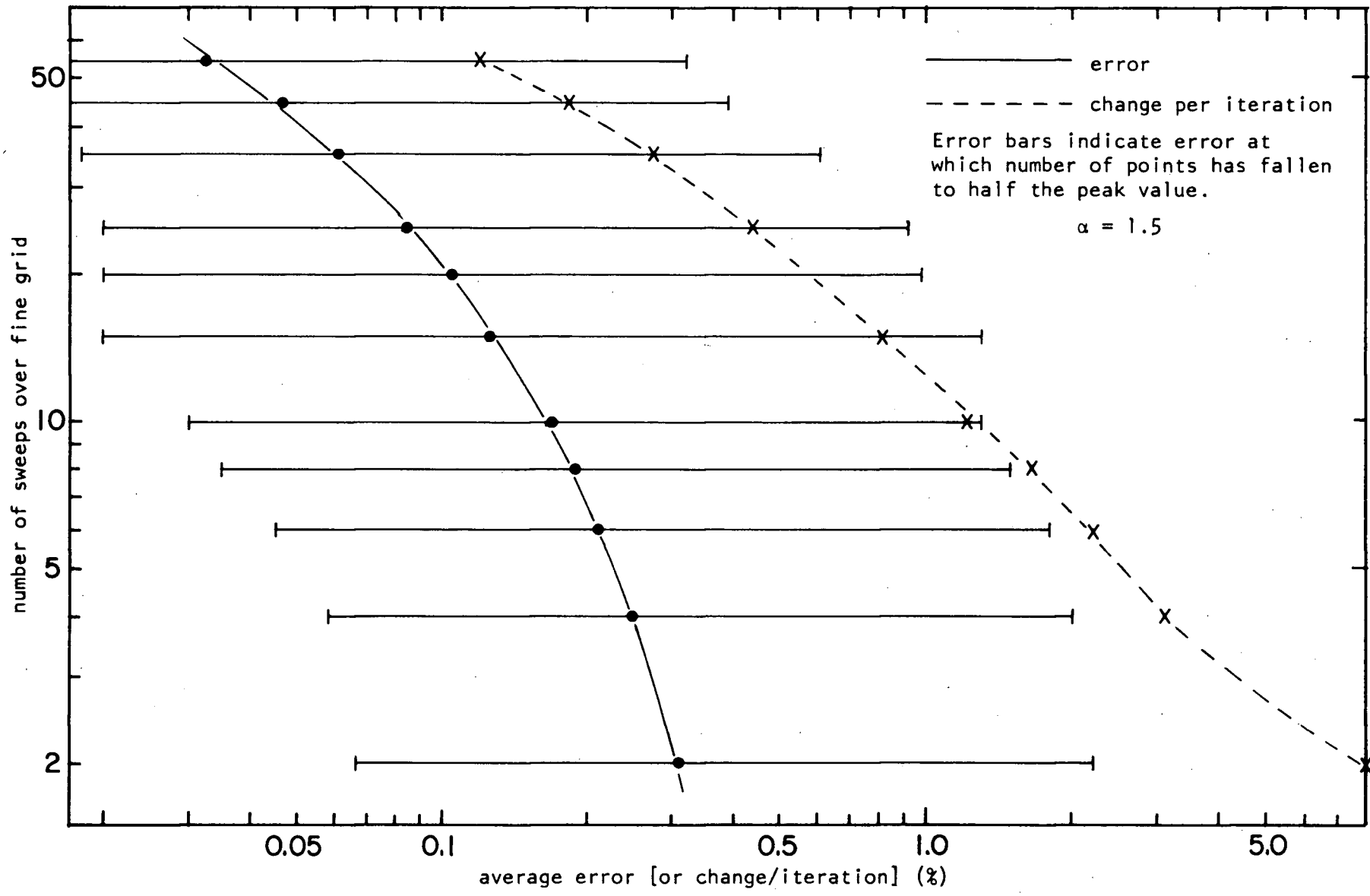


Fig. 2.2 Average error and average change per iteration vs number of sweeps over large volume

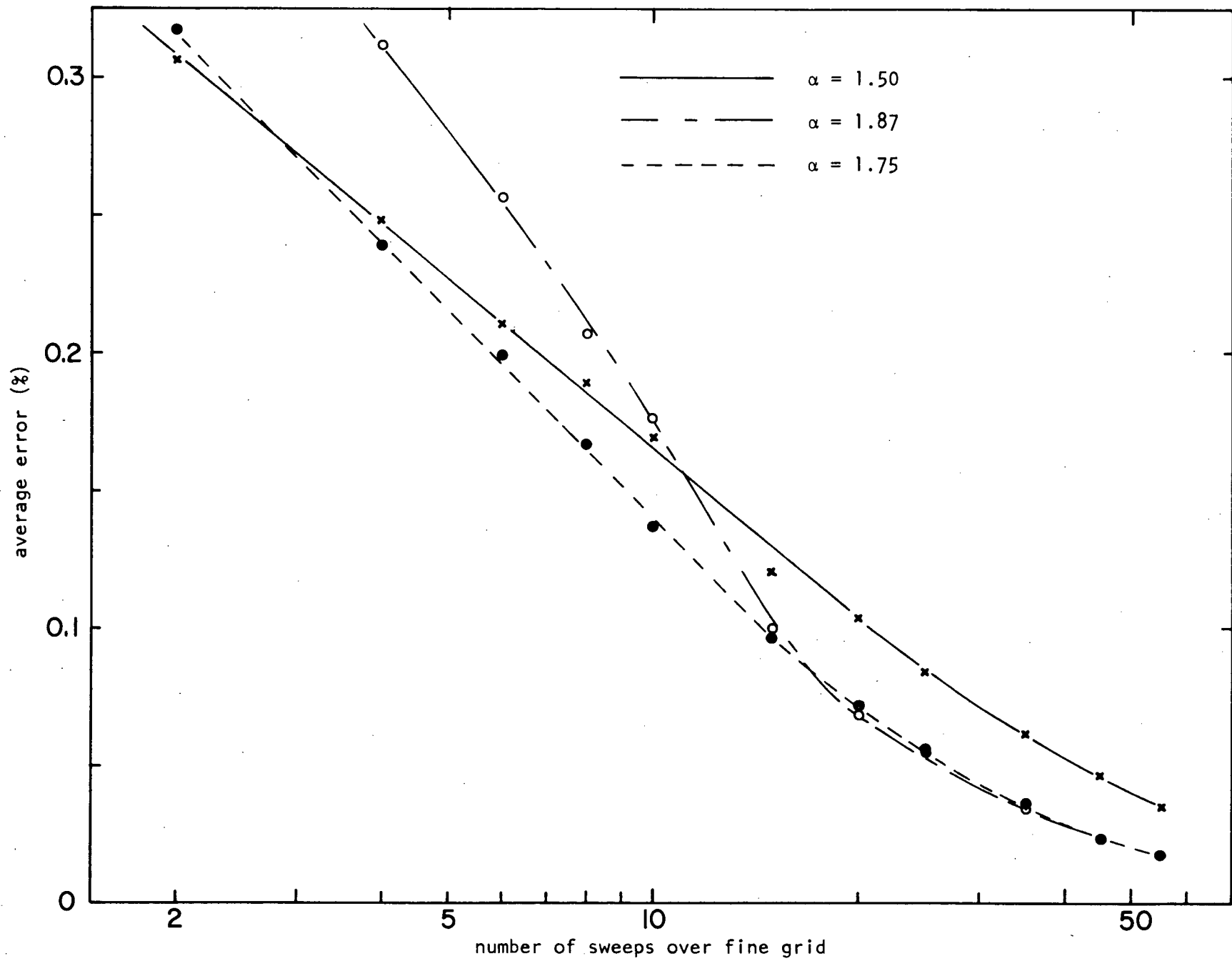


Fig. 2.3 Average error vs number of sweeps over large volume for various values of  $\alpha$

number of nodes with error indicated

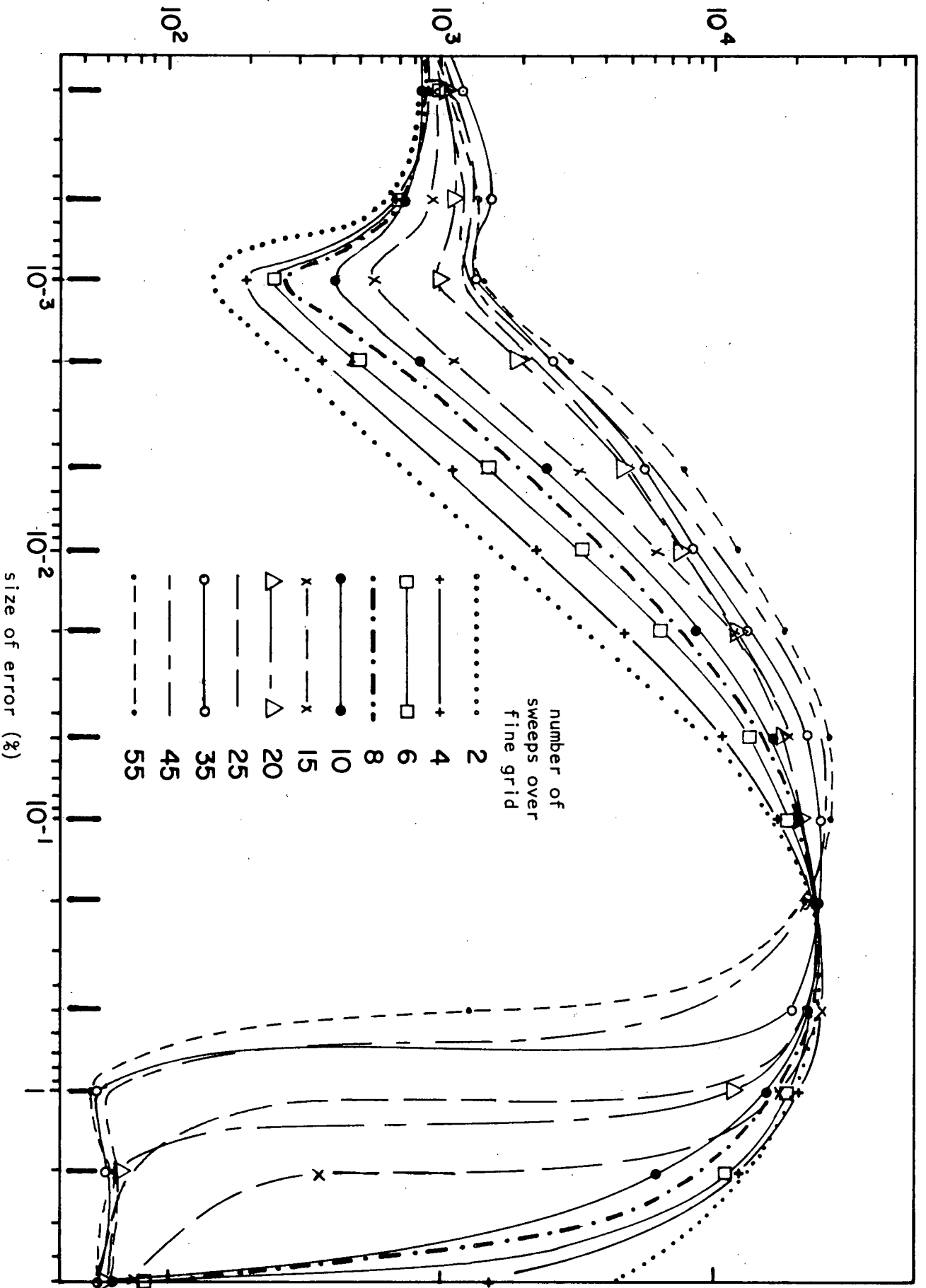


Fig. 2.4 Number of nodes with a given error vs size of error for various number of sweeps over large volume

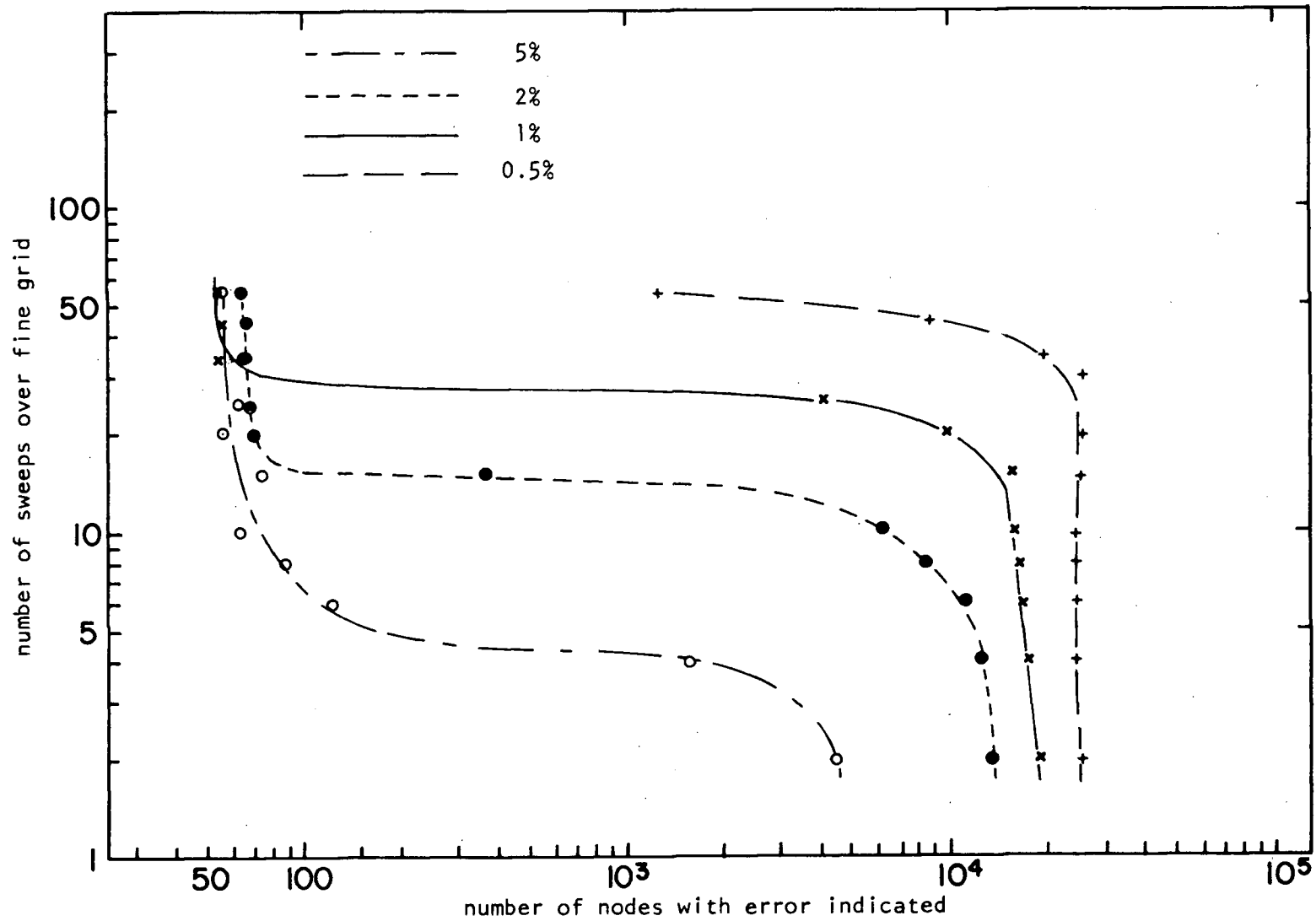


Fig. 2.5 Number of nodes with a given error vs number of sweeps over large volume for various size errors

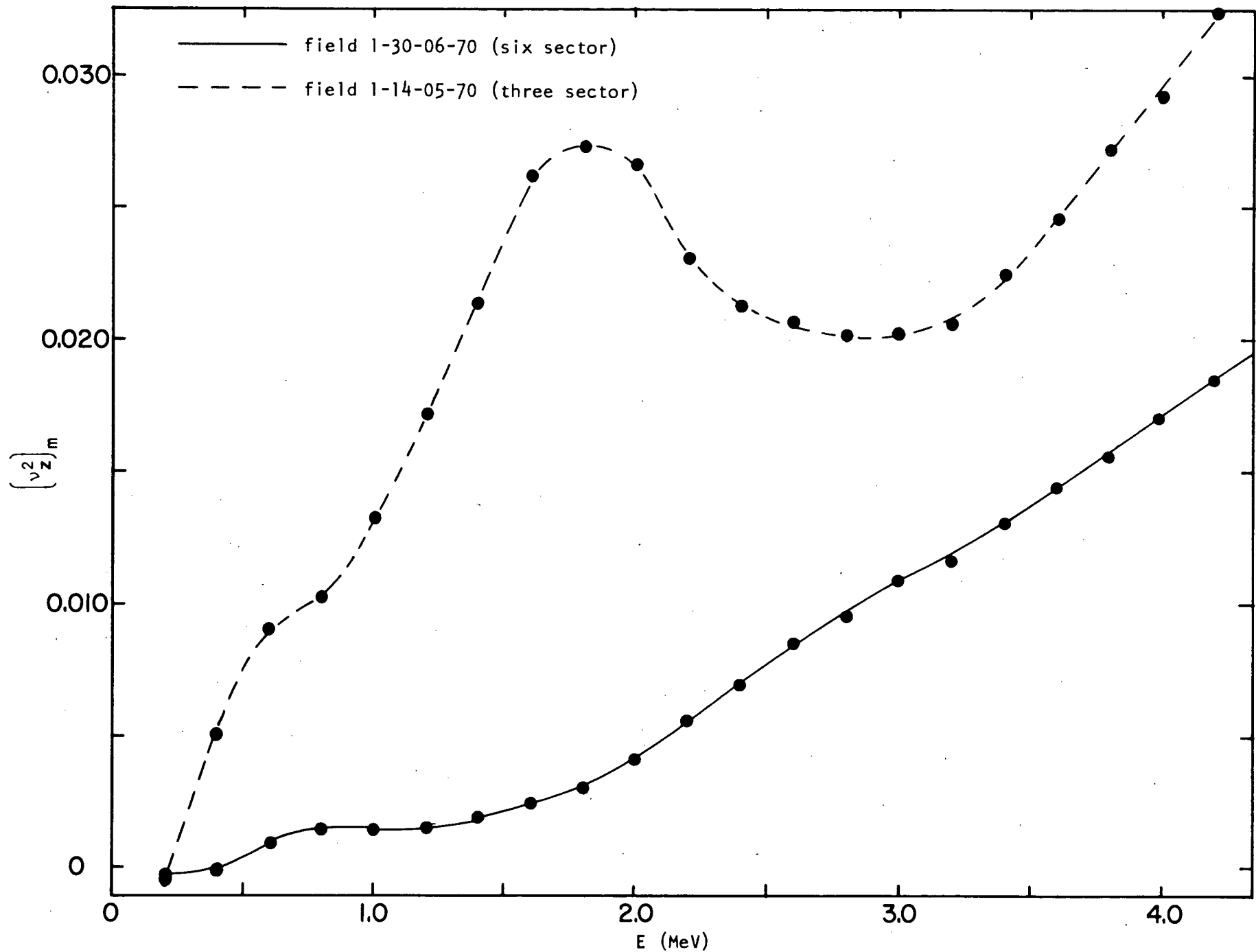


Fig. 3.1 Magnetic axial focusing frequency  $(v_z^2)$  vs energy for three- and six-sector magnetic geometries

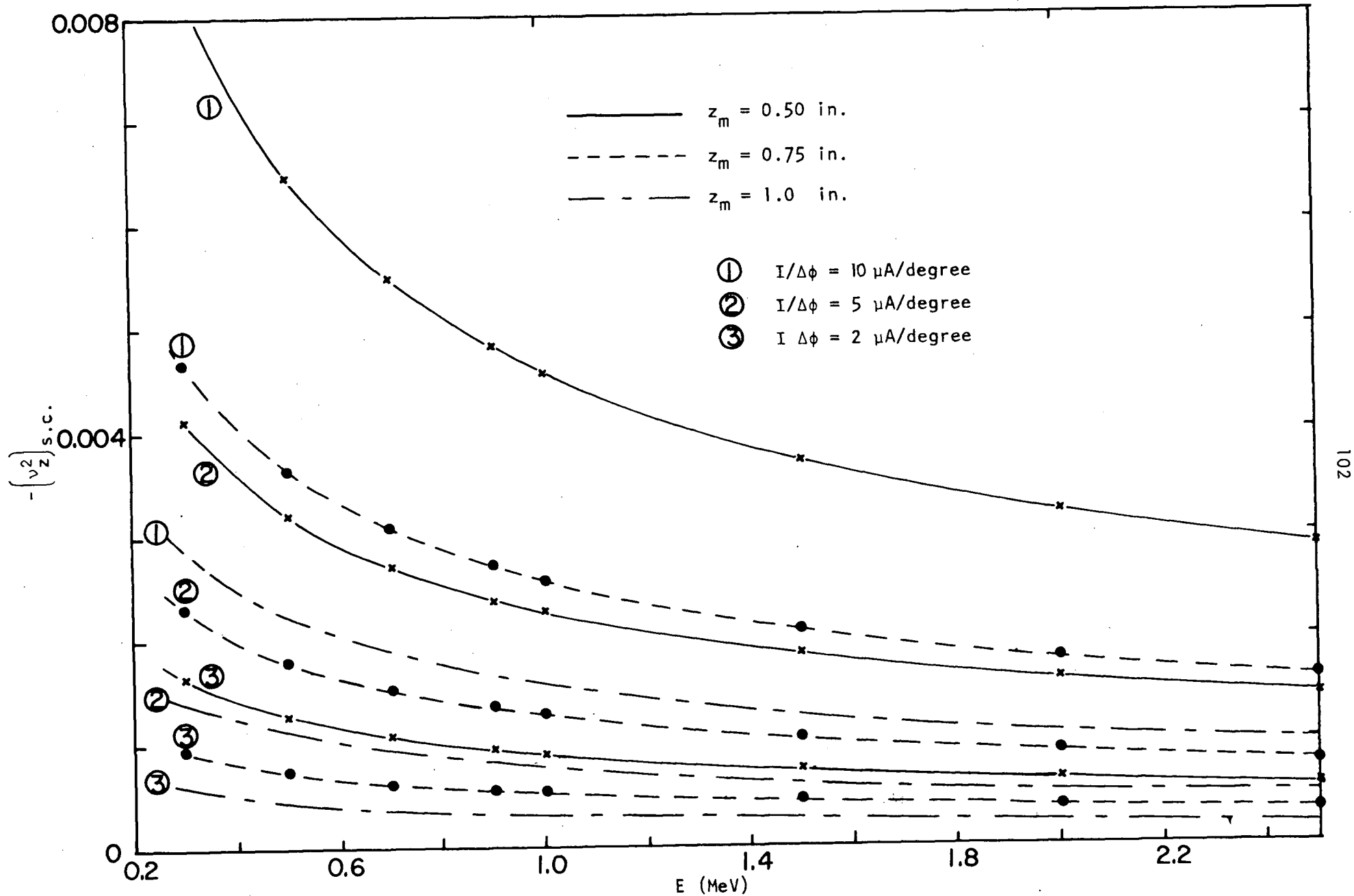


Fig. 3.2 Equivalent axial focusing frequency produced by space charge forces vs energy for various beam currents and axial beam heights

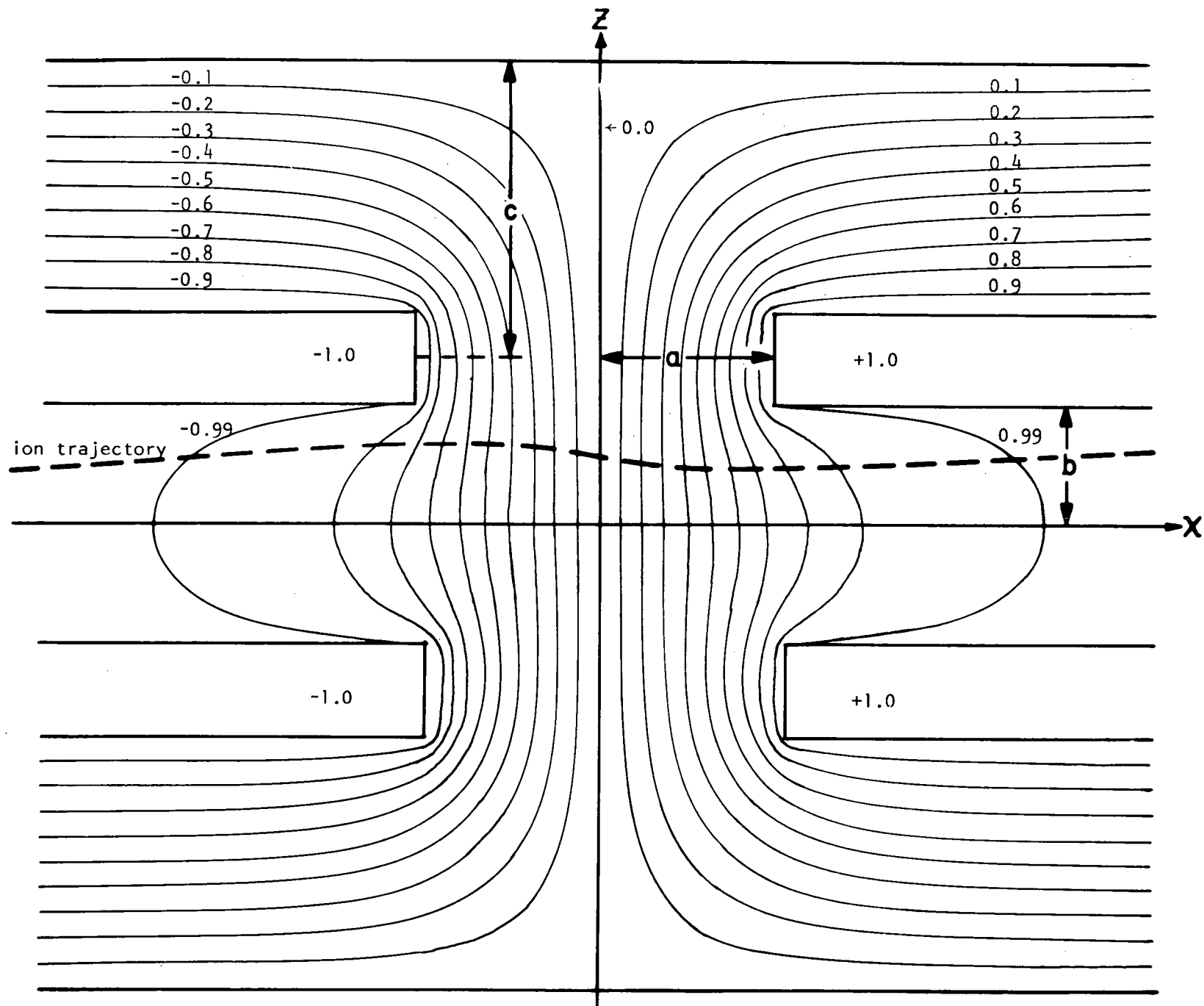


Fig.3.3 Cross-section of dees near accelerating region showing electric equipotentials and (schematically) an ion trajectory

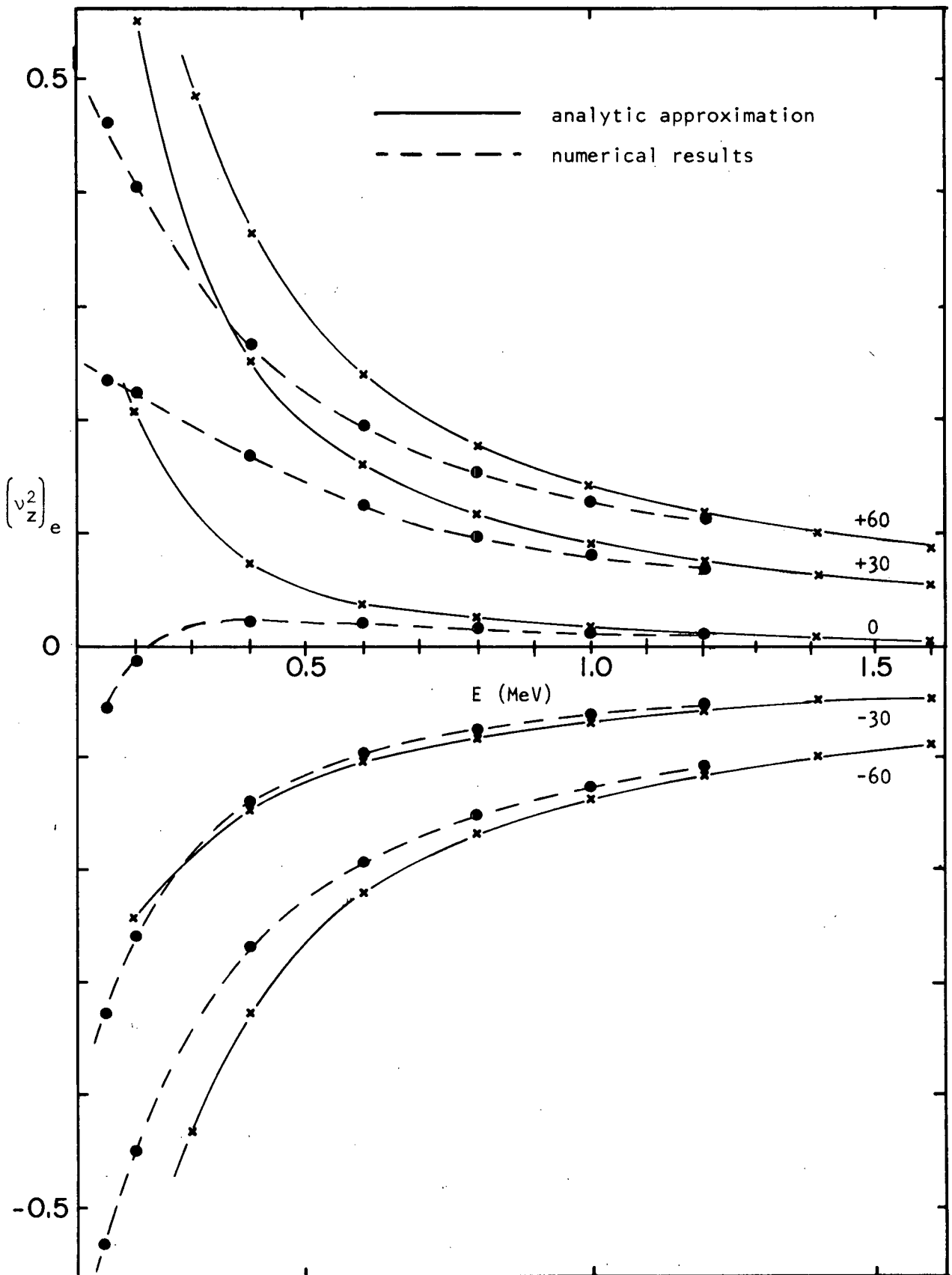


Fig. 3.4 Comparison between equivalent electric axial focusing frequencies predicted by the thin lens approximation and determined by numerical integration

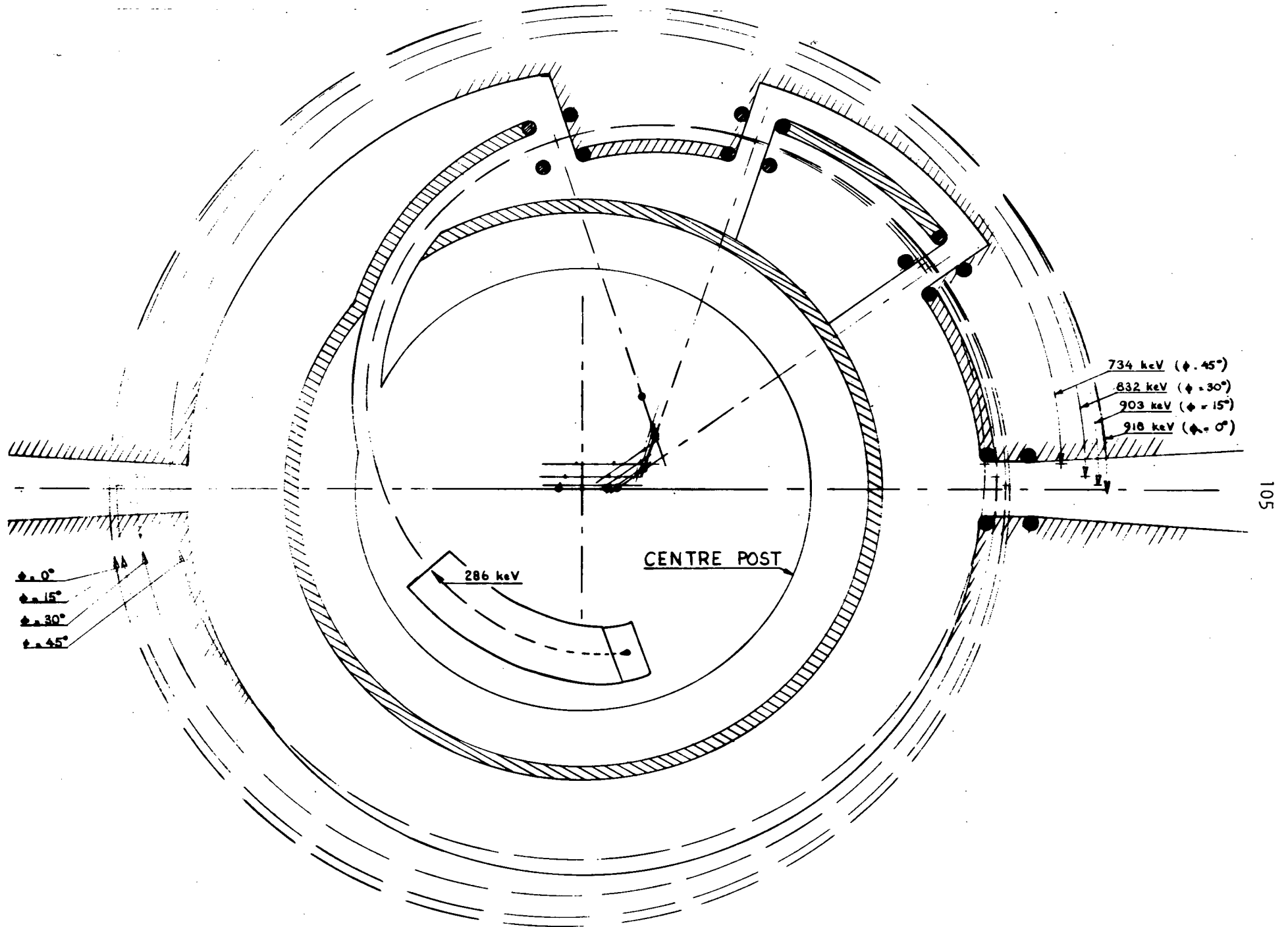


Fig. 3.5 Possible TRIUMF central geometry with three accelerating gaps in the first half-turn

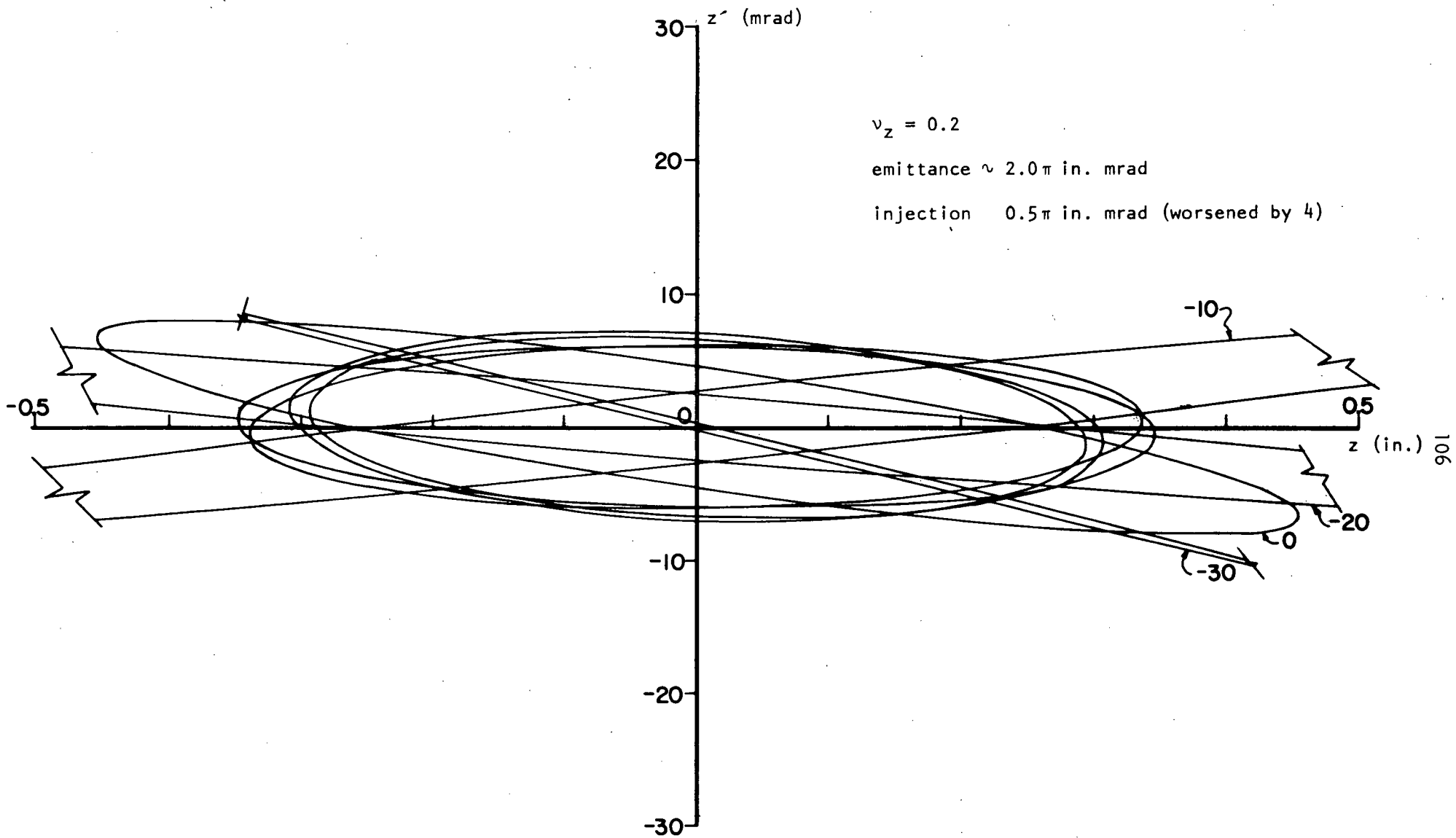


Fig. 3.6 Axial emittance ellipses required at injection for various RF phases

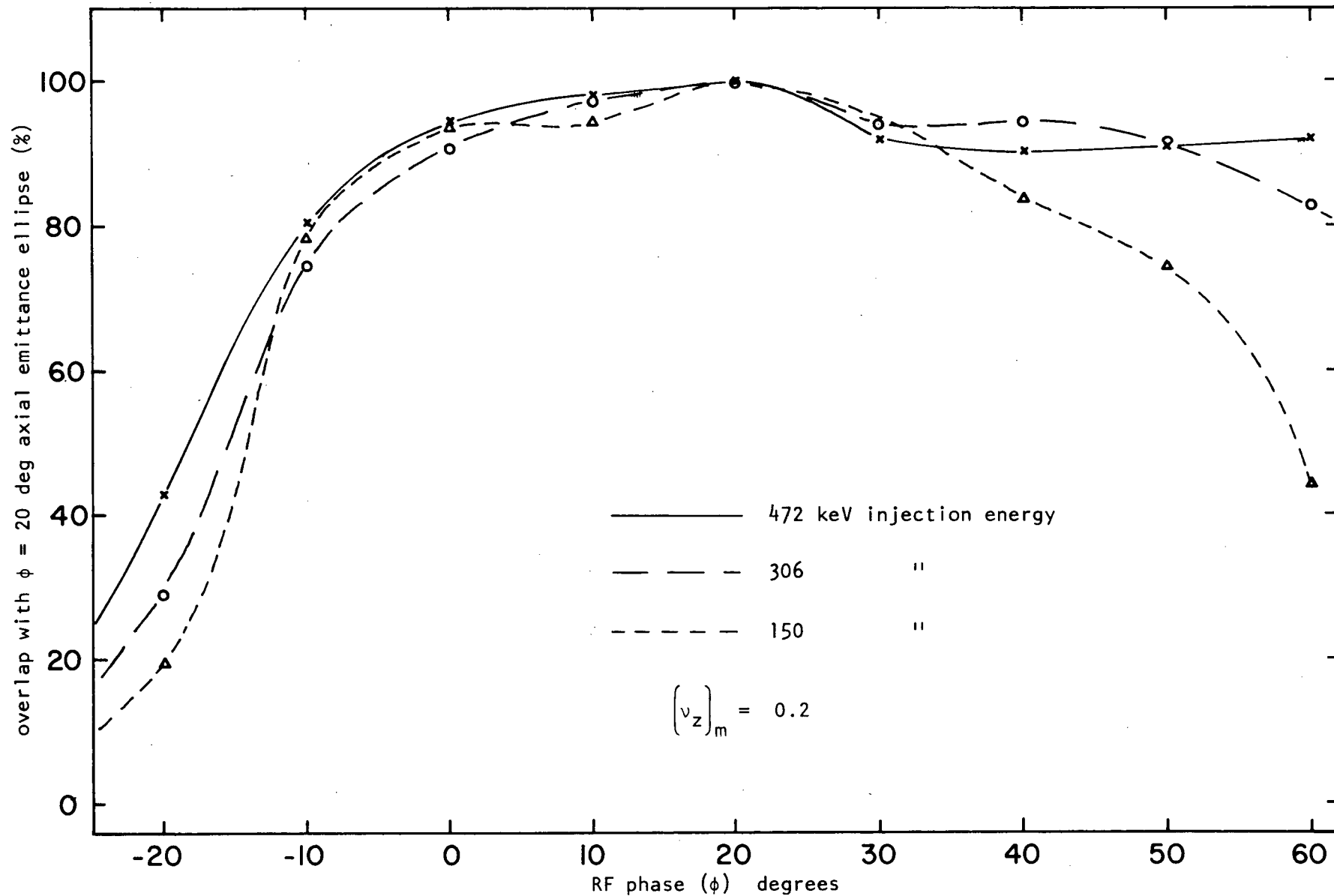


Fig. 3.7 Axial acceptance vs RF phase for various injection energies (one accelerating gap in the first half-turn)

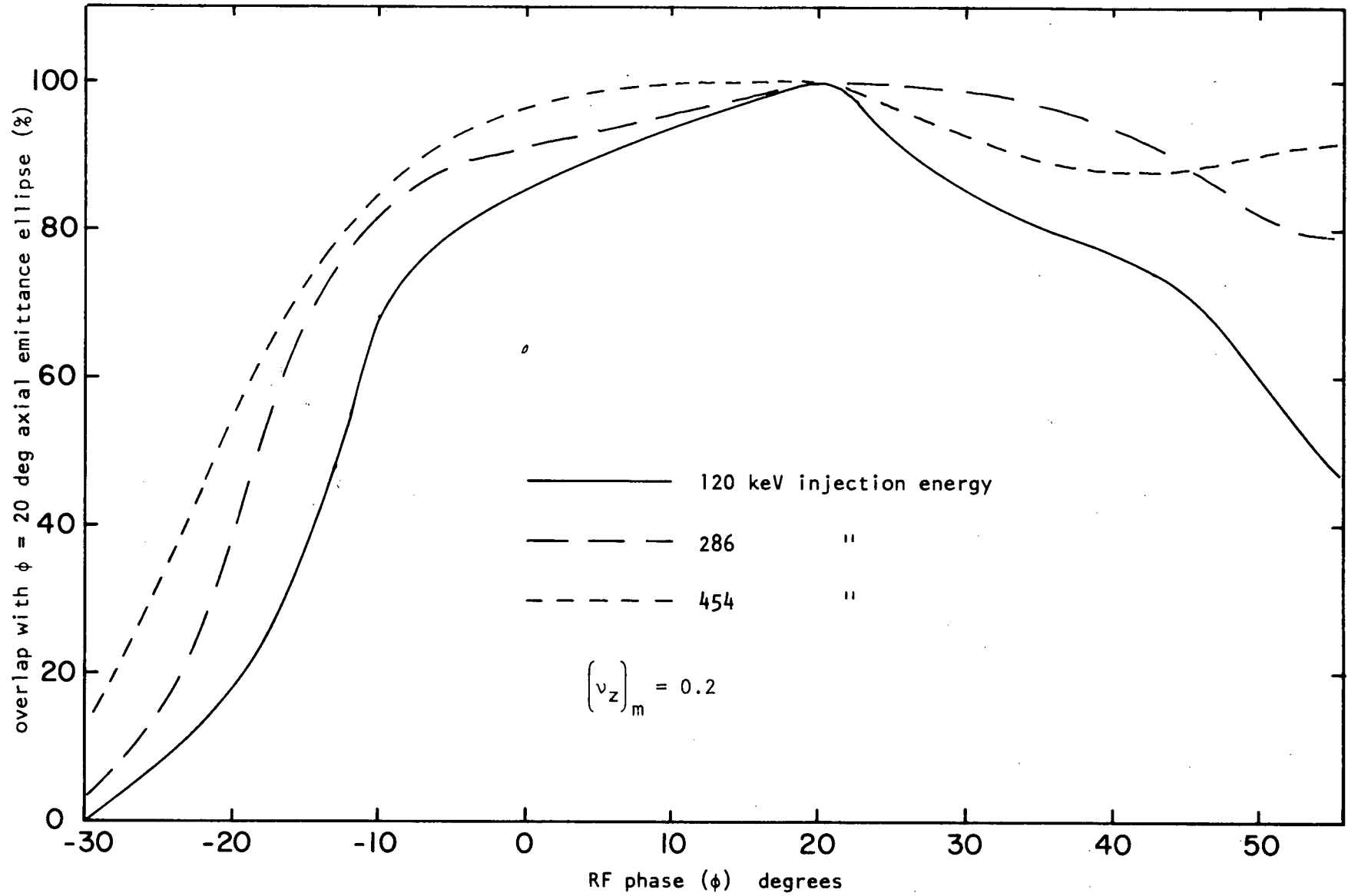


Fig. 3.8 Axial acceptance vs RF phase for various injection energies (three accelerating gaps in the first half-turn)

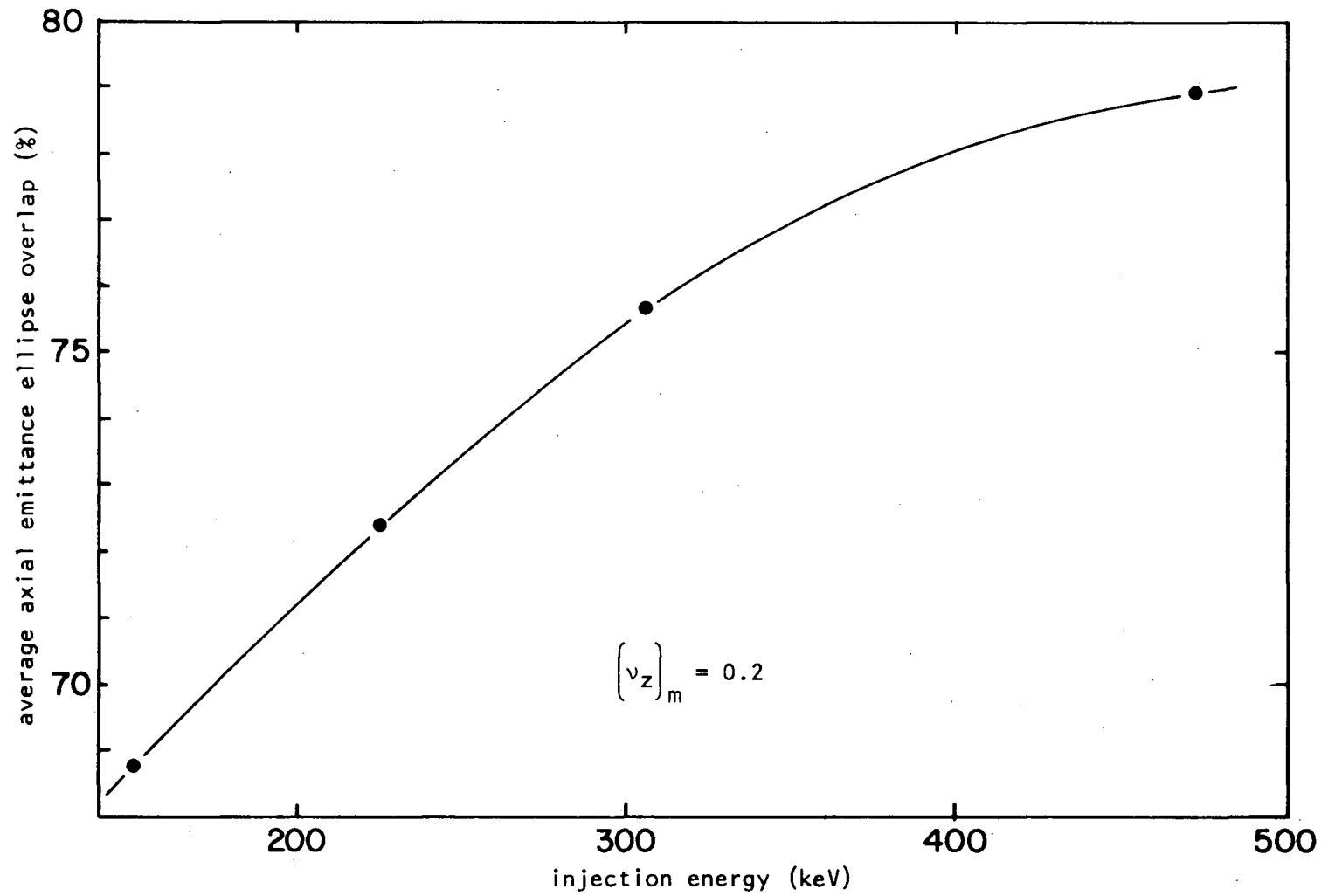


Fig. 3.9 Average axial acceptance (averaged from -30 deg to +60 deg) vs injection energy (one accelerating gap in the first half-turn)

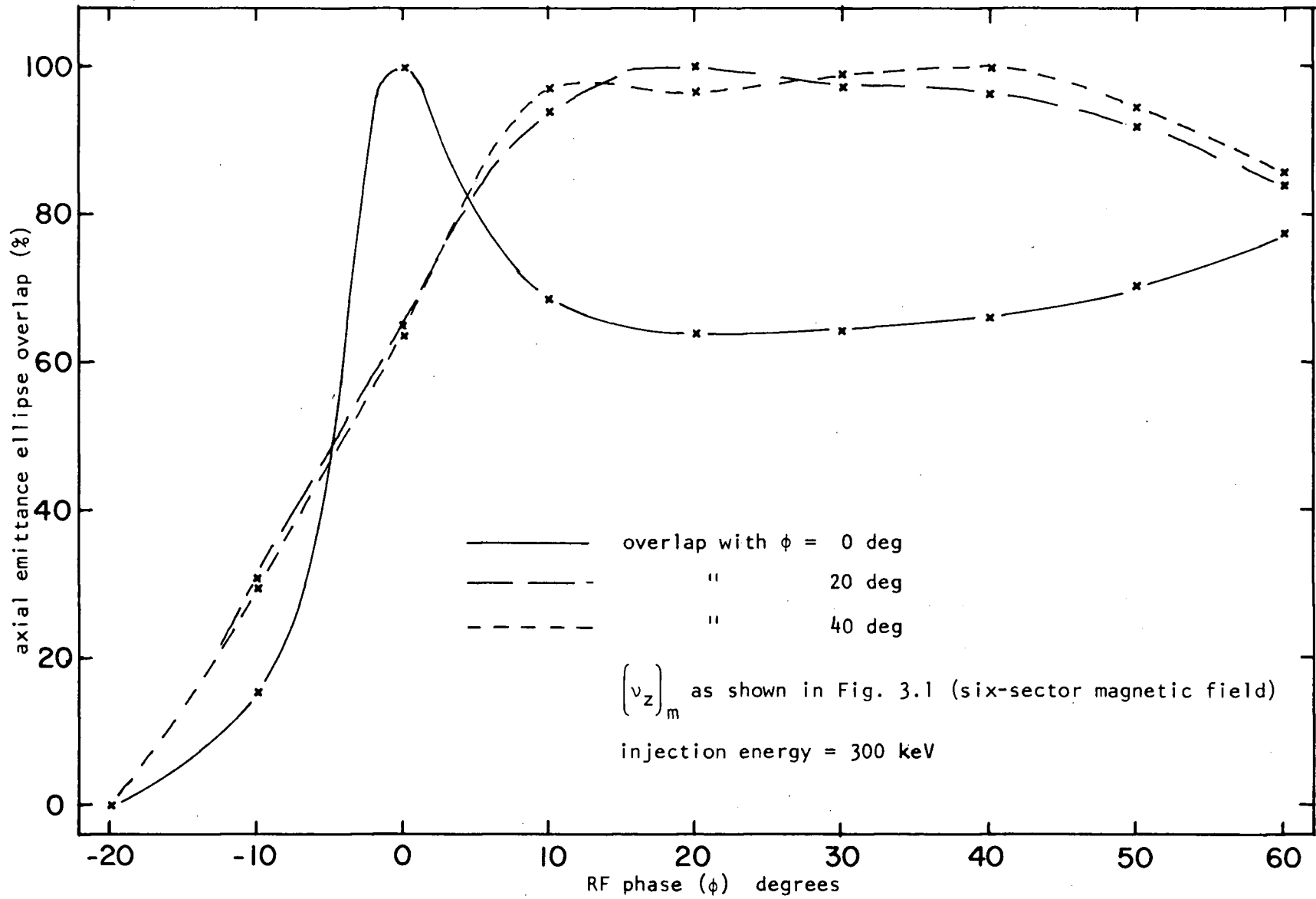


Fig. 3.10. Axial acceptance vs RF phase for various choices of the initial emittance ellipse

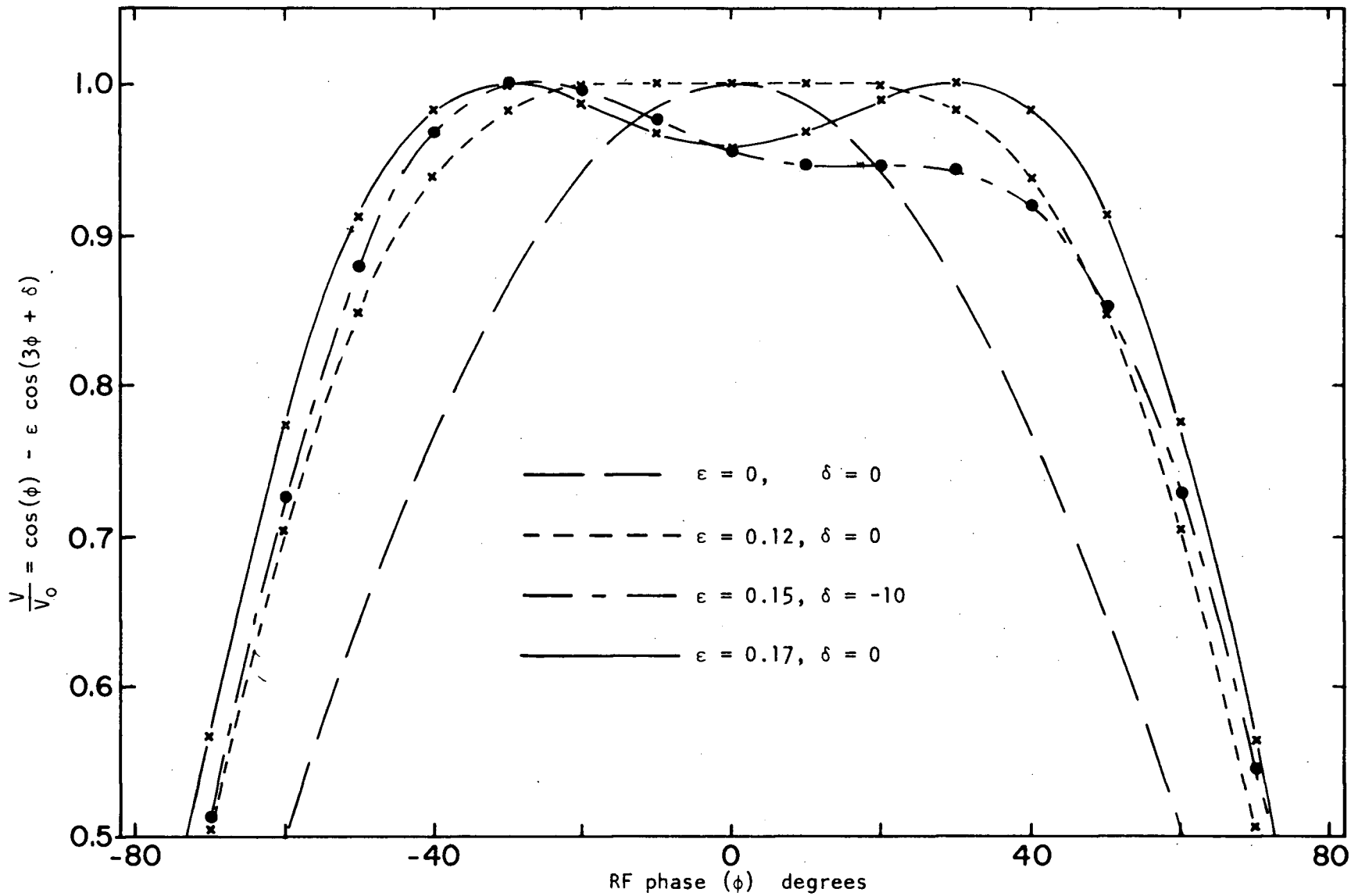


Fig. 3.11 RF voltage waveforms with various amounts of third harmonic and phase shift between fundamental and third harmonic

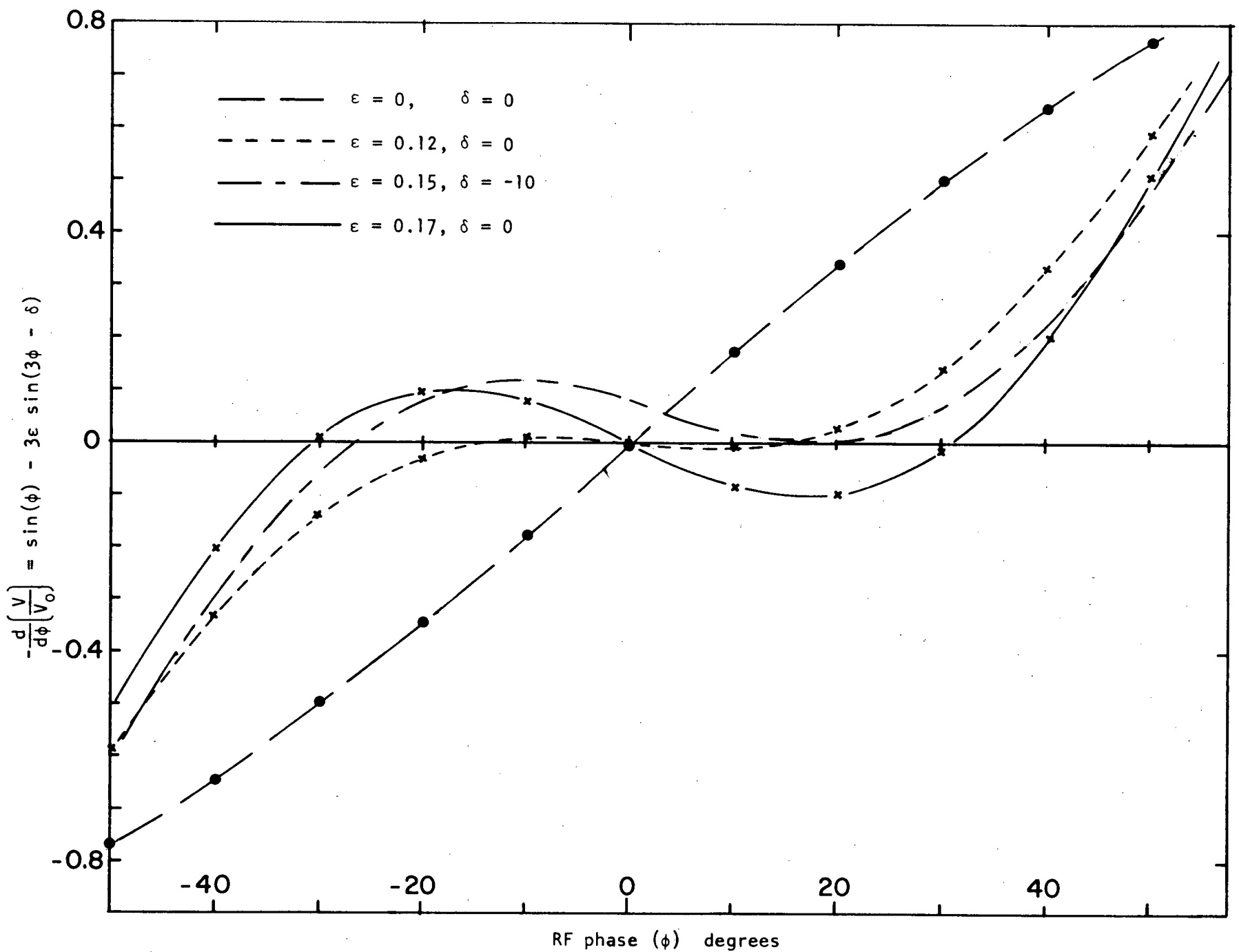


Fig. 3.12 Slope of RF voltage waveform with various amounts of third harmonic and phase shift between fundamental and third harmonic

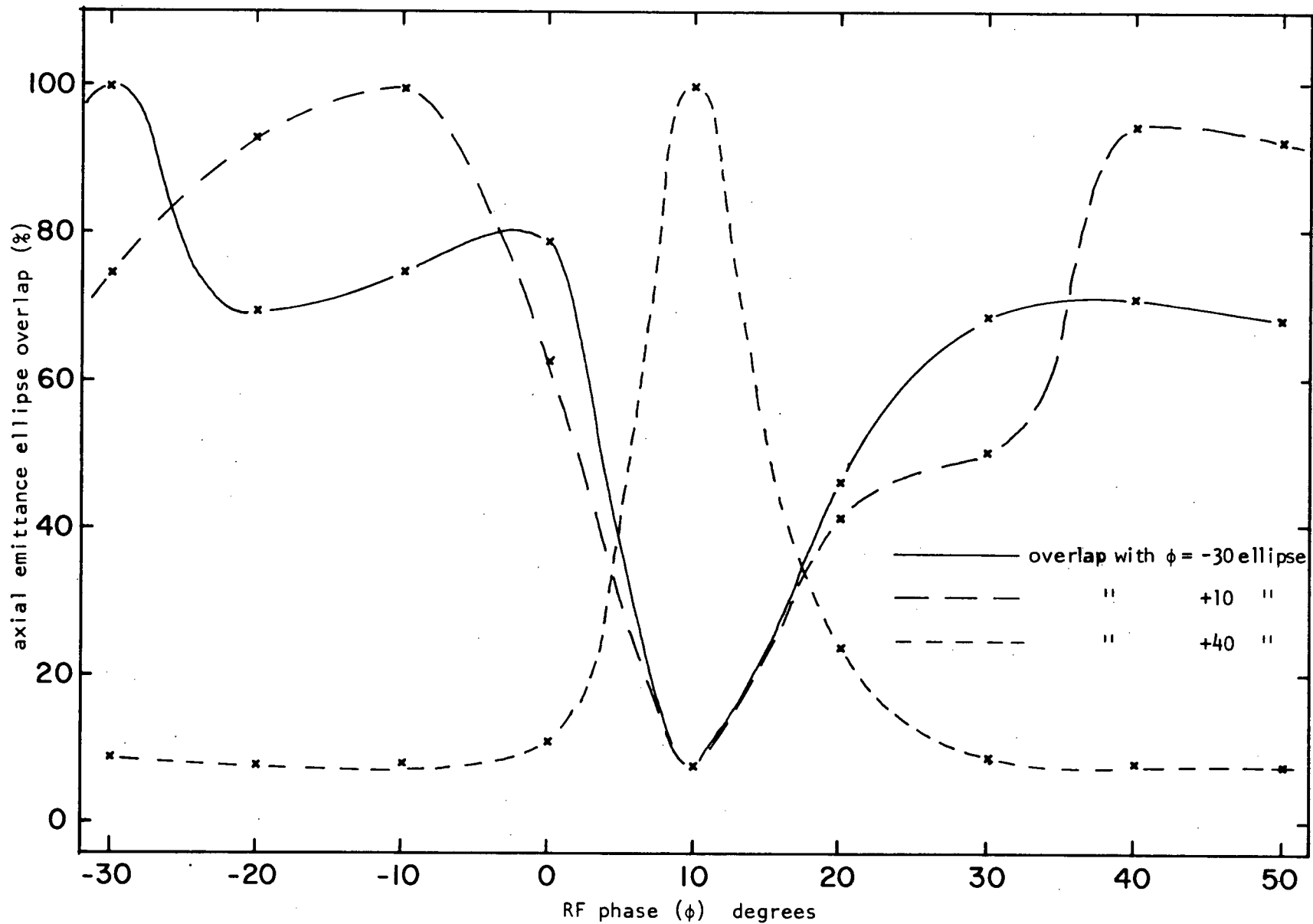


Fig. 3.13 Axial acceptance vs RF phase for various choices of the initial emittance ellipse,  $\epsilon = 0.17$ ,  $\delta = 0$

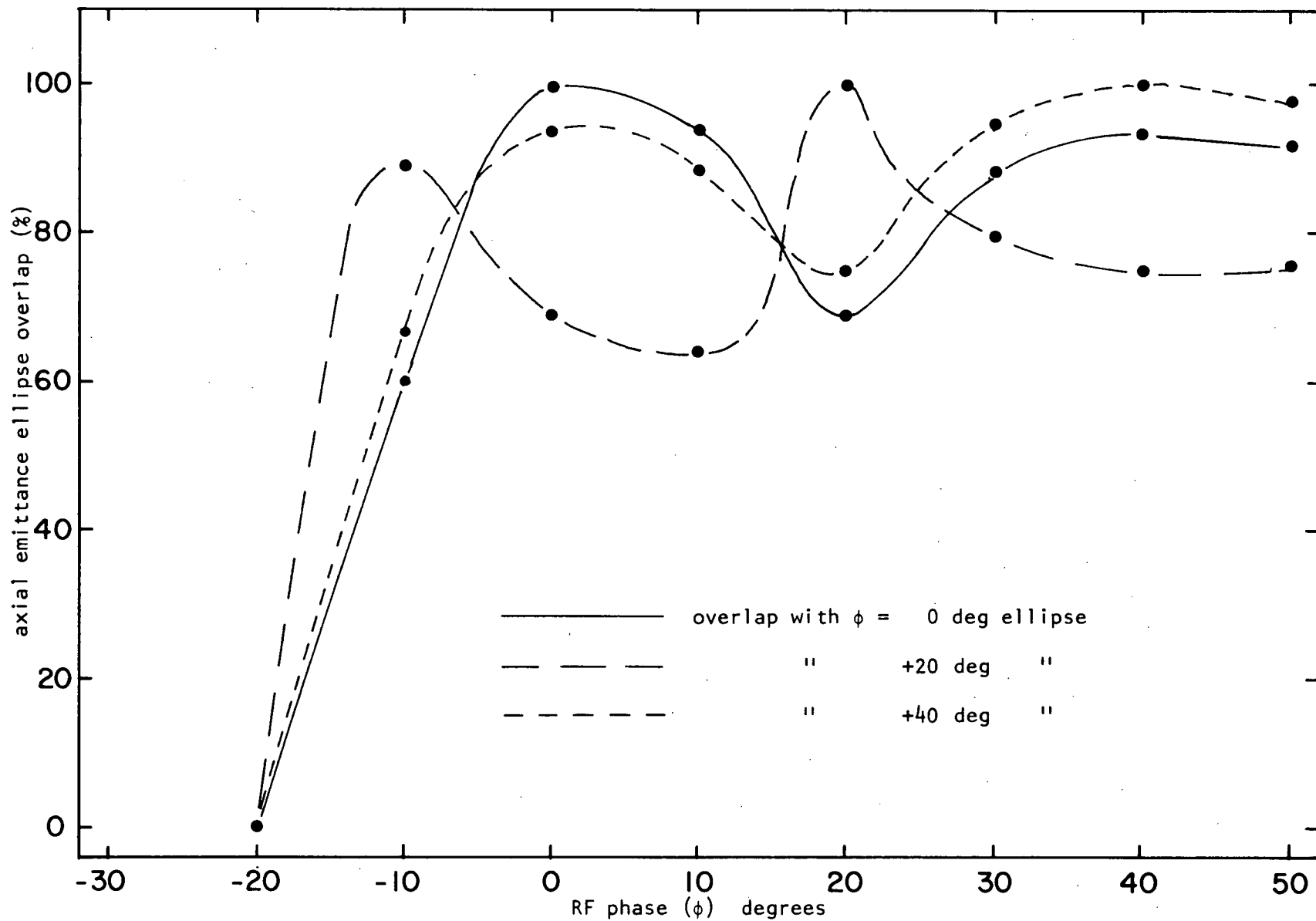


Fig. 3.14 Axial acceptance vs RF phase for various choices of the initial emittance ellipse,  $\epsilon = 0.12$ ,  $\delta = 0$

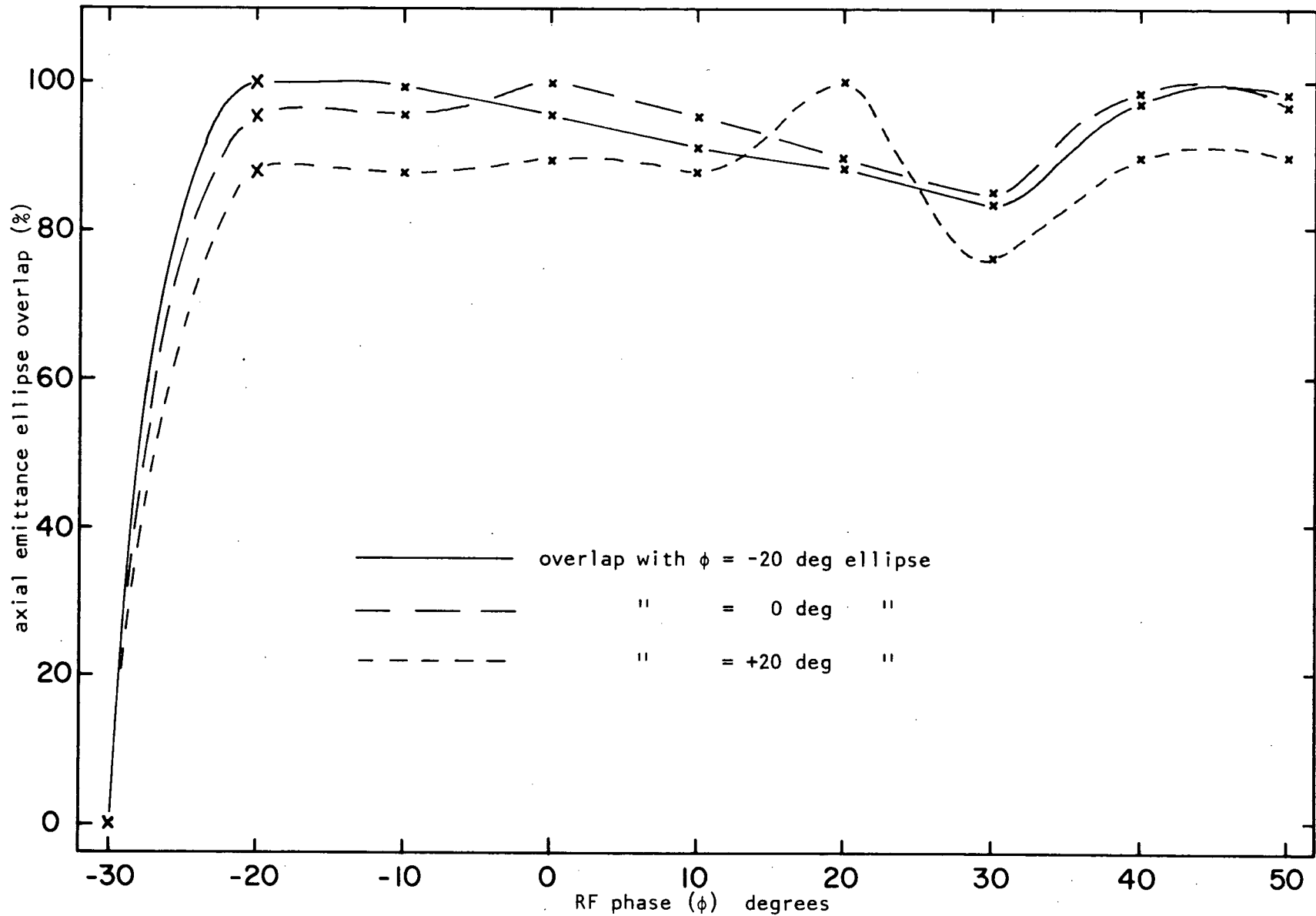


Fig. 3.15 Axial acceptance vs RF phase for various choices of the initial emittance ellipse,  $\epsilon = 0.15$ ,  $\delta = -10$  deg

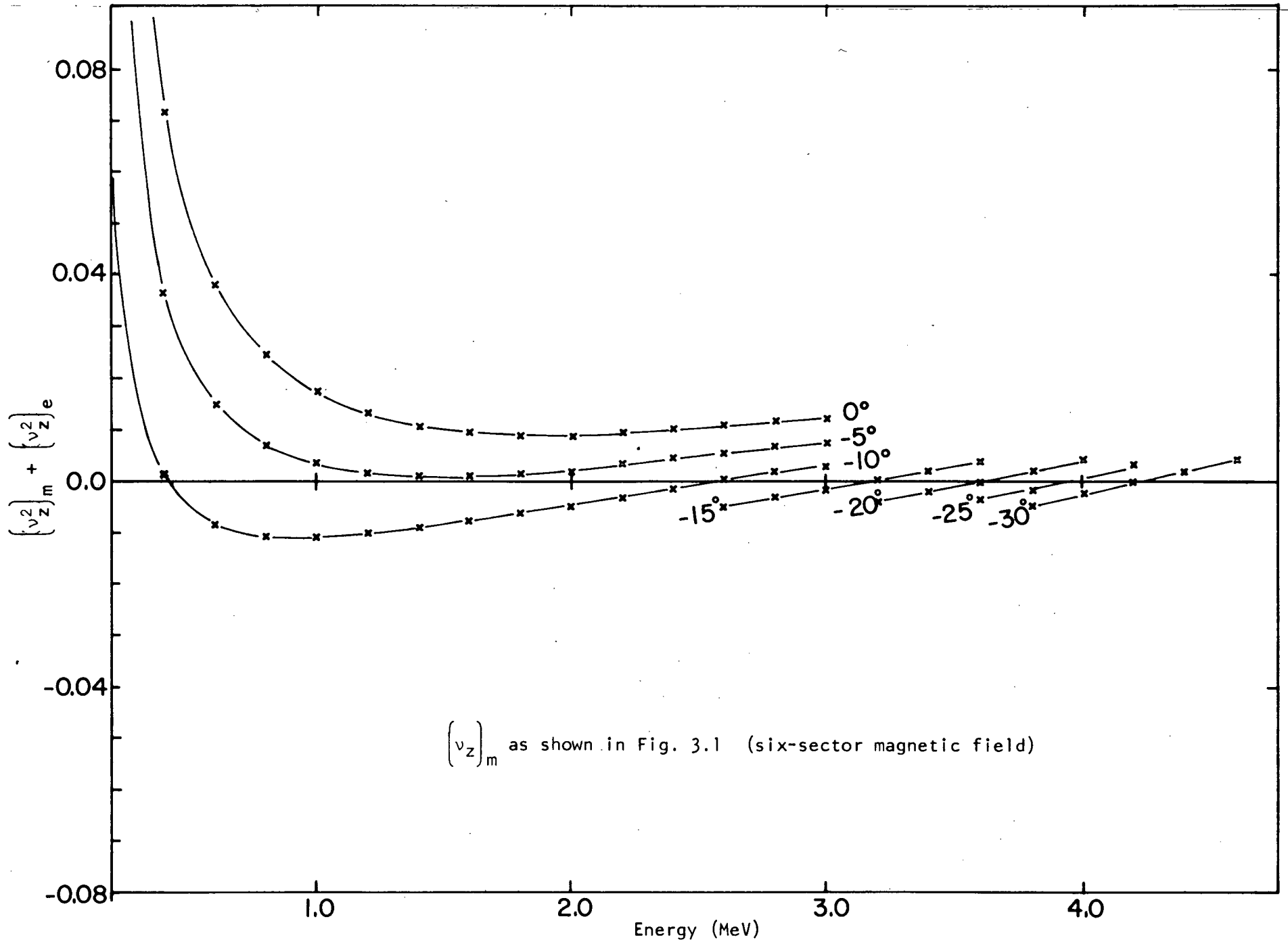


Fig. 3.16 Total (Magnetic and electric) equivalent axial focusing frequency vs energy for various RF phases

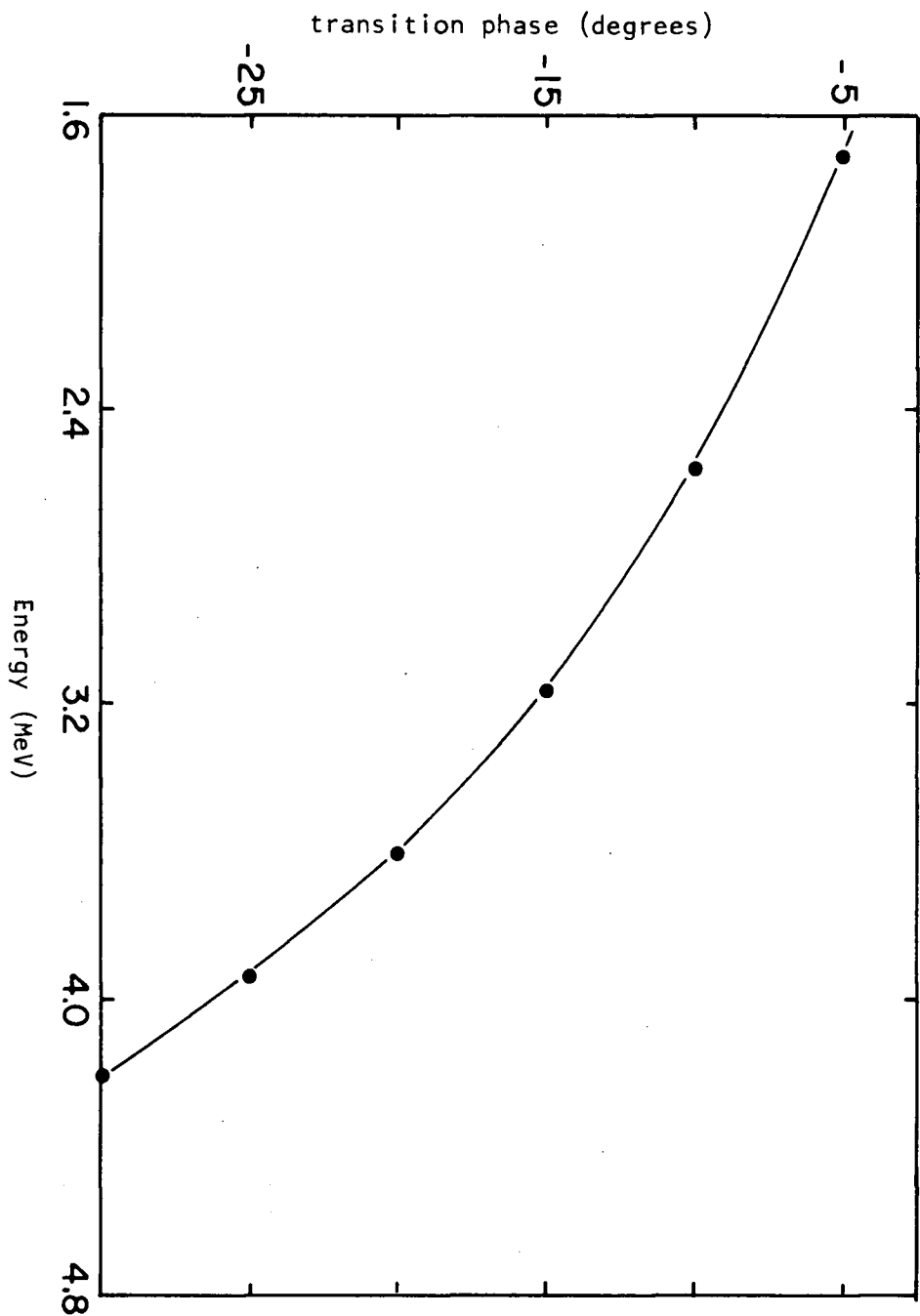


Fig. 3.17 Transition phase (of total axial focusing from negative to positive) vs energy

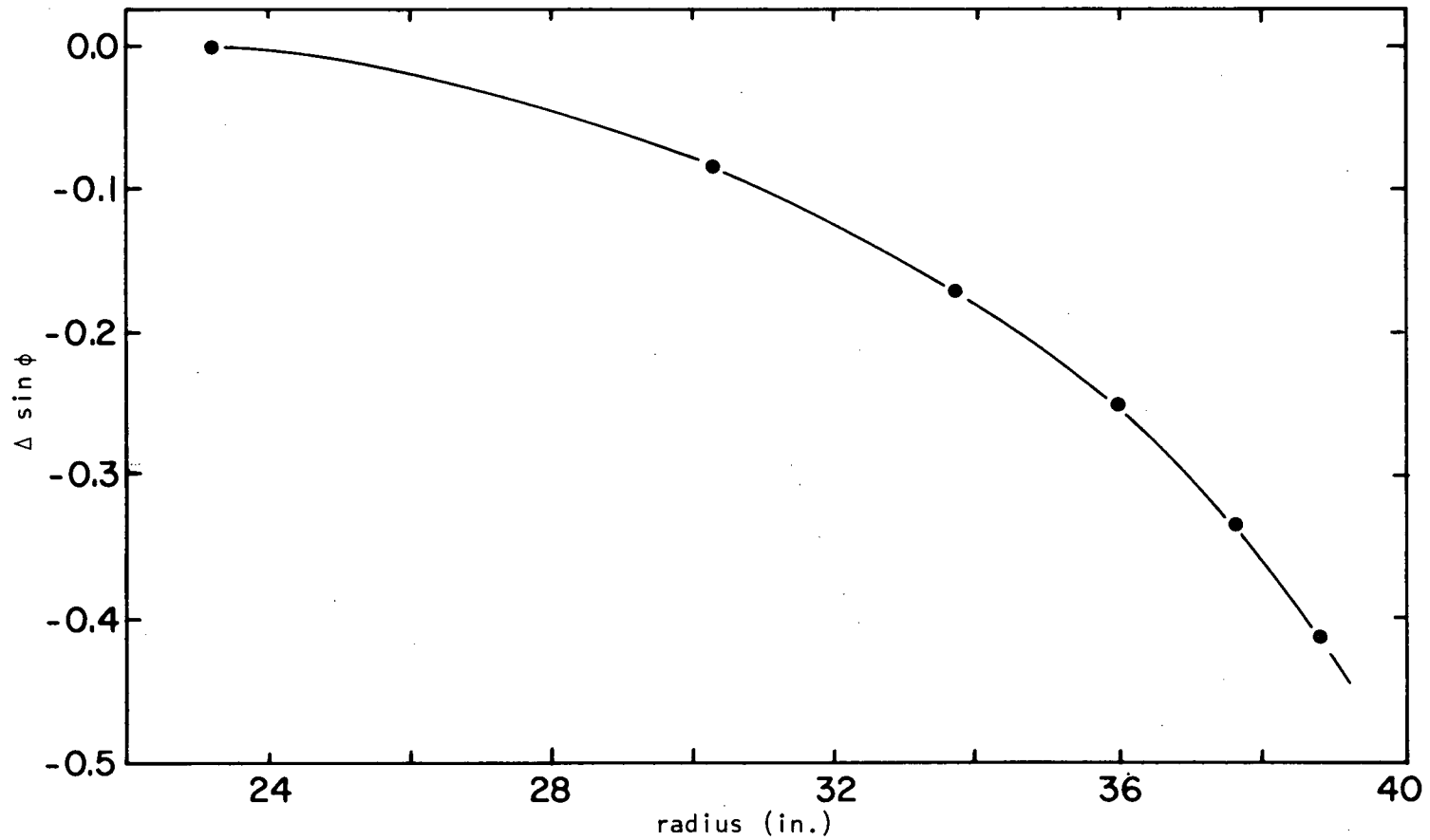


Fig. 3.18 Change in sine of RF phase required to keep ion at transition phase vs radius

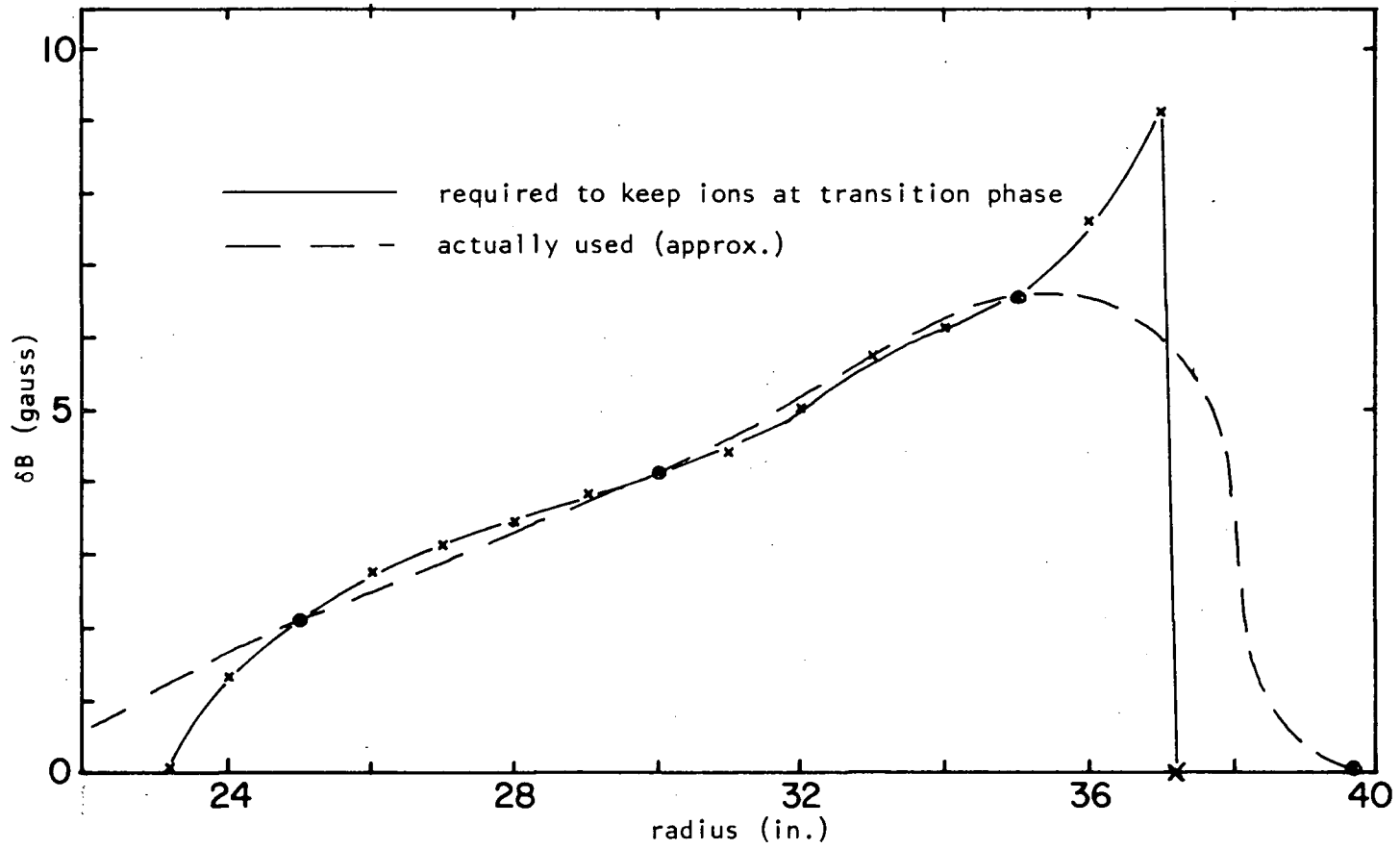


Fig. 3.19 Magnetic field bump required to keep ion at transition phase vs radius

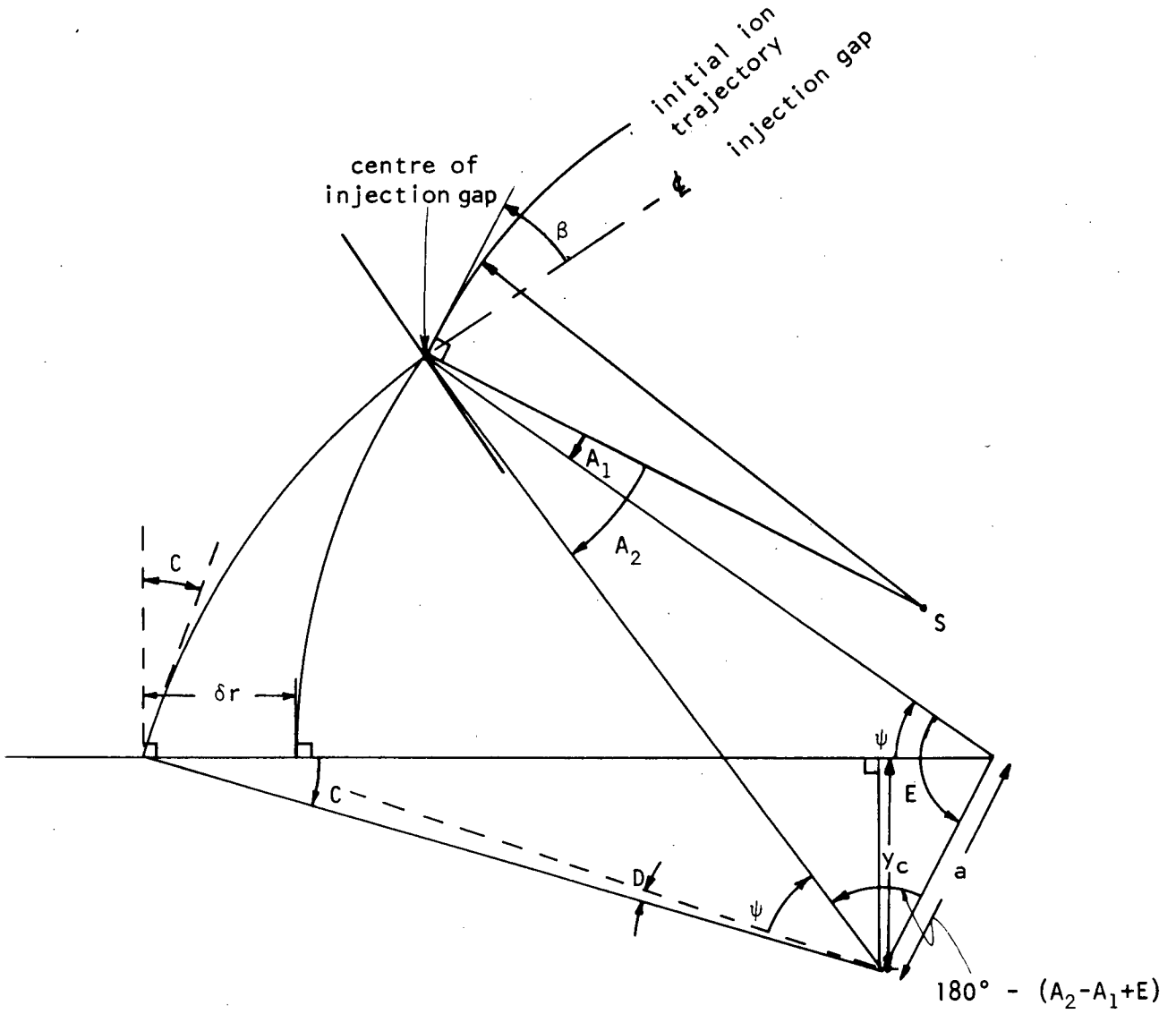


Fig. 4.1 Geometry of injection gap and first main gap for two RF phases

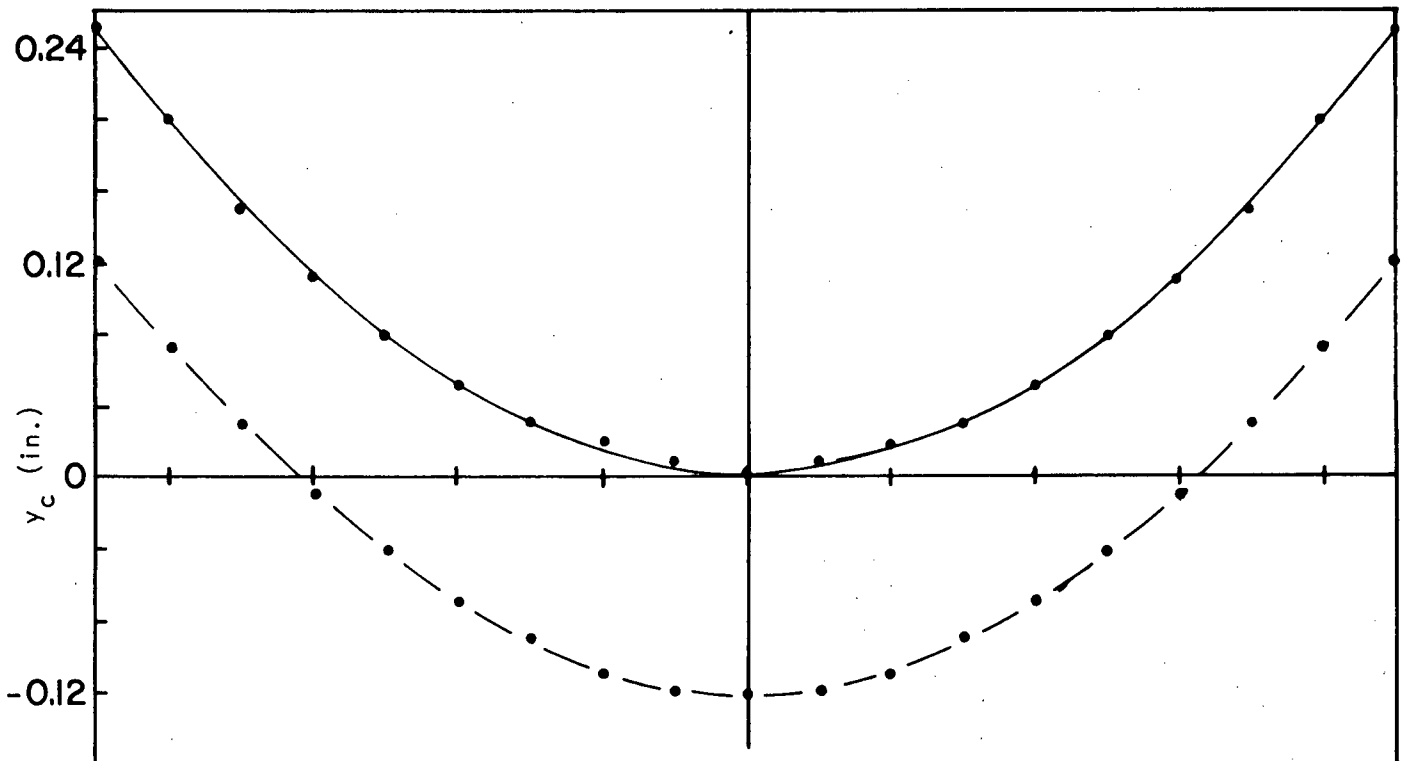


Fig. 4.2  $y_c$  vs RF phase at injection gap for various injection gap positions

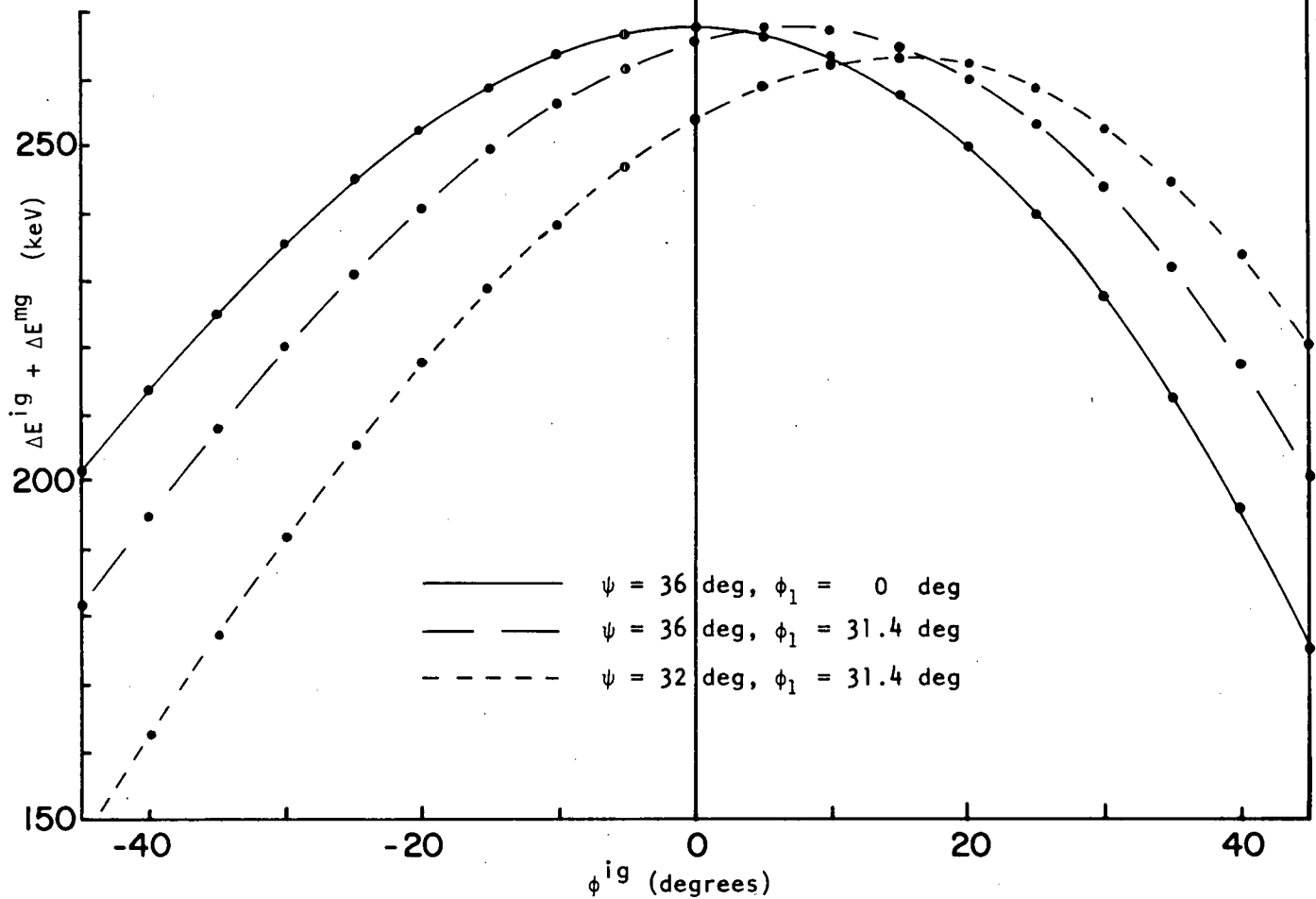


Fig. 4.3 Energy gain in injection gap and first main gap vs RF phase at injection gap for various injection gap positions

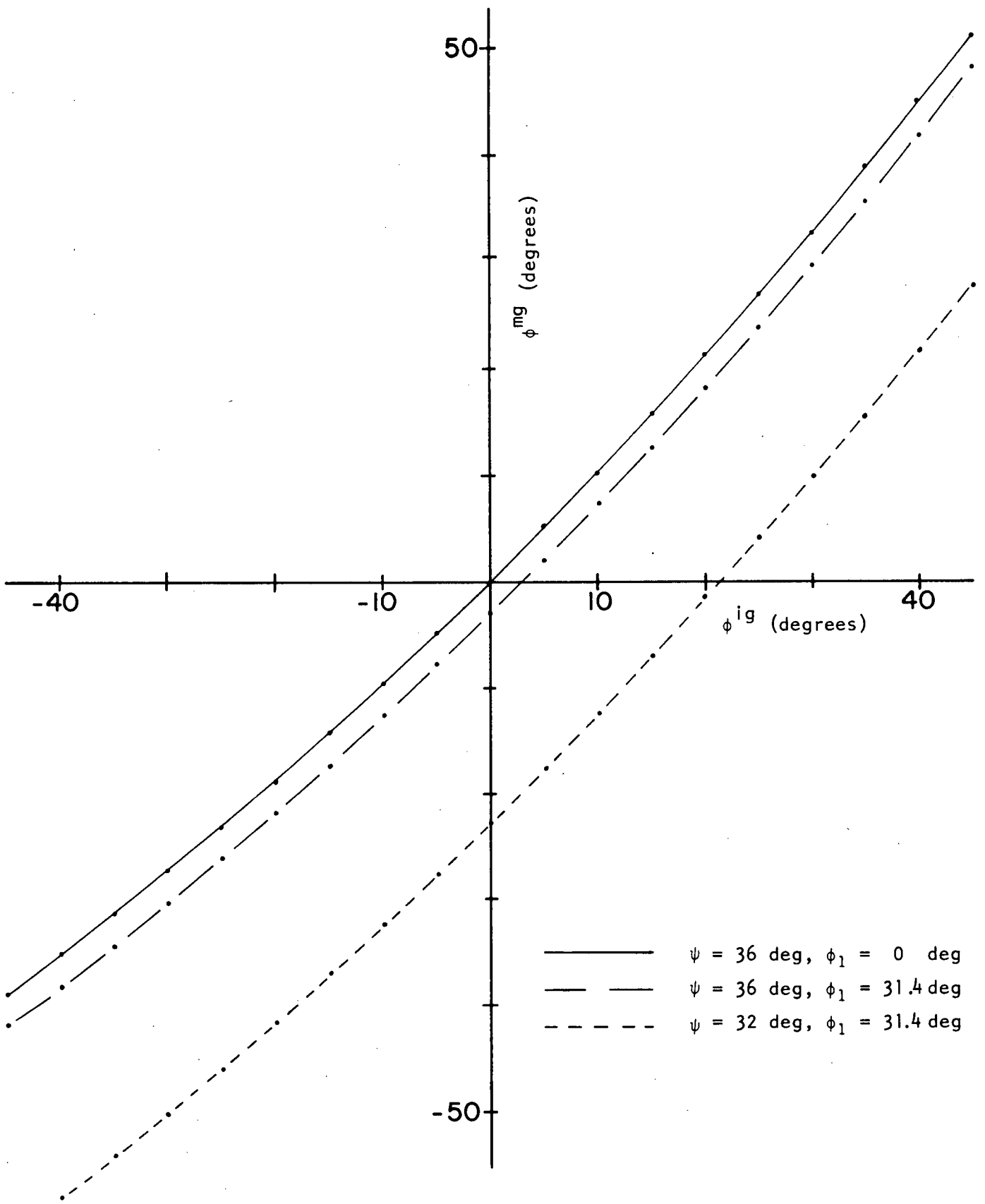


Fig. 4.4 RF phase at first main gap vs RF phase at injection gap for various injection gap positions

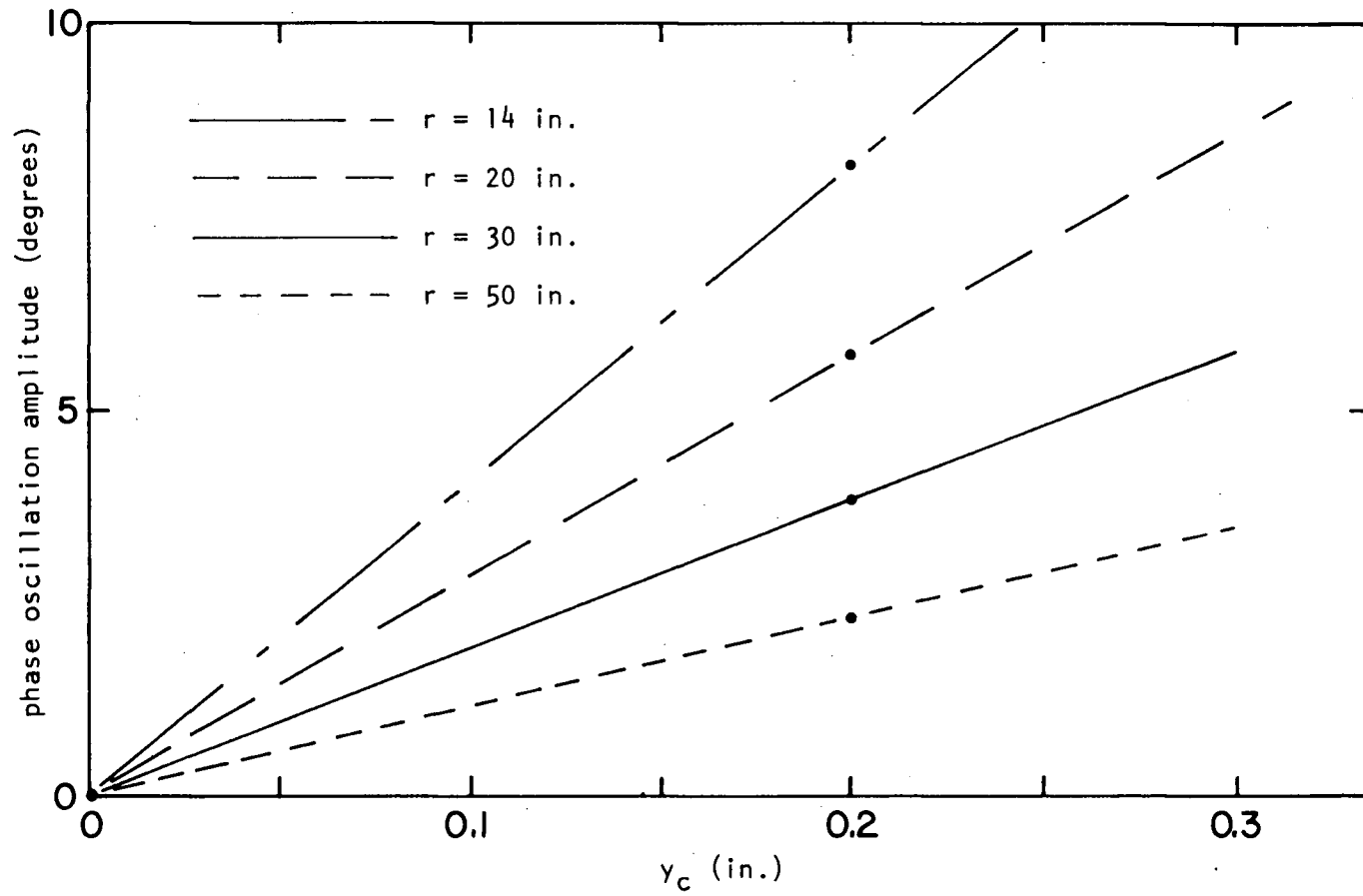


Fig. 4.5 Phase oscillation amplitude vs centring error at various radii

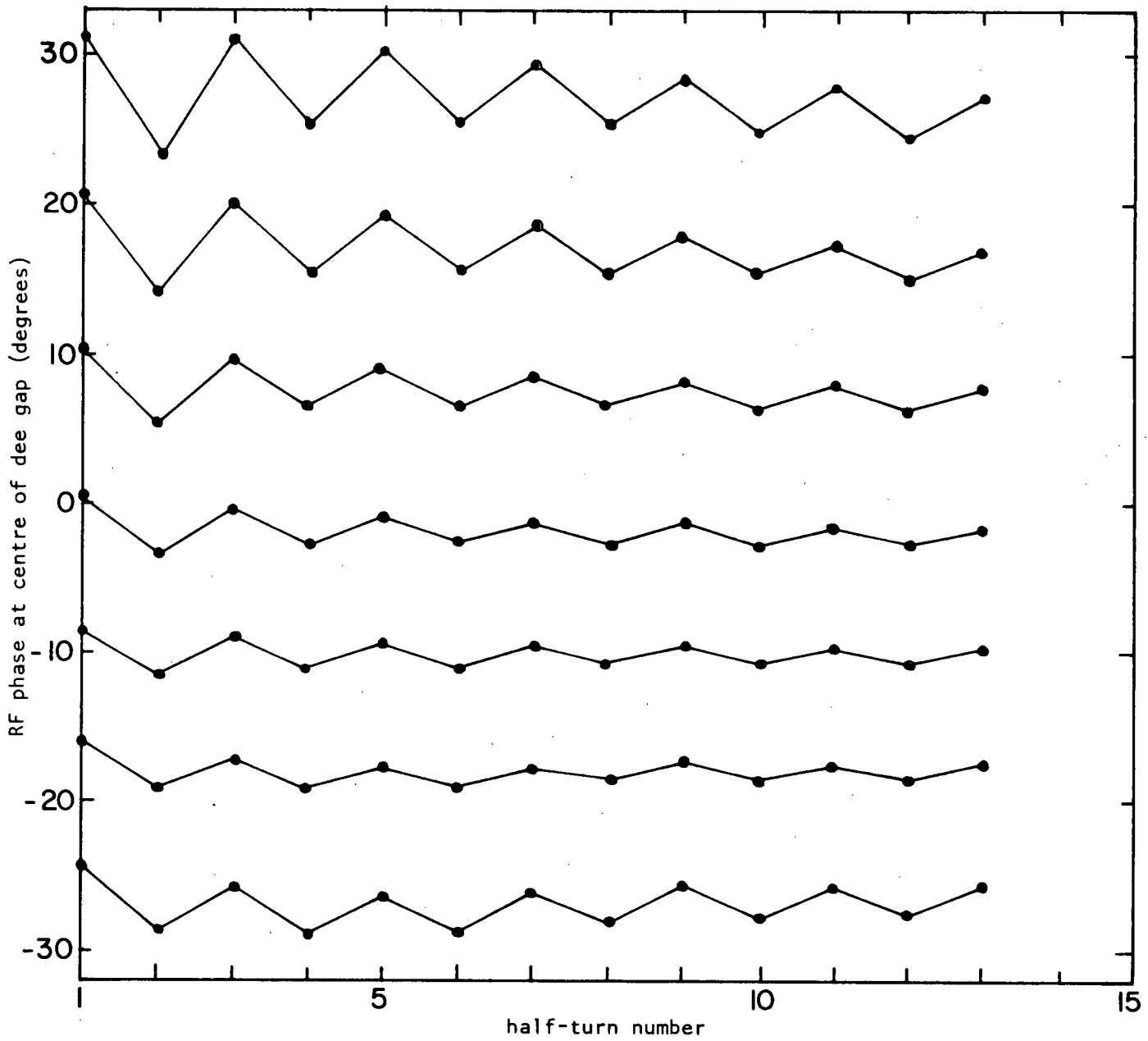


Fig. 4.6 RF phase vs half-turn number for various initial phases with no flutter in the magnetic field

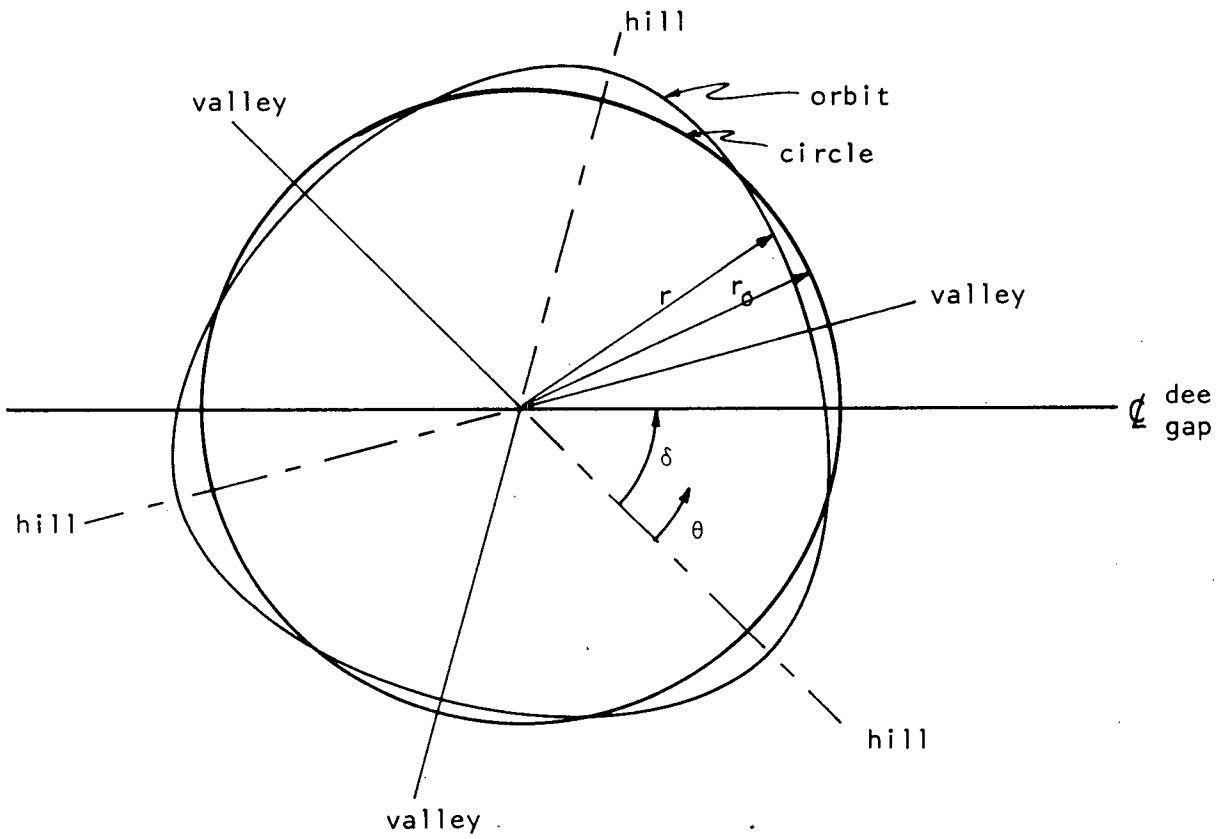


Fig. 4.7 Geometry of an orbit in a three-sector magnetic field

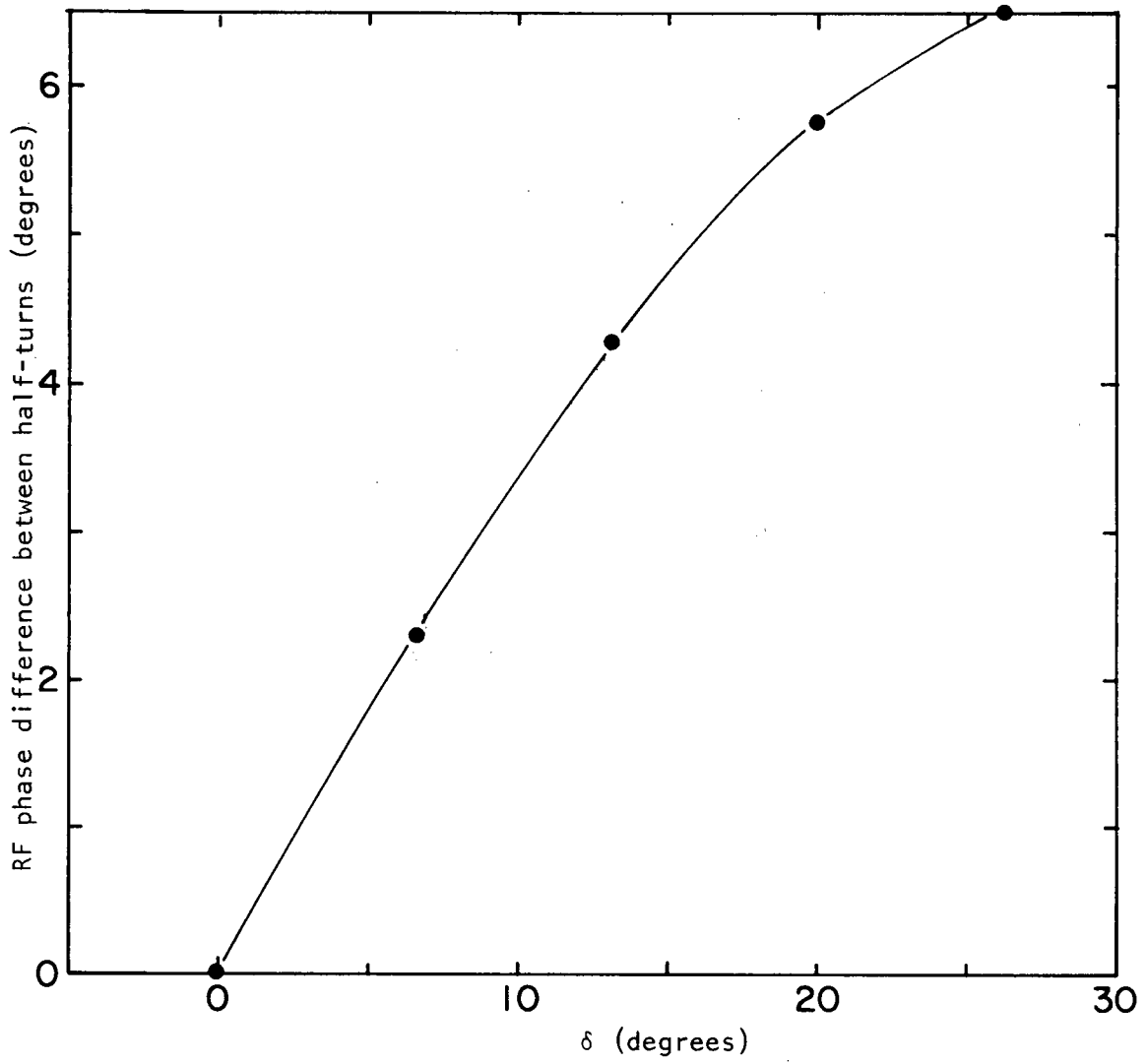


Fig. 4.8 RF phase difference on succeeding half-turns as a function of orientation of the dee gap ( $\delta$ )

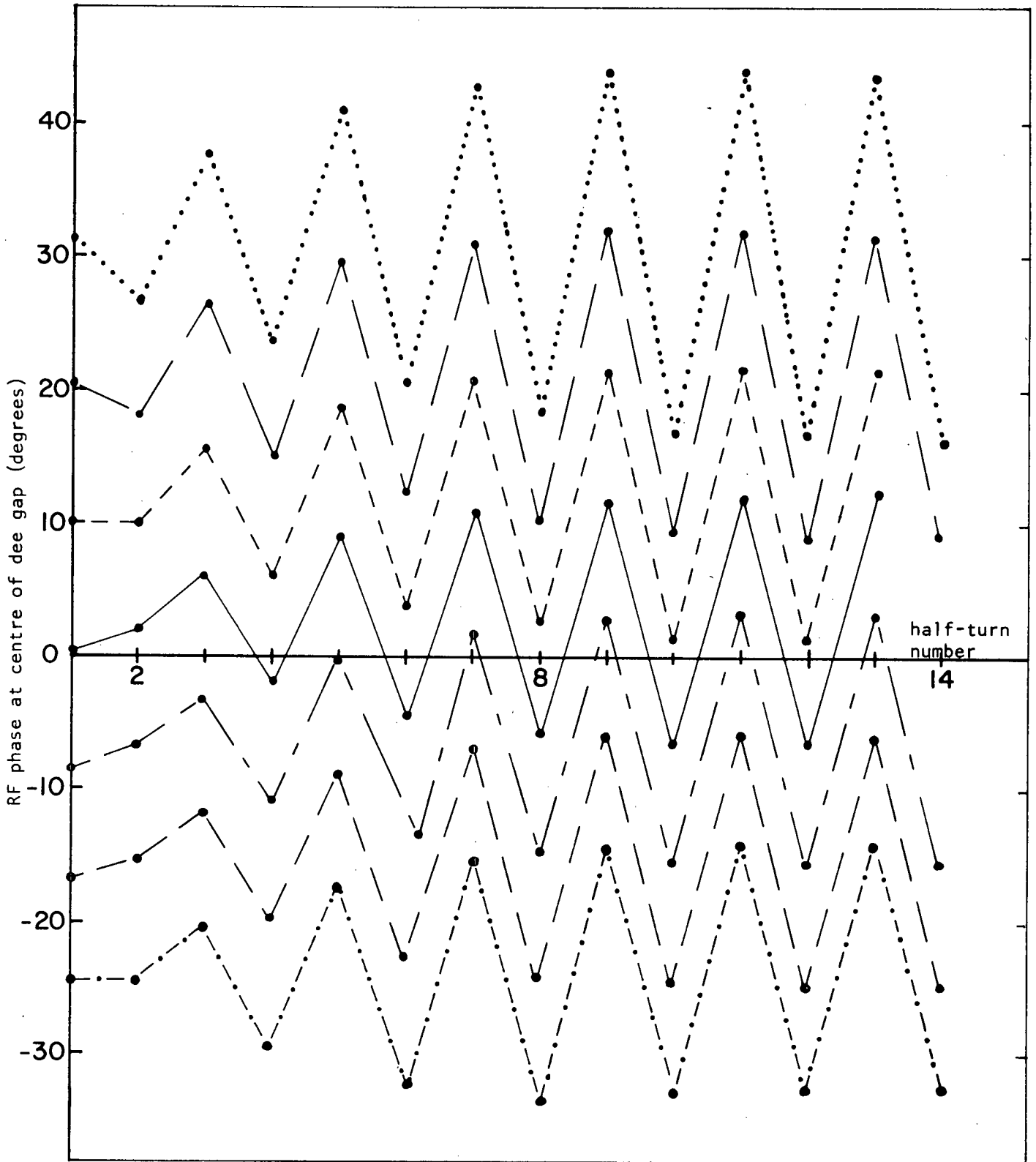


Fig. 4.9 RF phase vs half-turn number for various initial phases with a three-sector magnetic field ( $\delta = 30$  deg)

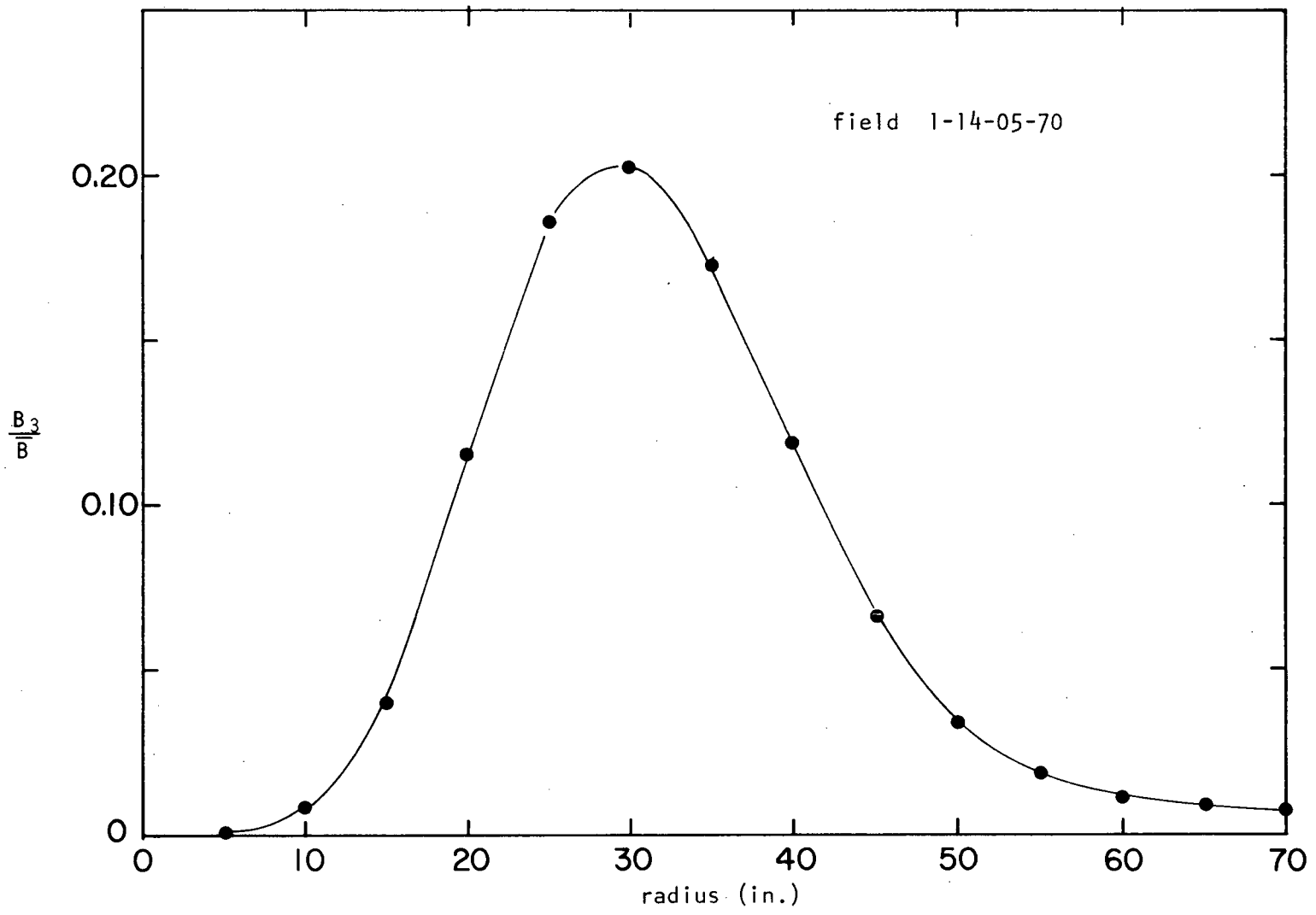


Fig. 4.10 Ratio of third harmonic amplitude in magnetic field to average field vs radius for (three-sector) field 1-14-5-70

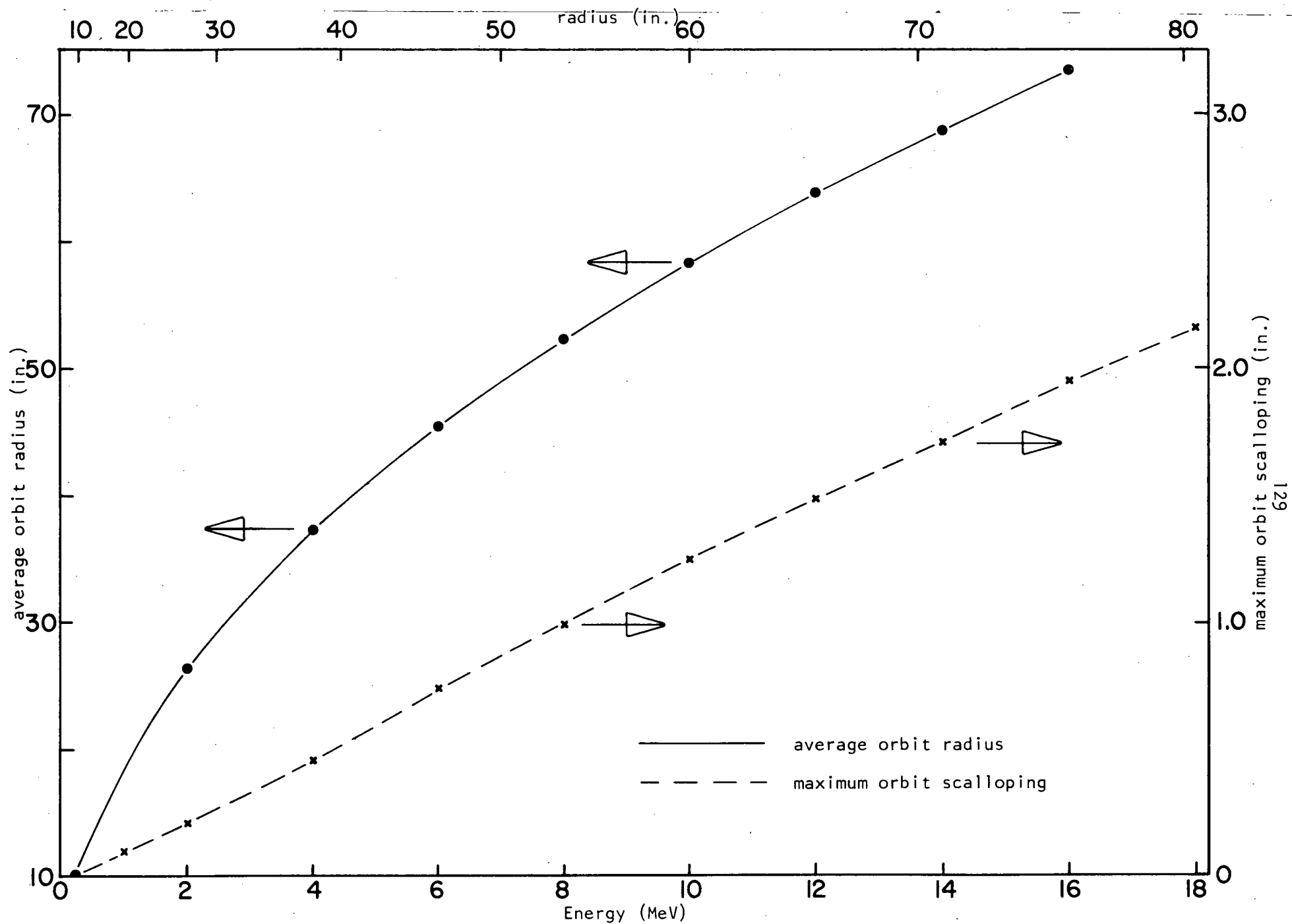


Fig. 4.11 Average orbit radius and maximum orbit scalloping vs radius for (six-sector) field 1-30-06-70

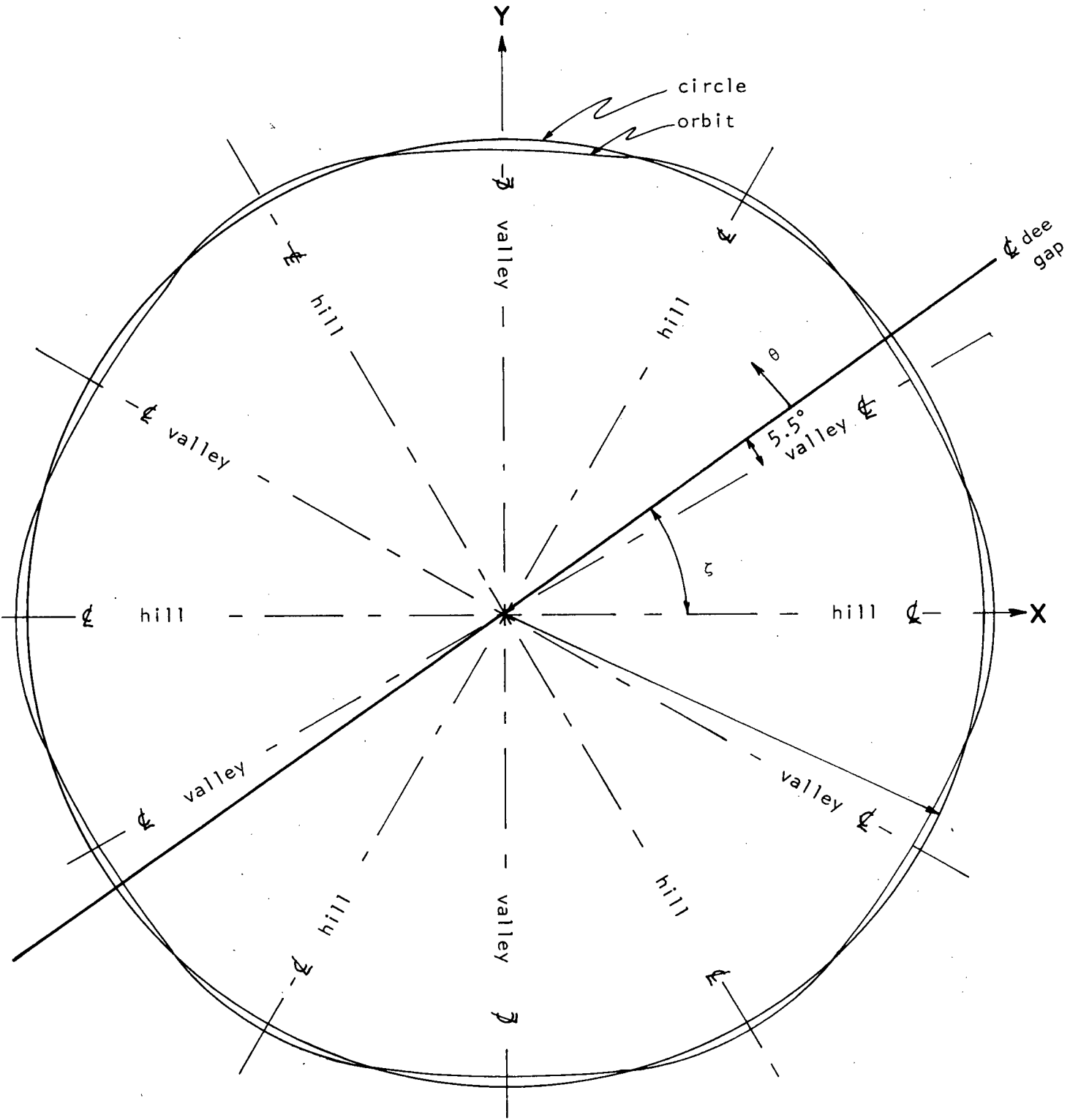


Fig. 4.12 Geometry of an orbit in a six-sector magnetic field

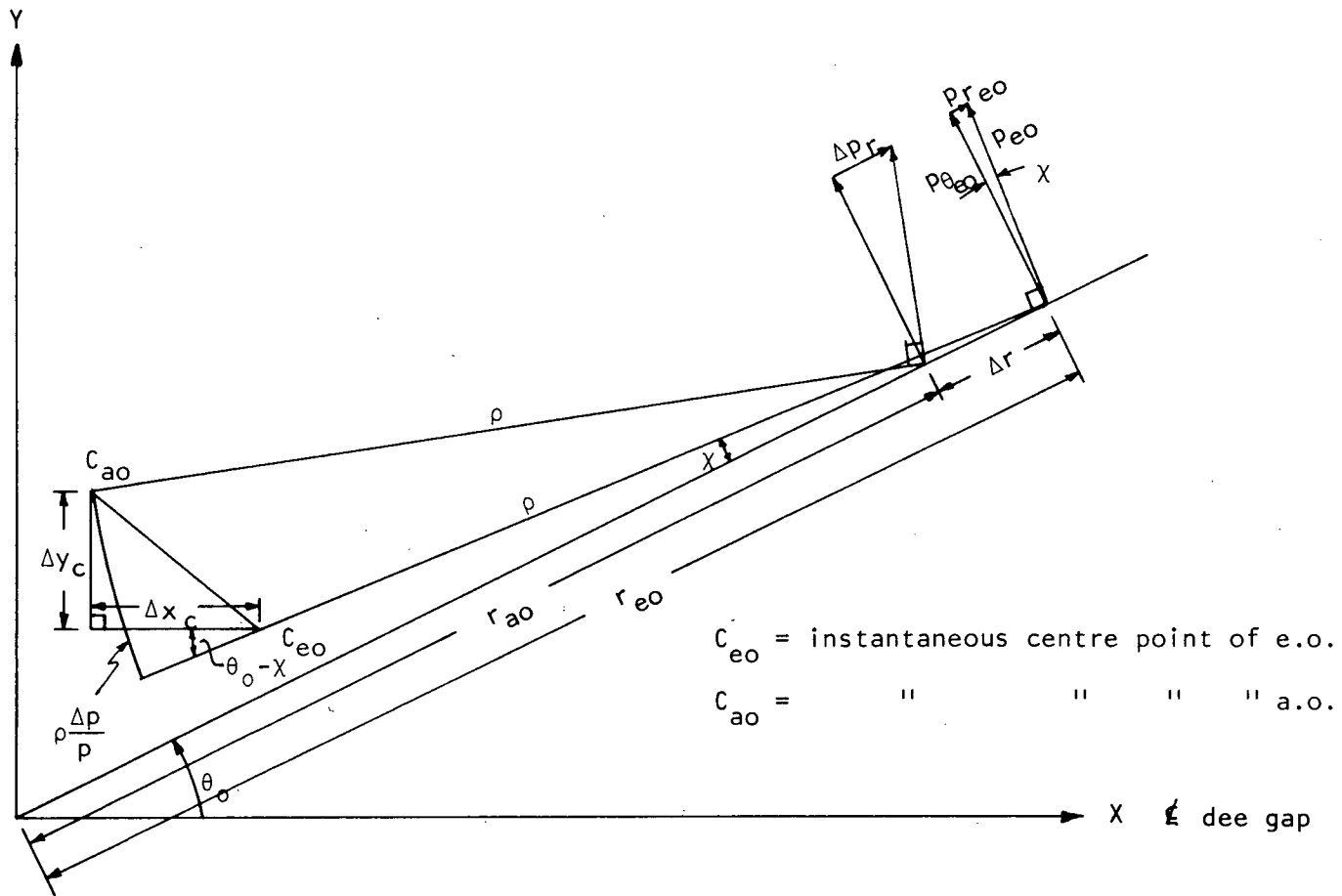


Fig. 4.13 Geometry of the difference between an equilibrium orbit and an accelerated orbit

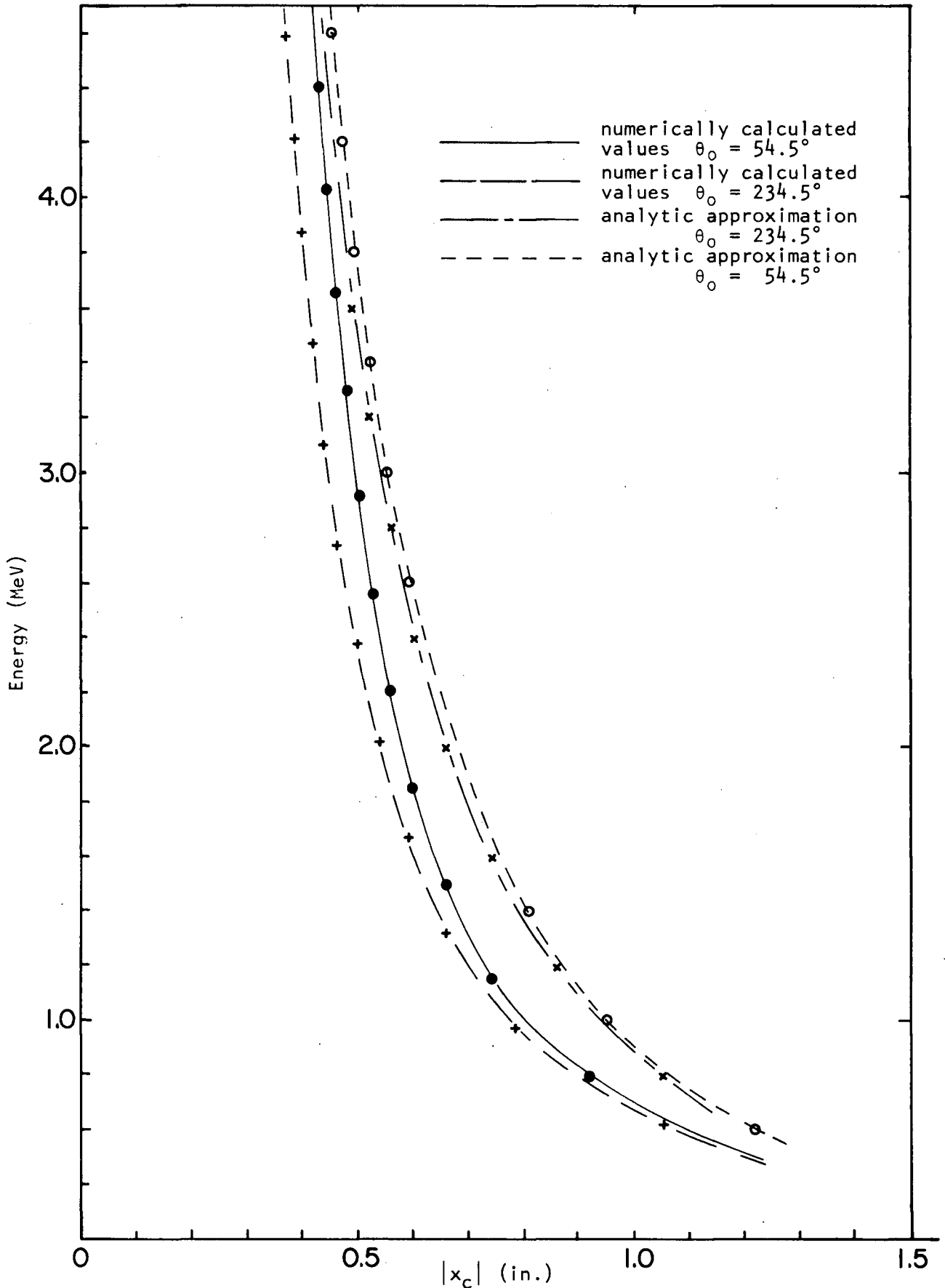


Fig. 4.14 Centre-point displacement along the dee gap vs energy showing values from numerical orbit tracks and from an analytic approximation

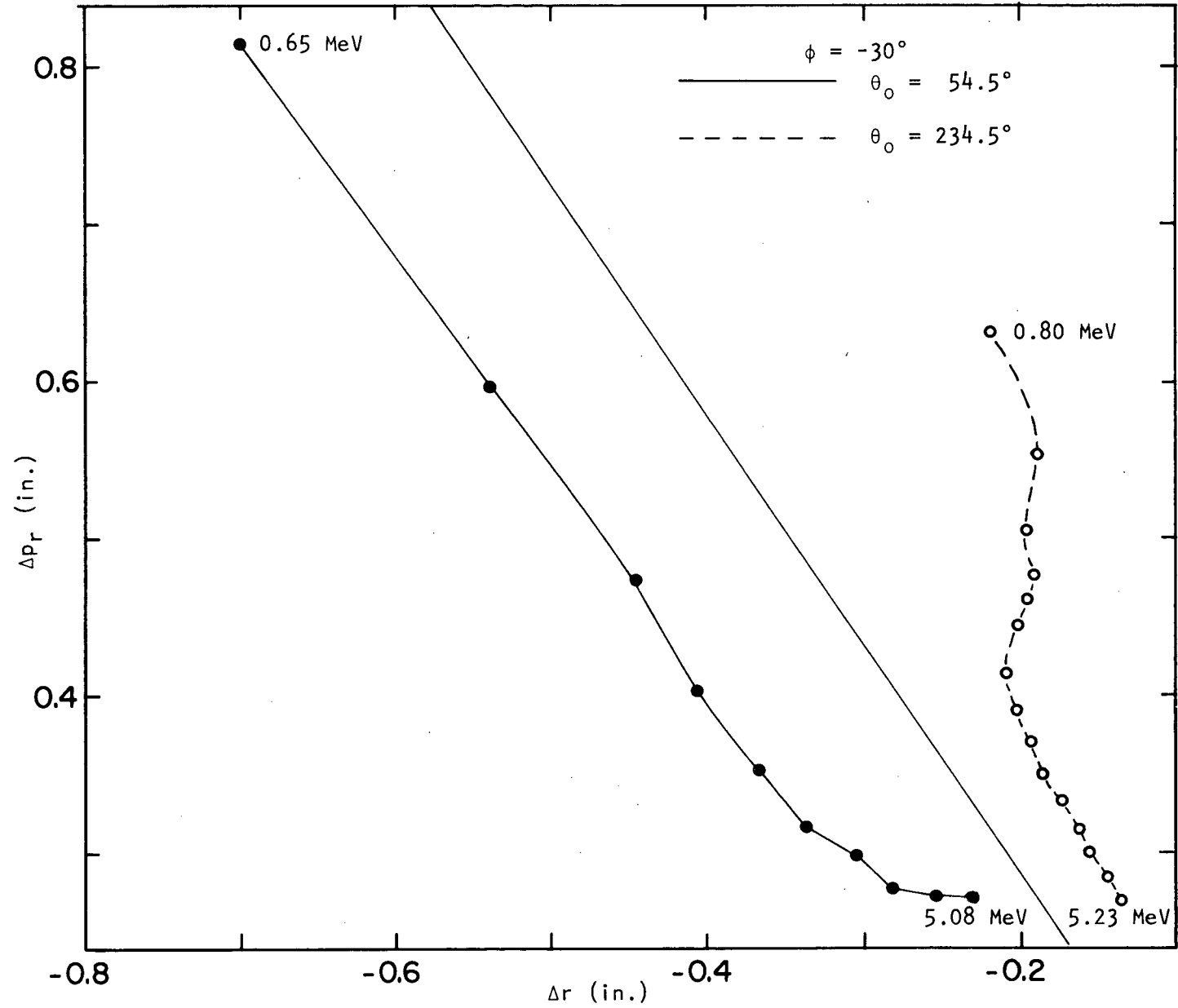


Fig. 4.15 Accelerated phase plot inwards from 5 MeV,  $\phi = -30$  deg

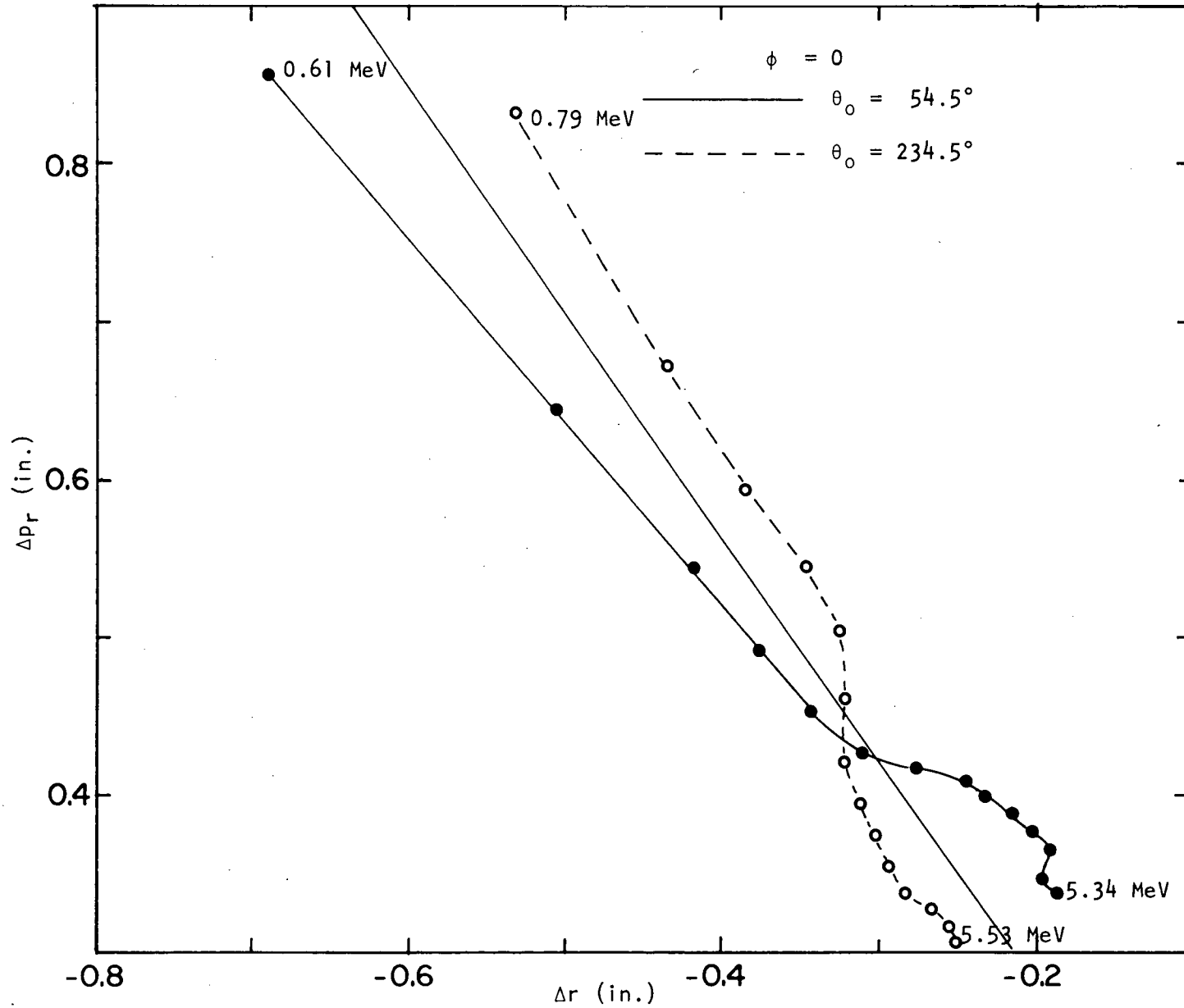


Fig. 4.16 Accelerated phase plot inwards from 5 MeV,  $\phi = 0$  deg

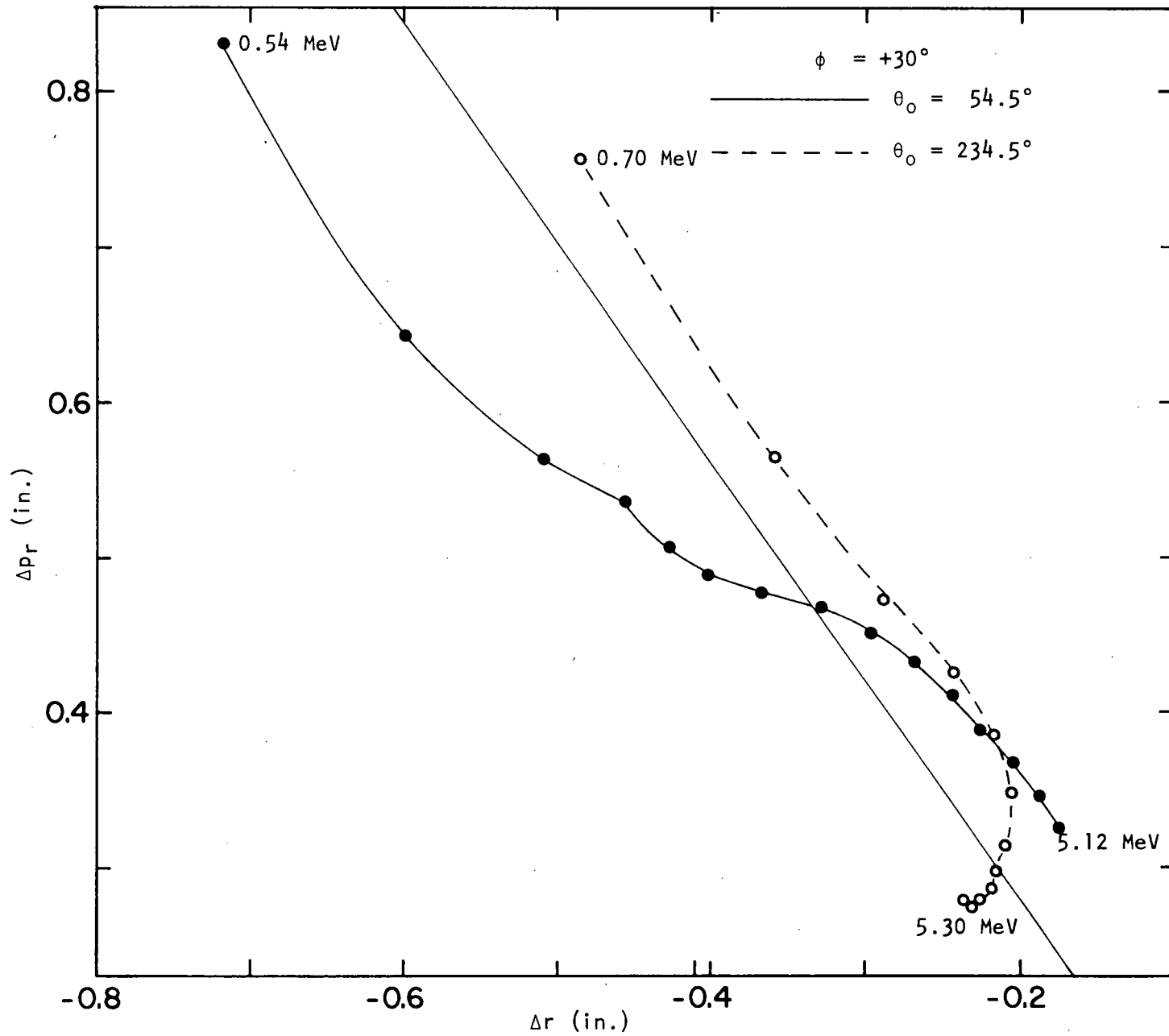


Fig. 4.17 Accelerated phase plot inwards from 5 MeV,  $\phi = +30$  deg

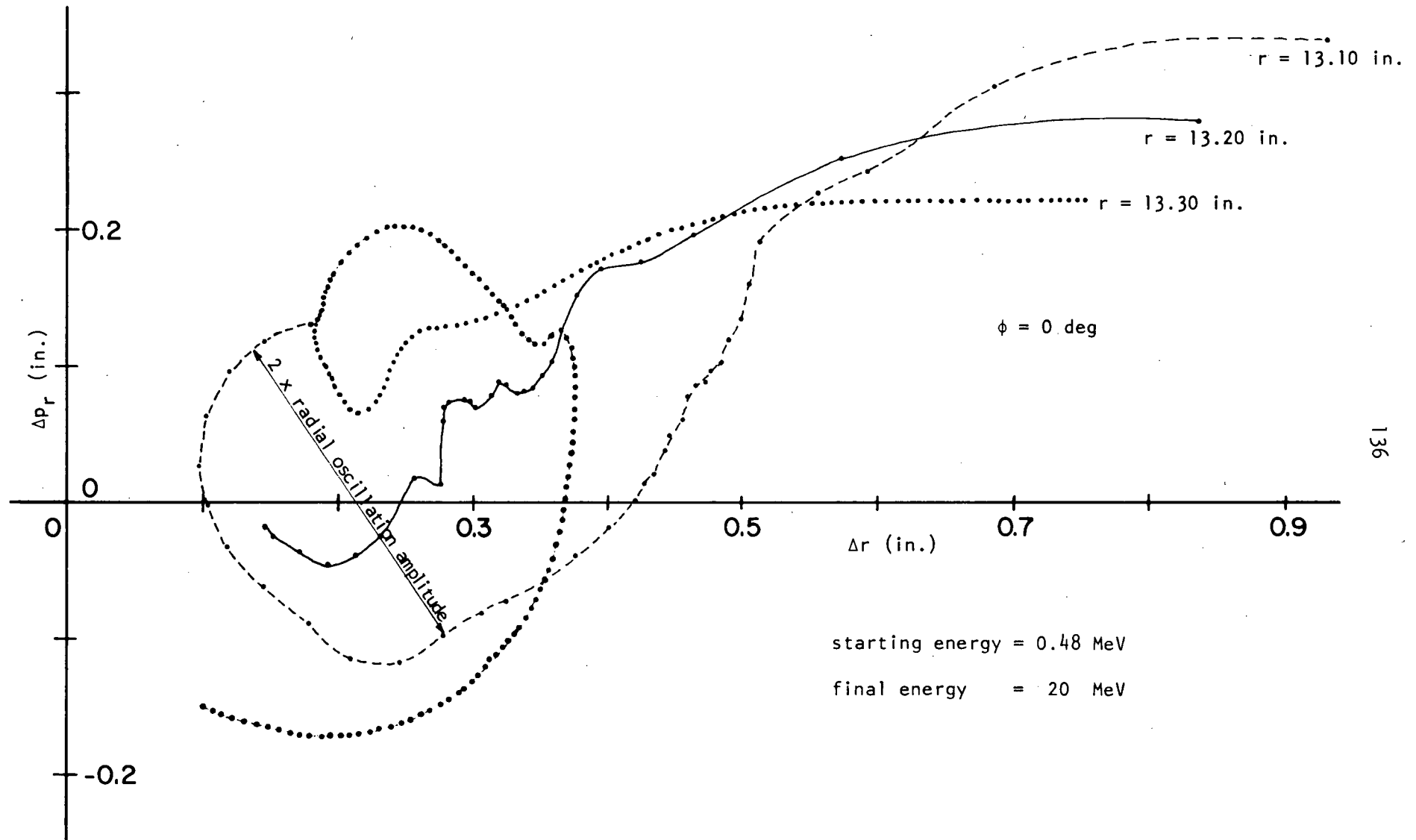


Fig. 4.18 Accelerated phase plot outwards for various radii at first main dee gap,  $\phi = 0$  deg

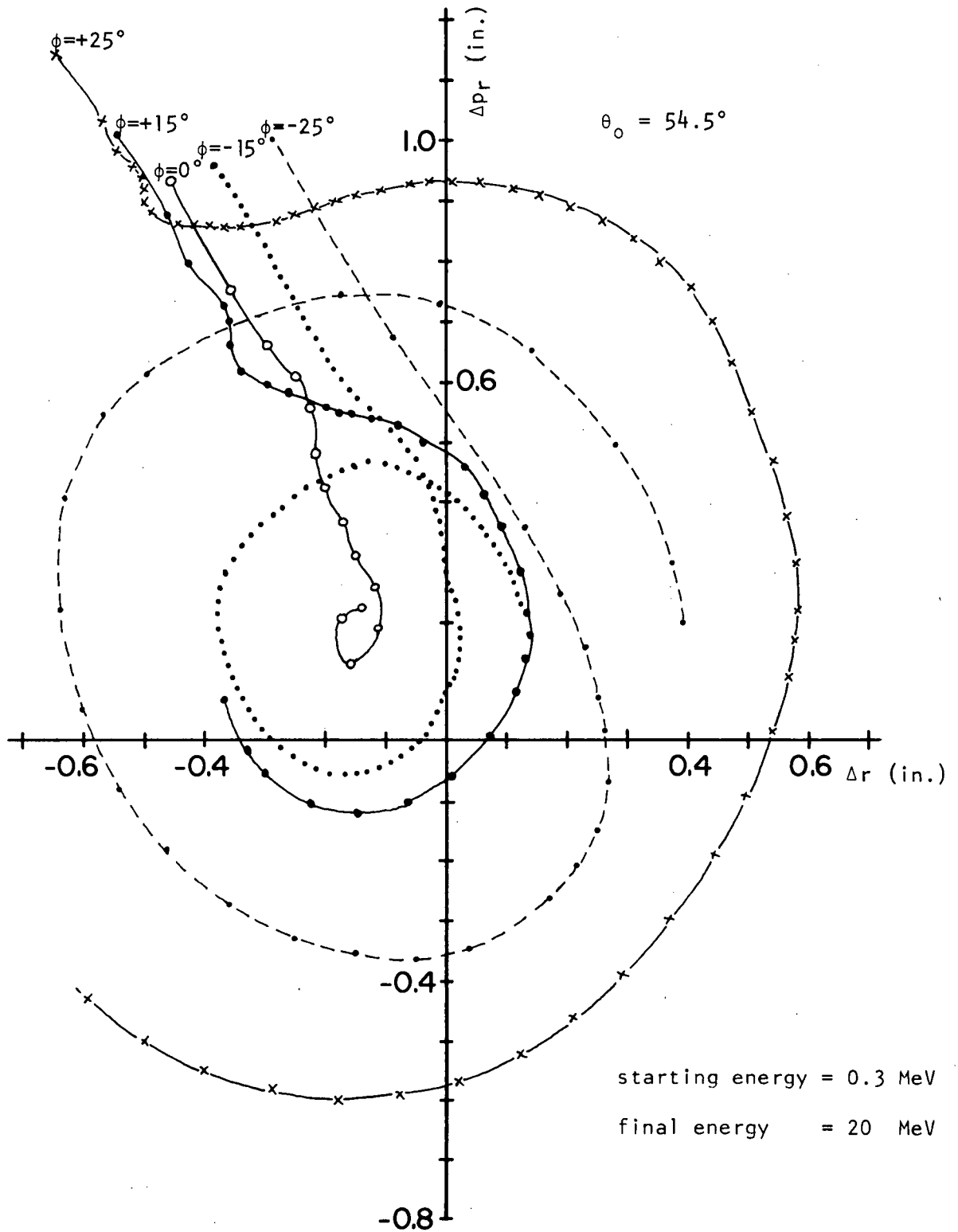


Fig. 4.19 Accelerated phase plot outwards from inflector exit for various phases; ion with  $\phi = 0$  is centred

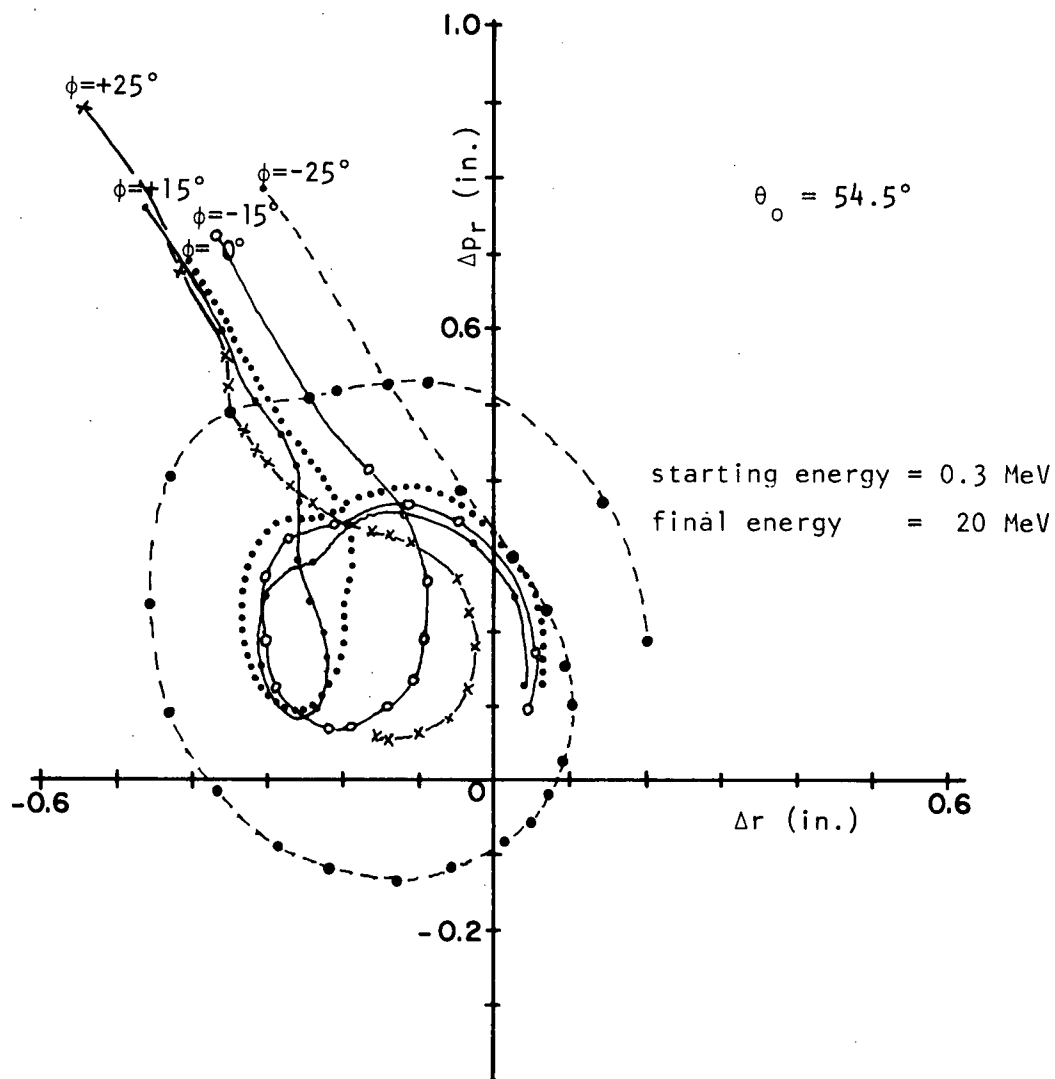


Fig. 4.20 Accelerated phase plot outwards from inflector exit for various phases; ion with  $\phi = +17$  deg is centred

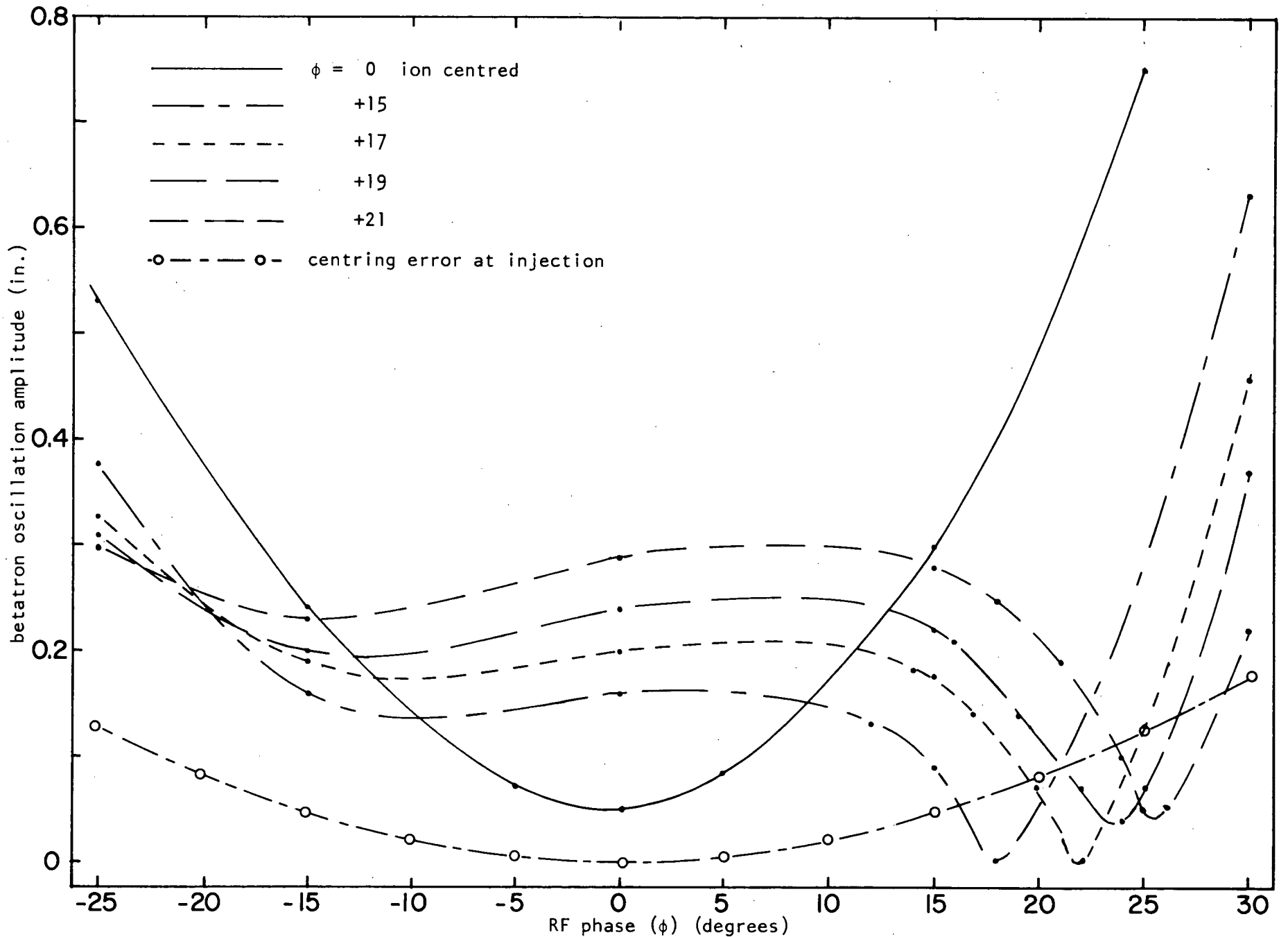


Fig. 4.21 Betatron oscillation amplitude vs RF phase for various starting conditions

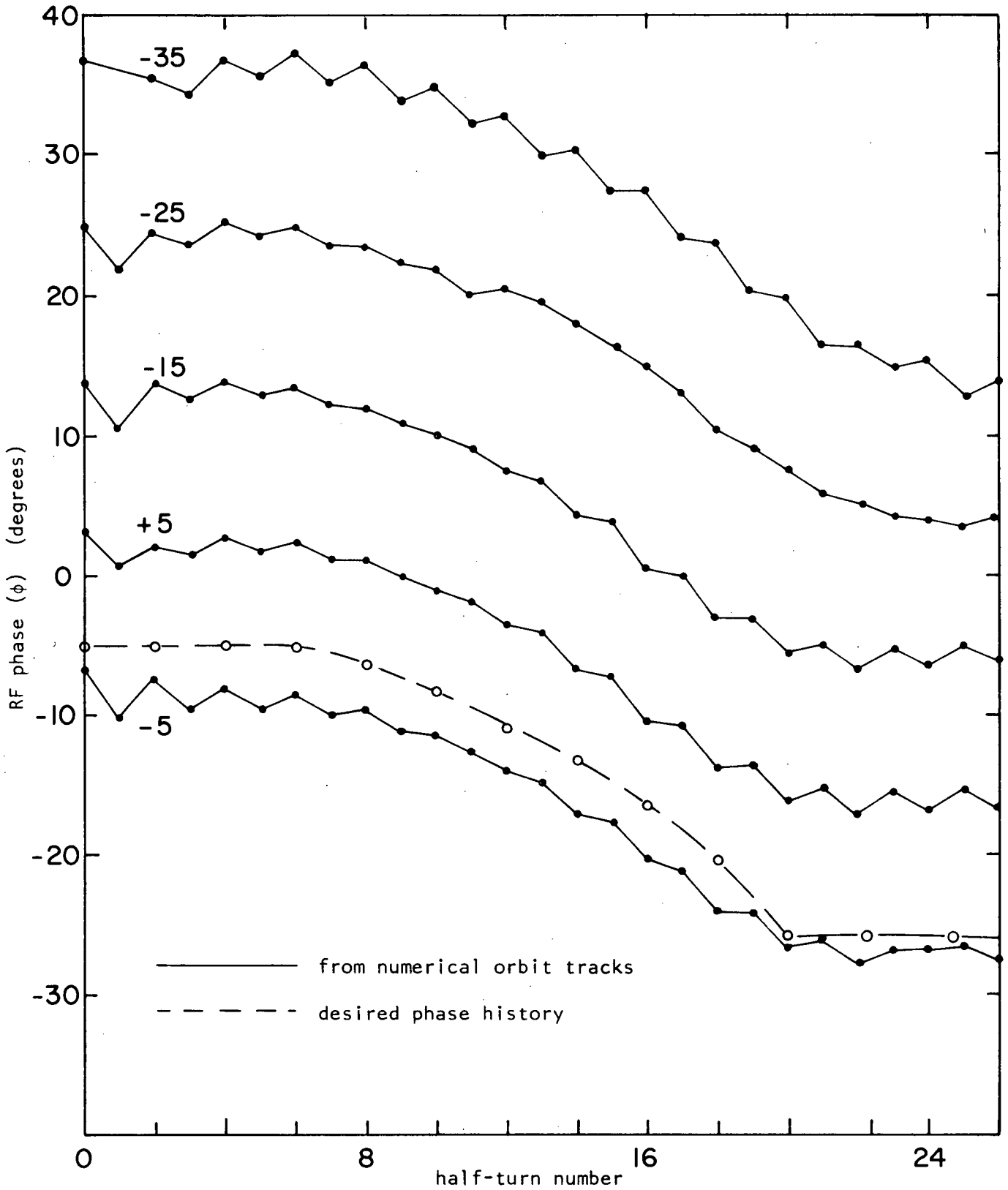


Fig. 4.22 Phase histories of ions with various starting phases in a magnetic field with a field bump

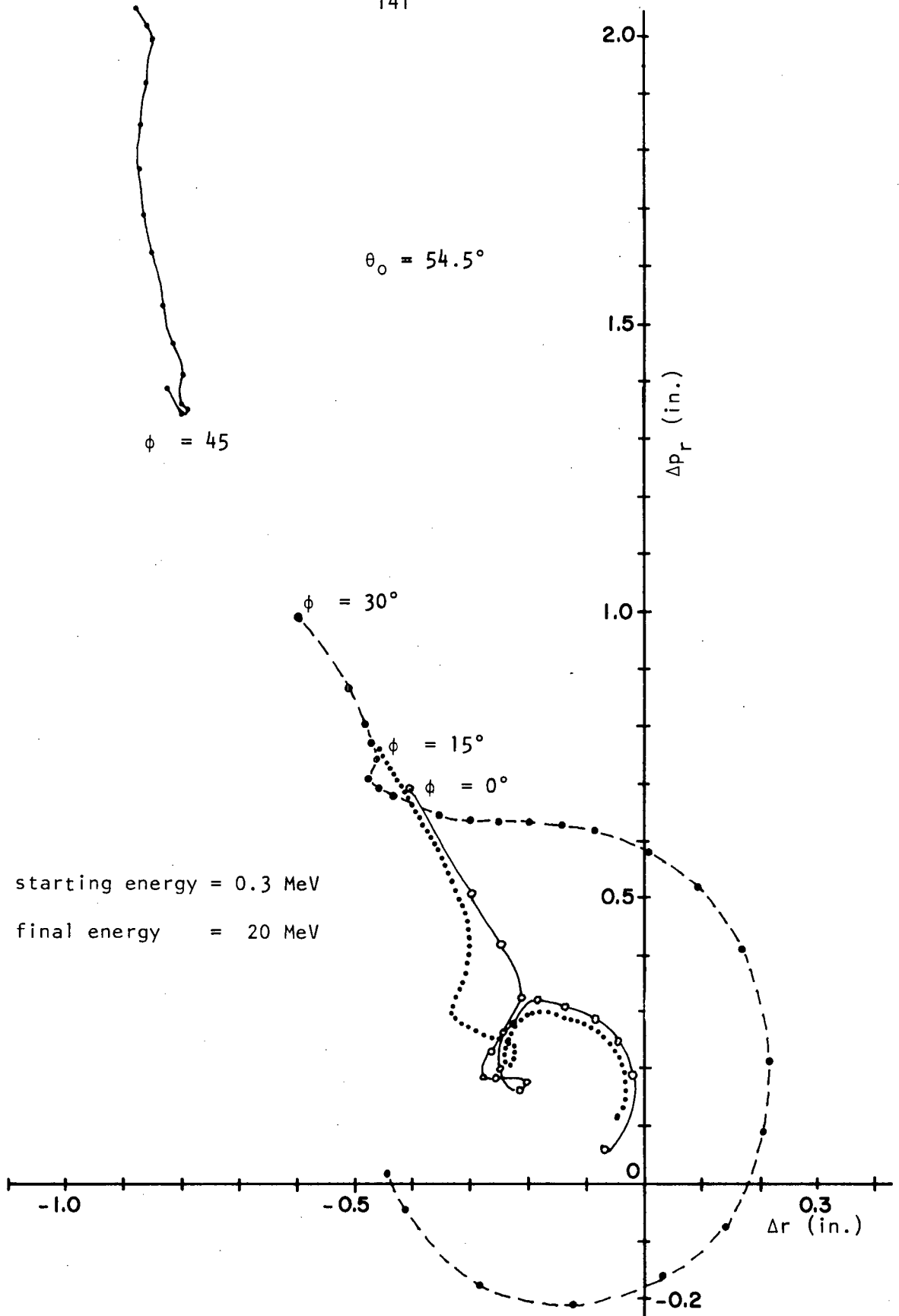


Fig. 4.23 Accelerated phase plot outwards from inflector exit for various phases using the magnetic field with the field bump; ion with  $\phi = 17$  deg is centred

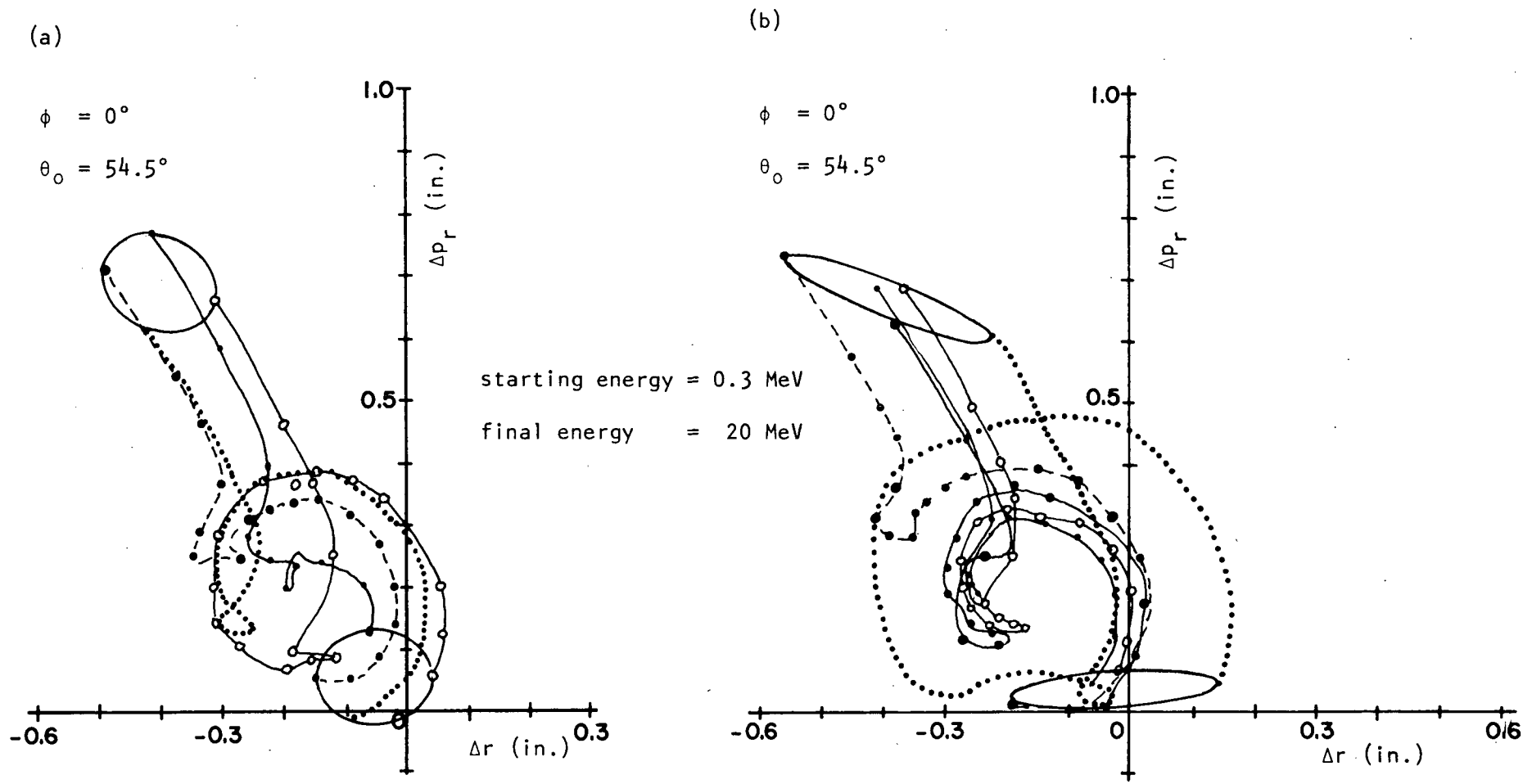


Fig. 4.24 Accelerated phase plots with  $\phi = 0$  deg for four points on the edge of the emittance ellipse a) matched to  $v_r = 1$ , and b) chosen to reduce the radial oscillation amplitude over the phase range  $-5$  deg to  $+25$  deg

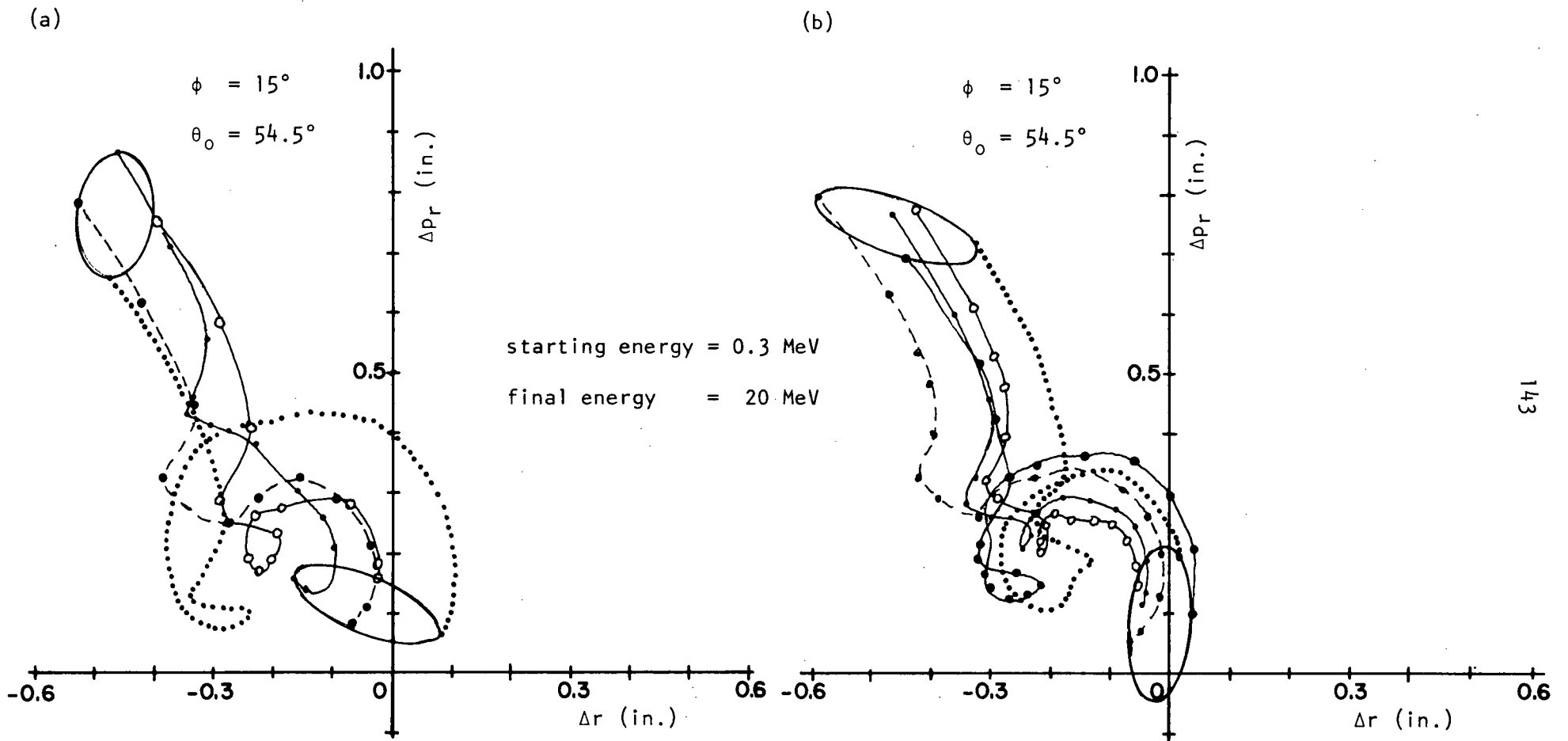


Fig. 4.25 Accelerated phase plots with  $\phi = +15$  deg for four points on the edge of the emittance ellipse a) matched to  $v_r = 1$ , and b) chosen to reduce the radial oscillation amplitude over the phase range  $-5$  deg to  $+25$  deg

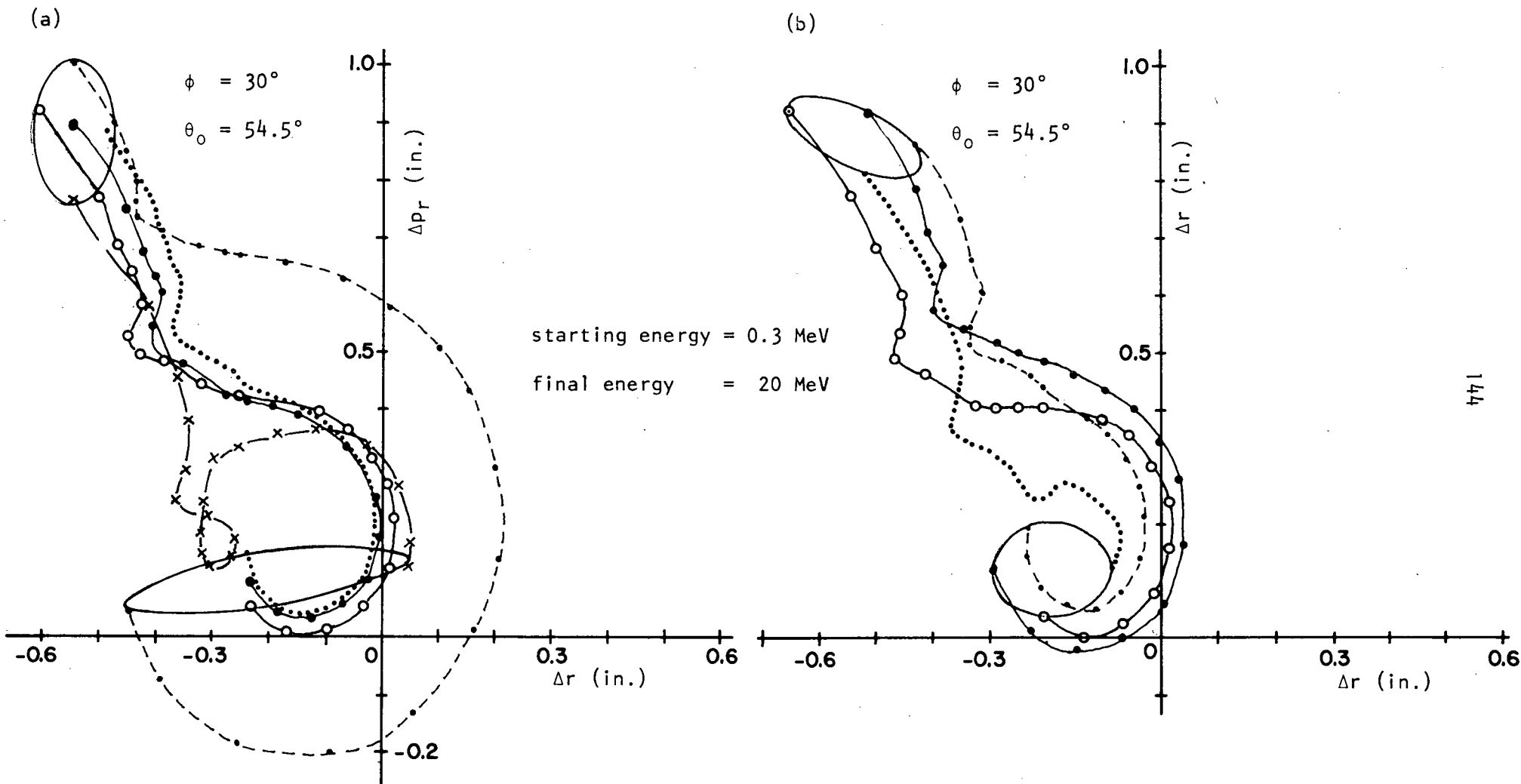


Fig. 4.26 Accelerated phase plots with  $\phi = +25$  deg for four points on the edge of the emittance ellipse a) matched to  $v_r = 1$ , and b) chosen to reduce the radial oscillation amplitude over the phase range  $-5$  deg to  $+25$  deg

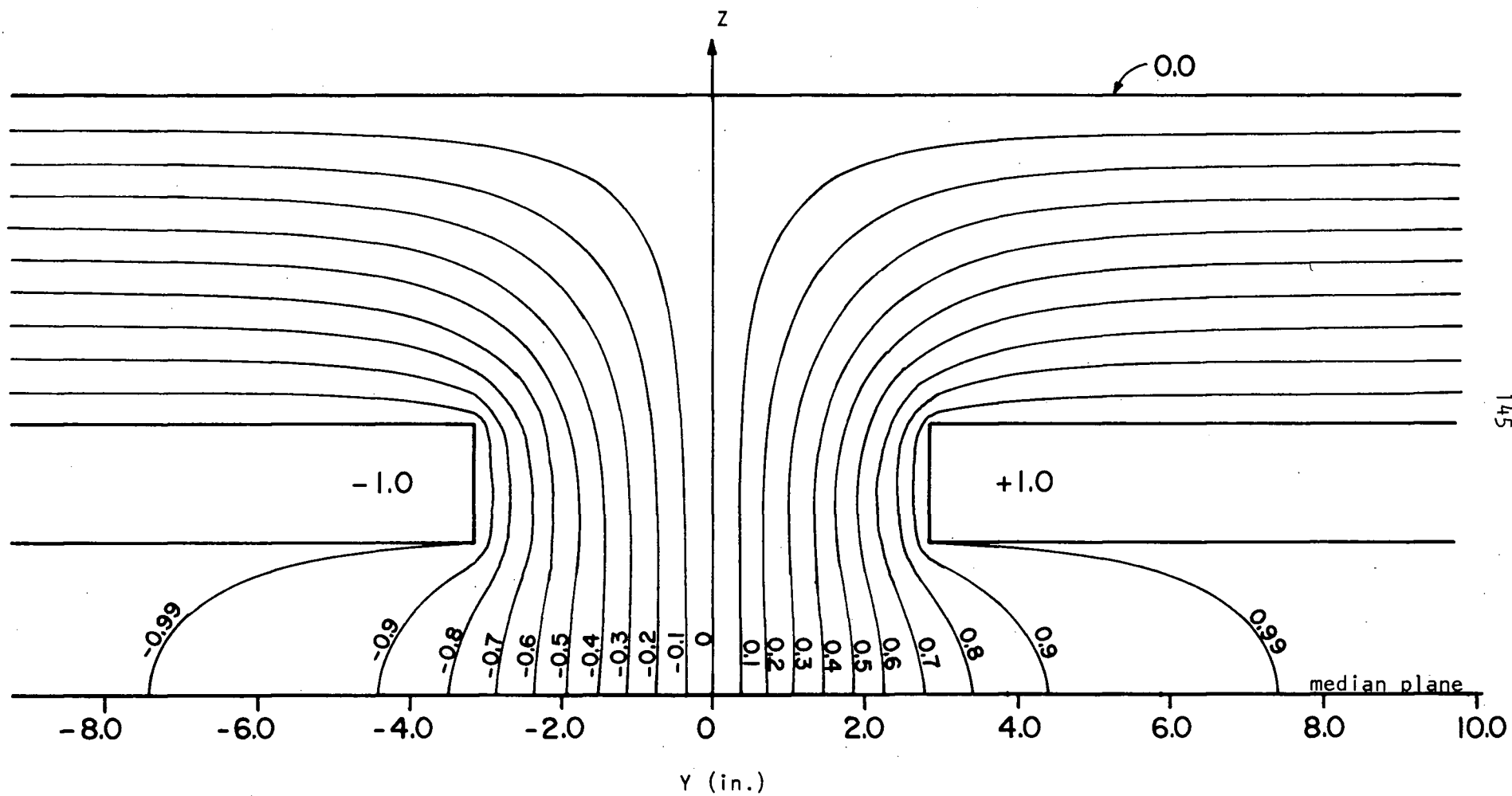


Fig. 5.1 Cross-section of a dee gap showing electric equipotentials

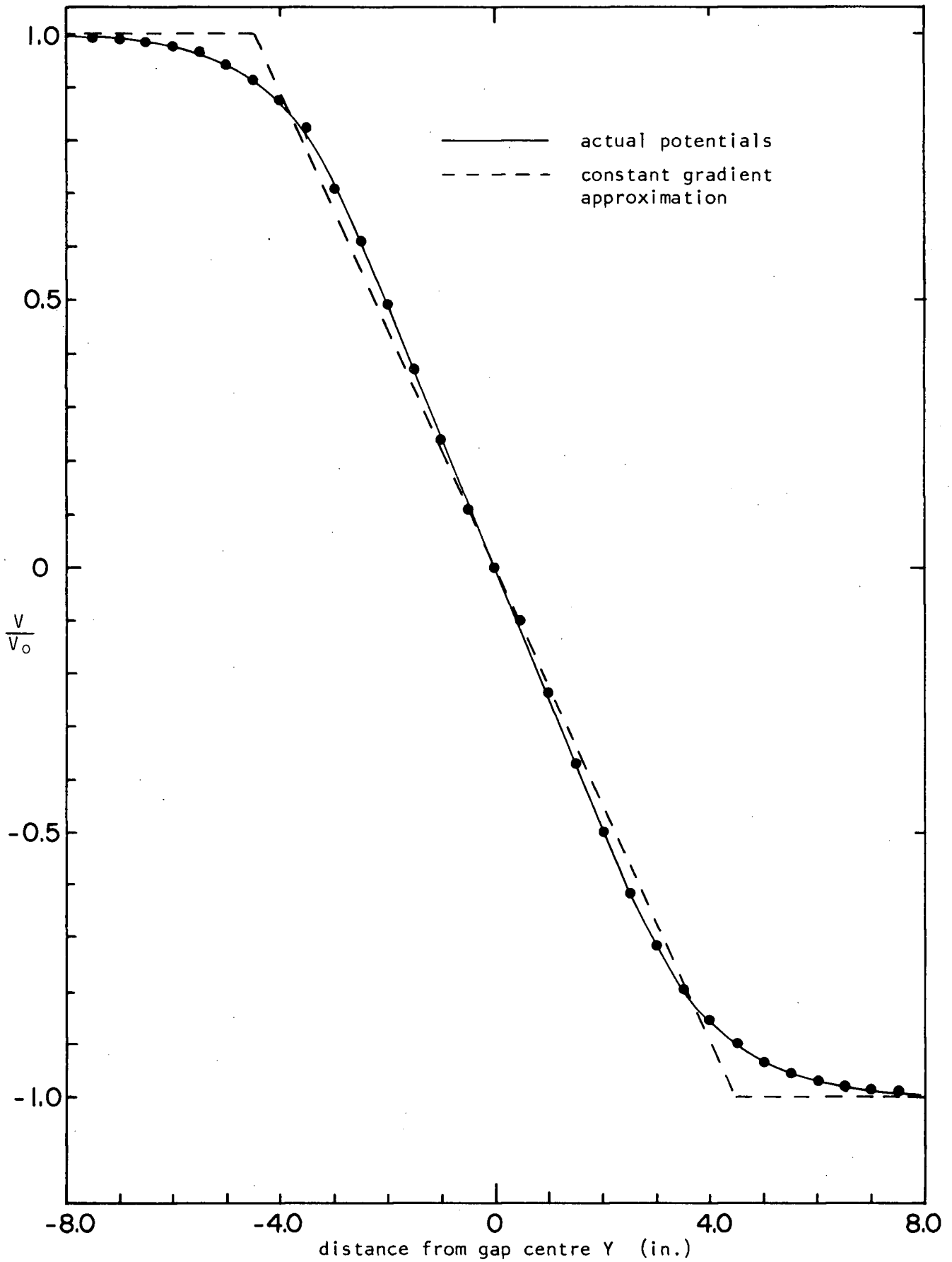


Fig. 5.2 Electric potential vs distance from dee gap centre showing actual values and constant gradient approximation

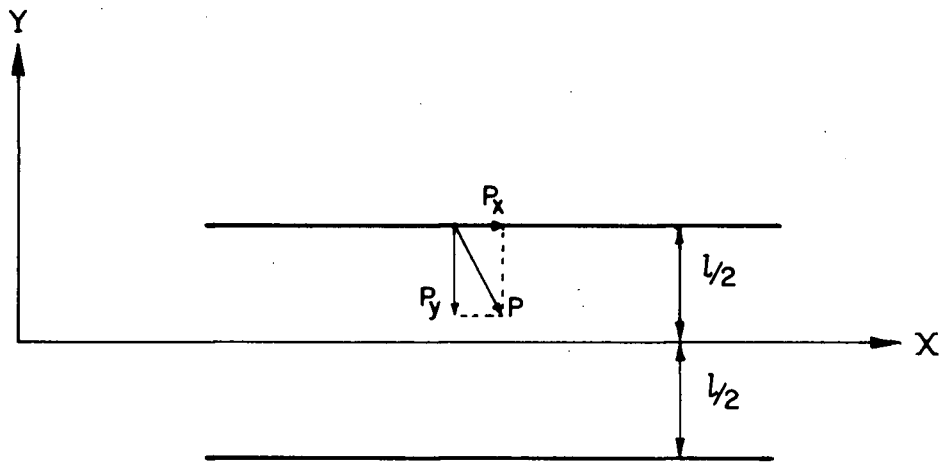


Fig. 5.3 Geometry of an ion crossing a dee gap

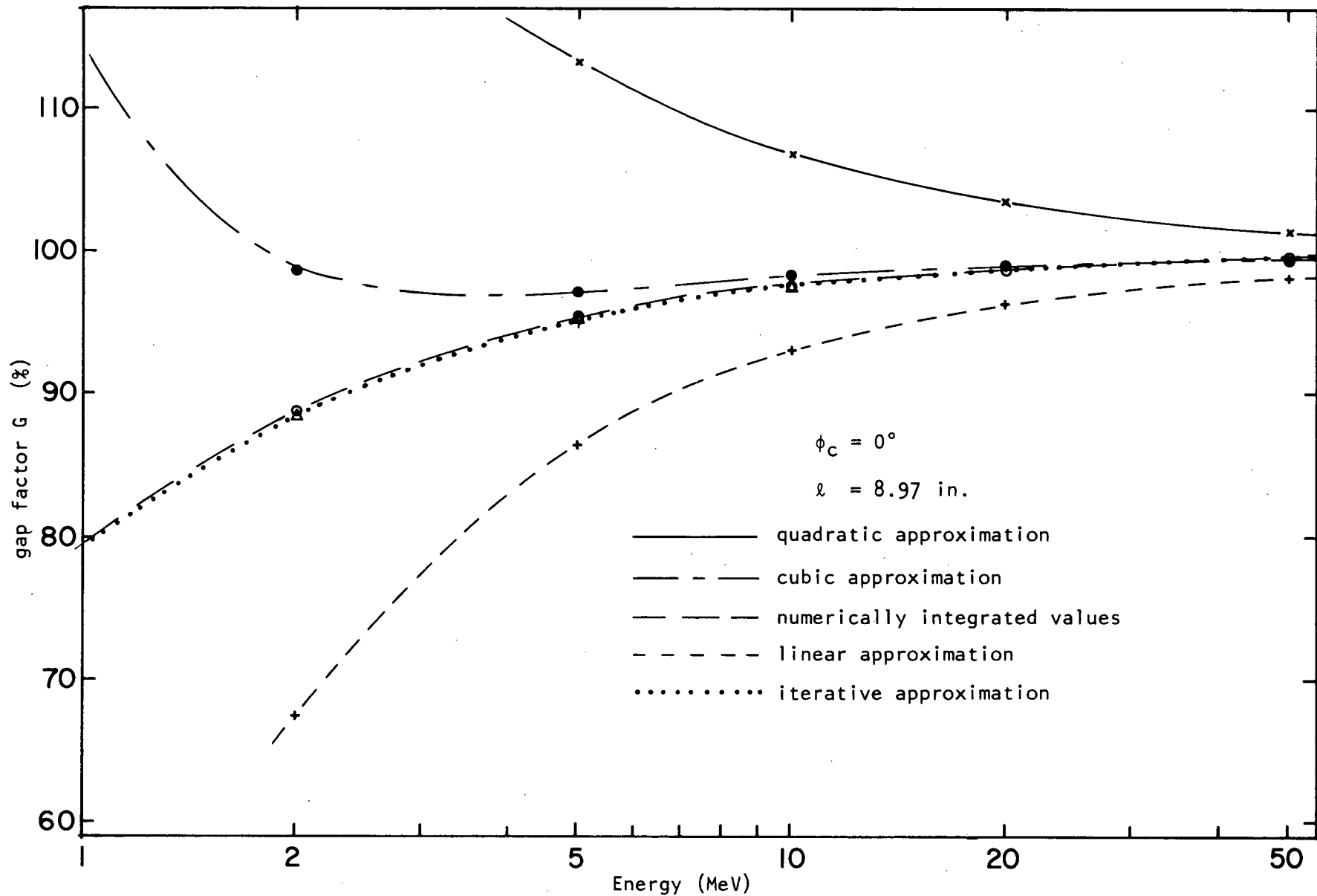


Fig. 5.4 Gap factors vs energy for  $\phi_c = 0 \text{ deg}$

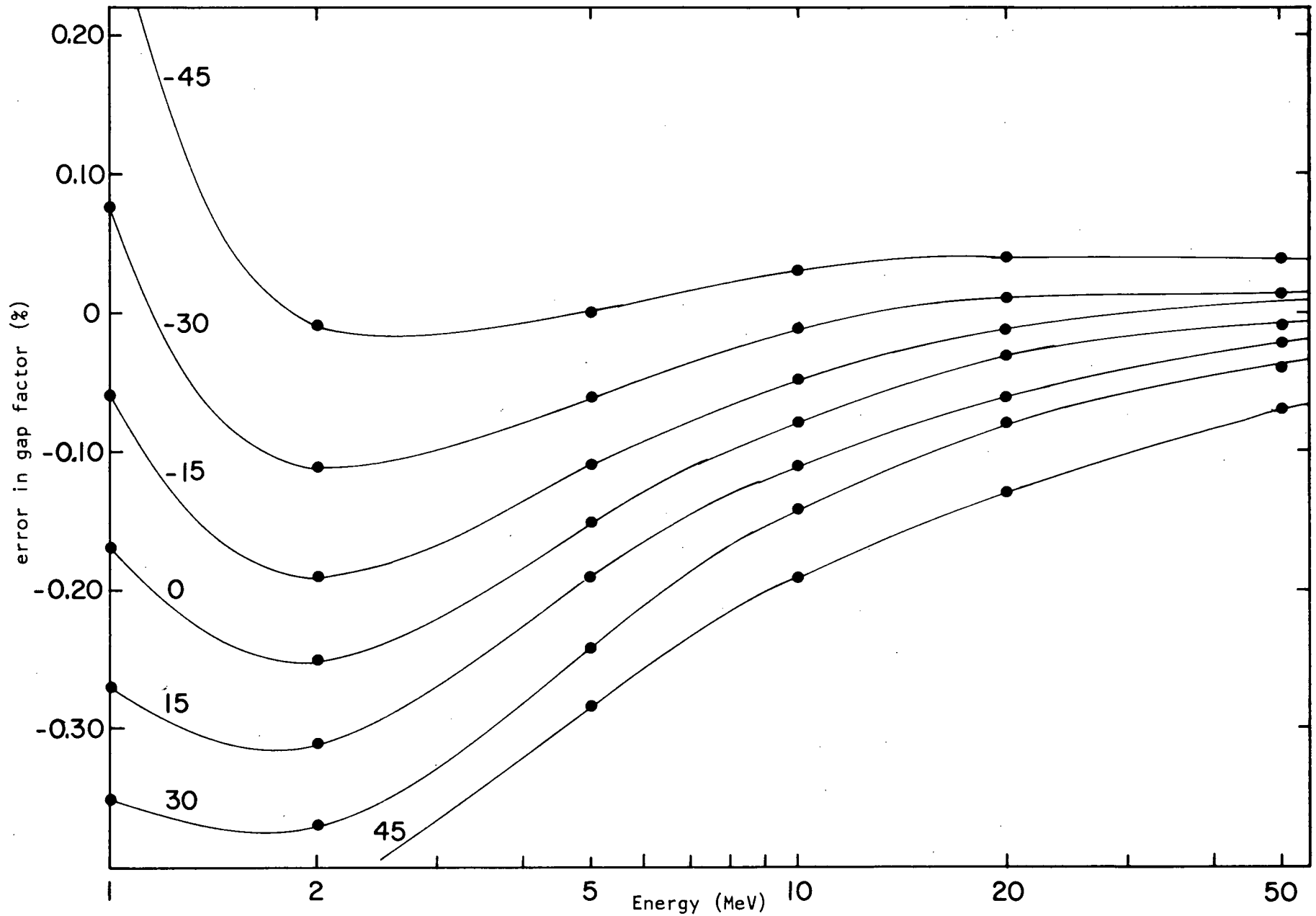


Fig. 5.5 Differences between gap factors obtained from numerical integration and those obtained from the constant gradient approximation as a function of energy, no magnetic field

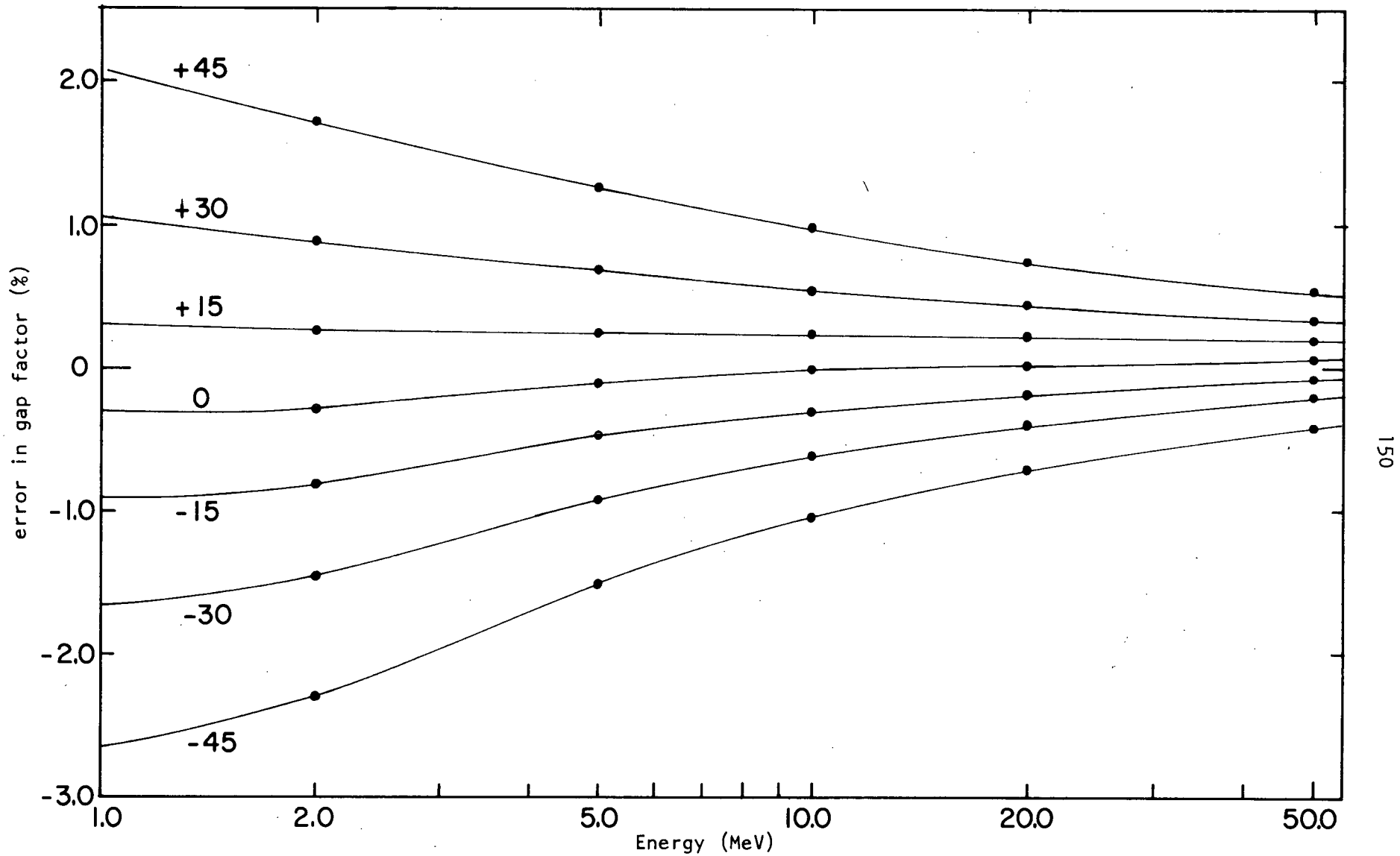


Fig. 5.6 Differences between gap factors obtained from numerical integration and those obtained from the constant gradient approximation as a function of energy, with an isochronous magnetic field

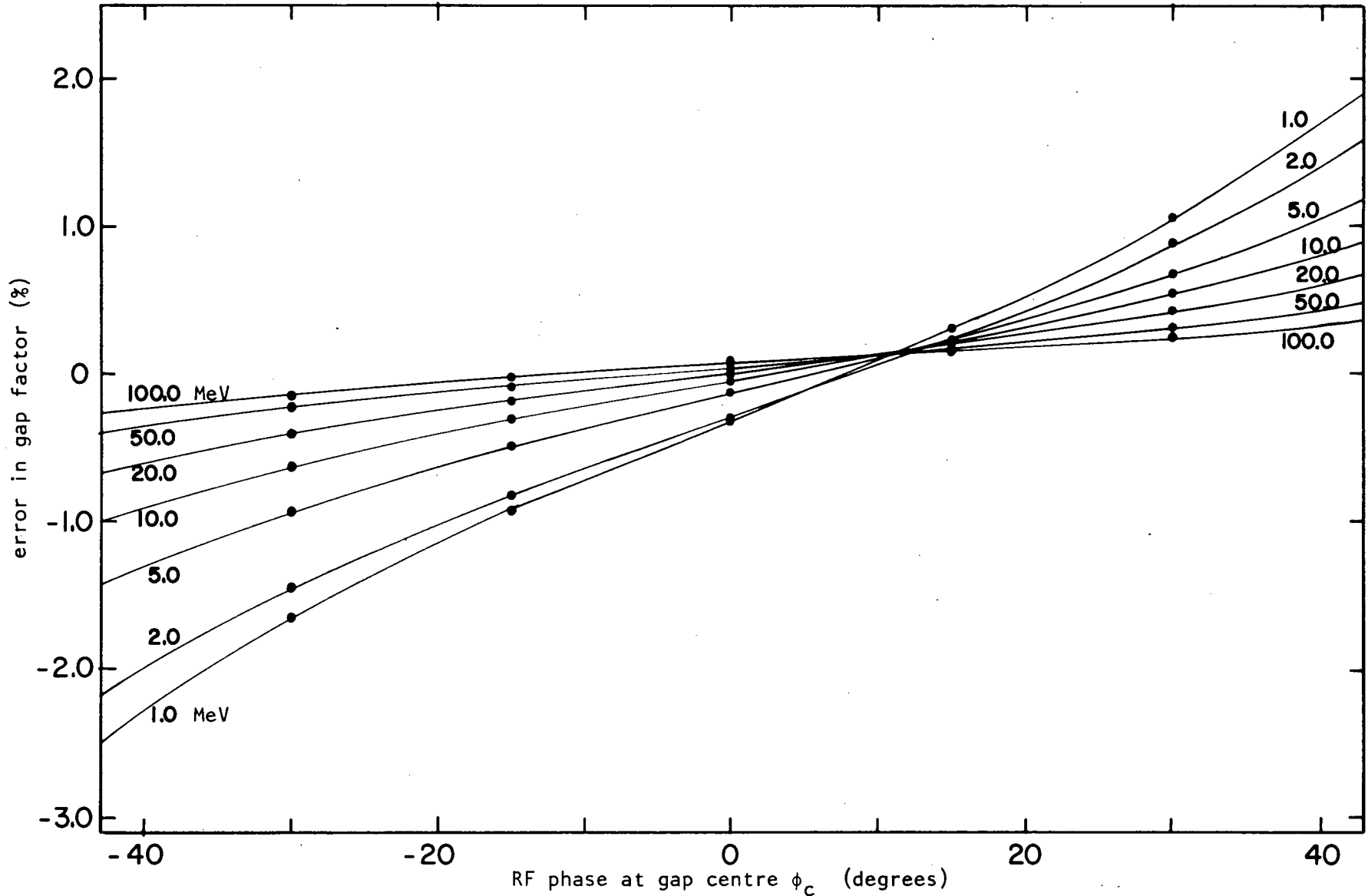


Fig. 5.7 Differences between gap factors obtained from numerical integration and those obtained from the constant gradient approximation as a function of RF phase, with an isochronous magnetic field.

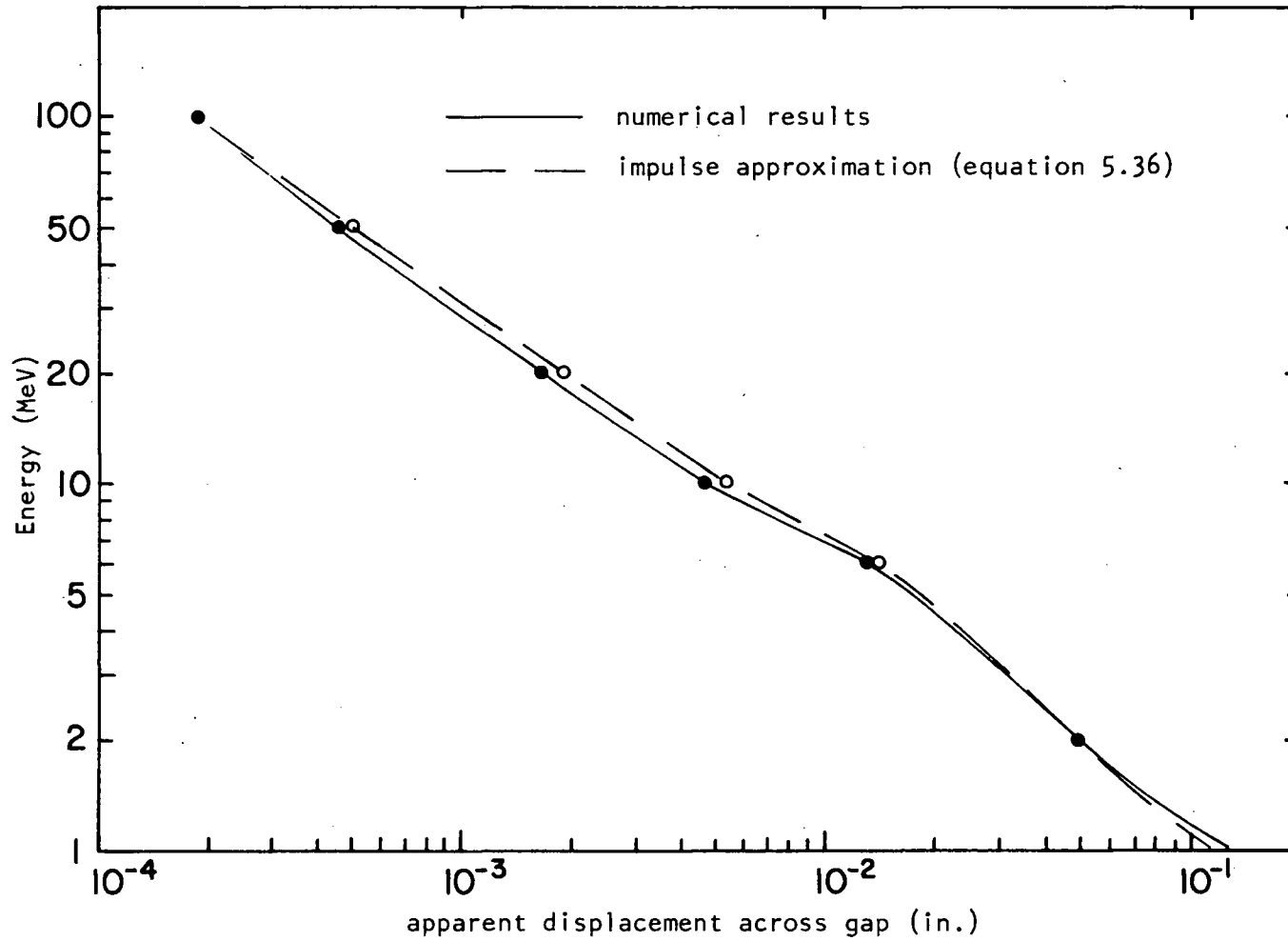


Fig. 5.8 Apparent displacement due to change in radius of curvature of the ion path while crossing the dee gap

Appendix A: THEORY OF SUCCESSIVE OVER-RELAXATION

We wish to solve a system of equations described by

$$\phi_{ijk} = \frac{1}{6} \left\{ \phi_{i-1jk} + \phi_{i+1jk} + \phi_{ij-1k} + \phi_{ij+1k} + \phi_{ijk-1} + \phi_{ijk+1} \right\}$$

[interior nodes]

$$= b_{ijk}$$

[boundary nodes]

$$i = 0, 1, 2 \dots p$$

$$j = 0, 1, 2 \dots q$$

$$k = 0, 1, 2 \dots r$$

The system contains N equations where  $N = (p + 1)(q + 1)(r + 1)$ .

We will start with some initial approximation for each unknown value of  $\phi$  denoted  $\phi_{ijk}^0$ . We will sequentially modify each of these values in the order

$$\begin{aligned} &\phi_{111} \phi_{211} \dots \phi_{p11} \phi_{121} \phi_{221} \dots \phi_{p21} \dots \dots \phi_{pq1} \phi_{112} \phi_{212} \dots \phi_{p12} \phi_{p22} \dots \\ &\dots \phi_{pq2} \dots \dots \dots \phi_{pqr} \end{aligned}$$

or in the opposite order.

The successive over-relaxation method can be described by the iterative sequence.

$$\phi_{ijk}^{n+1} = \phi_{ijk}^n + \frac{\alpha}{6} \left\{ \phi_{i-1jk}^{n+1} + \phi_{i+1jk}^n + \phi_{ij-1k}^{n+1} + \phi_{ij+1k}^n + \phi_{ijk-1}^{n+1} + \phi_{ijk+1}^n - 6 \phi_{ijk}^n \right\}$$

[interior nodes]

$$= b_{ijk}$$

[boundary nodes] (A.1)

$\phi_{ijk}^n$  is the  $n^{\text{th}}$  estimate of the value of the value of the potential at the node  $ijk$  and  $\alpha$  is a constant.

Now we define the error at the node  $ijk$  at the  $n^{\text{th}}$  iteration as

$$\varepsilon_{ijk}^n = \phi_{ijk}^n - \phi_{ijk} \quad (\text{A.2})$$

where  $\phi_{ijk}$  is the correct value at this node, then

$$\begin{aligned} \varepsilon_{ijk}^{n+1} + \phi_{ijk} = & \varepsilon_{ijk}^n + \phi_{ijk} + \frac{\alpha}{6} \left[ \varepsilon_{i-1jk}^{n+1} + \phi_{i-1jk} + \varepsilon_{i+1jk}^n + \phi_{i+1jk} + \right. \\ & \varepsilon_{ij-1k}^{n+1} + \phi_{ij-1k} + \varepsilon_{ij+1k}^n + \phi_{ij+1k} + \varepsilon_{ijk-1}^{n+1} + \phi_{ijk-1} + \\ & \left. \varepsilon_{ijk+1}^n + \phi_{ijk+1} - 6\varepsilon_{ijk}^n - 6\phi_{ijk} \right]. \end{aligned}$$

According to eqn.(2.2), the terms in  $\phi$  in the square bracket cancel, leaving

$$\begin{aligned} \varepsilon_{ijk}^{n+1} = & \varepsilon_{ijk}^n + \frac{\alpha}{6} \left( \varepsilon_{i-1jk}^{n+1} + \varepsilon_{i+1jk}^n + \varepsilon_{ij-1k}^{n+1} + \varepsilon_{ij+1k}^n + \varepsilon_{ijk-1}^{n+1} + \varepsilon_{ijk+1}^n \right. \\ & \left. - 6\varepsilon_{ijk}^n \right) \quad [\text{interior points}] \\ = 0 & \quad [\text{boundary points}] \quad (\text{A.3}) \end{aligned}$$

or

$$\begin{aligned} \varepsilon_{ijk}^{n+1} - \frac{\alpha}{6} \left( \varepsilon_{i-1jk}^{n+1} + \varepsilon_{ij-1k}^{n+1} + \varepsilon_{ijk-1}^{n+1} \right) = & \varepsilon_{ijk}^n + \frac{\alpha}{6} \left( \varepsilon_{i+1jk}^n + \varepsilon_{ij+1k}^n \right. \\ & \left. + \varepsilon_{ijk+1}^n \right). \end{aligned}$$

Clearly this method of iteration leads to a linear dependence of the  $\varepsilon_{ijk}^{n+1}$  on the  $\varepsilon_{ijk}^n$ , so we may write

$$\varepsilon_{ijk}^{n+1} = K\varepsilon_{ijk}^n \quad (\text{A.4})$$

and 
$$\varepsilon_{ijk}^{n+1} = K\varepsilon_{ijk}^n = K^2\varepsilon_{ijk}^{n-1} = \dots = K^n\varepsilon_{ijk}^0$$

where  $\varepsilon^{n+1}$  and  $\varepsilon^n$  are N-vectors whose elements are the N errors after n+1 and n iterations respectively. K is an N by N matrix which depends on  $\alpha$ , p, q and r, but not on n.

For an individual error  $\varepsilon_{ijk}$ , eqn.(A.4) can be written

$$\varepsilon_{ijk}^{n+1} = \sum_{i'j'k'} K_{ijk i'j'k'} \varepsilon_{i'j'k'}^n \quad (\text{A.5})$$

Now we denote the  $N$  eigenvalues of  $k$  by  $\lambda_\ell$  ( $\ell = 1, 2, \dots, N$ ) and the corresponding eigenvectors by  $\beta_\ell$ ,

$$k\beta_\ell = \lambda_\ell \beta_\ell. \quad (\text{A.6})$$

Since the eigenvectors form an orthogonal set, we can express the error vectors as a sum over the eigenvectors

$$\epsilon^n = \sum_\ell c_\ell^n \beta_\ell \quad (\text{A.7})$$

from eqn. (A.4)

$$\epsilon^{n+1} = \sum_\ell c_\ell^n k\beta_\ell = \sum_\ell c_\ell^n \lambda_\ell \beta_\ell \quad (\text{A.8})$$

hence 
$$c_\ell^{n+1} = \lambda_\ell c_\ell^n = \dots = \lambda_\ell^{n+1} c_\ell^0.$$

Now to evaluate the eigenvalues, we substitute eqns. (A.7) and (A.8) into (A.3), giving

$$\begin{aligned} \left( \sum_\ell c_\ell^{n+1} \beta_\ell \right)_{ijk} &= \left( \sum_\ell c_\ell^n \beta_\ell \right)_{ijk} + \frac{\alpha}{6} \left[ \left( \sum_\ell c_\ell^{n+1} \beta_\ell \right)_{i-1jk} + \left( \sum_\ell c_\ell^n \beta_\ell \right)_{i+1jk} \right. \\ &+ \left. \left( \sum_\ell c_\ell^{n+1} \beta_\ell \right)_{ij-1k} + \left( \sum_\ell c_\ell^n \beta_\ell \right)_{ij+1k} + \left( \sum_\ell c_\ell^{n+1} \beta_\ell \right)_{ijk-1} \right. \\ &+ \left. \left( \sum_\ell c_\ell^n \beta_\ell \right)_{ijk+1} - 6 \left( \sum_\ell c_\ell^n \beta_\ell \right)_{ijk} \right]. \end{aligned}$$

Using the second part of eqn. (A.8), this becomes

$$\begin{aligned} \sum_\ell c_\ell^n \left[ \left( \lambda_\ell^{-1} + \alpha \right) \left( \beta_\ell \right)_{ijk} - \frac{\alpha}{6} \left[ \lambda_\ell \left( \beta_\ell \right)_{i-1jk} + \left( \beta_\ell \right)_{i+1jk} + \lambda_\ell \left( \beta_\ell \right)_{ij-1k} \right. \right. \\ \left. \left. + \left( \beta_\ell \right)_{ij+1k} + \lambda_\ell \left( \beta_\ell \right)_{ijk-1} + \left( \beta_\ell \right)_{ijk+1} \right] \right] = 0. \end{aligned}$$

But this must be true for any error  $\epsilon^n$ , i.e. for any set of  $c_\ell^n$ ; hence

$$\begin{aligned} (\lambda_\ell^{-1} + \alpha) \left( \beta_\ell \right)_{ijk} &= \frac{\alpha}{6} \left[ \lambda_\ell \left( \beta_\ell \right)_{i-1jk} + \left( \beta_\ell \right)_{i+1jk} + \lambda_\ell \left( \beta_\ell \right)_{ij-1k} \right. \\ &\quad \left. + \left( \beta_\ell \right)_{ij+1k} + \lambda_\ell \left( \beta_\ell \right)_{ijk-1} + \left( \beta_\ell \right)_{ijk+1} \right] \quad (A.9) \end{aligned}$$

$$\ell = 1, 2, \dots, N$$

and

$$\left( \beta_\ell \right)_{0jk} = \left( \beta_\ell \right)_{i0k} = \left( \beta_\ell \right)_{ij0} = \left( \beta_\ell \right)_{pjk} = \left( \beta_\ell \right)_{iqk} = \left( \beta_\ell \right)_{ijr} = 0. \quad (A.10)$$

To evaluate the eigenvectors and eigenvalues we will follow the procedure first given by Frankel.<sup>39</sup> A more general treatment has been given by Young.<sup>40</sup> The elements  $\left( \beta_\ell \right)_{ijk}$  of the eigenfunctions are evidently<sup>41</sup>

$$\left( \beta_\ell \right)_{ijk} = A^i \sin \frac{\pi s i}{p} B^j \sin \frac{\pi t j}{q} C^k \sin \frac{\pi u k}{r} \quad (A.11)$$

where  $s = 1, 2, \dots, p - 1$

$t = 1, 2, \dots, q - 1$

$u = 1, 2, \dots, r - 1$

Substituting eqn. (A.11) into eqn. (A.9) gives

$$(\lambda^{-1} + \alpha) A^i \sin \frac{\pi s i}{p} B^j \sin \frac{\pi t j}{q} C^k \sin \frac{\pi u k}{r} = \quad (A.12)$$

$$\begin{aligned} &\frac{\alpha}{6} \left[ B^j \sin \frac{\pi t j}{q} C^k \sin \frac{\pi u k}{r} \left( \lambda A^{i-1} \sin \frac{\pi s (i-1)}{p} + A^{i+1} \sin \frac{\pi s (i+1)}{p} \right) \right. \\ &+ A^i \sin \frac{\pi s i}{p} C^k \sin \frac{\pi u k}{r} \left( \lambda B^{j-1} \sin \frac{\pi t (j-1)}{q} + B^{j+1} \sin \frac{\pi t (j+1)}{q} \right) \\ &\left. + A^i \sin \frac{\pi s i}{p} B^j \sin \frac{\pi t j}{q} \left( \lambda C^{k-1} \sin \frac{\pi u (k-1)}{r} + C^{k+1} \sin \frac{\pi u (k+1)}{r} \right) \right]. \end{aligned}$$

For eqn.(A.12) to be satisfied for all values of  $i, j$  and  $k$ , we must have

$$\lambda = A^2, \lambda = B^2, \lambda = C^2.$$

Since multiplication of  $A$  (or  $B$  or  $C$ ) by  $-1$  is equivalent to replacing  $s$  by  $p-s$  (or  $t$  by  $q-t$  or  $u$  by  $r-u$ ), we may take  $A = +B = +C$ .

Then eqn.(A.12) becomes

$$\begin{aligned} (A^2-1 + \alpha)A^i \sin\frac{\pi si}{p} A^j \sin\frac{\pi tj}{q} A^k \sin\frac{\pi uk}{r} = \\ \frac{\alpha}{6} \left( A^j \sin\frac{\pi tj}{q} A^k \sin\frac{\pi uk}{r} 2A^{i+1} \sin\frac{\pi si}{p} \cos\frac{\pi s}{p} \right. \\ \left. + A^i \sin\frac{\pi si}{p} A^k \sin\frac{\pi uk}{r} 2A^{i+1} \sin\frac{\pi tj}{q} \cos\frac{\pi t}{q} \right. \\ \left. + A^i \sin\frac{\pi si}{p} A^j \sin\frac{\pi tj}{q} 2A^{i+1} \sin\frac{\pi uk}{r} \cos\frac{\pi u}{r} \right) \\ = \frac{\alpha}{3} A \left( A^i \sin\frac{\pi si}{p} A^j \sin\frac{\pi tj}{q} A^k \sin\frac{\pi uk}{r} \left( \cos\frac{\pi s}{p} + \cos\frac{\pi t}{q} + \cos\frac{\pi u}{r} \right) \right) \end{aligned}$$

so

$$(A^2-1 + \alpha) = \frac{\alpha}{3} A \left( \cos\frac{\pi s}{p} + \cos\frac{\pi t}{q} + \cos\frac{\pi u}{r} \right)$$

$$A^2 - A\alpha v + (\alpha-1) = 0 \tag{A.13}$$

$$A = \frac{1}{2} \left( \alpha v \pm \sqrt{\alpha^2 v^2 - 4(\alpha-1)} \right) \tag{A.14}$$

where 
$$v = \frac{1}{3} \left( \cos\frac{\pi s}{p} + \cos\frac{\pi t}{q} + \cos\frac{\pi u}{r} \right) = \cos \theta.$$

Now in order to investigate the convergence rate we note that we have expressed the error vectors as linear combinations of the eigenvectors, and eqn.(A.8) can be written

$$\varepsilon^n = \sum_{\ell} c_{\ell}^n \beta_{\ell} = \sum_{\ell} \lambda_{\ell}^n c_{\ell}^0 \beta_{\ell}. \quad (\text{A.15})$$

We will call the  $\lambda_{\ell}$  with the largest absolute value  $\lambda_m$ . We can then write eqn. (A.15) as

$$\frac{\varepsilon^n}{\lambda_m^n} = c_m^0 \beta_m + \sum_{\substack{\ell \\ \ell \neq m}} \left( \frac{\lambda_{\ell}}{\lambda_m} \right)^n c_{\ell}^0 \beta_{\ell},$$

but since  $\lambda_m > \lambda_{\ell}$ ,  $\left( \frac{\lambda_{\ell}}{\lambda_m} \right)^n$  goes to zero as  $n$  becomes large and we obtain, for large  $n$ ,

$$\varepsilon^n = c_m^0 \beta_m \lambda_m^n. \quad (\text{A.16})$$

So, to achieve the maximum convergence rate, we want  $\lambda_m$  ( $= A^2$ , etc.) to be as small as possible. ( $\lambda_m$  must be less than one if the process is to converge.) Returning to our equation for  $A$ , then if we consider

$$\alpha^2 v^2 \leq 4(\alpha - 1), \quad (\text{A.17})$$

the roots of eqn. (A.14) are complex conjugates with magnitude  $|A|^2 = \alpha - 1$ ; however, if  $\alpha^2 v^2 > 4(\alpha - 1)$ , the roots will be real and unequal. Since the product of the roots is  $(\alpha - 1)$ , one of the roots must have a magnitude greater than  $\sqrt{\alpha - 1}$ . Hence, the minimum  $\lambda_m = \max \left\{ |A_1|^2, |A_2|^2 \right\}$  occurs for  $\alpha$  in the range  $\alpha^2 v^2 \leq 4(\alpha - 1)$ . Since the magnitude of  $\lambda_m$  in this range is  $(\alpha - 1)$ , the value of  $\alpha$  (called  $\alpha_b$ ) giving the smallest  $\lambda_m$  is the smaller of the two roots of

$$\alpha_b^2 v^2 = 4(\alpha_b - 1),$$

$$\text{i.e.} \quad \alpha_b = \frac{2}{1 + \sin \theta} = \frac{2 - 2\sqrt{1-v^2}}{v^2} = 1 + \left( \frac{v}{1 + \sqrt{1-v^2}} \right)^2 \quad (\text{A.18})$$

and

$$\lambda_m = A^2 = \left( \frac{\alpha_b v}{2} \right)^2 = \frac{1 - \sin \theta}{1 + \sin \theta} = \alpha_b - 1 = \frac{2}{v^2} (1 - \sqrt{1 - v^2}) - 1.$$

Since we are calculating the minimum of the maximum values of  $A$ , we must take the worst case, i.e. the largest value of  $v$ , which is

$$v = \frac{1}{3} \left( \cos \frac{\pi}{p} + \cos \frac{\pi}{q} + \cos \frac{\pi}{r} \right). \quad (\text{A.19})$$

In practical problems,  $p$ ,  $q$  and  $r$  are  $\gg 1$ , and we can obtain approximate expressions for  $\alpha_b$  and  $\lambda_m$

$$v \approx 1 - \frac{\pi^2}{6} \left( \frac{1}{p^2} + \frac{1}{q^2} + \frac{1}{r^2} \right), \quad \sin \theta \approx \pi \sqrt{\frac{1}{p^2} + \frac{1}{q^2} + \frac{1}{r^2}}, \quad (\text{A.20})$$

$$\alpha_b \approx 2 - 2\pi \sqrt{\frac{1}{3} \left( \frac{1}{p^2} + \frac{1}{q^2} + \frac{1}{r^2} \right)}, \quad (\text{A.21})$$

$$\lambda_m \approx 1 - 2\pi \sqrt{\frac{1}{3} \left( \frac{1}{p^2} + \frac{1}{q^2} + \frac{1}{r^2} \right)} = \alpha_b - 1. \quad (\text{A.22})$$

Now that we have found the value of  $\alpha$  which gives fastest convergence, the question of interest is how fast does it converge. Referring to eqn. (A.8), each iteration reduces each error by at least a factor  $\lambda_m$ ; hence  $n$  iterations reduce the error by at least a factor  $(\lambda_m)^n$ . Hence, to reduce the errors by a factor  $f$ , the number of iterations required is

$$n = \frac{\log f}{\log \lambda_m}. \quad (\text{A.23})$$

## Appendix B. BOUNDARY CONDITIONS FOR RELAXATION CALCULATIONS

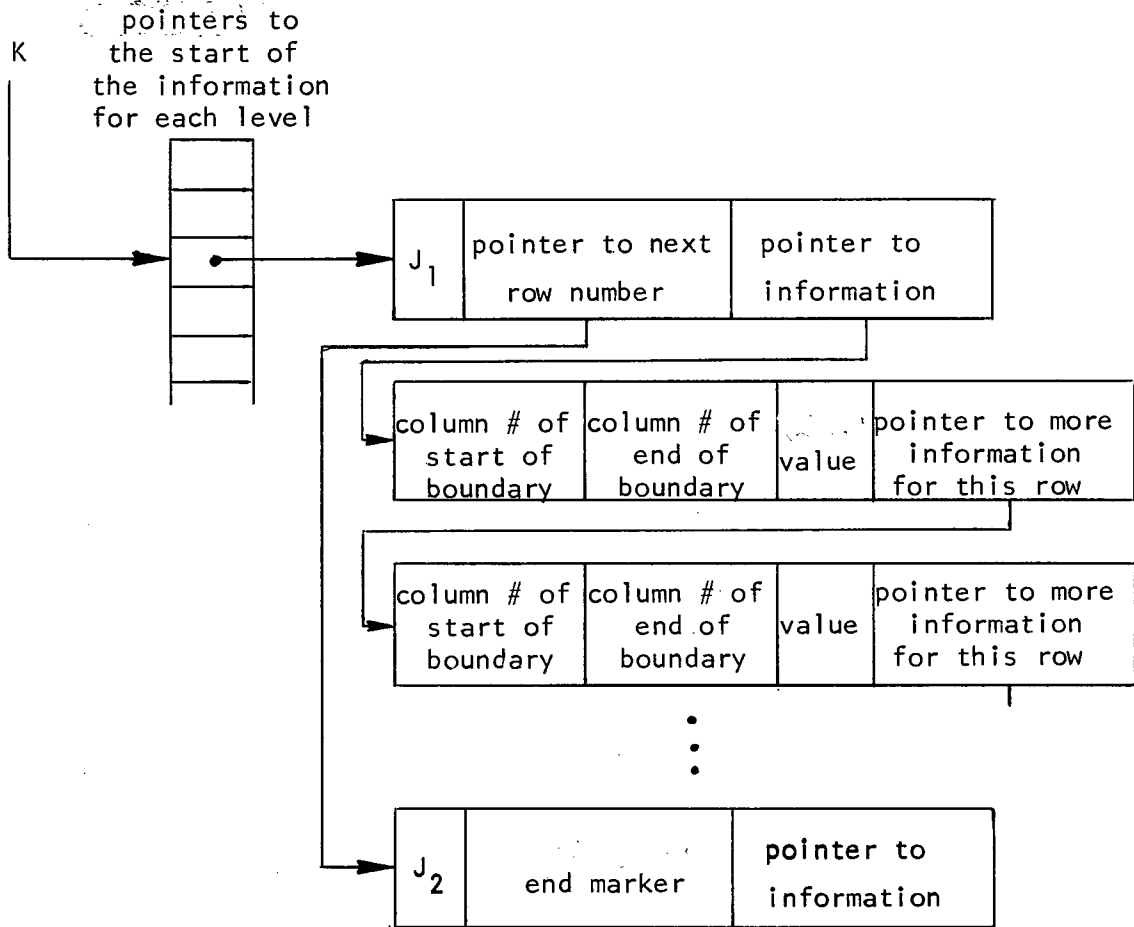
The relaxation program requires that boundary conditions be set before calculation starts. This consists of setting the boundary value for every point which lies on a boundary. Since typical problems contain  $10^5$  to  $10^6$  points, some automatic method must be found.

The relaxation program allows the user to supply a subroutine (BOUND) which returns boundary value when given the co-ordinates of each point. For complicated boundary shapes, this subroutine may be complicated to write and slow to execute. The program described here is fast and easy to use because it takes advantage of two characteristics of cyclotron-like geometries. First, these (three dimensional) geometries can be separated into several two dimensional geometries (planes) then the description of each plane and its vertical extent completely describes the three dimensional geometry. In the case of cyclotrons, it is natural to take these planes parallel to the median plane.

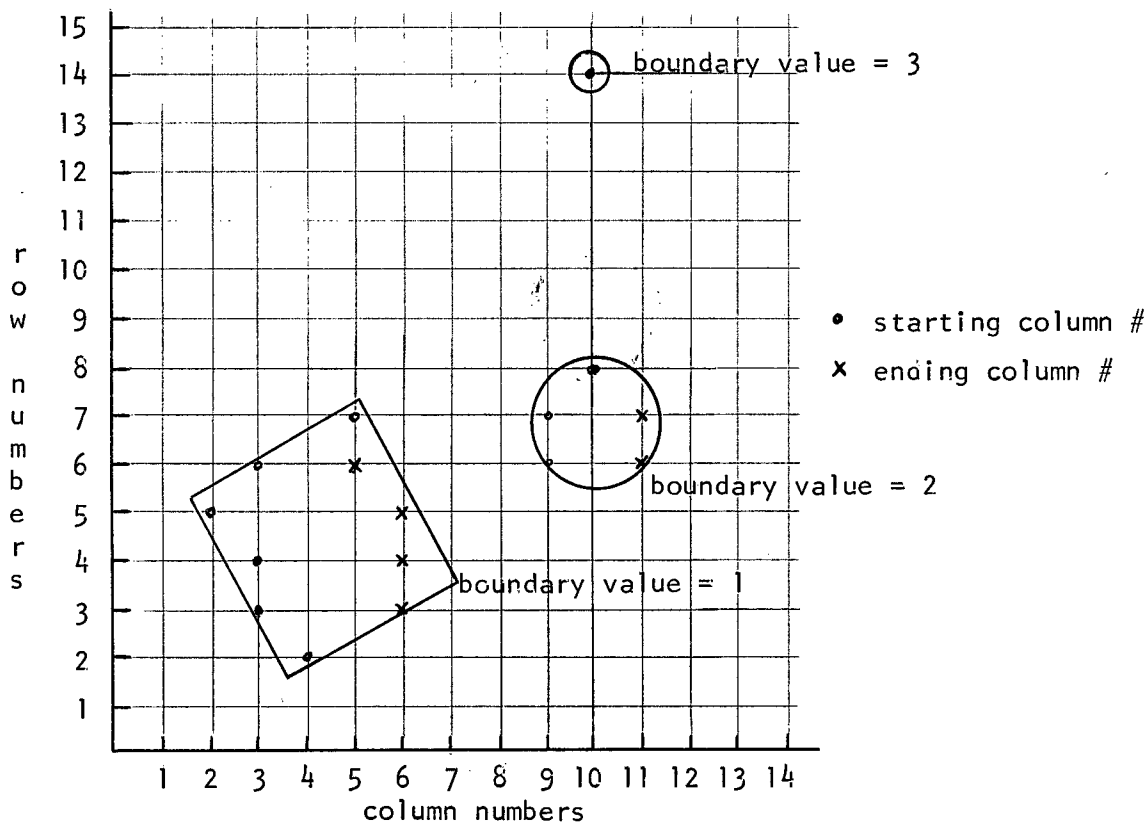
Secondly, the geometry of each of these planes can be made up from relatively simple shapes. If both these conditions are met then it is possible to devise a linked list structure which allows the boundaries to be entered in a simple way and produces output suitable for the relaxation program to read. In addition, the storage used by the program depends on the first power of the grid size (the storage required would vary as the third power of the grid size if all points were stored).

Consider a grid as shown in Fig. 2.1, a line of points with  $I$  and  $K$  constant is a column, with  $J$  and  $K$  constant is a row and a plane with  $K$  constant is a level. Now we choose to store information only about those points which fall on boundaries. The information stored is, for each

level, those rows which have boundaries in them, and for each of these rows, the start and end column number of the boundary and its boundary value. Note that one row may have several "pieces" of boundary in it hence there may be several entries for one row. The list scheme may be depicted schematically as follows, for level K, supposing rows  $J_1$  and  $J_2$  have boundaries in them.

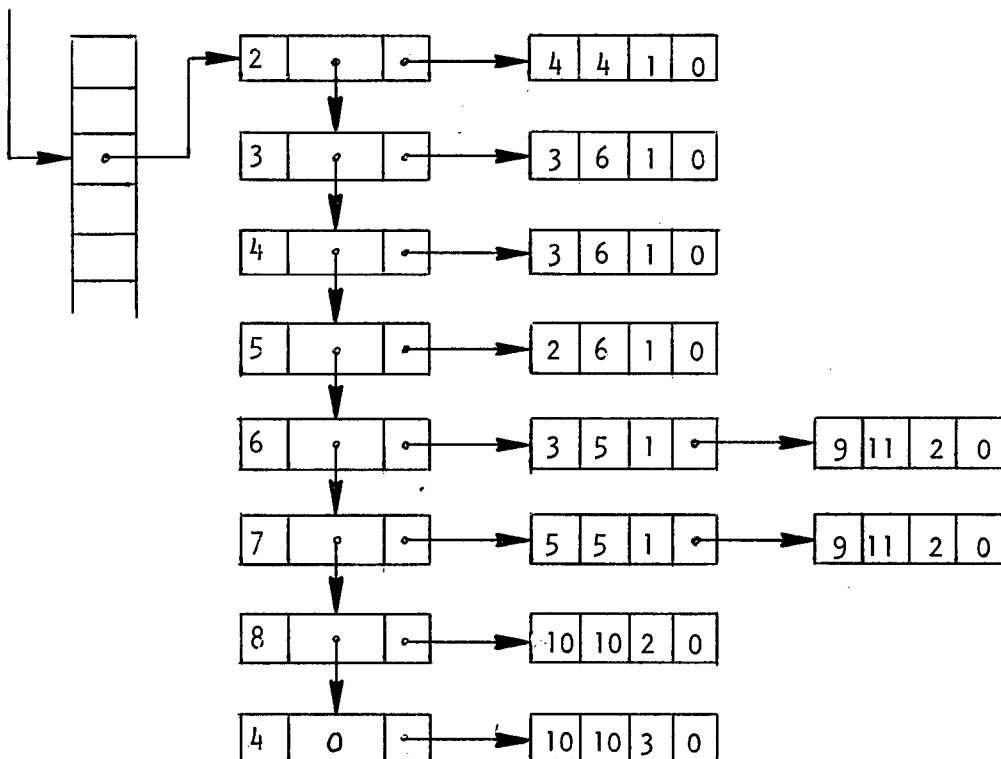


For example, if in level three we have the boundaries shown in the following figure



Then the list which describes this would look like

K = 3



There is no restriction on the number of boundaries which may cross any row. All of the storage comes out of one pool as required so that it is not necessary to know in advance how much storage will be required for each level or row. A test problem containing about  $10^5$  grid points required about 1500 words to store the boundary information.

Building the lists consists of reading a piece of the boundary and performing the following steps:

1. for each level involved, has a list been started?  
if not, start it.
2. search along the list for this level looking for the appropriate row number, if the row number is not in the list, enter it.
3. search along the list for this row, for an entry which overlaps the column numbers of the current entry. If an overlapping entry is found, modify its starting and ending column numbers so that it includes both the old entry and the current entry. If no overlapping entry is found, insert the current entry.
4. go on to the next row

The lists are maintained in order by row number but the entries for each row number are unordered.

Writing a tape containing values for every point requires an exhaustive search of the list for each point since it is not known that a point is not on a boundary until an entry for this point cannot be found in the list. This is done taking advantage of the fact that many levels are the same and is quite fast. The sample problem mentioned above required 0.6 minutes on an IBM 360/67 to set the boundaries and write the tape for the relaxation program.

## DATA REQUIRED

## 1. Problem Setup

first card (3F10.0, 3I5)

- 1) minimum X of grid
- 2) minimum Y of grid
- 3) grid spacing
- 4) # rows (a row has  $X = \text{constant}$ )
- 5) # columns (a column has  $Y = \text{constant}$ )
- 6) # levels

second, third . . . cards (3I5)

- 1) representative level number
- 2) level number of bottom of this representative level
- 3) level number of top of this representative level

subsequent cards define other representative levels, up to 32 are allowed, they can be entered in any order.

This input should be terminated by a blank card.

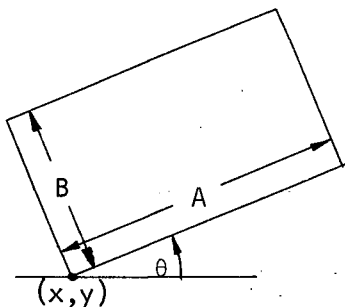
Next card (3F10.0)

- 1) the potential value to be dumped for boundary value 1
- 2) the potential value to be dumped for boundary value 2
- 3) the potential value to be dumped for boundary value 3

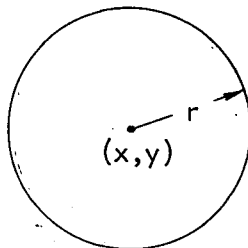
The relaxation program requires that the boundary conditions be in the range 0.0 to -1.0. BDRY requires that the boundary values be 1, 2 or 3. The above input allows the conversion to be made.

## 2. Description of Boundaries

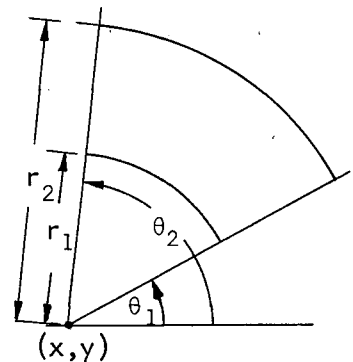
The shapes which the boundary must be broken into are



type = 1



type = 2



type = 3

These areas may overlap and may extend outside the grid.

One data card is required for each area.

(2I5, 6F10.0, 12, 1X, 2I2)  
P1, P2...P7,P8, P9,P10

	Rectangle	Circle	Annulus
	P1 = 1	P1 = 2	P1 = 3
P2	X	X	X
P3	Y	Y	Y
P4	$\theta$	R	$\theta_1$
P5	A		$\theta_2$
P6	B		R <sub>1</sub>
P7			R <sub>2</sub>
P8	the representative level number of the start of this section of boundary		
P9	the representative level number of the end of this section of boundary		
P10	the boundary value		

The program requires  $\theta_1 < \theta_2$  and the interval  $\theta_1, \theta_2$  must not contain zero (some annuli will have to be entered in two parts).

As many data cards as required can be used, terminated by a blank card.

### 3. Output of Results. (2F10.0) P1, P2

Two types of output are available

- 1) a printout of the boundary values at each grid point for one level
- 2) a dump of the boundary information in a form that the relaxation routine RESTOR can read.

A single card is required (for either output).

- P1     1 for dump of one level onto printer  
       2 for dump of all boundaries for relaxation program
- P2     if dump on printer, = level number to be dumped  
       if dump for relaxation program, = logical unit to dump onto

A series of these may be used (for example to display several levels on the printer then dump onto tape).

This input should be terminated by a blank card.

```

INTEGER LOROW ,HIROW,LOCOL,HICOL
INTEGER ISTART(10),IEND(10),VAL(10),HEADL(20),HEADR(500,3),
1 INFO(6000),POINT
COMMON IPLACE,ISTART,IEND,VAL,HEADL,HEADR,INFO,IINFO,IHEADR,POINT
CALL SET(BEGIN)
COMMON/QUA/QUAL(3)
COMMON/SIZE/NROW,NCOL,NLEV
COMMON/CORR/UNRL(20),BOT(20),TOP(20),NUMB
INTEGER UNRL,BOT,TOP
C READ GRID SPECS
READ(5,100)XO,YO,DELT,NROW,NCOL,NLEV
100 FORMAT(3F10.0,3I5)
WRITE(6,101)XO,YO,DELT,NROW,NCOL,NLEV
101 FORMAT('1',
1 ' ', 'GRID POINT 1,1 IS AT X= ',F10.3,' Y= ',F10.3,/
1 ' ', 'GRID SPACING IS= ',F10.3/
2 ' ', 'GRID SIZE (ROW BY COL BY LEVEL) IS',
6I5,' BY ',I5,' BY ',I5/
3 ' INCREASING ROW NUMBER IS IN DIRECTION OF INCREASING X'/
4 ' INCREASING COLUMN NUMBER IS IN DIRECTION OF INCREASING Y'//)
I=0
234 I=I+1
READ(5,232)UNRL(I),BOT(I),TOP(I)
232 FORMAT(3I5)
IF (UNRL(I).NE.0)GO TO 234
NUMB=I-1
DO 236 I=1,NUMB
WRITE(6,237)UNRL(I),BOT(I),TOP(I)
237 FORMAT(' LEVEL ',I3,' EXTENDS FROM ',I3,' TO ',I3)
236 CONTINUE
WRITE(6,803)
803 FORMAT(//)
READ(5,805)(QUAL(I),I=1,3)
806 FORMAT(1X,'INTERNAL VALUE= ',I3,'VALUE DUMPED=',F10.7)
DO 804 I=1,3
WRITE(6,806)I,QUAL(I)
804 CONTINUE
805 FORMAT(3F10.0)
WRITE(6,802)
802 FORMAT(1X,'INPUT DATA')
C READ BOUNDARY SPECS
900 READ(5,102,END=996)ITYPE,VALUE,T1,T2,T3,T4,T5,T6,IAA,IAB
CALL CLOCK
102 FORMAT(2I5,6F10.0,I2,1X,I2)
C
C CHECK FOR INVALID CODE
IF(ITYPE.EQ.0)GO TO 996
IF(ITYPE.GT.0.AND.ITYPE.LT.5) GO TO 5
WRITE(6,103)ITYPE,VALUE,T1,T2,T3,T4,T5,T6,IAA,IAB
103 FORMAT(' INVALID TYPE CODE , OFFENDING CARD IS'/
11X,2I5,6F10.3,2I4)
GO TO 900
C
C BRANCH FOR DIFFERENT BOUNDARY AREA TYPES
5 GO TO (1,2,3),ITYPE
C TYPE 1 THE AREA IS A RECTANGLE
1 X=T1
Y=T2
THETA=T3

```

```

A=T4
B=T5
WRITE(6,110)X,Y,THETA,A,B,VALUE,IAA,IAB
110 FORMAT(' RECTANGLE',T11,'X= ',F9.3,T24,'Y= ',F9.3,T37,
1'THETA= ',F9.3,T55,'A= ',F9.3,T73,'B= ',F9.3,T103,'VALUE= ',I2,
1T113,'LEVELS',I2,' TO ',I2)
THETA=THETA/57.29578
DIAG=SQRT(A*A+B*B)
ANG=ATAN(B/A)
LOCOL=IFIX ((Y-YO)/DELT)
HICOL=IFIX ((Y+DIAG*SIN(THETA+ANG)-YO)/DELT)+1
LOROW=IFIX ((X-B*SIN(THETA)-XO)/DELT)
HIROW=IFIX ((X+A*COS(THETA)-XO)/DELT)+1
IF(LOROW.LT.1)LOROW=1
IF(LOCOL.LT.1)LOCOL=1
IF(HIROW.GT.NROW)HIROW=NROW
IF(HICOL.GT.NCOL)HICOL=NCOL
C WRITE(6,876)LOROW,HIROW,LOCOL,HICOL
C 876 FORMAT(' LOROW=',I4,' HIROW=',I4,' LOCOL=',I4,' HICOL=',I4)
DO 10 I=LOROW,HIROW
DO 11J=LOCOL,HICOL
XX=FLOAT(I-1)*DELT+XO
YY=FLOAT(J-1)*DELT+YO
C
C TRANSFORM TO COORDINATE SYSTEM ORIENTED WITH RECTANGLE
XS=XX
YS=YY
XX=(XS-X)*COS(THETA)+(YS-Y)*SIN(THETA)
YY=(YS-Y)*COS(THETA)-(XS-X)*SIN(THETA)
C IF(XX.GE.0.0.AND.XX.LE.A.AND.YY.GE.0.0.AND.YY.LE.B)
C *WRITE(6,884)XS,YS
C 884 FORMAT(1X,2E12.3)
IF(XX.GE.0.0.AND.XX.LE.A.AND.YY.GE.0.0.AND.YY.LE.B)
1CALL SAVE(J,VALUE)
11 CONTINUE
IF(IPLACE.NE.0)CALL INSERT(I,IAA,IAB)
DO 781 IQZ=1,IPLACE
1START(IQZ)=0
1END(IQZ)=0
781 VAL(IQZ)=0
IPLACE=0
10 CONTINUE
C
GO TO 900
C
C
C
C TYPE 2 , THE AREA IS A CIRCLE
2 X=T1
Y=T2
R=T3
WRITE(6,120)X,Y,R,VALUE,IAA,IAB
120 FORMAT(' CIRCLE',T11,'X= ',F9.3,T24,'Y= ',F9.3,T37,'R= ',F9.3,
1T103,'VALUE= ',I2,T113,'LEVELS',I2,' TO ',I2)
C
LOCOL=IFIX((Y-R-YO)/DELT)
HICOL=IFIX((Y+R-YO)/DELT)+1
LOROW=IFIX((X-R-XO)/DELT)
HIROW=IFIX((X+R-XO)/DELT)+1
IF(LOROW.LT.1)LOROW=1

```

```

      IF (LOCAL.LT.1)LOCAL=1
      IF (HIROW.GT.NROW)HIROW=NROW
      IF (HICOL.GT.NCOL)HICOL=NCOL
      DO 20 I=LOROW,HIROW
      DO 21 J=LOCAL,HICOL
      XX=FLOAT(I-1)*DELTA+XO
      YY=FLOAT(J-1)*DELTA+YO
C      IF ((XX-X)**2+(YY-Y)**2.LE.R*R)WRITE(6,884)XX,YY
      IF ((XX-X)**2+(YY-Y)**2.LE.R*R)CALL SAVE (J,VALUE)
C
C 21 CONTINUE
      IF (IPLACE.NE.0)CALL INSERT(I,IAA,IAB)
      DO 782 IQZ=1,IPLACE
      ISTART(IQZ)=0
      IEND(IQZ)=0
      782 VAL(IQZ)=0
      IPLACE=0
C 20 CONTINUE
      GO TO 900
C
C
C
C 3 TYPE 3 , THE AREA IS AN ANNULUS
      X=T1
      Y=T2
      THETA1=T3
      THETA2=T4
      R1=T5
      R2=T6
      WRITE(6,130)X,Y,THETA1,THETA2,R1,R2,VALUE,IAA,IAB
C 130 FORMAT(' ANNULUS',T11,'X= ',F9.3,T24,'Y= ',F9.3,T37,'THETA1= ',
      1F9.3,T55,'THETA2= ',F9.3,T73,'R1= ',F9.3,T88,'R2= ',F9.3,T103,
      1'VALUE= ',I2,T113,'LEVELS',I2,' TO ',I2)
      THETA1=THETA1/57.29578
      THETA2=THETA2/57.29578
C
C90=1.5707963
C180=3.1415927
C270=4.7123890
      IAX=IFIX((X-R2*COS(C180-THETA2)-XO)/DELTA)
      IAY=IFIX((Y+R2*SIN(C180-THETA2)-YO)/DELTA)
      IBX=IFIX((X-R1*COS(C180-THETA2)-XO)/DELTA)
      IBY=IFIX((Y+R1*SIN(C180-THETA2)-YO)/DELTA)
      ICX=IFIX((X+R2*COS(THETA1)-XO)/DELTA)
      ICY=IFIX((Y+R2*SIN(THETA1)-YO)/DELTA)
      IDX=IFIX((X+R1*COS(THETA1)-XO)/DELTA)
      IDY=IFIX((Y+R1*SIN(THETA1)-YO)/DELTA)
      IX=IAX
      IY=IAY
      JX=IAX
      JY=IAY
      IF (THETA1.LT.C90.AND.THETA2.GT.C90) IY=IFIX((Y+R2-YO)/DELTA)
      IF (THETA1.LT.C180.AND.THETA2.GT.C180) JX=IFIX((X-R2-XO)/DELTA)
      IF (THETA1.LT.C270.AND.THETA2.GT.C270) JY=IFIX((Y-R2-YO)/DELTA)
      IF (THETA1.LT.0.0.AND.THETA2.GT.0.0) IX=IFIX((X+R2-XO)/DELTA)
      LOCAL=MINO (IAY,IBY,ICY,IDY,JY)
      HICOL=MAXO(IAY,IBY,ICY,IDY,IY)+1
      LOROW=MINO(IAX,IBX,ICX,IDX,JX)
      HIROW=MAXO(IAX,IBX,ICX,IDX,IX)+1
      IF (LOROW.LT.1)LOROW=1

```

```

      IF(LOCOL.LT.1)LOCOL=1
      IF(HIROW.GT.NROW)HIROW=NROW
      IF(HICOL.GT.NCOL)HICOL=NCOL
      DO 30 I=LOROW,HIROW
      DO 31 J=LOCOL,HICOL
      XX=FLOAT(I-1)*DELT +X0
      YY=FLOAT(J-1)*DELT +Y0
      TRANSFORM TO POLAR COORDINATES
C
C
      RR=SQRT((XX-X)**2+(YY-Y)**2)
      IF(RR.EQ.0.0)GO TO714
      TT=ATAN2(YY-Y,XX-X)
      IF(TT.LT.0.0)TT=TT+6.2831852
C
C
      IF(TT.GE.THETA1.AND.TT.LE.THETA2.AND.
      *RR.GE.R1.AND.RR.LE.R2)WRITE(6,823)
C
C
      *TT,THETA1,THETA2,RR,R1,R2,XX,YY
C 823 FORMAT(1X,8E12.3)
C
      IF(TT.GE.THETA1.AND.TT.LE.THETA2.AND.
      1 RR.GE.R1.AND.RR.LE.R2)CALL SAVE(J,VALUE)
      714 CONTINUE
C
C
31 CONTINUE
      IF(IPLACE.NE.0)CALL INSERT(I,IAA,IAB)
      DO 783 IQZ=1,IPLACE
      ISTART(IQZ)=0
      IEND(IQZ)=0
      783 VAL(IQZ)=0
      IPLACE=0
30 CONTINUE
      GO TO 900
C
C
C
999 READ(5,231,END=9999)IJ,IK
231 FORMAT(2I3)
      IF(IJ.EQ.0)GO TO 9999
      IF(IJ.EQ.1)CALL OUTPUT(NROW,NCOL,BEGIN,TLAST,IK)
      IF(IJ.EQ.2)CALL DUMP(IK)
996 WRITE(6,107)IHEADR,IINFO
107 FORMAT(1X,I5,' PLACES USED IN ROW HEADR ARRAY'/
      11X,I5,' PLACES USED IN INFORMATION ARRAY')
      GO TO 999
9999 STOP
      END
      SUBROUTINE SAVE(NCOL,VALUE)
      INTEGER ISTART(10),IEND(10),VAL(10),HEADL(20),HEADR(500,3),
      1 INFO(6000),POINT
      COMMON IPLACE,ISTART,IEND,VAL,HEADL,HEADR,INFO,IINFO,IHEADR,POINT
      INTEGER VALUE
      IF(IPLACE.EQ.0)GO TO 1
      IF(VALUE.EQ.VAL(IPLACE))GO TO 2
      1 IPLACE=IPLACE+1
      ISTART(IPLACE)=NCOL
      IEND(IPLACE)=NCOL
      VAL(IPLACE)=VALUE
C
C
      WRITE(6,66)IPLACE,VAL(IPLACE)
C 66 FORMAT(' IPLACE=',I5,' VAL(IPLACE)=' ,I5)
      RETURN
      2 IF(NCOL.NE.IEND(IPLACE)+1)GO TO 1

```

```

IEND(IPLACE)=NCOL
RETURN
END
SUBROUTINE SET
INTEGER ISTART(10),IEND(10),VAL(10),HEADL(20),HEADR(500,3),
1 INFO(6000),POINT
COMMON IPLACE,ISTART,IEND,VAL,HEADL,HEADR,INFO,IINFO,IHEADR,POINT
DO 1 I=1,20
1 HEADL(I)=0
DO 2 I=1,500
DO 2 J=1,3
2 HEADR(I,J)=0
DO 3 I=1,6000
3 INFO(I)=0
DO 4 I=1,10
ISTART(I)=0
IEND(I)=0
4 VAL(I)=0
IINFO=1
IHEADR=1
IPLACE=0
RETURN
END
SUBROUTINE INSERT(NROW,IAA,IAB)
DIMENSION LEVEL(20)
INTEGER ISTART(10),IEND(10),VAL(10),HEADL(20),HEADR(500,3),
1 INFO(6000),POINT
INTEGER START,END,VALUE
COMMON IPLACE,ISTART,IEND,VAL,HEADL,HEADR,INFO,IINFO,IHEADR,POINT
C INITIALLY , LEVEL HEADERS ARE SET TO ZERO
C IINFO POINTS TO THE FIRST EMPTY SPACE IN THE INFO ARRAY
C IHEADR POINTS TO THE FIRST EMPTY SPACE IN THE HEADR ARRAY
C LOOP OVER THE ARRAY LEVEL TO SEE WHICH LEVELS
C TO ENTER THE BOUNDARY CONDITIONS INTO
C
555 CONTINUE
DO 800 I=IAA,IAB
C
C HEADL(I) POINTS TO THE FIRST ENTRY IN THE LIST OF ROW NUMBERS
C
INDEX=HEADL(I)
C
C IF INDEX=0 , THE ROW LIST FOR THIS LEVEL IS EMPTY , START IT
C
IF(INDEX.NE.0)GO TO 150
C
HEADL(I)=IHEADR
INDEX=IHEADR
IHEADR=IHEADR+1
HEADR(INDEX,1)=NROW
C WRITE(6,503)HEADR(INDEX,1),NROW
C 503 FORMAT(' HEADR(INDEX,1)=' ,I5,5X, 'NROW=' ,I5)
GO TO 600
C
C IS THE CURRENT ENTRY IN THE ROW NUMBER LIST THE REQUIRED ONE ?
C
150 IF(NROW.EQ.HEADR(INDEX,1))GO TO 600
C IT IS NOT THE REQUIRED ONE SHOULD IT BE INSERTED BEFORE
C THE FIRST ENTRY IN THE LIST ?
C IF((NROW.LT.HEADR(INDEX,1)).AND.(INDEX.EQ.HEADL(I)))GO TO 197

```

```

C
C   IT IS NOT THE REQUIRED ONE IS IT THE LAST ONE ?
C
C   IF(HEADR(INDEX,3).EQ.0)GO TO 198
C
C   IS IT BRACKETED BY THE CURRENT ONE AND THE NEXT ONE ?
C
C   IF(NROW.GT.HEADR(INDEX,1).AND.NROW.LT.HEADR(HEADR(INDEX,3),1)
1)GO TO 198
C
C   OTHERWISE , GO ON TO THE NEXT ONE
C
C   INDEX=HEADR(INDEX,3)
C   GO TO 150
C
C   INSERT A ROW HEADER FOR NROW AFTER THE CURRENT ENTRY
198  ITEMP=HEADR(INDEX,3)
C   HEADR(INDEX,3)=IHEADR
C   HEADR(IHEADR,1)=NROW
C   HEADR(IHEADR,3)=ITEMP
C   INDEX=IHEADR
C   IHEADR=IHEADR+1
C   GO TO 600
C   INSERT A ROW HEADER FOR NROW BEFORE THE FIRST ENTRY IN THE LIST
197  ITEMP=HEADL(I)
C   HEADL(I)=IHEADR
C   HEADR(IHEADR,1)=NROW
C   HEADR(IHEADR,3)=ITEMP
C   INDEX=IHEADR
C   IHEADR=IHEADR+1
C
C   THE LIST FOR NROW IS STARTED , INSERT THE ENTRIES
C
C
C   600  DO 300 K=1,10
C   WRITE(6,1021)ISTART(K),IEND(K),VAL(K),NROW,IAA,IAB
C1021  FORMAT(1X,6I8)
C   IF ISTART IS ZERO , ALL ENTRIES HAVE BEEN MADE
C   WRITE(6,504)ISTART(K)
C 504  FORMAT(' ISTART(K)=',I5)
C   IF(ISTART(K).EQ.0)GO TO 301
C
C   NDEX=HEADR(INDEX,2)
C   WRITE(6,505)NDEX
C 505  FORMAT(' NDEX=',I5)
C
C   IF NDEX=0 , THE LIST IS EMPTY , START IT
777  IF(NDEX.NE.0)GO TO 700
C   INSERT A NEW ENTRY
C   HEADR(INDEX,2)=IINFO
C   NDEX=IINFO
C   CALL PACK(ISTART(K),IEND(K),VAL(K),0,INFO(NDEX))
C   IINFO=IINFO +1
C   GO TO 300
C
C   UNPACK THE CURRENT ENTRY
700  CALL UNPACK(START,END,VALUE,POINT,INFO(NDEX))
C   DO THE INTERVALS INTERSECT ?
C   IF(START.LE.ISTART(K).AND.END.GE.IEND(K).AND.VAL(K).EQ.VALUE)
1GO TO 300

```

```

C     IF THEY DON'T INTERSECT GO ON TO THE NEXT ONE
      IF(START.GT.IEND(K).OR.END.LT.ISTART(K))GO TO 701
C     IF THEY INTERSECT CHECK VALUES
706  IF(VAL(K).NE.VALUE)GO TO 707
C     VALUES ARE THE SAME MODIFY END POINTS
      IF(ISTART(K).LT.START)START=ISTART(K)
      IF(IEND(K).GT.END)END=IEND(K)
      CALL PACK(START,END,VALUE,POINT,INFO(NDEX))
      GO TO 300
707  WRITE(6,818)ISTART(K),IEND(K),VAL(K),START,END,
      *VALUE,NROW,I
818  FORMAT(1X,'ATTEMPT TO INSERT ENTRY START=',I4,
      *'END=',I4,'VALUE=',I4,'CONFLICTS WITH ENTRY START=',
      *I4,'END=',I4,'VALUE=',I4,'AT ROW',I4,'LEVEL',I4)
      GO TO 300

C
C     GO ON TO THE NEXT ENTRY
701  NSAVE=NDEX
      NDEX=POINT
C     IF NDEX=0 , THE END OF THE LIST HAS BEEN REACHED
      IF(NDEX.NE.0)GO TO 700
C     INSERT A NEW ENTRY
C     SET NEW POINTER
      CALL PACK(START,END,VALUE,IINFO,INFO(NSAVE))
C     PUT THE INFO IN
      CALL PACK(ISTART(K),IEND(K),VAL(K),0,INFO(IINFO))
      IINFO=IINFO+1
300  CONTINUE
301  CONTINUE
800  CONTINUE
556  CONTINUE
      RETURN
      END

SUBROUTINE PACK(START,END,VALUE,POINT,Z)
C     THE INFORMATION IS PACKED AS FOLLOWS , BITS NUMBERED RIGHT TO LEFT
C           POINTER                FIRST 13 BITS
C           COLUMN NUMBER OF END    NEXT    8 BITS
C           VALUE OF BOUNDARY CONDITION NEXT    2 BITS
C           COLUMN NUMBER OF START  NEXT    8 BITS
C      $Z=2^{23}*START+2^{21}*VALUE+2^{13}*END+POINT$ 
      INTEGER ST,EN,VA,PO,Z
      INTEGER START,END,VALUE,POINT,Z,SHFTL
      Z=POINT+SHFTL(EN,13)+SHFTL(VALUE,21)+SHFTL(START,23)
C     CALL UNPACK(ST,EN,VA,PO,Z)
C     IF(START.NE.ST.OR.END.NE.EN.OR.VA.NE.VALUE.OR.PO.NE.POINT)STOP 1234
      RETURN
      END

SUBROUTINE UNPACK(START,END,VALUE,POINT,Z)
      INTEGER START,END,VALUE,POINT,Z,SHFTR
      DATA M1/Z00001FFF/,M2/Z001FE000/,M3/Z00600000/,M4/Z7F800000/
      START=SHFTR(LAND(M4,Z),23)
      VALUE=SHFTR(LAND(M3,Z),21)
      END=SHFTR(LAND(M2,Z),13)
      POINT=LAND(M1,Z)
      RETURN
      END

SUBROUTINE OUTPUT(NROW,NCOL,BEGIN,TLAST,K)
C     THIS SUBROUTINE EXAMINES THE VALUE OF EACH POINT IN
C     THE ARRAY WHICH HAS BEEN SET UP FROM THE BOUNDARY CONDITIONS

```

C THERE ARE FOUR POSSIBLE VALUES AT EACH POINT  
 C THESE ARE AND WILL BE PRINTED AS FOLLOWS  
 C

C	BOUNDARY VALUE 1	1
C	BOUNDARY VALUE 2	2
C	BOUNDARY VALUE 3	3
C	NO BOUNDARY VALUE	0

C DIMENSION IJ(100)  
 C INTEGER ONE,TWO,THRE,BLANK,X  
 C INTEGER IEND(10),ISTART(10)  
 C DATA ONE/'1'/,TWO/'2'/,THRE/'3'/,BLANK/' '/,X/'X'/  
 C INTEGER VAL(10),HEADL(20),HEADR(500,3),INFO(6000),POINT  
 C COMMON IPLACE,ISTART,IEND,VAL,HEADL,HEADR,INFO,IINFO,IHEADR,POINT  
 C COMMON/L/LINE(250)

C  
 C  
 C CALL CLOCK  
 C IF(HEADL(K).NE.0)GO TO 1  
 C WRITE(6,10)K  
 10 FORMAT(' LEVEL ',I2,' IS EMPTY')  
 C GO TO 99  
 1 WRITE(6,11)K  
 11 FORMAT('1','LEVEL ',I2)  
 C IS=1  
 C IJK=0  
 C IE=NCOL  
 C IF(NCOL.GE.101) IE=IS+99  
 13 DO 100 I=1,NROW  
 C DO 201 J=1,100  
 201 IJ(J)=BLANK  
 C CALL BOUND(K,I,IS,IE)  
 C DO 101 J=IS,IE  
 C IB=LINE(J)  
 C IND=J-IJK  
 C ITEMP=X  
 C IF(IB.EQ.0)ITEMP=BLANK  
 C IF(IB.EQ.1)ITEMP=ONE  
 C IF(IB.EQ.2)ITEMP=TWO  
 C IF(IB.EQ.3)ITEMP=THRE  
 101 IJ(IND)=ITEMP  
 C WRITE(6,222)(IJ(J),J=1,100),I  
 222 FORMAT(1X,100A1,5X,I5)  
 100 CONTINUE  
 C IF(IE.GE.NCOL) GO TO 99  
 C IS=IE+1  
 C IJK=IS-1  
 C IE=IS+99  
 C IF(IE.GT.NCOL)IE=NCOL  
 C GO TO 13  
 99 RETURN  
 C END  
 C SUBROUTINE DUMP(NTAPE)  
 C COMMON/size/NROW,NCOL,NLEV  
 C COMMON/CORR/UNRL(20),BOT(20),TOP(20),NUMB  
 C COMMON/L/LINE(250)  
 C COMMON/QUA/QUAL(3)  
 C INTEGER UNRL,BOT,TOP

```

DIMENSION B(16,16,8)
CALL CLOCK
IBLSZ=2048
WRITE(6,100)NTAPE
100 FORMAT(18H DUMP ON LOGICAL      I3)
NBX=NROW/16
NBY=NCOL/16
NBZ=NLEV/8
ITOTAL=NBX*NBY*NBZ
IPROD=ITOTAL/NBZ
REWIND NTAPE
WRITE(NTAPE)ITOTAL
DO 20 I=1,ITOTAL
DO 500 I11=1,16
DO 500 I22=1,16
DO 500 I33=1,8
500 B(I11,I22,I33)=0.0
C   FIND BLOCK COORDINATES
KBLK=((I-1)/IPROD)+1
NPLACE=I-(KBLK-1)*IPROD
JBLK=((NPLACE-1)/NBX)+1
IBLK=NPLACE-(JBLK-1)*NBX
C   FIND GRID COORDINATES
IS=(IBLK-1)*16+1
IE=IS+15
JS=(JBLK-1)*16+1
JE=JS+15
KS=(KBLK-1)*8+1
KE=KS+7
C   WRITE(6,327)IS,IE,JS,JE,KS,KE
C 327 FORMAT(6I10)
429 DO 93 KI=1,NUMB
IF(KE.LT.BOT(KI).OR.KS.GT.TOP(KI))GO TO 93
KK=UNRL(KI)
KBOT=KS
IF(BOT(KI).GT.KS)KBOT=BOT(KI)
KTOP=KE
IF(TOP(KI).LT.KE)KTOP=TOP(KI)
94 DO 19 IIQ=IS,IE
IB=IIQ-(IBLK-1)*16
CALL BOUND(KK,IIQ,JS,JE)
DO 50 K=KBOT,KTOP
KB=K-(KBLK-1)*8
DO 50 JQ=JS,JE
JB=JQ-(JBLK-1)*16
ZQUA=0.0
IF(LINE(JQ).NE.0)ZQUA=-QUAL(LINE(JQ))
50 B(IB,JB,KB)=ZQUA
19 CONTINUE
93 CONTINUE
427 WRITE(NTAPE)B
IF(I.EQ.23)WRITE(6,555)B
555 FORMAT(' ',16F6.3)
20 CONTINUE
REWIND NTAPE
CALL CLOCK
RETURN
END
SUBROUTINE BOUND(NLEV,NROW,IS,IE)
INTEGER VAL(10),HEADL(20),HEADR(500,3),INFO(6000),POINT

```

```
INTEGER IEND(10), ISTART(10)
COMMON IPLACE, ISTART, IEND, VAL, HEADL, HEADR, INFO, IINFO
*, IHEADR, POINT
COMMON/L/LINE(250)
DO 1 I=1,250
1 LINE(I)=0
INDEX=HEADL(NLEV)
2 IF(INDEX.EQ.0)RETURN
IF(HEADR(INDEX,1)=NROW)3,4,5
4 III=HEADR(INDEX,2)
6 IF(III.EQ.0)RETURN
CALL UNPACK(IST,IEN,IIVA,IOINT,INFO(III))
IF(IST.GT.IE.OR.IEN.LT.IS)GO TO 8
IF(IST.LT.IS)IST=IS
IF(IEN.GT.IE)IEN=IE
DO 7 I=IST,IEN
7 LINE(I)=IIVA
8 III=IOINT
GO TO 6
3 INDEX=HEADR(INDEX,3)
GO TO 2
5 RETURN
END
SUBROUTINE CLOCK
LOGICAL START
DATA START/.FALSE./
IF(START) GO TO 1
BEGIN=SCLOCK(0.0)
START=.TRUE.
TLAST=0.0
1 T=SCLOCK(BEGIN)/60.0
ETIM=T-TLAST
TLAST=T
WRITE(6,2)T,ETIM
2 FORMAT(' TOTAL TIME USED= ',F8.3,' INCREMENT= ',F8.3)
RETURN
END
```

Appendix C. NEW RELAXATION ITERATION ROUTINES

Changes were made in the relaxation program to allow the sequence that the blocks are iterated to be either forward or backward and to allow the iterations over the physical work area to be either forward or backward. In addition, the routine RLX3D was rewritten in assembly language to increase the speed. The increase in speed achieved was about a factor of 12. Listings of the new routines MAINB and RLX3D are given on the following pages. These are compatible with the program as distributed by Nelson.<sup>14</sup>

```

SUBROUTINE MAINB(A, ID, JD, KD, IDIR, JDIR, *)
COMMON/CORSIZ/ IZ, JZ, KZ, IH, JH, KH
DIMENSION A(ID, JD, KD)
COMMON /TAU/ TIME
COMMON /SSW/ SS2, SS3, SS4
LOGICAL SS2, SS3, SS4
COMMON /CARD/ P1, P2, P3, P4, P5, P6, P7, P8
COMMON /BC/ EP(6)
DIMENSION EQ(6)
COMMON /PSA/ LX, LY, LZ, P(22)
COMMON /VOLUME/ NX, NY, NZ, NB KX, NB KY, NB KZ, LXS, LYS, LZS, IDEL, JDEL, KD
XDEL
CALL DATA(&999)
IF(IDIR.EQ. 1)GO TO 201
IF(IDIR.EQ.=1)GO TO 202
PRINT 203
203 FORMAT(' UNDEFINED ITERATION DIRECTION IDIR=1 ASSUMED')
IDIR=1
GO TO 201
202 LXS=MAX1((P1+P2=2.), 1.)
NBLKX=P2
LYS=MAX1((P3+P4=2.), 1.)
NBLKY=P4
LZS=MAX1((P5+P6=2.), 1.)
NBLKZ=P6
IDEL==1
JDEL==1
KDEL==1
LOOPX=P1
LOOPY=P3
LOOPZ=P5
GO TO 205
201 LXS=P1
NBLKX=P2
LYS=P3
NBLKY=P4
LZS=P5
NBLKZ=P6
IDEL=1
JDEL=1
KDEL=1
LOOPX=NBLKX=1
LOOPY=NBLKY=1
LOOPZ=NBLKZ=1
205 N=P7
IF(JDIR.EQ.=1)N==N
C=P8
K=1
PRINT 1, K, N, C
1 FORMAT(10H ITERATE 2I6, F10.5)
5 LZ=LZS
10 LY=LYS
20 LX=LXS
30 CALL LODA(LX, LY, LZ, A, ID, JD, KD, &999)
DO 31 I=1, 6
31 EQ(I)=1.
IF(LX.EQ.1)EQ(1)=EP(1)
IF(LY.EQ.1)EQ(3)=EP(3)
IF(LZ.EQ.1)EQ(5)=EP(5)

```

```

IF(LX.GE.NBKX-1)EQ(2)=EP(2)
IF(LY.GE.NBKY-1)EQ(4)=EP(4)
IF(LZ.GE.NBKZ-1)EQ(6)=EP(6)
CALL CLOCK(&999)
PRINT 100
C IF(SS3)PRINT 100
100 FORMAT(12H RELAXATION )
R=0.
RN=0.
L=(NBKX-1)*((NBKY-1)*(LZ-1)+LY-1)+LX
CALL RLX3D(A,IZ,JZ,KZ,1,1,1,MINO(NX=IH*(LX-1),IZ),MINO(NY=JH*(LY-1
X),JZ),MINO(NZ=KH*(LZ-1),KZ),C,1,N,R,RN,EQ)
PRINT 101,R,RN
C IF(SS3)PRINT 101,R,RN
101 FORMAT(12H RESIDUE = ,2E14.5)
IF(IDIR.EQ.1)GO TO 214
LX=LX+IDEL
IF(LX.GE.LOOPX)GO TO 30
LY=LY+JDEL
IF(LY.GE.LOOPY)GO TO 20
LZ=LZ+KDEL
IF(LZ.GE.LOOPZ)GO TO 10
GO TO 211
214 LX=LX+IDEL
IF(LX.LE.LOOPX) GO TO 30
LY=LY+JDEL
IF(LY.LE.LOOPY) GO TO 20
LZ=LZ+KDEL
IF(LZ.LE.LOOPZ) GO TO 10
211 K=K-1
IF(K.GT.0) GO TO 5
LX=LXS
LY=LYS
LZ=LZS
CALL CLOCK(&999)
800 CALL UNLOAD
RETURN
999 RETURN 1
END

```

```

MACRO
&LABEL BOT    &D1,&D2,&D3,&D4,&LABEL
        LE     0,128(1,5)
        LTER   0,0
        BM     *+74
        AR     1,5
        LE     0,&D1.(1)
        LPER   2,0
        LE     0,&D2.(1)
        LPER   0,0
        AUR    2,0
        LE     0,&D3.(1)
        LPER   0,0
        AUR    2,0
        LE     0,&D4.(1)
        LPER   0,0
        AUR    2,0
        AR     1,8
        LE     0,128(1)
        LPER   0,0
        AUR    2,0
        AUR    2,0
        SR     1,8
        DE     2,=E'6'
        LE     0,128(1)
        SUR    2,0
        ME     2,72(0,14)
        AUR    0,2
        LPER   0,0
        STE    0,128(1)
        SR     1,5
        MEND
MACRO
&LABEL TOP    &D1,&D2,&D3,&D4,&LABEL
        LE     0,128(1,5)
        LTER   0,0
        BM     *+74
        AR     1,5
        LE     0,&D1.(1)
        LPER   2,0
        LE     0,&D2.(1)
        LPER   0,0
        AUR    2,0
        LE     0,&D3.(1)
        LPER   0,0
        AUR    2,0
        LE     0,&D4.(1)
        LPER   0,0
        AUR    2,0
        SR     1,8
        LE     0,128(1)
        LPER   0,0
        AUR    2,0
        AUR    2,0
        AR     1,8
        DE     2,=E'6'
        LE     0,128(1)
        SUR    2,0
        ME     2,72(0,14)

```

```

AUR      0,2
LPER     0,0
STE      0,128(1)
SR       1,5
MEND
MACRO
&LABEL  INT      &D1,&D2,&D3,&D4,&LABEL
        LE       0,128(1,5)
        LTER     0,0
        BM       *+84
        AR       1,5
        LE       0,&D1.(1)
        LPER     2,0
        LE       0,&D2.(1)
        LPER     0,0
        AUR      2,0
        LE       0,&D3.(1)
        LPER     0,0
        AUR      2,0
        LE       0,&D4.(1)
        LPER     0,0
        AUR      2,0
        AR       1,8
        LE       0,128(1)
        LPER     0,0
        AUR      2,0
        SR       1,8
        SR       1,8
        LE       0,128(1)
        LPER     0,0
        AUR      2,0
        AR       1,8
        DE       2,=E'6'
        LE       0,128(1)
        SUR      2,0
        ME       2,72(0,14)
        AUR      0,2
        LPER     0,0
        STE      0,128(1)
        SR       1,5
MEND
MACRO
SYM      &D,&BRANCH
L        10,76(0,14)
LE       0,&D.(10)
LTER     0,0
BNZ      &BRANCH
MEND
RLX      TITLE  'RLX3D VERSION 4'
        CSECT
        ENTRY  RLX3D
        USING  *,12
RLX3D    STM    14,12,12(13)
        LR     12,15
        ST     13,ASAVE

```

\*\*\*\*\*R1 CONTAINS ADDRESS OF FIRST CALLING PARAMETER

\*\*\*\*\*SET UP LOOPS FOR 32 BY 32 BY 16 ARRAY

\*\*\*\*\*CALL RLX3D(A,IZ,JZ,KZ, 1, 1, 1,IL,JL,KL, C, 1, N, R,RN,EQ)

\*\*\*\*\* 0 4 8 12 16 20 24 28 32 36 40 44 48 52 56 60

\*



	S	11,=F'2'	CALC J LIMIT
	M	10,=F'128'	
	ST	11,24(0,14)	
	A	11,=F'128'	
	ST	11,52(0,14)	
	L	10,20(0,1)	
	L	11,0(0,10)	
	S	11,=F'1'	
	M	10,=F'128'	
	ST	11,16(0,14)	
	ST	11,60(0,14)	
	L	10,36(0,1)	ADDRESS OF KZ
	L	11,0(0,10)	LOAD KZ
	S	11,=F'2'	CALC K LIMIT
	M	10,=F'4096'	
	A	11,AA	
	ST	11,32(0,14)	
	A	11,=F'4096'	
	ST	11,48(0,14)	
	L	10,24(0,1)	
	L	11,0(0,10)	
	S	11,=F'1'	
	M	10,=F'4096'	
	A	11,AA	
	ST	11,12(0,14)	
	ST	11,68(0,14)	
	L	10,48(0,1)	LOAD ADDRESS OF N
	L	0,0(0,10)	LOAD N
	L	9,=F'1'	
	LTR	0,0	DETERMINE STARTING ITERATION DIRECTION
	BP	ST	
	LPR	0,0	
	LNR	9,9	
ST	ST	9,IDIR	
	L	10,40(0,1)	LOAD ADDRESS OF C
	LE	0,0(0,10)	LOAD C
	STE	0,72(0,14)	STORE C
	L	10,52(0,1)	LOAD ADDRESS OF R
	LE	4,0(0,10)	LOAD R
	L	10,56(0,1)	LOAD ADDRESS OF RN
	LE	6,0(0,10)	LOAD RN
	L	10,60(0,1)	LOAD ADDRESS OF EQ
	ST	10,76(0,14)	STORE ADDRESS OF EQ
	LA	14,SAVEAR	ADDRESS OF SAVE AREA
	ST	14,8(0,13)	SET FORWARD POINTER
	ST	13,4(0,14)	SET BACKWARD POINTER
	LR	13,14	
*****	START	ITERATION LOOP	
ITER	L	14,IDIR	
	LTR	14,14	
	BP	FWD	
	L	15,=V(RLXBWD)	
	B	SWTCH	
FWD	L	15,=V(RLXFWD)	
SWTCH	LNR	14,14	
	ST	14,IDIR	
	BALR	14,15	
FIN	BCT	0,ITER	
*****	ITERATIONS FINISHED,SAVE	REQUIRED VALUES	
	L	1,ALIST	LOAD ADDRESS OF LIST

```

L      10,52(0,1)      ADDRESS OF RS
STE    4,0(0,10)      STORE RS
L      10,56(0,1)      ADDRESS OF RN
STE    6,0(0,10)      STORE RN
*****RESTORE REGISTERS AND RETURN
L      13,ASAVE
LM     14,12,12(13)
SR     15,15
BCR    15,14
ASAVE  DS      A
IDIR   DS      F
AA     DS      A
ALIST  DS      F
SAVEAR DS     18F
LTORG
REGS   COM
DS     20F
END
RLXF   CSECT
ENTRY  RLXFWD
USING  *,12
RLXFWD STM     14,12,12(13)
LR     12,15
ST     13,ASAVE
L      14,=V(REGS)
LM     1,9,0(14)
*****START LOOP OVER K
*****DO BOTTEM PLANE
SYM    16,INSIDE
LR     5,4              SET J TO CURRENT K
LR     7,5              SET J LIMIT
A      7,24(0,14)
L      1,0(0,14)       SET I
SYM    0,LQ1
BOT    132,132,256,256 CORNER
LQ1    AR     1,2       INCREMENT I
SYM    8,LQ2
ILOOP1 BOT    132,124,256,256,ILOOP1
BXLE   1,2,ILOOP1
LQ2    NOPR   14
SYM    4,LL1
BOT    124,124,256,256 CORNER
LL1    AR     5,6       INCREMENT J
JLOOP1 L      1,0(0,14) SET I
SYM    0,LL2
BOT    132,132,0,256
LL2    AR     1,2       INCREMENT I
*****DO INTERIOR POINTS IN BOTTEM PLANE
ILOOP2 LE     0,128(1,5)
LTER   0,0
BM     SKIP
LE     0,132(1,5)
LPER   2,0
LE     0,124(1,5)
LPER   0,0
AUR    2,0
LE     0,256(1,5)
LPER   0,0
AUR    2,0
LE     0,0(1,5)

```

```

LPER 0,0
AUR 2,0
AR 1,8
LE 0,128(1,5)
LPER 0,0
AUR 2,0
AUR 2,0
SR 1,8
DE 2,=E'6'
LE 0,128(1,5)
SUR 2,0
BP POS
AUR 6,2
SUR 4,2
ME 2,72(0,14)
AUR 0,2
LPER 0,0
STE 0,128(1,5)
B SKIP
POS AUR 4,2
ME 2,72(0,14)
AUR 0,2
STE 0,128(1,5)
SKIP BXLE 1,2,ILOOP2
SYM 4,LQ3
LQ3 BOT 124,124,0,256 EDGE
BXLE 5,6,JLOOP1
L 1,0(0,14) SET X INDEX
SYM 0,LQ4
LQ4 BOT 132,132,0,0 CORNER
AR 1,2 INCREMENT I
SYM 12,LQ5
ILOOP3 BOT 124,132,0,0,ILOOP3
BXLE 1,2,ILOOP3
LQ5 NOPR 14
SYM 4,INSIDE
BOT 124,124,0,0 CORNER
*****BOTTEM PLANE DONE
INSIDE AR 4,8 INCREMENT K
KLOOP1 LR 5,4 RESET Y INDEX
LR 7,5 SET J LIMIT
A 7,24(0,14)
L 1,0(0,14) RESET X INDEX
SYM 0,LL3
LL3 INT 132,132,256,256
AR 1,2 INCREMENT X
SYM 8,LL13
ILOOP4 INT 132,124,256,256,ILOOP4
BXLE 1,2,ILOOP4
LL13 NOPR 14
SYM 4,NEXT
INT 124,124,256,256
NEXT AR 5,6 INCREMENT J
JLOOP3 L 1,0(0,14) RESET X INDEX
SYM 0,NEXU
INT 132,132,0,256 EDGE
NEXU AR 1,2 INCREMENT I
*****INTERIOR POINTS OF INTERIOR PLANES
ILOOP8 LE 0,128(1,5)
LTER 0,0

```

```

BM      SKJP
LE      0,132(1,5)
LPER    2,0
LE      0,124(1,5)
LPER    0,0
AUR     2,0
LE      0,256(1,5)
LPER    0,0
AUR     2,0
LE      0,0(1,5)
LPER    0,0
AUR     2,0
AR      1,8
LE      0,128(1,5)
LPER    0,0
AUR     2,0
SR      1,8
SR      1,8
LE      0,128(1,5)
LPER    0,0
AUR     2,0
AR      1,8
DE      2,=E'6'
LE      0,128(1,5)
SUR     2,0
BP      POZ
AUR     6,2
SUR     4,2
ME      2,72(0,14)
AUR     0,2
LPER    0,0
STE     0,128(1,5)
B       SKJP
POZ     AUR     4,2
        ME      2,72(0,14)
        AUR     0,2
        STE     0,128(1,5)
SKJP    BXLE    1,2,ILOOP8
        SYM     4,NEXV
        INT     124,124,0,256
NEXV    BXLE    5,6,JLOOP3
        L       1,0(0,14)          RESET I
        SYM     0,LL12
        INT     132,132,0,0
LL12    AR      1,2              INCREMENT I
        SYM     12,LL14
ILOOP6  INT     124,132,0,0,ILOOP6
        BXLE    1,2,ILOOP6
LL14    NOPR    14
        SYM     4,NEXS
        INT     124,124,0,0
NEXS    BXLE    4,8,KLOOP1
*****INTERIOR PLANES DONE DO TOP PLANE
        SYM     20,FIN
        L       1,0(0,14)          RESET I
        LR      5,4              RESET J
        LR      7,5
        A       7,24(0,14)
        SYM     0,LQ10
        TOP     132,132,256,256    CORNER

```

```

LQ10      AR      1,2          INCREMENT I
          SYM      8,LQ11
ILOOP7    TOP     132,124,256,256,ILOOP7
          BXLE     1,2,ILOOP7
LQ11      NOPR    14
          SYM      4,LL4
          TOP     124,124,256,256    CORNER
LL4       AR      5,6
JLOOP4    L       1,0(0,14)        RESET I
          SYM      0,LL5
          TOP     132,132,0,256    EDGE
LL5       AR      1,2          INCREMENT I
*****DO INTERIOR POINTS IN TOP PLANE
ILOOPX    LE      0,128(1,5)
          LTER     0,0
          BM       SKKP
          LE      0,132(1,5)
          LPER     2,0
          LE      0,124(1,5)
          LPER     0,0
          AUR      2,0
          LE      0,256(1,5)
          LPER     0,0
          AUR      2,0
          LE      0,0(1,5)
          LPER     0,0
          AUR      2,0
          SR       1,8
          LE      0,128(1,5)
          LPER     0,0
          AUR      2,0
          AUR      2,0
          AR       1,8
          DE      2,=E'6'
          LE      0,128(1,5)
          SUR      2,0
          BP       POR
          AUR      6,2
          SUR      4,2
          ME      2,72(0,14)
          AUR      0,2
          LPER     0,0
          STE     0,128(1,5)
          B       SKKP
POR       AUR      4,2
          ME      2,72(0,14)
          AUR      0,2
          STE     0,128(1,5)
SKKP     BXLE     1,2,ILOOPX
          SYM      4,LL6
          TOP     124,124,0,256
LL6       BXLE     5,6,JLOOP4
          L       1,0(0,14)        SET I
          SYM      0,LQ12
          TOP     132,132,0,0
LQ12     AR      1,2          INCREMENT I
          SYM      12,LQ13
ILOOP9    TOP     124,132,0,0,ILOOP9
          BXLE     1,2,ILOOP9
LQ13     NOPR    14

```

```

SYM      4,FIN
TOP      124,124,0,0
*****TOP PLANE DONE
FIN      L      13,ASAVE
          LM     14,12,12(13)
          SR     15,15
          BCR    15,14
ASAVE    DS     A
          LTORG
REGS     COM
          DS     20F
          END
RLXB     CSECT
          ENTRY  RLXBWD
          USING *,12
RLXBWD   STM     14,12,12(13)
          LR     12,15
          ST     13,ASAVE
          L      14,=V(REGS)
          LM     1,9,36(14)
*****START LOOP OVER K
*****DO TOP PLANE
SYM      20,INSIDE
LR       5,4           SET J TO CURRENT K
LR       7,5           SET J LIMIT
A        5,52(0,14)
L        1,36(0,14)
SYM      4,LQ1
BOT     0,0,124,124   CORNER
LQ1     AR      1,2     INCREMENT I
SYM     12,LQ2
ILOOP1  BOT     132,124,0,0,ILOOP1
BXH     1,2,ILOOP1
LQ2     NOPR    14
SYM     0,LL1
BOT     0,0,132,132   CORNER
LL1     AR      5,6     INCREMENT J
JLOOP1  L       1,36(0,14) SET I
SYM     4,LL2
BOT     124,124,0,256
LL2     AR      1,2     INCREMENT I
*****DO INTERIOR POINTS IN TOP PLANE
ILOOP2  LE      0,128(1,5)
          LTER   0,0
          BM     SKIP
          LE     0,132(1,5)
          LPER   2,0
          LE     0,124(1,5)
          LPER   0,0
          AUR    2,0
          LE     0,256(1,5)
          LPER   0,0
          AUR    2,0
          LE     0,0(1,5)
          LPER   0,0
          AUR    2,0
          AR     1,8
          LE     0,128(1,5)
          LPER   0,0
          AUR    2,0

```

```

AUR 2,0
SR 1,8
DE 2,=E'6'
LE 0,128(1,5)
SUR 2,0
BP POS
AUR 6,2
SUR 4,2
ME 2,72(0,14)
AUR 0,2
LPER 0,0
STE 0,128(1,5)
B SKIP
POS AUR 4,2
ME 2,72(0,14)
AUR 0,2
STE 0,128(1,5)
SKIP BXH 1,2,ILOOP2
SYM 0,LQ3
BOT 132,132,0,256 EDGE
LQ3 BXH 5,6,JLOOP1
L 1,36(0,14)
SYM 4,LQ4
BOT 124,124,256,256 CORNER
LQ4 AR 1,2 INCREMENT I
SYM 8,LQ5
ILOOP3 BOT 124,132,256,256,ILOOP3
BXH 1,2,ILOOP3
LQ5 NOPR 14
SYM 0,INSIDE
BOT 256,256,132,132
*****TOP PLANE DONE
INSIDE AR 4,8 INCREMENT K
KLOOP1 LR 5,4 RESET Y INDEX
LR 7,5 SET J LIMIT
A 5,52(0,14)
L 1,36(0,14) RESET X INDEX
SYM 4,LL3
INT 124,124,0,0
LL3 AR 1,2 INCREMENT X
SYM 12,LL13
ILOOP4 INT 132,124,0,0,ILOOP4
BXH 1,2,ILOOP4
LL13 NOPR 14
SYM 0,NEXT
INT 0,0,132,132
NEXT AR 5,6 INCREMENT J
JLOOP3 L 1,36(0,14) RESET X INDEX
SYM 4,NEXU
INT 124,124,0,256 EDGE
NEXU AR 1,2 INCREMENT I
*****INTERIOR POINTS OF INTERIOR PLANES
ILOOP8 LE 0,128(1,5)
LTER 0,0
BM SKJP
LE 0,132(1,5)
LPER 2,0
LE 0,124(1,5)
LPER 0,0
AUR 2,0

```

```

LE      0,256(1,5)
LPER    0,0
AUR     2,0
LE      0,0(1,5)
LPER    0,0
AUR     2,0
AR      1,8
LE      0,128(1,5)
LPER    0,0
AUR     2,0
SR      1,8
SR      1,8
LE      0,128(1,5)
LPER    0,0
AUR     2,0
AR      1,8
DE      2,=E'6'
LE      0,128(1,5)
SUR     2,0
BP      POZ
AUR     6,2
SUR     4,2
ME      2,72(0,14)
AUR     0,2
LPER    0,0
STE     0,128(1,5)
B       SKJP
POZ     AUR     4,2
        ME      2,72(0,14)
        AUR     0,2
SKJP    STE     0,128(1,5)
        BXH    1,2,ILOOP8
        SYM    0,NEXV
NEXV    INT     132,132,0,256
        BXH    5,6,JLOOP3
        L      1,36(0,14)          RESET I
        SYM    4,LL12
        INT     124,124,256,256
LL12    AR      1,2              INCREMENT I
        SYM    8,LL14
ILOOP6  INT     124,132,256,256,ILOOP6
        BXH    1,2,ILOOP6
LL14    NOPR    14
        SYM    0,NEXS
        INT     256,256,132,132
NEXS    BXH     4,8,KLOOP1
*****INTERIOR PLANES DONE DO BOTTEM PLANE
        SYM    16,FIN
        L      1,36(0,14)          RESET I
        LR     5,4              RESET J
        LR     7,5
        A      5,52(0,14)
        SYM    4,LQ10
        TOP    124,124,0,0          CORNER
LQ10    AR      1,2              INCREMENT I
        SYM    12,LQ11
ILOOP7  TOP     132,124,0,0,ILOOP7
        BXH    1,2,ILOOP7
LQ11    NOPR    14
        SYM    0,LL4

```

```

TOP      132,132,0,0
LL4      AR      5,6
JLOOP4   L        1,36(0,14)          RESET I
          SYM     4,LL5
          TOP     124,124,0,256      EDGE
LL5      AR      1,2                  INCREMENT I
*****DO INTERIOR POINTS IN BOTTEM PLANE
ILOOPX   LE      0,128(1,5)
          LTER    0,0
          BM      SKKP
          LE      0,132(1,5)
          LPER    2,0
          LE      0,124(1,5)
          LPER    0,0
          AUR     2,0
          LE      0,256(1,5)
          LPER    0,0
          AUR     2,0
          LE      0,0(1,5)
          LPER    0,0
          AUR     2,0
          SR      1,8
          LE      0,128(1,5)
          LPER    0,0
          AUR     2,0
          AUR     2,0
          AR      1,8
          DE      2,=E'6'
          LE      0,128(1,5)
          SUR     2,0
          BP      POR
          AUR     6,2
          SUR     4,2
          ME      2,72(0,14)
          AUR     0,2
          LPER    0,0
          STE     0,128(1,5)
          B       SKKP
POR       AUR     4,2
          ME      2,72(0,14)
          AUR     0,2
          STE     0,128(1,5)
SKKP     BXH     1,2,ILOOPX
          SYM     0,LL6
          TOP     132,132,0,256
LL6      BXH     5,6,JLOOP4
          L        1,36(0,14)          SET I
          SYM     4,LQ12
          TOP     124,124,256,256
LQ12     AR      1,2                  INCREMENT I
          SYM     8,LQ13
ILOOP9   TOP     124,132,256,256,ILOOP9
          BXH     1,2,ILOOP9
LQ13     NOPR    14
          SYM     0,FIN
          TOP     256,256,132,132
*****BOTTEM PLANE DONE
FIN      L        13,ASAVE
          LM      14,12,12(13)
          SR      15,15

```

ASAVE	BCR	15,14
	DS	A
	LTORG	
REGS	COM	
	DS	20F
	END	

Appendix D. PROGRAM AXCENT.

This program performs the axial acceptance calculations described in Section 3. The data input consists of a description of the beam (emittance and energy) followed by data describing a sequence of focusing elements (dee gaps or magnetic field regions). The  $v_z$  used for the magnetic field can be entered on the data cards or determined by interpolation from a table of values. The program tracks particles with various phases through the focusing elements up to some maximum energy. When the tracking is complete, the program can match the beam to a specified  $v_z$  and then calculate, for each phase what elliptical emittance shape is required at injection to produce a beam matched to the final  $v_z$ . Various plots of ion trajectories and beam envelopes are available.

## Description of Data for AXCENT

All data is read in free format by subroutine DATA. Each card has 8 numeric fields (cols 1 to 40) and an alphanumeric (comment) field (cols 41 to 60). Trailing parameters not specified are set to zero. Fields are separated by any character except +, -, ., !, ... 9, 0.

In general, the first number on each piece of data is an index which specifies what operation is to be performed while the other fields contain data.

1, P2, P3, P4, P5, P6; Initialize the problem

if P2  $\neq$  0 initialize transfer matrix, E and S only (no data required)

P3 = C =  $\epsilon \cos \delta$      $\epsilon = \frac{\text{amplitude of 3rd harmonic}}{\text{amplitude of 1st harmonic}}$

P4 = phase of third harmonic with respect to the fundamental ( $\delta$ )

if P5  $\neq$  0 use table of phase slips read from logical unit 1

if P6  $\neq$  0 use table of  $v_z$  values read from logical unit 2

one data card required

P1 = initial energy (M V)  
 P2 = emittance in in. (mrad. at energy P1)  
 P3 =  $z_{max}$   
 P4 =  $\phi$  (ellipse parameter as defined by Steffen (24))  
 P5  $\neq 0$  then track backwards (otherwise forward)  
 P6 = maximum energy for outward track if P6 = 0, no maximum is set  
 P7 = initial phase of "zero" phase

2 Transfer to subroutine TRACK, requires data as follows:

- 1, P2, P3 thin lens  
 P2 = peak voltage across gap (MV)  
 P3 = reduction factor (set to 1.0 if not specified)
- 2, P2, P3 constant  $v_z$  magnetic field region  
 P2 =  $v_z$  (not used if a table of values is provided)  
 P3 = angular length (degrees)
- 3, P2 repeat the previous two elements (which must be different i.e. one thin lens and an  $v_z$  region) P2 times
- 4, P2 print after each element (initially yes)  
 P2 = 1 yes  
 P2 = 0 no
- 5, P2, P3, P4  
 P2 = 1 turn plot output on (must be done before start of tracking)  
 P3 = # turns/inch on X axis (default to 1.0)  
 P4 = # z inches/plot inch on Y axis (default to 0.5)  
 P2 = 2 turn plot output off  
 P3 = 3,4,5,...9 causes plots to be produced according to the following table

<u>P2</u>	<u>Z1</u>	<u>Z2</u>	<u>envelope</u>
3	X		
4		X	
5			X
6	X	X	
7	X		X
8		X	X
9	X	X	X

if P4 = 999 all phases are plotted, otherwise phases P4 to P5 are plotted

6 RETURN to MAIN

3, P2 Transform back to initial starting point, match to  
 $v_z = P2$

4, P2, P3 Draw ellipses

P2 = # z inches per plot inch (typically 0.1)

P3 = # z<sup>1</sup> radians per plot inch (typically 0.01)

5 Compute overlap of current ellipses

6 Stop

```

C*****MAIN
C   THIS PROGRAMME CAN PERFORM THE FOLLOWING TASKS:
C
C   (1) TRACK PARTICLES AND PHASE SPACE ELLIPSES THROUGH
C   A SERIES OF ELECTRIC THICK LENSES AND MAGNETIC FIELDS
C   WITH CONSTANT FOCUSING PROPERTIES
C
C   (2) MATCH A PHASE SPACE ELLIPSE TO A SPECIFIED MAGNETIC FIELD
C
C   (3) TRANSFORM BACK THROUGH A SYSTEM TO DETERMINE
C   WHAT INITIAL ELLIPSE IS REQUIRED TO PRODUCE THE REQUIRED
C   FINAL ELLIPSE
C
C   (4) CALCULATE THE COMMON AREA BETWEEN PHASE SPACE ELLIPSES
C   FOR DIFFERENT PHASES
C
C   (5) DRAW PHASE SPACE ELLIPSES ON A CALCOMP PLOTTER
C
C   (6) PLOT TRAJECTORIES AND ENVELOPES ON A CALCOMP PLOTTER
C
C   -THIS ROUTINE READS DATA AND TRANSFERS
C   CONTROL TO THE SUBROUTINES.
C   -TRANSFER IS CONTROLLED BY THE FIRST
C   NUMBER ON THE DATA CARD.
C   -ALL DATA IS READ IN FREE FORMAT BY
C   SUBROUTINE"DATA"AND TRANSMITTED THROUGH
C   COMMON AREA "CARD".
COMMON/CARD/P(8),MNT(5)
COMMON/PLT/IS,PRNT
COMMON/START/ESTART,Z1(13),Z1P(13),Z2(13),Z2P(13),EPS,EMAX
COMMON/START2/FIO,DELTA,C,THTA
COMMON /SLIP/NPS,EOS,DELES,PS(100)
COMMON /VNUZ/NUUZ,EOZ,DELEZ,UZ(100)
LOGICAL IS,PRNT
1 CALL PAGE(2)
CALL DATA(&999)
I=P(1)
GO TO(100,200,300,400,500,600),I
CALL PAGE(1)
WRITE(6,20)
20 FORMAT(' INVALID DATA IGNORED')
GO TO 1
C
C   INDEX=1 INITIALIZE
C   -IF P2=0 INITIALIZE TRANSFER MATRIX
C   ENERGY AND S ONLY (THROUGH ENTRY "INITA")
100 IF(P(2).EQ.1)GO TO 101
C=P(3)
DELTA=P(4)/57.29578
NPS=0
NUUZ=0
IF(P(5).EQ.0.0)GO TO 50
READ(1,111)NPS,EOS,DELES
READ(1,112)(PS(I),I=1,NES)
50 IF(P(6).EQ.0.0)GO TO 51
READ(2,111)NUUZ,EOZ,DELEZ
READ(2,112)(UZ(I),I=1,NUUZ)
111 FORMAT(I5,5X,2F10.0)

```

```

112 FORMAT(8F10.0)
51 CALL PAGE(1)
WRITE(6,19)
WRITE(3,68)MNT
68 FORMAT(' ',5A4)
19 FORMAT(' INITIALIZE')
CALL INIT
GO TO 1
101 CALL PAGE(1)
WRITE(6,11)
11 FORMAT(' INITIALIZE TRANSFER MATRIX ONLY')
CALL INITA
GO TO 1

```

```

C
C   -TRANSFER TO SUBROUTINE "TRACK"

```

```

200 CALL PAGE(1)
WRITE(6,12)
12 FORMAT(' TRACK')
CALL TRACK
GO TO 1

```

```

C
C   -MATCH TO NUZ=P2

```

```

300 CALL PAGE(1)
WRITE(6,13)
13 FORMAT(' TRANSFORM BACK')
CALL UNTRK(P(2))
GO TO 1

```

```

C
C   -DRAW ELLIPSES ON PLOTTER

```

```

400 CALL PAGE(1)
WRITE(6,14)
14 FORMAT(' DRAW ELLIPSES')
CALL DRAW(P(2),P(3))
GO TO 1

```

```

C
C   -CALCULATE ELLIPSE OVERLAPS

```

```

500 CALL PAGE(1)
WRITE(6,15)
15 FORMAT(' CALCULATE ELLIPSE OVERLAPS')
CALL COMP
GO TO 1

```

```

C
C   -END OF RUN

```

```

600 WRITE(6,16)
16 FORMAT(' END OF RUN')
IF(IS)CALL PLOTND
STOP 1
999 STOP 999
END

```

```

SUBROUTINE INIT

```

```

C*****INIT

```

```

C   -THIS ROUTINE DOES ALL INITIALIZATION
C   AND SHOULD BE CALLED ONCE FOR EACH
C   CASE TO BE RUN.
C   -ONE DATA CARD IS REQUIRED
COMMON/USD/USED
COMMON/ELST/AL(13),BE(13),GA(13)
COMMON/ELLIPS/ALFA(13),BETA(13),GAMMA(13)
COMMON/CARD/P(8),MNT(5)
COMMON/TT/T(2,2,13),E(13),S(13),PASE(13)

```

```

COMMON/DIR/BKWD,END(13),BAD(13)
COMMON/START/ESTART,Z1(13),Z1P(13),Z2(13),Z2P(13),EPS,EMAX
COMMON/START2/FIO,DELTA,C,THTA
COMMON/PLT/IS,PRNT
COMMON/MORPLT/IZ1,IZ2,IEV
COMMON/PGE/N,NPAGE,NAME(5)
DATA IFST/0/
IF(IFST.EQ.1)GO TO 5674
IFST=1
USED=0.0
5674 CONTINUE
DOUBLE PRECISION AL,BE,GA
DOUBLE PRECISION ALFA,BETA,GAMMA,T,E
LOGICAL BKWD,END,PRNT,IS,ERR,BAD
LOGICAL IZ1,IZ2,IEV
IZ1=.FALSE.
IZ2=.FALSE.
IEV=.FALSE.
PRNT=.TRUE.
BKWD=.FALSE.
N=0
NPAGE=0
DO 239 I=1,5
239 NAME(I)=MNT(I)
CALL PAGE(61)
CALL PAGE(2)
CALL DATA(&999)
FIO=P(7)/57.29578
FISAVE=FIO
THTA=FIO
IF(P(5).NE.0.0)BKWD=.TRUE.
EMAX=100000.
IF(P(6).NE.0.0)EMAX=P(6)
ESTART=P(1)
SQE=SQRT(ESTART)
ALF=P(4)
ZMAX=P(3)
EPS=P(2)*SQE/1000.
BET=ZMAX**2/EPS
GAM=(1.0+ALF*ALF)/(BET)
SQEPS=SQRT(EPS)
DO 94 I=1,13
ALFA(I)=ALF
BETA(I)=BET
BAD(I)=.FALSE.
94 GAMMA(I)=GAM

C
C   -THIS ENTRY INITIALIZES THE TRANSFER
C   MATRIX ENERGY AND S ONLY
ENTRY INITA
THTA=FIO
THTA=0.0
DO 96 I=1,13
PASE(I)=((I-7)*10.+FISAVE)/57.295779
AL(I)=ALFA(I)
BE(I)=BETA(I)
GA(I)=GAMMA(I)
Z1(I)=SQEPS/DSQRT(GAMMA(I))
Z1P(I)=0.0
Z2(I)=0.0

```

```

Z2P(I)=SQEPS/(DSQRT(BETA(I)))
END(I)=.FALSE.
E(I)=ESTART
S(I)=0.0
T(1,1,I)=1.0
T(1,2,I)=0.0
T(2,1,I)=0.0
96 T(2,2,I)=1.0
CALL PAGE(1)
WRITE(6,100)
100 FORMAT(' INITIAL VALUES')
CALL PRINT
CALL POINTS
RETURN
999 STOP 998
END
SUBROUTINE TRACK
C*****TRACK
C THIS SUBROUTINE READS THE DATA CARDS
C WHICH DESCRIBE THE ELEMENTS AND
C TRANSFERS CONTROL TO SUBROUTINES WHICH
C CALCULATE THE ACTUAL MATRIX ELEMENTS.
COMMON/CARD/P(8),MNT(5)
COMMON/PLT/IS,PRNT
COMMON/MORPLT/IZ1,IZ2,IEV
COMMON/SQALE/XSKALE,YSKALE
COMMON /SLIP/NPS,EOS,DELES,PS(100)
COMMON /VNUZ/NUZ,EOZ,DELEZ,UZ(100)
LOGICAL IZ1,IZ2,IEV
LOGICAL LENS,PRNT,IS
LOGICAL LLL,LALL
LLL=.FALSE.
11 CALL PAGE(2)
CALL DATA(&999)
KOUNT=1
I=P(1)
GO TO(1,2,3,4,5,6),I
CALL PAGE(1)
WRITE(6,100)
100 FORMAT(' INVALID DATA IGNORED BY TRACK')
GO TO 11
C THIN LENS
1 LENS=.TRUE.
T2=P(2)
T3=P(3)
21 CALL TLEN(T2,T3)
IF(PRNT)CALL PRINT
IF(LLL) CALL POINTQ
KOUNT=KOUNT-1
IF (KOUNT.NE.0)GO TO 22
GO TO 11
C CONSTANT NUZ REGION
2 LENS=.FALSE.
Q2=P(2)
Q3=P(3)
22 CALL NUZ(Q2,Q3)
IF(PRNT)CALL PRINT
IF(LLL)CALL POINTQ
KOUNT=KOUNT-1
IF(KOUNT.NE.0)GO TO 21

```

```

      GO TO 11
C     SET UP KOUNT FOR REPETITION OF PREVIOUS TWO ELEMENTS
      3 KOUNT=2.*(P(2)-1.)
      IF(LENS)GO TO 22
      GO TO 21
C     SET PRINT ON OR OFF
      4 IF(P(2).NE.0.0)GO TO 8
      CALL PAGE(1)
      WRITE(6,200)
200   FORMAT(' PRINT OFF')
      PRNT=.FALSE.
      GO TO 11
      8 IF(P(2).NE.1.0)GO TO 11
      CALL PAGE(1)
      WRITE(6,201)
201   FORMAT(' PRINT ON')
      PRNT=.TRUE.
      GO TO 11
C     SET SWITCHES TO CONTROL PLOTTING OF Z1,Z2, AND ENV
      5 I=P(2)
      IF(I.NE.1)GO TO 61
      LLL=.TRUE.
      XSKALE=P(3)
      YSKALE=P(4)
      IF(XSKALE.EQ.0.0)XSKALE=1.0
      IF(YSKALE.EQ.0.0)YSKALE=0.5
      GO TO 11
      61 IF(I.NE.2)GO TO 62
      LLL=.FALSE.
      GO TO 11
      62 IZ1=.FALSE.
      IZ2=.FALSE.
      IEV=.FALSE.
      LALL=.FALSE.
      IF(I.EQ.3)IZ1=.TRUE.
      IF(I.EQ.4)IZ2=.TRUE.
      IF(I.EQ.5)IEV=.TRUE.
      IF(I.NE.6)GO TO 63
      IZ1=.TRUE.
      IZ2=.TRUE.
      63 IF(I.NE.7)GO TO 64
      IZ1=.TRUE.
      IEV=.TRUE.
      64 IF(I.NE.8)GO TO 65
      IZ2=.TRUE.
      IEV=.TRUE.
      65 IF(I.NE.9)GO TO 66
      IZ1=.TRUE.
      IZ2=.TRUE.
      IEV=.TRUE.
      66 IF(P(3).EQ.999.)LALL=.TRUE.
      CALL PLO(IZ1,IZ2,IEV,LALL,IFIX(P(3)),IFIX(P(4)))
      GO TO 11
C     RETURN TO MAIN
      6 RETURN
999   STOP 1234
      END
      SUBROUTINE NUZ(P1,P2)
C*****
C     =THIS ROUTINE CALCULATES THE MATRIX

```

```

C     ELEMENTS FOR CONSTANT NUZ MAGNETIC
C     FIELD REGIONS.
COMMON/DIR/BKWD,END(13),BAD(13)
COMMON/TT/T(2,2,13),E(13),S(13),PASE(13)
COMMON/ELEM/EL(2,2)
COMMON/PLT/IS,PRNT
COMMON/START2/FIO,DELTA,C,THTA
COMMON /SLIP/NPS,EDS,DELES,PS(100)
COMMON /VNUZ/NUUZ,EOZ,DELEZ,UZ(100)
DIMENSION REM(13)
LOGICAL IS,PRNT
DOUBLE PRECISIONT,EL,E
LOGICAL BKWD,END,BAD
T1=P1
THT=P2*5.0/57.29578
FIO=FIO+THT
THTA=THTA+THT
T2=P2
IREM=1
REM(1)=P1
105 FORMAT('OMAGNETIC FIELD ,  ANGULAR LENGTH=',F7.2,
+ ' NUZ=',13F6.2)
DO 70 I=1,13
IF(END(I))GO TO 70
IF(BAD(I))GO TO 70
EE=E(I)
SQE=SQRT(EE)
IF(NNUZ.EQ.0)GO TO 117
T1=UTERP(EE)
C WRITE(6,129)T1
C 129 FORMAT(' ',E16.8)
IREM=IREM+1
REM(IREM-1)=T1
117 R=18.94*SQE
SS=R*T2/57.2957795130823209
S(I)=S(I)+SS
PASE(I)=PASE(I)+THT
IF(NPS.NE.0)PASE(I)=PASE(I)+STERP(EE)
Q=T1*SS/R
SI=SIN(Q)
CO=COS(Q)
EL(1,1)=CO
EL(1,2)=SS*SI/(Q*SQE)
EL(2,1)=-Q*SI*SQE/SS
EL(2,2)=CO
CALL MATMUL(I)
CALL UPDATE(I)
70 CONTINUE
IF(.NOT.PRNT)GO TO 32
IREM=IREM-1
CALL PAGE(2)
WRITE(6,105)P2,(REM(I),I=1,IREM)
32 RETURN
END
SUBROUTINE TLEN(P1,P2)
C*****
C     THIS ROUTINE CALCULATES THE PHASE
C     AND ENERGY GAIN REQUIRED TO COMPUTE
C     THE ELECTRIC LENS EFFECTS.
C     SUBROUTINE TLENS CALCULATES THE

```

```

C   CHANGES IN SLOPE AND DISPLACEMENT
C   CAUSED BY THE LENS.
COMMON/DIR/BKWD,END(13),BAD(13)
COMMON/TT/T(2,2,13),E(13),S(13),PASE(13)
COMMON/ELEM/EL(2,2)
COMMON/START/ESTART,Z1(13),Z1P(13),Z2(13),Z2P(13),EPS,EMAX
COMMON/PLT/IS,PRNT
COMMON/START2/FIO,DELTA,C,THTA
LOGICAL IS,PRNT
DOUBLE PRECISION T,EL,E
DP1=P1
DP2=P2
LOGICAL BKWD,END,BAD
104 FORMAT('OTHIN LENS ENERGY GAIN= ',F7.3,' REDUCTION FACTOR= '
+,F7.3,' R.F PHASE AT GAP WITH NO PHASE SLIP IS'F8.2,
+' (' ,F6.2, ' )')
DIMENSION ZZZ(13),ZZX(13)
DO 60 I=1,13
FI=PASE(I)-THTA
C   THE FOLLOWING EXPRESSION FOR THE ENERGY GAIN ALLOWS THE
C   MIXTURE OF THIRD HARMONIC TO BE SPECIFIED BY DELTA (THE PHASE
C   DIFFERENCE BETWEEN THE FIRST AND THIRD HARMONIC) AND C WHERE
C   C=EPSILON*COS(DELTA); EPSILON IS THE RELATIVE AMPLITUDE OF THE FIRST
C   AND THIRD HARMONICS
DELE=DP1*(COS(FI)-C*COS(3.*FI)+C*TAN(DELTA)*SIN(3.*FI))
IF(BKWD)DELE=-DELE
IF(E(I)+DELE.LT.0.0)END(I)=.TRUE.
IF(E(I).GT.EMAX)END(I)=.TRUE.
IF(END(I))GO TO 60
IF(BAD(I))GO TO 60
CALL TLENS(E(I)+DELE/2.,FI,DP1,A)
ZA=DSQRT(E(I))/DSQRT(E(I)+DBLE(DELE))
ZA=1.0-ZA
IF(BKWD)A=-A
IF(BKWD)ZA=-ZA
IF(DP2.EQ.0.0)GO TO 20
A=DP2*A
ZA=DP2*ZA
20 ZZZ(I)=A
ZZX(I)=ZA
EL(1,1)=1.0-ZA
EL(2,1)=-A*(DSQRT(E(I))+DSQRT(E(I)+DBLE(DELE)))/2.
EL(2,2)=1.0
EL(1,2)=-A*(1.0-EL(1,1))/EL(2,1)
E(I)=E(I)+DELE
CALL MATMUL(I)
CALL UPDATE(I)
60 CONTINUE
IF(.NOT.PRNT)GO TO 734
CALL PAGE(4)
THPN=THTA*57.29578
THPM=AMOD(THPN,360.)
WRITE(6,104)P1,P2,THPN,THPM
WRITE(6,1001)ZZZ,ZZX
1001 FORMAT(' ',13F7.3)
734 RETURN
END
SUBROUTINE TLENS(E,THETA,DELE,ZZ)
C*****
C   -THIS ROUTINE CALCULATES THE DISPLACEMENT

```

```

C*****
C   -THIS ROUTINE CALCULATES THE DISPLACEMENT

```

```

C   AND SLOPE CHANGES CAUSED BY THE THIN LENS.
C   -F1 AND F2 ARE THE FACTORS DESCRIBED BY
C   ROSE IN=
C       PHYS, REV. VOL(53),392(1938)
C   - F3, F4, AND F5 ARE THE FACTORS DESCRIBED
C   BY COHEN IN=
C       REV. SCC. INSTR. VOL.24, 589(1953)
C   -THE NUMERICAL VALUES ARE THOSE APPROPRIATE
C   TO THE TRIUMF DEE GEOMETRY.
COMMON/START/ESTART,Z1(13),Z1P(13),Z2(13),Z2P(13),EPS,EMAX
COMMON/START2/FIO,DELTA,C,THTA
PI=3.1415926535897932
SI=SIN(THETAR)=3.*C*COS(3.*THETAR)*TAN(DELTA)=3.*C*SIN(3.*THETAR)
CO=COS(THETAR)=C*COS(3.*THETAR)+C*TAN(DELTA)*SIN(3.*THETAR)
EVOEC=.5*DELE/E
C   WRITE(6,100)E,THETAR,DELE,SI,CO,EVOEC
C   IF(E.LT.0.0)STOP 456
C   R=18.94*SQRT(E)
C   IF(DELE.NE.0.1)GO TO 1
C   F=.975
C   GO TO 3
1  IF(R.GT.30.0)GO TO 2
C   F=1.07-0.0155*R
C   GO TO 3
2  F=0.605
3  F1=5.*EVOEC*SI/R
C   F2=2*F*EVOEC*EVOEC*CO*CO/(PI*2.0)
C   F3=-EVOEC*EVOEC*SI*SI/(.2*R)
C   F4=-.4*EVOEC*EVOEC*CO*CO/R
C   F5= 5.*EVOEC*EVOEC*SI/R
C   F12=F1+F2
C   F15=F12+F3+F4+F5
C   ZZ=F12
C   ZZ=F15
C   WRITE(6,100)F1,F2,R,ZZ
C   RETURN
C 100 FORMAT(' ',6G10.3)
C   END
C   SUBROUTINE UPDATE(I)
C *****UPDATE
C   -THIS ROUTINE CALCULATES
C   THE NEW ELLIPSE COEFFICIENTS FROM THE
C   INITIAL VALUES OF THE COEFFICIENTS AND
C   THE CURRENT 2X2 TRANSFER MATRIX.
COMMON/ELST/AL(13),BE(13),GA(13)
COMMON/ELLIPS/ALFA(13),BETA(13),GAMMA(13)
COMMON/TT/T(2,2,13),E(13),S(13),PASE(13)
COMMON/ELEM/EL(2,2)
COMMON/DIR/BKWD,END(13),BAD(13)
LOGICAL BKWD,END,BAD
DOUBLE PRECISION AL,BE,GA,TEST
DOUBLE PRECISION T,ALFA,BETA,GAMMA,EL
DOUBLE PRECISION C,CP,SS,SP,ALF,BET,GAM,E
C=T(1,1,I)
CP=T(2,1,I)
SS=T(1,2,I)
SP=T(2,2,I)
ALF=AL(I)
BET=BE(I)
GAM=GA(I)

```

```

C THE FOLLOWING THREE TESTS CAUSE TERMINATION OF THE
C CALCULATION FOR ANY PHASE FOR WHICH ANY ONE OF THE
C FOLLOWING CONDITIONS OCCUR:
C (1) BETA < 0
C (2) GAMMA > 0
C (3) BETA*GAMMA=ALFA**2=1 > 0.001
C THESE CONDITIONS OCCUR WHEN BETA OR GAMMA BECOME LARGE
C SO THAT THERE IS NOT SUFFICIENT PRECISION TO
C CALCULATE THEM PROPERLY
C BETA(I)=C*C*BET=2.*C*SS*ALF+SS*SS*GAM
C IF(BETA(I).GE.0.0)GO TO 200
C CALL PAGE(1)
C IP=(I-7)*10
C WRITE(6,1)IP
C BAD(I)=.TRUE.
C BETA(I)=BETA(I)
C RETURN
200 ALFA(I)=C*CP*BET+(C*SP+SS*CP)*ALF-SS*SP*GAM
C GAMMA(I)=CP*CP*BET=2.*CP*SP*ALF+SP*SP*GAM
C IF(GAMMA(I).GE.0.0)GO TO 201
C CALL PAGE(1)
C IP=(I-7)*10
C WRITE(6,2)IP
C BAD(I)=.TRUE.
C GAMMA(I)=GAMMA(I)
C RETURN
201 TEST=BETA(I)*GAMMA(I)-ALFA(I)*ALFA(I)-1.
C IF(DABS(TEST).LT.0.001)RETURN
C CALL PAGE(1)
C IP=(I-7)*10
C WRITE(6,3)IP
C BAD(I)=.TRUE.
1 FORMAT(' CALCULATION OF FI= ',I4,' TERMINATED DUE '
X' TO NEGATIVE BETA')
2 FORMAT(' CALCULATION OF FI= ',I4,' TERMINATED DUE '
X' TO NEGATIVE GAMMA')
3 FORMAT(' CALCULATION OF FI= ',I4,' TERMINATED DUE '
X' TO B*G=A*A NOT EQUAL TO 1.')
C RETURN
C END
C SUBROUTINE MATMUL(I)
C *****MATMUL
C -THIS ROUTINE MULTIPLIES THE OLD
C TRANSFER MATRIX BY THE MATRIX FOR THE CURRENT ELEMENT TO
C PRODUCE THE NEW TRANSFER MATRIX
C COMMON/TT/T(2,2,13),E(13),S(13),PASE(13)
C COMMON/ELEM/EL(2,2)
C COMMON/DIR/BKWD,END(13),BAD(13)
C LOGICAL BKWD,END,BAD
C DOUBLE PRECISION T,EL,E
C DOUBLE PRECISION T11,T12,T21,T22,TA
C LOGICAL ERR
C T11=T(1,1,I)
C T12=T(1,2,I)
C T21=T(2,1,I)
C T22=T(2,2,I)
C T(1,1,I)=T11*EL(1,1)+T21*EL(1,2)
C T(1,2,I)=T12*EL(1,1)+T22*EL(1,2)
C T(2,1,I)=T11*EL(2,1)+T21*EL(2,2)
C T(2,2,I)=T12*EL(2,1)+T22*EL(2,2)

```

```

C      -THE FOLLOWING STATEMENTS CHECK THAT THE DETERMINANT
C      OF THE TRANSFER MATRIX IS WITHIN .001 OF 1
C      -IF NOT, THE CALCULATION IS TERMINATED
C      -THIS OCCURS WHEN THE MATRIX ELEMENTS BECOME LARGE
C      SO THAT THE DETERMINANT CANNOT BE CALCULATED ACCURATELY
C      TA=T(1,1,I)*T(2,2,I)-T(1,2,I)*T(2,1,I)-1.
C      IF(DABS(TA).LT.0.001)RETURN
C      CALL PAGE(1)
C      IP=(I-7)*10
C      WRITE(6,100)IP
100  FORMAT(' CALCULATION OF FI= ',I4,' TERMINATED DUE'
C      X' TO DET OF T NOT EQUAL TO 1.')
C      BAD(I)=.TRUE.
C      RETURN
C      END
C      SUBROUTINE UNTRK(XNUZ)
C *****UNTRK
C      PARAMETERS WHICH ARE REQUIRED TO MATCH
C      THE BEAM ELLIPSE TO THE GIVEN NUZ.
C      THEN IT CALCULATES THE INVERSE OF THE
C      CURRENT 3X3 TRANSFER MATRIX FOR THE
C      ELLIPSE COEFFICIENTS, AND MULTIPLIES THE
C      REQUIRED FINAL VECTOR BY THE INVERSE
C      MATRIX TO DETERMINE WHAT STARTING ELLIPSE
C      PARAMETERS WILL GIVE THE REQUIRED FINAL VECTOR.
C      COMMON /CARD/P(8),MNT(5)
C      COMMON/TT/T(2,2,13),E(13),S(13),PASE(13)
C      COMMON/ELLIPS/ALFA(13),BETA(13),GAMMA(13)
C      COMMON/START/ESTART,Z1(13),Z1P(13),Z2(13),Z2P(13),EPS,EMAX
C      COMMON/DIR/BKWD,END(13),BAD(13)
C      COMMON /VNUZ/NNUZ,EOZ,DELEZ,UZ(100)
C      LOGICAL BKWD,END,BAD
C      DOUBLE PRECISION T,ALFA,BETA,GAMMA,E
C      DOUBLE PRECISION T11,T12,T21,T22
C      DOUBLE PRECISION EO(3,3),EI(3,3),ST(3),EN(3)
C      IF(NNUZ.NE.0)XNUZ=UTERP(EMAX)
C      CALL PAGE(1)
C      WRITE(6,109)XNUZ
109  FORMAT(' MATCH TO NUZ= ',F7.3)
C      ST(1)=18.94/XNUZ
C      ST(3)=1./ST(1)
C      ST(2)=0.0
C      DO 800 K=1,13
C      IF(BAD(K))GO TO 800
C      FI=FLOAT(K-7)*10
C      CALL PAGE(8)
C      WRITE(6,103)FI
103  FORMAT('OPHASE= ',F4.0/
C      X' MATRIX',40X,'INVERSE')
C      T11=T(1,1,K)
C      T12=T(1,2,K)
C      T21=T(2,1,K)
C      T22=T(2,2,K)
C      3 X 3 MATRIX COMPONENTS
C      EO(1,1)=T11*T11
C      EO(1,2)=-2.*T11*T12
C      EO(1,3)=T12*T12
C      EO(2,1)=-T11*T21
C      EO(2,2)=T11*T22+T21*T12
C      EO(2,3)=-T12*T22

```

```

EO(3,1)=T21*T21
EO(3,2)=-2.*T21*T22
EO(3,3)=T22*T22
C 3 X 3 INVERSE MATRIX COMPONENTS
EI(1,1)=T22*T22
EI(1,2)=2.*T12*T22
EI(1,3)=T12*T12
EI(2,1)=T21*T22
EI(2,2)=T11*T22+T21*T12
EI(2,3)=T11*T12
EI(3,1)=T21*T21
EI(3,2)=2.*T11*T21
EI(3,3)=T11*T11
DO 10 IJ=1,3
WRITE(6,100)(EO(IJ,IL),EI(IJ,IL),IL=1,3)
100 FORMAT(' ',3E11.3,13X,3E11.3)
10 CONTINUE
DO 67 I=1,3
67 EN(I)=EI(I,1)*ST(1)+EI(I,2)*ST(2)+EI(I,3)*ST(3)
WRITE(6,102)ST,EN
102 FORMAT(' INITIAL VECTOR ',3E16.8/
X' FINAL VECTOR ',3E16.8)
BETA(K)=EN(1)
ALFA(K)=EN(2)
GAMMA(K)=EN(3)
800 CONTINUE
RETURN
999 STOP 999
END
SUBROUTINE DRAW(S1,S2)
C *****DRAW
C -THIS ROUTINE DRAWS THE ELLIPSES ON A
C CALCOMP PLOTTER. THE SCALE USED IS
C READ IN ON THE DATA CARD WHICH CAUSES
C TRANSFER TO THIS ROUTINE
C -ELLIPSES WHICH WOULD GO OFF THE PAGE
C ARE TRUNCATED
COMMON/USD/USED
COMMON/PLT/IR,PRNT
COMMON/ELLIPS/ALFA(13),BETA(13),GAMMA(13)
COMMON/START/ESTART,Z1(13),Z1P(13),Z2(13),Z2P(13),EPS,EMAX
COMMON/TT/T(2,2,13),E(13),S(13),PASE(13)
COMMON/DIR/BKWD,END(13),BAD(13)
LOGICAL BKWD,END,BAD
COMMON/PGE/N,NPAGE,NAME(5)
DOUBLE PRECISION T,ALFA,BETA,GAMMA,E
LOGICAL IR,IS,PRNT
DIMENSION X(1000),Y(1000)
DATA DELPHI/.00628318/
DATA IS/.FALSE./
IR=IS
IF(IS)GO TO 1
CALL PLOTS
IS=.TRUE.
IR=.TRUE.
1 CALL PLOT(USED,0.0,-1)
USED=12.0
CALL AXIS(5.,5.,10HZ (INCHES),10,5.,0.0,0.0,S1)
CALL AXIS(5.,5.,12HZ (RADIAN),12,5.,90.,0.0,S2)
CALL AXIS(5.,5.,1H ,-1,5.,180.,0.0,-S1)

```

```

CALL AXIS(5.,5.,1H ,=-1,5.,270.,0.0,=S2)
CALL SYMBOL(5.1,9.0,.25,NAME(1),0.0,20)
DO 2 K=1,13
  IF(BAD(K))GO TO 2
  SQE=DSQRT(E(K))
  A=ALFA(K)
  B=BETA(K)*SQE
  G=GAMMA(K)/SQE
  TEM=G*S1*S1=B*S2*S2
C   IF(TEM.GT.0.1E-25)GO TO 521
C   ANG=1.5708
C   GO TO 522
C   THE FOLLOWING 5 STATEMENTS CALCULATE THE ANGLE AT WHICH
C   TO LABEL THE ELLIPSE.
521 ANG=.5*ATAN(2.*A*S1*S2/TEM)
522 IF(TEM.LE.0.0)GO TO 634
   IF(A.LT.0.0)ANG=ANG+1.5708
   IF(A.GE.0.0)ANG=ANG-1.5708
634 IF(ANG.LT.0.0)ANG=ANG+6.28318
   EPQ=EPS/SQE
   PHI=0.0
   DO 3 I=1,500
     CO=COS(PHI)
     SI=SIN(PHI)
C   SCALE FACTORS
C     S1=Z INCHES PER PLOT INCH
C     S2=Z' RADIANS PER PLOT INCH
   TEN=G*S1*S1*CO*CO+B*S2*S2*SI*SI+2.0*A*S1*S2*SI*CO
   IF(TEN.GT.0.1E-25)GO TO 523
   R=100.
   GO TO 524
523 R=SQRT(EPQ/TEN)
524 X(I)=R*CO+5.
   Y(I)=R*SI+5.
   X(I+500)=-R*CO+5.
   Y(I+500)=-R*SI+5.
   PHINEW=PHI+DELPHI
   IF(PHI.LT.ANG.AND.PHINEW.GT.ANG)LAB=I
   PHI=PHINEW
3 CONTINUE
  IRST=1000
C   WRITE(3,2345)LAB
C2345 FORMAT(' ',I6)
  DO 5 I=1,1000
    IF(X(I).LT.0.0.OR.X(I).GT.10.0.OR.
X    Y(I).LT.0.0.OR.Y(I).GT.10.0)GO TO 5
    IF(I.LT.IRST)IRST=I
5 CONTINUE
  CALL PLOT(X(IRST),Y(IRST),3)
  XNUM=FLOAT(K-6)*10.
  DO 4 I=1,1000
    IF(X(I).LT.0..OR.X(I).GT.10..OR.Y(I).LT.0..OR.Y(I).GT.10.)
XGO TO 12
    XX=X(I)
    YY=Y(I)
    CALL PLOT(XX,YY,2)
12 IF(I.EQ.LAB)CALL NUMBER(XX,YY,.14,XNUM,0.0,0)
4 CONTINUE
2 CONTINUE
  CALL PLOT(XX,YY,3)

```

RETURN

END

SUBROUTINE PRINT

C\*\*\*\*\*PRINT

C -THIS ROUTINE PRINTS THE CURRENT TRANSFER  
 C MATRIX, ENERGY, S, ELLIPSE COEFFICIENTS,  
 C ENVELOPE, AND PRINCIPLE TRAJECTORIES FOR  
 C EACH PHASE

COMMON/TT/T(2,2,13),E(13),S(13),PASE(13)

COMMON/ELLIPS/ALFA(13),BETA(13),GAMMA(13)

COMMON/START/ESTART,Z1(13),Z1P(13),Z2(13),Z2P(13),EPS,EMAX

COMMON/DIR/BKWD,END(13),BAD(13)

LOGICAL BKWD,END,BAD

DOUBLE PRECISION ALFA,BETA,E,GAMMA,T,TA

CALL PAGE(3)

WRITE(6,101)

101 FORMAT(/' AFTER LAST ELEMENT '

X/ 4X,'PHASE',6X,'T11',8X,'T12',9X,'T21'

X,8X,'T22',7X,'E',5X,'S',5X,'ALFA',

X6X,'BETA',6X,'GAMMA',2X

X,2X,'ENV',2X,'ENV''',2X,'Z1',2X,'Z1''',3X,'Z2',4X,'Z2''')

DO 40 I=1,13

IF(BAD(I))GO TO 40

SQE=DSQRT(E(I))

CALL PAGE(1)

FI=FLOAT(I-7)\*10.

C TA=BETA(I)\*GAMMA(I)-ALFA(I)\*ALFA(I)-1.0

C IF(DABS(TA).LT.0.0001)GO TO 236

C CALL PAGE(1)

C WRITE(6,667)TA

C 667 FORMAT(' \*\*\*\*\*WARNING\*\*\*\*\* BETA\*GAMMA-ALFA\*\*2-1 NOT ZERO'

C X,' VALUE= ',E16.8)

236 IF(BETA(I).LT.0.0.OR.GAMMA(I).LT.0.0)GO TO 500

100 FORMAT(1X,F4.0,1X,F6.1,4E11.3,F6.3,F6.2,3E10.3,6F5.2)

EX=DSQRT(EPS\*BETA(I))

EXP=DSQRT(EPS\*GAMMA(I))/SQE

GO TO 600

500 EX=0.0

EXP=0.0

600 ZPA=T(1,1,I)\*Z1(I)+T(1,2,I)\*Z1P(I)

ZPB=(T(2,1,I)\*Z1(I)+T(2,2,I)\*Z1P(I))/SQE

ZQA=T(1,1,I)\*Z2(I)+T(1,2,I)\*Z2P(I)

ZQB=(T(2,1,I)\*Z2(I)+T(2,2,I)\*Z2P(I))/SQE

PSE=AMOD(PASE(I)\*57.2958,360.)

WRITE(6,100)FI,PSE,T(1,1,I),T(1,2,I),

XT(2,1,I),T(2,2,I),E(I),S(I),ALFA(I),BETA(I),GAMMA(I)

X,EX,EXP,ZPA,ZPB,ZQA,ZQB

40 CONTINUE

RETURN

END

SUBROUTINE COMP

C\*\*\*\*\*COMP

C -THIS ROUTINE SETS UP THE CALLS TO SUBROUTINE REGION WHICH  
 C CALCULATES THE ELLIPSE OVERLAPS

COMMON/START/ESTART,Z1(13),Z1P(13),Z2(13),Z2P(13),EPS,EMAX

COMMON/ELLIPS/ALFA(13),BETA(13),GAMMA(13)

COMMON/DIR/BKWD,END(13),BAD(13)

LOGICAL BKWD,END,BAD

DOUBLE PRECISION ALFA,BETA,GAMMA

DIMENSION A(13),VALUE(13,13),SUM(13)

```

CALL PAGE(18)
WRITE(6,102)
102 FORMAT('OFRACATIONAL OVERLAP OF ELLIPSES')
WRITE(6,100)
100 FORMAT('O',6X,' -60      -50      '
X,' -40      -30      -20      -10      '
X'  0      10      20'
X,'      30      40      50      60')
DO 1 I=1,13
N=(I-7)*10
DO 2 J=1,I
A(J)=99.
IF(BAD(J).OR.BAD(I))GO TO 59
CALL REGION(I,J,A(J))
59 CONTINUE
VALUE(I,J)=A(J)
C WRITE(2,549) A(J)
C 549 FORMAT(' ',G16.8)
JJ=J
2 CONTINUE
WRITE(6,101)N,(A(K),K=1,JJ)
101 FORMAT(' ',I4,13(2X,F5.3,2X))
1 CONTINUE
DO 8 I=1,13
JJ=I
SUM(I)=-1.0
DO 62 J=1,JJ
62 IF(VALUE(I,J).LE.1.0)SUM(I)=SUM(I)+VALUE(I,J)
DO 11 K=JJ,13
11 IF(VALUE(K,JJ).LE.1.0)SUM(I)=SUM(I)+VALUE(K,JJ)
8 CONTINUE
DO 9 I=1,13
SUM(I)=SUM(I)/13.
IF(SUM(I).LT.0.0)SUM(I)=99.
9 CONTINUE
WRITE(6,103)SUM
103 FORMAT(' ', ' SUM',13(2X,F5.3,2X))
RETURN
END
SUBROUTINE REGION(I,J,FRAC)
C*****
C SUBROUTINE REGION CALCULATES FRACTIONAL OVERLAP OF ELLIPSES
COMMON/START/ESTART,Z1(13),Z1P(13),Z2(13),Z2P(13),EE,EMAX
COMMON/TT/T(2,2,13),EAB(13),S(13),PASE(13)
DOUBLE PRECISION T,EAB
COMMON/ELLIPS/ALFA(13),BETA(13),GAMMA(13)
DOUBLE PRECISION ALFA,BETA,GAMMA ,A1,B1,G1,A2,B2,G2,E
DOUBLE PRECISION SUM1,SUM2,DIFF1,DIFF2,RATIO1,RATIO2
DOUBLE PRECISION A,B,G,BINV,DISCR,STUFF1,STUFF2,X1,X2,TEMP
DOUBLE PRECISION PSIPOS,PSINEG,H1,H2,BASIC1,BASIC2,CHI1,CHI2
DOUBLE PRECISION DP1,DP2,DN1,DN2,TPLUS,TMINUS,FIPOS,FINEG
SQEI=DSQRT(EAB(I))
SQEJ=DSQRT(EAB(J))
A1=ALFA(I)
A2=ALFA(J)
B1=BETA(I)*SQEI
B2=BETA(J)*SQEJ
G1=GAMMA(I)/SQEI
G2=GAMMA(J)/SQEJ
E=EE

```

```

LOGICAL L1,L2,L3,LL1,LL2
REAL*8 MAJ1,MAJ2,MIN1,MIN2,MAJDIF
SUM1=G1+B1
SUM2=G2+B2
DIFF1=G1-B1
DIFF2=G2-B2
RATIO1=0.5*(SUM1+DSQRT(SUM1*SUM1-4.))
RATIO2=0.5*(SUM2+DSQRT(SUM2*SUM2-4.))
MAJ1=DSQRT(E*RATIO1)
MAJ2=DSQRT(E*RATIO2)
A=A1-A2
B=B1-B2
G=G1-G2
L1=A.EQ.0..AND.B.EQ.0.
L2=A.EQ.0..AND.G.EQ.0.
L3=B.EQ.0..AND.G.EQ.0.
C THE ELLIPSES COINCIDE
IF(L1.OR.L2.OR.(L1.AND.L2)) GO TO 621
C POINTS OF INTERSECTION ARE AT 0 AND 90 DEGREES
IF(L3) GO TO 622
C ONE POINT OF INTERSECTION IS AT 90 DEGREES
IF(B.EQ.0..AND.G.NE.0.) GO TO 623
C NONE OF THE ABOVE SPECIAL CASES
C CALCULATE ANGLES OF INTERSECTION
BINV=1./B
DISCR=DSQRT(A*A-B*G)
STUFF1=-BINV*A
STUFF2=B INV*DISCR
X1=STUFF1+STUFF2
X2=STUFF1-STUFF2
IF(B.GT.0.) GO TO 624
TEMP=X2
X2=X1
X1=TEMP
624 PSIPOS=DATAN(X1)
PSINEG=DATAN(X2)
GO TO 686
623 PSIPOS=1.5707963
PSINEG=0.5*G/A
GO TO 500
622 PSIPOS=1.5707963
PSINEG=0.
C CALCULATE ORIENTATIONS OF MAJOR AXES
C TEST TO SEE IF ELLIPSE #1 IS A CIRCLE
686 IF(DIFF1.EQ.0.0)GO TO 400
500 H1=2.*A1/DIFF1
BASIC1=0.5*DATAN(H1)
IF(DIFF1.LT.0.)GO TO 503
IF(A1)501,502,502
501 CH1=BASIC1+1.5707963
GO TO 687
502 CH1=BASIC1-1.5707963
GO TO 687
503 CH1=BASIC1
GO TO 687
400 CH1=0.
C TEST TO SEE IF ELLIPSE #2 IS A CIRCLE
687 IF(DIFF2.EQ.0.0)GO TO 401
H2=2.*A2/DIFF2
504 BASIC2=0.5*DATAN(H2)

```

```

IF(DIFF2.EQ.0.)GO TO 401
IF(DIFF2.LT.0.)GO TO 507
IF(A2) 505,506,506
505 CHI2=BASIC2+1.5707963
GO TO 508
506 CHI2=BASIC2-1.5707963
GO TO 508
507 CHI2=BASIC2
GO TO 508
401 CHI2=0.
C   THERE ARE 3 POSSIBLE CASES:
C   (1) ONE MAJOR AXIS LIES OUTSIDE PTS. OF INTERSECTION
C   (2) BOTH AXES LIE INSIDE
C   (3) BOTH AXES LIE OUTSIDE
508 DP1=PSIPOS=CHI1
DP2=PSIPOS=CHI2
DN1=PSINEG=CHI1
DN2=PSINEG=CHI2
LL1=DN1.LE.0..AND.DP1.GE.0.
LL2=DN2.LE.0..AND.DP2.GE.0.
C   TEST CASE (2)
IF(LL1.AND.LL2) GO TO 511
C   TEST CASE (3)
IF(.NOT.LL1.AND..NOT.LL2) GO TO 512
C   CASE (1)
IF(LL1.AND..NOT.LL2) GO TO 509
IF(.NOT.LL1.AND.LL2) GO TO 510
C   MORE CALCULATION AND TESTING REQUIRED TO DETERMINE
C   WHICH ELLIPSE TO USE FOR AREA SECTOR CALCULATION
509 TPLUS=DSIN(DP2)/DCOS(DP2)
TMINUS=DSIN(DN2)/DCOS(DN2)
GO TO 513
510 TPLUS=DSIN(DP1)/DCOS(DP1)
TMINUS=DSIN(DN1)/DCOS(DN1)
GO TO 514
511 MAJDIF=MAJ1=MAJ2
IF(MAJDIF)510,510,509
512 MAJDIF=MAJ1=MAJ2
IF(MAJDIF)509,509,510
513 FIPOS=DATAN(RATIO2*TPLUS)
IF(DP2.GE.=1.5707963.AND.DP2.LE.1.5707963)GO TO 402
FIPOS=FIPOS+3.1415927
402 FINEG=DATAN(RATIO2*TMINUS)
IF(DN2.GE.=1.5707963.AND.DN2.LE.1.5707963)GO TO 450
FINEG=FINEG+3.1415927
GO TO 450
514 FIPOS=DATAN(RATIO1*TPLUS)
IF(DP1.GE.=1.5707963.AND.DP1.LE.1.5707963)GO TO 403
FIPOS=FIPOS+3.1415927
403 FINEG=DATAN(RATIO1*TMINUS)
IF(DN1.GE.=1.5707963.AND.DN1.LE.1.5707963)GO TO 450
FINEG=FINEG+3.1415927
GO TO 450
621 FRAC=1.0
GO TO 700
450 FRAC=(2./3.1415927)*(FIPOS-FINEG)
700 CONTINUE
RETURN
END
SUBROUTINE PAGE(NREQD)

```

```

C*****PAGE
C      -THIS ROUTINE WRITES THE TITLE
C      PAGE NUMBER ON EACH NEW PAGE
COMMON/PGE/N,NPAGE,NAME(5)
COMMON/START/ESTART,Z1(13),Z1P(13),Z2(13),Z2P(13),EPS,EMAX
COMMON/START2/FIO,DELTA,C,THTA
DIMENSION D(2),T(2)
IF(N+NREQD.GT.60)GO TO 1
N=N+NREQD
RETURN
1 NPAGE=NPAGE+1
CALL DATE(D,T)
DZA=DELTA*57.29578
WRITE(6,101)NAME,C,DZA,D,T,NPAGE
101 FORMAT('1 CASE ',5A4,3X,'C= '
X,F7.3,3X,'DELTA= '
X,F7.3,3X,2A4,2X,2A4,42X,'PAGE ',I3//)
N=4+NREQD
IF(NREQD.EQ.61)N=4
RETURN
END
SUBROUTINE POINTS
C      WRITE(5,9)
C 9    FORMAT(' ','POINTS CALLED')
DIMENSION C(13),Q(13)
COMMON/PTS/X(13,200),Y(3,13,200),PH(13),M,TURNS
COMMON/START/ESTART,Z1(13),Z1P(13),Z2(13),Z2P(13),EPS,EMAX
DOUBLE PRECISION ALFA,BETA,GAMMA,T,E
COMMON/TT/T(2,2,13),E(13),S(13)
COMMON/ELLIPS/ALFA(13),BETA(13),GAMMA(13)
COMMON/START2/FIO,DELTA,CDUM,THTA
COMMON/SQALE/XSKAL,YSKAL
DATA A,B/.01745329,.03183098/
C      WRITE(5,10)(BETA(I),I=1,13),(T(1,1,I),T(1,2,I),T(2,1,I),
C      2T(2,2,I),I=1,13),THTA
C 10   FORMAT(1X,10E13.6)
DO 200 I=1,13
C      IF(I.EQ.1) WRITE(5,15)
C 15   FORMAT('0',T10,'I',T30,'PHI',T50,'C',//)
PH(I)=10.*(I-6)
C(I)= COS(PH(I)*A)*B
C      WRITE(5,20) I,PH(I),C(I)
C 20   FORMAT(' ',T9,I2,T27,F6.1,T46,F10.6)
200   CONTINUE
J=1
RETURN
ENTRY POINTQ
300   DO 400 I=1,13
C      IF(I .EQ. 1) WRITE(5,40) J
C 40   FORMAT('0',T30,' J = ',I4,//)
C      IF(I.EQ.1)WRITE(5,30)
C 30   FORMAT(' ',T20,'Y1',T40,'Y2',T60,'Y3',T80,'X',//)
Y(1,I,J)=(T(1,1,I)*Z1(I) + T(1,2,I)*Z1P(I))/YSKAL + 5.
Y(2,I,J)=(T(1,1,I)*Z2(I) + T(1,2,I)*Z2P(I))/YSKAL + 5.
Y(3,I,J)=(DSQRT(EPS*BETA(I)))/YSKAL + 5.
X(I,J) = THTA*C(I)/XSKAL
C      WRITE(8,35)Y(1,I,J),Y(2,I,J),Y(3,I,J),X(I,J)
C 35   FORMAT(' ',4F10.4)
400   CONTINUE
M=J

```

J=J+1  
 RETURN  
 END

SUBROUTINE PLO(LZ1,LZ2,LENV,LALL,IST,LAST)

C\*\*\*\*\*PLO

C

C THIS SUBROUTINE DRAWS AXES AND LABELS AND DECIDES  
 C WHICH PHASES ARE TO BE PLOTTED

C

C WRITE(5,25)

C 25 FORMAT(' ', 'PLO HAS BEEN CALLED'//)

INTEGER IST, LAST, M, PN

COMMON/PLT/IS, PRNT

COMMON/USD/USED

COMMON/PTS/X(13,200), Y(3,13,200), PH(13), M, TURNS

COMMON/PGE/N, NPAGE, NAME(5)

COMMON/SQALE/XSKALE, YSKALE

COMMON/DIR/BKWD, END(13), BAD(13)

LOGICAL BKWD, END, BAD

LOGICAL LZ1, LZ2, LENV, LALL, LPN, IS, PRNT

URNS=M/6

URNS=URNS/XSKALE

HALF=URNS/2.

C WRITE(5,105) TURNS, HALF

C105 FORMAT('0', T30, 'URNS=', F10.5, T50, 'HALF=', F10.5, //)

IF(IS) GO TO 10

CALL PLOTS

IS=.TRUE.

10 CALL PLOT(USED, 0.0, =1)

YSTT=-5.\*YSKALE

CALL AXIS(0., 0., 'Z', 1, 10., 90., YSTT, YSKALE)

CALL AXIS(0., 5., 'URNS X COS(PHASE)', =18, TURNS, 0., 0.0, XSKALE)

CALL SYMBOL(HALF=1.8, 9., .21, NAME(1), 0., 20)

IF(.NOT.LZ1) GO TO 200

CALL SYMBOL(HALF=.9, 8.75, .21, 'Z1', 0., 2)

DO 120 I=1, 13

PN=PH(I)

LPN=(PN.LT.IST).OR.(PN.GT.LAST)

IF(LP.N.AND..NOT.LALL) GO TO 120

IF(BAD(I))GO TO 120

CALL DP(1, I)

120 CONTINUE

200 IF(.NOT.LZ2) GO TO 300

CALL SYMBOL(HALF=.36, 8.75, .21, 'Z2', 0., 2)

DO 220 I=1, 13

PN=PH(I)

LPN=(PN.LT.IST).OR.(PN.GT.LAST)

IF(LP.N.AND..NOT.LALL)GO TO 220

IF(BAD(I))GO TO 220

CALL DP(2, I)

220 CONTINUE

300 IF(.NOT.LENV) GO TO 400

CALL SYMBOL(HALF+.18, 8.75, .21, 'ENV', 0., 3)

DO 320 I=1, 13

PN=PH(I)

LPN=(PN.LT.IST).OR.(PN.GT.LAST)

IF(LP.N.AND..NOT.LALL) GO TO 320

IF(BAD(I))GO TO 320

CALL DP(3, I)

320 CONTINUE

```

400 IF(LALL)GO TO 500
    CALL SYMBOL(HALF=1.98,8.5,.21,'PHASES TO INCL',
10.,22)
    FLT1=IST
    FLT2=LAST
    CALL NUMBER(HALF=.72,8.5,.21,FLT1,0.,=1)
    CALL NUMBER(HALF+.54,8.5,.21,FLT2,0.,=1)
500 CONTINUE
    CALL WHERE(XNOW,YNOW)
    CALL PLOT(XNOW,YNOW,3)
    USED=TURNS+2.
    RETURN
    END
    SUBROUTINE DP(N,K)
C*****DP
C
C          THIS SUBROUTINE DRAWS THE LINES
C
    COMMON/PTS/X(13,200),Y(3,13,200),PH(13),M,TURNS
    INTEGER P,K,N,M
    LOGICAL LYB,LYS,LXB,LMOD,ON
666 CONTINUE
    DIMENSION V(200),W(200)
C    V IS X=COORD. W IS Y=COORD.
C    WRITE(5,115) N,K
C115  FORMAT('0',T20,'DP CALLED',T30,'N=',I2,T40,'K=',I2,/)
    CALL QPRS(P,ON)
    DO 100 J=1,M
C    IF(J.EQ.1) WRITE(5,50)
C 50  FORMAT('0',T10,'J',T25,'V(J)',T45,'W(J)',/)
C    WRITE(5,135)J,V(J),W(J)
C 135  FORMAT(' ',T8,I4,T20,F10.6,T40,F10.6)
    LYB=(Y(N,K,J).LT.10.)
    LYS=(Y(N,K,J).GT.0.)
    LXB=(X(K,J).LT.TURNS)
    LMOD=(MOD(J,24).EQ. 0)
    IF(LYB.AND.LYS.AND.LXB.AND.LMOD)CALL NUMBER(V(J),W(J),
1.1,PH(K),0.,=1)
    IF(LYB.AND.LYS) GO TO 120
    IF(LYS) GO TO 110
C    Y TOO SMALL STOP LINE AT BOTTOM OF PAGE
    CALL OPQ(ON,N,K,&100,&130,&121)
121  P=P+1
    V(P)=(X(K,J)-X(K,J-1))*Y(N,K,J-1)/(Y(N,K,J-1)-Y(N,K,J))+X(K,J-1)
    W(P)=0.
C    WRITE(5,65)
C 65  FORMAT(' ', 'LAST Y TOO SMALL',T20,'NEWX=',F10.5,
C    2T40,'NEWY=',F10.5)
    CALL NUMBER(V(P),W(P),.2,PH(K),0.,=1)
    GO TO 100
C    Y IS TOO BIG. STOP LINE AT TOP OF PAGE
110  CALL OPQ(ON,N,K,&100,&130,&122)
122  P=P+1
    V(P)=(X(K,J)-X(K,J-1))*(10.-Y(N,K,J-1))/(Y(N,K,J)-Y(N,K,J-1))
    X+X(K,J-1)
    W(P)=10.
C    WRITE(5,95) V(J),W(J)
C 95  FORMAT(' ', 'LAST Y TOO BIG',T20,'NEWX=',F10.5,
C    3T40,'NEWY=',F10.5)
    CALL NUMBER(V(P)+.01,W(P)-.05,.1,PH(K),0.,=1)

```

```

GO TO 100
120 IF(LXB) GO TO 99
C   X IS TOO BIG STOP LINE AT END OF X=AXIS
CALL OPQ(ON,N,K,&100,&130,&123)
123 P=P+1
    W(P)=(Y(N,K,J)-Y(N,K,J-1))*(TURNS=X(K,J-1))/(X(K,J)-X(K,J-1))
    X+Y(N,K,J-1)
    V(P)=TURNS
C   WRITE(5,60) V(J),W(J)
C 60  FORMAT(' ', 'LAST X TOO BIG', T20, 'NEWX=', F10.5,
C     4T40, 'NEWY=', F10.5)
    CALL NUMBER(V(P)+.01, W(P)-.05, .1, PH(K), 0., -1)
    GO TO 100
99  P=P+1
    V(P)=X(K,J)
    W(P)=Y(N,K,J)
    ON=.TRUE.
100 CONTINUE
130 WRITE(8,669) (V(NM), W(NM), NM=1, P)
669 FORMAT(' ', 2G12.3)
    CALL LINE(V,W,P,1)
C   WRITE(5,125) N,K,P
C125 FORMAT('0', T20, 'LINE CALLED FOR N=', I2, 2X, 'K=', I2, 2X, 'P=', I4,
C     5T60, 'RETURN TO PLO')
667 CONTINUE
    RETURN
    END
    SUBROUTINE OPQ(ON,N,K,*,*,*)
C*****OPQ
    LOGICAL OFF(13),ON
    INTEGER P
    IF(.NOT.ON) RETURN 1
    ON=.FALSE.
    IF(OFF(K)) RETURN 2
    OFF(K)=.TRUE.
    RETURN 3
    ENTRY QPRS(P,ON)
    DO 1 I=1,13
1   OFF(I)=.FALSE.
    ON=.FALSE.
    P=0
    RETURN
    END
    SUBROUTINE DATA(*)
    COMMON /CARD/P(8),MNT(5)
    DIMENSION A(40)
    READ 100,A,MNT
100  FORMAT(40A1,5A4)
    PRINT 101,A,MNT
101  FORMAT(6HODATA/40A1,1H/5A4,1H/)
    DO 15 I=1,8
15  P(I)=0.
    CALL SCAN(A,40,P,8)
    CALL CLOCK($999)
    RETURN
999 RETURN 1
    END
    SUBROUTINE SCAN(A,NCH,T,MAX)
    DIMENSION A(1),T(1),C(12)
    LOGICAL MINUS,NUMBER,PERIOD,FRACT,OPEN

```

```

DATA C/1H0,1H1,1H2,1H3,1H4,1H5,1H6,1H7,1H8,1H9,1H.,1H=/
K=0
NFPT=0
4 CONTINUE
OPEN=.FALSE.
FRACT=.FALSE.
MINUS=.FALSE.
FPNINT=0.
FPNFRC=0.
NFRACT=0
SGN=1.
5 K=K+1
IF(K.GT.NCH.OR.NFPT.GT.MAX)RETURN
CH=A(K)
DO 10 I=1,12
IF(C(I).EQ.CH)GO TO 15
10 CONTINUE
IF(OPEN)GO TO 20
GO TO 5
15 PERIOD=I.EQ.11
MINUS=I.EQ.12
NUMBER=I.LT.11
OPEN=.TRUE.
IF(PERIOD)FRACT=.TRUE.
IF(FRACT)NFRACT=NFRACT+1
IF(MINUS)SGN=-1.
FPT=I-1
IF(NUMBER.AND.FRACT)FPNFRC=FPNFRC+FPT/FLOAT(10**(NFRACT-1))
IF(NUMBER.AND..NOT.FRACT)FPNINT=FPNINT*10.+FPT
GO TO 5
20 NFPT=NFPT+1
T(NFPT)=SGN*(FPNINT+FPNFRC)
GO TO 4
END
FUNCTION UTERP(E)
COMMON /VNUZ/NNUZ,EOZ,DELEZ,UZ(100)
P=(E-EOZ)/DELEZ
IT=P
P=P-IT
IT=IT+1
P2=P+P
P3=P2+P
PP=P*P
UTERP=(PP-P3+2.)*UZ(IT)/2.+(P2-PP)*UZ(IT+1)+(PP-P)*UZ(IT+2)/2.
UTERP=ABS(UTERP)
RETURN
END
FUNCTION STERP(E)
COMMON /SLIP/NPS,EOS,DELES,PS(100)
P=(E-EOS)/DELES
IT=P
P=P-IT
IT=IT+1
P2=P+P
P3=P2+P
PP=P*P
STERP=(PP-P3+2.)*PS(IT)/2.+(P2-PP)*PS(IT+1)+(PP-P)*PS(IT+2)/2.
RETURN
END

```